



# The physics of gamma-ray bursts & relativistic jets



Pawan Kumar<sup>a,\*</sup>, Bing Zhang<sup>b</sup>

<sup>a</sup> Department of Astronomy, University of Texas at Austin, Austin, TX 78712, USA

<sup>b</sup> Department of Physics & Astronomy, University of Nevada Las Vegas, Las Vegas, NV 89154, USA

## ARTICLE INFO

### Article history:

Accepted 22 September 2014

Available online 23 December 2014

editor: M.P. Kamionkowski

## ABSTRACT

We provide a comprehensive review of major developments in our understanding of gamma-ray bursts, with particular focus on the discoveries made within the last fifteen years when their true nature was uncovered. We describe the observational properties of photons from the radio to 100s GeV bands, both in the prompt emission and the afterglow phases. Mechanisms for the generation of these photons in GRBs are discussed and confronted with observations to shed light on the physical properties of these explosions, their progenitor stars and the surrounding medium. After presenting observational evidence that a powerful, collimated, jet moving at close to the speed of light is produced in these explosions, we describe our current understanding regarding the generation, acceleration, and dissipation of the jet. We discuss mounting observational evidence that long duration GRBs are produced when massive stars die, and that at least some short duration bursts are associated with old, roughly solar mass, compact stars. The question of whether a black-hole or a strongly magnetized, rapidly rotating neutron star is produced in these explosions is also discussed. We provide a brief summary of what we have learned about relativistic collisionless shocks and particle acceleration from GRB afterglow studies, and discuss the current understanding of radiation mechanism during the prompt emission phase. We discuss theoretical predictions of possible high-energy neutrino emission from GRBs and the current observational constraints. Finally, we discuss how these explosions may be used to study cosmology, e.g. star formation, metal enrichment, reionization history, as well as the formation of first stars and galaxies in the universe.

© 2014 Elsevier B.V. All rights reserved.

## Contents

1. Introduction .....	3
2. Radiative processes .....	6
2.1. Photon arrival time from a moving source, Doppler shift, Lorentz invariance of power etc. ....	6
2.2. Synchrotron radiation .....	8
2.2.1. Effect of synchrotron cooling on electron distribution .....	9
2.2.2. Synchrotron self-absorption frequency .....	10
2.2.3. Maximum energy of synchrotron photons .....	10
2.3. Inverse-Compton radiation .....	11
2.4. Hadronic processes .....	12
3. Afterglow theory .....	12
3.1. Relativistic shocks: basic scalings .....	12

\* Corresponding author.

E-mail addresses: [pk@astro.as.utexas.edu](mailto:pk@astro.as.utexas.edu) (P. Kumar), [zhang@physics.unlv.edu](mailto:zhang@physics.unlv.edu) (B. Zhang).

3.2.	Afterglow synchrotron spectrum and lightcurve .....	15
3.3.	Reverse shock.....	18
3.4.	Jet break.....	19
3.5.	Other effects.....	21
3.5.1.	Naked afterglow and high-latitude effect.....	21
3.5.2.	Energy injection .....	21
3.5.3.	Density bumps .....	22
3.5.4.	Synchrotron self-Compton.....	22
3.5.5.	Hard electron spectrum .....	22
3.5.6.	Effect of neutron decay.....	22
3.5.7.	Radiation front effect.....	23
3.5.8.	Transition to Newtonian phase.....	23
4.	Afterglow observations and interpretations .....	23
4.1.	Late time afterglow observations and interpretations .....	23
4.2.	Early afterglow observations and interpretations .....	24
4.2.1.	Steep decay of early X-ray light-curve .....	26
4.2.2.	Sudden increase in X-ray flux (flares) .....	26
4.2.3.	Plateaus in X-ray light-curves.....	26
4.2.4.	Steep decay following the plateau in X-ray light-curve .....	27
4.3.	High energy ( $>10^2$ MeV) afterglow radiation .....	28
5.	Collisionless shock properties from GRB afterglow observations .....	31
6.	Observational properties of GRB prompt radiation .....	34
6.1.	Temporal properties .....	34
6.2.	Spectral properties.....	35
6.2.1.	Spectral shapes and functions .....	35
6.2.2.	Spectral evolution .....	38
6.3.	Broad-band prompt emission .....	40
6.4.	Polarization .....	41
6.5.	Isotropic luminosity function .....	42
6.6.	Correlations between different observed parameters .....	42
6.6.1.	$E_{p,z}$ - $E_{\gamma,\text{iso}}$ (Amati) and $E_{p,z}$ - $L_{\gamma,\text{iso}}$ (Yonetoku) relations .....	42
6.6.2.	$E_{p,z}$ - $E_{\gamma}$ (Ghirlanda) relation.....	43
6.6.3.	$E_{p,z}$ - $E_{\gamma,\text{iso}}$ - $t_{b,z}$ (Liang-Zhang) relation .....	43
6.6.4.	$E_{p,z}$ - $L_{\gamma,\text{iso}}$ - $T_{0.45}$ (Fermani) relation .....	43
6.6.5.	$E_{\gamma,\text{iso}}$ - $\theta_j$ (Frail) relation: constant energy reservoir .....	44
6.6.6.	Luminosity-spectral lag ( $L-\tau$ ), Norris relation .....	44
6.6.7.	Luminosity-variability ( $L-V$ ) relation .....	44
6.6.8.	$E_{\gamma,\text{iso}}$ - $\Gamma$ and $L_{\gamma,\text{iso}}$ - $\Gamma$ relations .....	44
6.7.	GRB cosmography .....	44
7.	Progress toward understanding GRB prompt radiation .....	45
7.1.	Hot fireball model .....	46
7.1.1.	Dynamics of a hot fireball .....	46
7.1.2.	Photospheric radiation .....	49
7.2.	Distance from the central engine where $\gamma$ -rays are produced .....	49
7.3.	Internal shocks: conversion of outflow kinetic energy to radiation .....	51
7.4.	Viability of Synchrotron radiation mechanism for GRBs for shock heated plasma .....	52
7.5.	Constraints on Synchrotron-self-Compton mechanism for GRBs .....	54
7.6.	General constraints on electron Lorentz factor ( $\gamma_e$ ) .....	55
7.6.1.	Short lived acceleration phase for electrons .....	55
7.6.2.	Continuous/repeated acceleration of electrons .....	56
7.7.	Effects of neutrons on jet dynamics and radiation .....	56
7.8.	Prompt $\gamma$ -rays from photosphere: processed thermal photons .....	59
7.9.	Hadronic model for prompt $\gamma$ -ray radiation .....	61
7.9.1.	Photo-pion process for producing high energy photons .....	61
7.9.2.	Bethe-Heitler process .....	63
7.9.3.	Proton synchrotron model for producing $>10^2$ MeV photons .....	65
7.10.	Magnetic jet model .....	66
7.10.1.	Adiabatic expansion and acceleration of a Poynting jet .....	66
7.10.2.	Magnetic dissipation and jet acceleration .....	69
7.10.3.	Basic reconnection physics .....	71
7.10.4.	Forced reconnection of magnetic fields for a high- $\sigma$ GRB jet and prompt $\gamma$ -ray radiation .....	72
7.10.5.	Particle acceleration .....	73
7.11.	Some off-the-beaten-track ideas for GRB prompt radiation mechanism .....	74
8.	GRB central engine .....	75
8.1.	Hyper-accreting black holes .....	76
8.1.1.	Neutrino-dominated accretion flow (NDAF) and advection-dominated accretion flow (ADAF) .....	76

8.1.2.	Blandford–Znajek mechanism .....	77
8.1.3.	Magnetic jets launched from the accretion disk .....	78
8.1.4.	Effects of the stellar envelope in long GRBs .....	78
8.1.5.	Black hole engine in short GRBs .....	78
8.2.	Millisecond magnetars .....	78
8.3.	Models of late central engine activities .....	79
8.3.1.	X-ray flares .....	80
8.3.2.	X-ray “plateaus” .....	80
8.4.	Difference between the two types of engines .....	81
9.	Progenitors of GRBs .....	82
9.1.	Two physically distinct types of GRBs .....	82
9.2.	Massive star GRBs .....	83
9.2.1.	Properties of supernovae associated with GRBs .....	83
9.2.2.	Host galaxy properties of long GRBs .....	84
9.2.3.	Progenitor of long GRBs .....	84
9.3.	Compact star GRBs .....	84
9.3.1.	Non-detection of SN light .....	84
9.3.2.	Host galaxy properties of short GRBs .....	85
9.3.3.	Progenitor of short GRBs .....	85
9.4.	Gravitational wave diagnosis of GRB progenitor .....	85
10.	High energy neutrinos from GRBs .....	85
10.1.	PeV neutrinos .....	86
10.2.	Other neutrino emission components from GRBs .....	88
11.	GRBs from the first stars (pop III stars) and their use for investigating the high redshift universe .....	88
12.	Concluding thoughts and future prospects .....	90
	Acknowledgments .....	91
	References .....	91

## 1. Introduction

This introduction to Gamma-Ray Bursts (GRBs) is meant to provide a brief summary of their main properties so that someone not interested in details can obtain a quick overview, in a few pages, of the main properties of these explosions from the reading of this introduction.

The serendipitous discovery of Gamma-Ray Bursts (GRBs) in the late sixties by the Vela satellites<sup>1</sup> [1] puzzled astronomers for several decades: GRBs are irregular pulses of gamma-ray radiation (typically lasting for less than one minute), with a non-thermal (broken power-law) spectrum peaking at  $\sim 10\text{--}10^4$  keV, and are seen a few times a day at random locations in the sky e.g. [2–4]. Their spectacular nature, detection at redshift larger than 9 with current generation of instruments, and their connection with supernovae explosions and possibly black-holes formation, have led to a great deal of time and effort invested to their study (e.g. [5–13]).

The histogram of GRB duration has two distinct peaks. One at 0.3 s and the other at about 30 s, which are separated by a dip at 2 s. Bursts with duration less than 2 s are classified as short-GRBs and those that last for more than 2 s are called long-GRBs. Based only on the two peaks in the duration distribution, and well before anything was known about the distance or physical origin of GRBs, it was suspected that these peaks correspond to two physically distinct progenitors. Recent observations have confirmed that long-GRBs are one possible outcome of the collapses of massive stars (mass  $\gtrsim 15M_{\odot}$ ), and that at least some of the short-GRBs arise in the mergers of compact objects in binary systems (perhaps merger of two neutron stars or a neutron star and a black hole). The connection between the classifications based on burst duration and based on distinct physical origins turns out to be more complicated though, and is still not fully understood.

Distances to GRBs were completely uncertain until the launch of Compton-Gamma-Ray-Observatory (CGRO), from space shuttle Atlantis, on 5 April 1991 in a low earth orbit at 450 km (in order to avoid the Van Allen radiation belt that covers  $\sim 10^3\text{--}6 \times 10^4$  km altitude). It carried four instruments that provided a wide energy band coverage of 20 keV–30 GeV (at 17 tons, CGRO, was the heaviest astrophysical payload flown at that time). CGRO established that these bursts are isotropically distributed [4] and their number at the faint end (but well above the instrument threshold) deviates from the expected

<sup>1</sup> Vela – short for velador, meaning “watchman” in Spanish – were a group of 12 satellites (including 6 advanced Vela design) that were launched starting from October 17, 1963 until 1970, and the last satellite was decommissioned in 1984 (even though they were designed for a nominal life of 6–18 months). Vela satellites were launched to monitor compliance with the treaty “banning nuclear weapon tests in the atmosphere, in outer space and under water” signed by the governments of the Soviet Union, the United Kingdom and the United States, in Moscow on August 5, 1963 before being opened for signature by other countries. It was ratified by the US Senate on September 24, 1963. The treaty went into effect on October 10, 1963.

Euclidean count<sup>2</sup>  $N(> f) \propto f^{-3/2}$  (e.g. [14–16]). These two discoveries taken together convinced most astronomers that GRBs are located at distances much larger than the size of the local group of galaxies.

The confirmation of the cosmological distance to GRBs was obtained in 1997, when the BeppoSAX satellite, launched on April 30, 1996, provided angular position of bursts to within 4 arc-minutes – more than a factor 20 improvement compared with the Compton Gamma-ray Observatory – which enabled optical and radio astronomers to search for counterparts for these explosions. A rapidly fading X-ray & optical emission (the “afterglow”) accompanying a GRB was found on February 28, 1997, about 8 hours after the detection of the burst, and that led to the determination of redshift for this GRB to be 0.695 [17–19]. This launched a new era in the study of GRBs which has led to a wealth of new information and a much deeper understanding of these enigmatic explosions (e.g. [20–22,8,9,12,13]).

From burst redshift and flux we know that GRBs radiate between  $10^{48}$  and  $10^{55}$  ergs, if isotropic. This means that GRBs are the most energetic explosions in the Universe; the luminosity of the brightest bursts rivaling that of the entire Universe at all wavelengths albeit for only a few seconds [23].

Our understanding of GRBs has improved enormously in the last 18 years due to the observations made by several dedicated  $\gamma$ -ray/X-ray satellites (BeppoSAX, KONUS/Wind, HETE-2, Swift, Integral, AGILE, Fermi) and the follow-up observations carried out by numerous ground-based optical, IR, mm and radio observatories. Much of this progress has been made possible by the monitoring and theoretical modeling of long-lived afterglow emissions following the burst.

We know from breaks in optical & X-ray afterglow lightcurves that GRBs are highly beamed [24,25], and the true amount of energy release in these explosions is  $10^{48}–10^{52}$  ergs [26–32].

The follow-up of GRBs at longer wavelengths (X-ray, and optical) has established that afterglow light-curves often decay as a power-law with time ( $F_v \propto t^{-1}–t^{-2}$ ) and have a power-law spectrum ( $F_v \propto v^{-0.9 \pm 0.5}$ ). The synchrotron radiation from the external *forward-shock* – which results from the interaction of GRB-ejecta with the circumburst medium [33–36] – provides a good fit to the multi-wavelength afterglow data for GRBs (e.g. [37]).

In many cases, the decay of the optical or X-ray afterglow light-curve steepens to  $F_v \propto t^{-2.2}$  at  $\sim 1$  day after the burst. The most natural explanation for this steepening (foreseen by Rhoads [24]) is that GRB outflows are not spherical but collimated into narrow jets [25]. As the ejecta is decelerated and the strength of the relativistic beaming diminishes, the edge of the jet becomes visible to the observer. The finite angular extent of the ejecta leads to an achromatic faster decay of optical & X-ray lightcurves. This achromatic transition from a slower to a faster decay of lightcurves is called “jet-break”.

The initial opening angle of the jet and its kinetic energy can be obtained by modeling the broadband emission (radio to X-ray) of those GRB afterglows whose light-curve fall-off exhibited a jet-break. From these fits it is found that the opening angle of GRB jets is in the range of  $\sim 2$  – 10 degrees, thus the ejecta collimation reduces the required energy budget by a factor  $\sim 10^2$ – $10^3$  relative to the isotropic case; the true amount of energy release for most long duration GRB is found to be  $10^{49} \sim 10^{52}$  erg [24–28,32]. The medium within  $\sim 0.1$  pc of the burst is found to have a uniform density in many cases, and the density is of the order of a few protons per cm<sup>3</sup> [37]. This is a surprising result in the light of the evidence that long duration GRBs are produced in the collapse of a massive star – as suggested by Woosley [38], Paczynski [39], MacFadyen and Woosley [40] – where we expect the density to decrease with distance from the center as  $r^{-2}$  due to the wind from the progenitor star [41–44].

It was expected from theoretical considerations that GRB outflows are highly relativistic (e.g. [45–47,6]). A direct observational confirmation of this was provided by measurements of radio scintillation for GRB 970508 [48,20], and “superluminal” motion of the radio afterglow of a relatively nearby burst GRB 030329 [49] where the blastwaves were found to be still mildly relativistic several weeks after the explosion.

The evidence for association of long-duration GRBs (those lasting for more than 2 s) with core collapse SNe comes from two different kinds of observations: (i) GRBs are typically found to be in star forming regions of their host galaxies (e.g. [50–53]); (ii) For several GRBs, Type Ic supernovae have been detected spectroscopically associated with the GRBs. Most of the SNe-associated GRBs have luminosity significantly lower than typical GRBs,<sup>3</sup> e.g. GRB 980425 [56], 030329 [57,58], 060218 [59–61], 100316D [62,63], 101219B [64], and 120422A [65]. However, two nearby high-luminosity GRBs, i.e. 031203 [66] and 130427A [67,68], are also found to be associated with Type Ic SNe. Additionally, a subset of about a dozen GRBs show at late-times ( $\sim 10$  days) SNa-like “bump” in the optical data and simultaneously a change in color that is inconsistent with synchrotron emission, and suggests that optical flux from the underlying supernova is starting to overtake the GRB afterglow flux [22,10].

Significant progress toward answering the long standing question regarding the nature of short duration GRBs (those lasting for less than 2 s) was made possible by the Swift satellite’s more accurate localization of these bursts (3 arcmin vs. a few degrees for Compton-GRO). This led to the discovery that a fraction of these bursts are located in elliptical galaxies, i.e. associated with older stellar population, and were found to be on average less energetic and at a lower redshift [69–76]. These observations are consistent with the old idea that these bursts originate from neutron star mergers [77,78]. However, there is no conclusive proof for this model as yet.

<sup>2</sup> The easiest way to understand this relation is to consider sources of the same intrinsic luminosity,  $L$ , uniformly distributed in an Euclidean space. The observed flux decreases with distance  $R$  as  $R^{-2}$ , and the total number of sources within  $R$  grows as  $R^2$ . The observed flux from these sources is  $>f = L/(4\pi R^2)$ . Hence the total number of objects an observer sees with flux above  $f$  scales as  $f^{-3/2}$ . This argument is easy to generalize to consider a more realistic source luminosity function.

<sup>3</sup> These low-luminosity GRBs may not be representative of the main GRB population (e.g. [54,55]).

The Swift satellite, designed for the study of GRBs and launched in November 2004, has X-ray and UV-optical telescopes on board and provides localization of bursts to within 3 arcminutes. When Swift's gamma-ray telescope (Burst and Alert Telescope or BAT) detects a burst, the X-ray Telescope (XRT) and the UV-Optical Telescope (UVOT) on board Swift quickly slew to the GRB position within 60–100 s to observe the target, which provides excellent coverage of the transition from the prompt  $\gamma$ -ray phase to the lower-frequency afterglow emission phase.<sup>4</sup> Swift has provided a wealth of puzzling observations [79–81], and revealed that a variety of physical processes shape the early X-ray afterglow lightcurves [82]. Its XRT has found that for about 50% of GRBs the X-ray flux decays very rapidly after the burst ( $F_x \propto t^{-3}$ ), followed by a plateau during which the X-ray afterglow flux decrease is much slower ( $F_x \propto t^{-1/2}$ ) than expected in the standard forward-shock model. The former feature indicates that the  $\gamma$ -ray prompt radiation and afterglows are produced by two different mechanisms or arise from different outflows while the latter perhaps suggests that the forward shock that powers the afterglow takes a long time (of order several hours) to become a self-similar blast wave with constant energy (another possibility is that the observed X-ray radiation is not produced in the external shock).

Swift has also discovered episodes of a sharp increase in the X-ray flux (flares) minutes to hours after the end of the GRB [83–86]. The rapid rise time for the X-ray flux, with  $\delta t/t \sim 0.1$ , rules out the possibility that flares are produced as a result of inhomogeneity in the circumstellar medium where the curvature of the relativistic shock front limits  $\delta t \sim R/2c\Gamma^2 \sim t$  or  $\delta t/t \sim 1$  [87–89]. This suggests that the central engine in these explosions is active for a time period much longer than the burst duration<sup>5</sup> [83,82,92,93].

While the X-ray and optical data for  $t \gtrsim 10^4$  s (time measured from  $\gamma$ -ray trigger) are consistent with external forward shock emission, the features seen in the X-ray data prior to  $\sim 10^4$  s are not well understood. Similarly the expected achromatic breaks in the lightcurves (associated with finite jet angle) are seen in some bursts but not others [94–97,30, 29,31].

One of the foremost unanswered questions about GRBs is the physical mechanism by which prompt  $\gamma$ -rays – the radiation that triggers detectors on board GRB satellites – are produced. Is the mechanism the popular internal shock model<sup>6</sup> [98], the external shock model, or something entirely different? Are  $\gamma$ -ray photons generated via the synchrotron process or inverse-Compton process, or by a different mechanism? Answers to these questions will help us address some of the most important unsolved problems in GRBs – how is the explosion powered in these bursts? Does the relativistic jet produced in these explosions consist of ordinary baryonic matter, electron–positron pairs, or is the energy primarily in magnetic fields?

The Fermi satellite, a multi-purpose high energy satellite launched in June 2008, has provided useful data extending from  $\sim 10$  keV to  $> 300$  GeV to help answer some of these questions. It has made several important discoveries regarding GRBs [99–103]: (1) in most cases the high energy photons ( $> 10^2$  MeV) are detected with a delay of a few seconds with respect to the lower energy emission ( $\lesssim 1$  MeV); (2) high energy emission lasts for a time period much longer ( $\sim 10^3$  s) than emission below  $\sim 1$  MeV (which lasts for less than 1 min for most GRBs); (3) the broad-band prompt  $\gamma$ -ray spectra are found in most cases to consist of one peak and power law functions with different indices at low and high energies with a smooth transition from one to the other over a factor  $\lesssim 10$  in frequency (this is the so called “Band” spectrum), however in a few cases the spectrum has an addition component.

There are several different lines of strong evidence suggesting that the high energy photons ( $> 10^2$  MeV) we observe after the prompt phase ( $t \gtrsim 10$  s) are produced in the external forward shock via the synchrotron process [104,105]. On the other hand the origin of prompt  $\gamma$ -ray emission, low and high energies, remains a puzzle. Some of the proposed models are: synchrotron and inverse-Compton (IC) radiation processes in internal or external shocks or at sites where magnetic field in Poynting jet is dissipated (e.g. [33,106–108]); and photospheric radiation with contribution from multiple IC scatterings (e.g. [109–121,55]).

Swift satellite has found GRBs at high redshifts; the highest redshift GRB discovered to date is at  $z = 9.4$  when the universe was just 0.52 billion years old or 3.8% of its current age [122]. Swift is capable of detecting bursts of similar intrinsic brightness up to redshift of about 15. Because of their intrinsically simple spectrum and extremely high luminosity, GRBs are expected to offer a unique probe of the end of cosmic dark age when the first stars and galaxies were forming.

This review is organized in the order of the best understood GRB properties discussed first and the least well understood phenomena described last. We start with a brief review of radiation physics, and describe the theory of GRB afterglows which began to be developed even before the first detection of afterglow radiation. We then describe how well the afterglow theory does when confronted with observations. We first consider the late time afterglow observations (these observations starting from roughly half a day after the explosion can last for weeks to months), and what they have taught us about GRBs and the medium in their vicinity. This is followed by early afterglow observation – starting from  $\sim 30$  s (2 s) since the burst trigger for long (short) GRBs and spanning a duration of a few hours – and our current understanding of the puzzles they pose. Then

<sup>4</sup> Prior to the launch of Swift, there was a gap of typically about 7–8 hs between the detection of a burst in the  $\gamma$ -ray band and the follow up study of its afterglow emissions in the X-ray and lower energy bands.

<sup>5</sup> Well before the discovery of X-ray flares Katz and Piran [90] suggested a long lived central engine activity as an explanation for the high-energy  $\gamma$ -rays from GRB 940217 detected 5000 s after the GRO/BATSE trigger [91]. However, it is possible that these high energy photons might have been produced in an external shock.

<sup>6</sup> According to the internal shock model, a fraction of jet kinetic energy is converted to thermal energy when a faster moving segment of the jet collides with a slower moving part that was ejected at an earlier time. The thermal energy produced is then radiated away as  $\gamma$ -ray photons via a number of different mechanisms such as the synchrotron and inverse-Compton process.

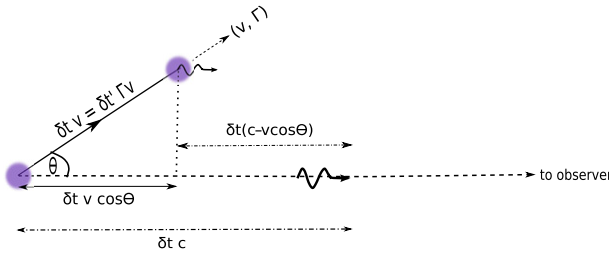


**Fig. 1.** The relation between pulse duration in source comoving frame,  $\delta t'$ , lab frame ( $\delta t$ ), and the time interval for pulse received by a distant observer is shown in this figure. The source is moving with speed  $v$  (Lorentz factor  $\Gamma$ ), at an angle  $\theta$  with respect to observer line of sight. One photon is emitted when the source was at the location at the left side of the figure. And a second photon is emitted  $\delta t'$  later when the photon has already traveled a distance  $c\delta t$  toward the observer, and the source is also a distance  $v \cos \theta \delta t$  closer. The difference between these two distances is the time interval in the observer frame for the arrival of the two photons which is given by Eq. (1).

the least well understood of all the data – properties of the GRB prompt radiation – and the strengths and weaknesses of various models proposed to explain these observations are reviewed. Next, we take up the properties of the central engine, and describe the two leading models: a new-born hyper-accreting black hole, and a strongly magnetized, rapidly spinning neutron star (magnetar). We then move on to discuss the possible progenitors of GRBs. We also devote a section to discussion of possible neutrino emission from GRBs.

## 2. Radiative processes

We provide in this section a brief overview of a few of the most important radiative processes in GRBs which will be used extensively in this review. There are excellent books that cover this topic in detail such as the monograph by Rybicki and Lightman [123], and books on high energy astrophysics by Longair [124], Krolik [125], Dermer and Menon [126], Kulsrud [127]. This section is no substitute for the extensive coverage of this topic provided in these books. The purpose here is to provide a quick summary of some of the main results we need in other sections, so as to make this review somewhat self-contained.

We describe synchrotron, inverse-Compton and photo-pion processes in this section. A few basic relativity results that are needed for understanding of radiative processes are also included here.

### 2.1. Photon arrival time from a moving source, Doppler shift, Lorentz invariance of power etc.

Consider a source moving with speed  $v$ , and corresponding Lorentz factor  $\Gamma$ , at an angle  $\theta$  with respect to the line of sight to the observer located far away from the source. Two photons are emitted  $\delta t'$  apart in the source comoving frame. In the lab frame (the frame in which the source is seen to move at speed  $v$ ), the time interval of emitting these two photons is  $\delta t = \Gamma \delta t'$ . The time difference for the arrival of these photons at the observer is given by (see Fig. 1):

$$\begin{aligned}\delta t_{obs} &= \delta t + [d - v \cos \theta(\delta t)]/c - d/c = \delta t(1 - v \cos \theta/c) \\ &= \delta t' \Gamma(1 - v \cos \theta/c) = \delta t' \mathcal{D}^{-1}\end{aligned}\quad (1)$$

where  $d$  is the distance to the source,

$$\mathcal{D} = [\Gamma(1 - v \cos \theta/c)]^{-1} \quad (2)$$

is the Doppler factor. For  $\theta \ll 1$  and  $\Gamma \gg 1$ , the above expression for  $\delta t_{obs}$  can be approximated as

$$\delta t_{obs} \approx \frac{\delta t'}{\Gamma} [1 + (\theta \Gamma)^2/2] = \frac{\delta t}{\Gamma^2} [1 + (\theta \Gamma)^2/2]. \quad (3)$$

The photon frequency in the observer frame,  $\nu$ , can be expressed in terms of the comoving frame frequency  $\nu'$  using the standard Lorentz transformation of photon 4-momentum in comoving frame –  $\nu'(1, \cos \theta', \sin \theta', 0)$  – to the lab frame 4-momentum  $\nu(1, \cos \theta, \sin \theta, 0)$

$$\nu = \nu' \Gamma (1 + v \cos \theta'/c) \quad \& \quad \nu \cos \theta = \nu' \Gamma (\cos \theta' + v/c) \quad (4)$$

or

$$\nu = \frac{\nu'}{\Gamma (1 - v \cos \theta/c)} \equiv \nu' \mathcal{D}, \quad (5)$$

which is the standard Doppler shift formula.

## Relativistic beaming of photons

The transverse component of momentum does not change under Lorentz transformation, i.e. its comoving and lab frame values are the same

$$v \sin \theta = v' \sin \theta' \quad \text{or} \quad \sin \theta = \sin \theta' / \mathcal{D}. \quad (6)$$

For large  $\Gamma, \theta \approx \theta'/\Gamma$ , i.e. photons are focused in the forward direction such that the angular size of the photon beam in the lab frame is smaller than it is in the comoving frame by a factor  $\sim \Gamma$ . The solid angle for a conical beam of photons in lab frame is smaller than in the comoving frame by a factor  $\sim \Gamma^2$ . A more precise expression for Lorentz transformation of solid angle is:

$$d\Omega = \sin \theta d\theta d\phi = \sin \theta' d\theta' d\phi' / \mathcal{D}^2 = d\Omega' / \mathcal{D}^2. \quad (7)$$

Next we show that the power<sup>7</sup> radiated by a particle is Lorentz invariant when the radiation beam is symmetric under parity transformation in particle rest-frame, i.e. the energy radiated per unit solid angle in directions  $(\theta, \phi) & (\pi - \theta, \pi + \phi)$  are equal. One of the easiest ways to see this is to consider the 4-momentum carried away by photons emitted in time interval  $\delta t'$  in the source frame, which is:  $P' \delta t'(1, 0, 0, 0)$ ; where  $P'$  is the power in source comoving frame, and the space components are zero because of parity symmetry. The 4-momentum and the elapsed time in the lab frame are:  $\Gamma P' \delta t'(1, v, 0, 0), \Gamma \delta t'$ . Hence the power in the lab frame is  $P = P' \Gamma \delta t' / (\Gamma \delta t') = P'$ .

## Transformation of specific luminosity and specific intensity

Another useful result concerns the Lorentz transformation of luminosity. Let us consider a source that is spherically symmetric and is expanding with Lorentz factor (LF)  $\Gamma$ . The observed specific luminosity,  $L_\nu$ , is the total energy that flows through a surface enclosing the source per unit time and frequency. Thus, it follows that

$$L_\nu = \frac{dE}{dv dt_{obs}} = \Gamma \frac{dE'}{dv' dt'} = \Gamma L'_{\nu'}, \quad (8)$$

where we made use of  $dvd t_{obs} = dv' dt'$  (see Eqs. (1) and (5)), and  $E = \Gamma E'$  when the 3-momentum vector is zero as it must for a spherically symmetric radiation source.

The specific intensity is defined as flux per unit frequency and per unit solid angle carried by photons traveling within a narrow conical beam with its axis perpendicular to surface  $dA$ , i.e.

$$I_\nu \equiv \frac{dE}{dv dt_{obs} dA d\Omega}. \quad (9)$$

Considering that  $E$  transforms as  $v, d\Omega$  transformation is given by Eq. (7), and  $dvd t_{obs} dA$  is Lorentz invariant, we find

$$I_\nu = \mathcal{D}^3 I'_{\nu'}. \quad (10)$$

## Observed lightcurve from a source that is suddenly turned off

Transient sources such as GRBs can turn off rapidly on a time scale of a second or less. Following [128,129] we consider a case here where a relativistic, conical, optically thin source moving with LF  $\Gamma$  turns off abruptly, and calculate how the flux declines with time as seen by a far away observer in a fixed frequency band.

We consider the source to be a thin shell, and points in the source are specified by  $(r, \theta, \phi)$  where angle  $\theta$  is measured with respect to the line of sight to the observer. The source turns off suddenly when it is at radius  $r = R_0$ . Photons released at  $(r = vt, \theta, \phi)$  arrive at the observer with a time delay with respect to a photon emitted at  $r = 0$  of

$$t_{obs} = t - r \cos \theta / c = t(1 - v \cos \theta / c) = t / (\Gamma \mathcal{D}). \quad (11)$$

We calculate the lightcurve at frequency  $\nu$  from the source after time  $t_{0,obs} \approx R_0 / (2c\Gamma^2)$  which corresponds to the arrival of photons from  $(R_0, 0, 0)$  at the observer. At  $t_{obs} > t_{0,obs}$  the observer sees photons which left the source when  $r < R_0$  as determined by Eq. (11). The time dependence of the observed flux, when the intrinsic spectrum is  $I'_{\nu'} = I' \nu'^{-\beta}$ , follows from the Lorentz transformation of specific intensity. At any given observer time  $t_{obs} > t_{0,obs}$  we receive radiation from  $\theta > \theta_t$ , where  $\theta_t$  is the angle corresponding to time  $t_{obs}$  such that  $t_{obs} = R_0(1/\nu - \cos \theta_t / c)$  (see Eq. (11)). Considering that the observed flux is proportional to the integral of  $I_\nu$  over the solid angle of the source, we find  $f_\nu \propto \int_{\theta_t} d\theta \sin \theta \mathcal{D}^{-(3+\beta)}$ . Or  $f_\nu \propto (1 - v \cos \theta_t / c)^{-(2+\beta)} \propto t_{obs}^{-(2+\beta)}$ . A more precise derivation of this result is outlined below.

The specific flux in observer frame from a relativistic source of comoving specific intensity  $I'_{\nu'}$  and spectrum  $\propto \nu'^{-\beta}$  is given by

$$f_\nu(t_{obs}) = \int d\Omega_{obs} I_\nu \cos \theta_{obs} = 2\pi \int d\theta_{obs} \frac{I'_{\nu'} \nu'^{\beta} \sin 2\theta_{obs} [(1+z)\Gamma]^{-(3+\beta)}}{2\nu^\beta [1 - v \cos(\theta + \theta_{obs})/c]^{3+\beta}}, \quad (12)$$

<sup>7</sup> Power is defined as the frequency integrated total energy radiated per unit time over  $4\pi$  steradians.

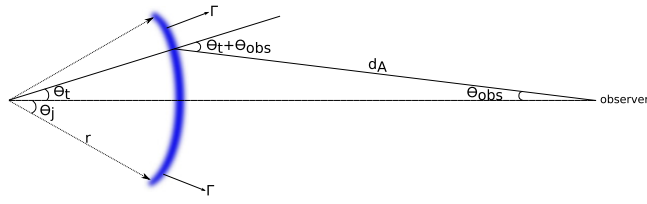


**Fig. 2.** A sketch of the various angles and distances for the large angle (or high latitude) emission when the  $\gamma$ -ray source turns off suddenly.

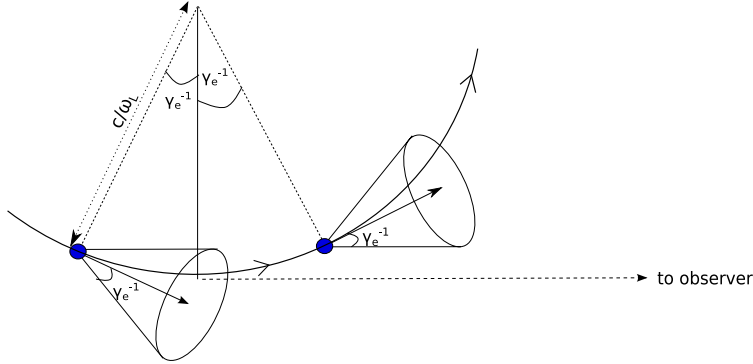


**Fig. 3.** The figure shows a segment of electron orbit that is moving in magnetic field with LF  $\gamma_e$ . Radiation from the electron is received by a distant observer only for a small segment of the orbit when the electron's velocity vector lies within  $\gamma_e^{-1}$  of the observer line of sight as a result of the beaming of photons in the forward direction in the lab frame (radiation in electron comoving frame is dipolar which covers almost  $4\pi$  steradians). The observed synchrotron peak frequency for emission from this electron follows from this simple property (Eq. (18)).

where  $\nu'_0$  is a frequency that lies on the power law segment of the spectrum for  $I'_{\nu'}$ , and we made use of the Lorentz transformation of specific intensity to obtain the last part of the above equation. The factor  $(1+z)^{3+\beta}$  in the above equation takes into account redshift of frequency for a source at  $z$ .

Using the law of sine for a triangle (see Fig. 2),  $\sin \theta/d_A = \sin \theta_{obs}/r$ , the above integral is transformed to

$$f_{\nu} \approx \frac{2\pi I' \nu'_0 \nu'^{\beta} \nu^{-\beta}}{[(1+z)\Gamma]^{3+\beta}} \left( \frac{R_0}{d_A} \right)^2 \int_{\theta_t}^{\pi/2} d\theta \frac{\sin \theta \cos \theta}{(1 - v \cos \theta/c)^{3+\beta}}. \quad (13)$$

We replaced  $\theta + \theta_{obs}$  in the denominator with  $\theta$  since  $\theta_{obs} \ll \theta$ . The above integral is straightforward to carry out and yields

$$f_{\nu}(t_{obs}) \propto (1 - v \cos \theta_t/c)^{-(2+\beta)} \nu^{-\beta} \propto t_{obs}^{-(2+\beta)} \nu^{-\beta}. \quad (14)$$

Thus, the observed radiation does not drop to zero as soon as the source is turned off, but the flux declines rapidly with time and eventually vanishes when  $\theta_t$  exceeds the angular size of the source ( $\theta_j$ ).

## 2.2. Synchrotron radiation

Consider an electron of Lorentz factor  $\gamma_e$ , and speed  $v_e$ , moving perpendicular to the magnetic field of strength  $B$ . The electric field in the electron rest frame is  $E = \gamma_e v_e B/c$ , and hence according to the Larmor's formula the power radiated due to electron acceleration in this electric field is

$$P_{syn} = \frac{2q^4 E^2}{3c^3 m_e^2} = \frac{2q^4 B^2 \gamma_e^2 v_e^2}{3c^5 m_e^2} = \sigma_T B^2 \gamma_e^2 v_e^2 / (4\pi c), \quad (15)$$

where  $\sigma_T = 8\pi q^4 / (3m_e^2 c^4)$  is the Thomson cross section. Since electric dipole radiation has parity symmetry,  $P_{syn}$  is a Lorentz invariant quantity (see Section 2.1), and hence the above equation gives the correct synchrotron power from an electron as viewed in the lab frame. The average power per electron, for isotropic pitch angle distribution, is smaller than the above expression by a factor 3/2.

The Larmor frequency of the electron (or its angular speed) is

$$\omega_L = \frac{qB}{\gamma_e m_e c}. \quad (16)$$

Due to relativistic beaming of photons described in Section 2.1 radiation from the electron that a distant observer receives is confined to the duration when the electron velocity vector lies within an angle  $\gamma_e^{-1}$  of the observer line of sight (Fig. 3).

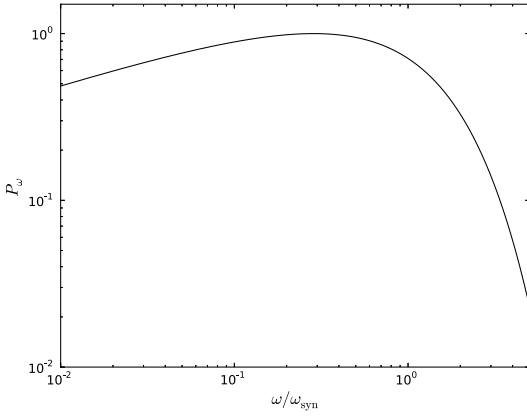


**Fig. 4.** This figure shows the synchrotron spectrum for a single electron; the x-axis is frequency in units of  $\omega_{\text{syn}}$  (see Eq. (18)), and the flux is normalized to unity at the peak.

The fraction of orbital time when this condition is satisfied is  $\sim 1/(\pi \gamma_e)$ , and therefore the duration of the radiation pulse received by the observer in each orbit is:

$$\delta t_{\text{obs}} \sim \frac{2}{\gamma_e \omega_L} \frac{1}{2\gamma_e^2} \sim \frac{m_e c}{qB\gamma_e^2}, \quad (17)$$

where we used Eq. (1) that relates the comoving time,  $\delta t' = \delta t/\gamma_e$ , to the observer frame time duration for photon pulse arrival. The inverse of this time is the characteristic frequency for synchrotron radiation which is given by

$$\omega_{\text{syn}} \sim \frac{qB\gamma_e^2}{m_e c} \quad \text{and} \quad \nu_{\text{syn}} = \frac{\omega_{\text{syn}}}{2\pi} \sim \frac{qB\gamma_e^2}{2\pi m_e c}, \quad (18)$$

where  $\nu_{\text{syn}}$  is the cyclic frequency. A more precise treatment has an additional factor  $(3/2) \sin \alpha$ ;  $\alpha$  is the pitch angle between the electron's velocity and the magnetic field. The synchrotron spectrum peaks at  $\sim \nu_{\text{syn}}$ . The spectrum below the peak scales as  $P_{\text{syn}}(\nu) \propto \nu^{1/3}$  (this behavior is determined by the Fourier transform of the synchrotron pulse profile), and it declines exponentially for  $\nu > \nu_{\text{syn}}$  (see Fig. 4); we refer to [123] for the calculation of synchrotron spectrum. The power per unit frequency  $P_{\text{syn}}(\nu)$  at the peak of the spectrum is

$$P_{\text{syn}}(\nu_{\text{syn}}) \sim P_{\text{syn}}/\nu_{\text{syn}} \sim \frac{\sigma_T B m_e c^2}{2q}. \quad (19)$$

The synchrotron spectrum for a power-law distribution of electrons,  $d\eta_e/d\gamma_e \propto \gamma_e^{-p}$ , is  $f_\nu \propto \nu^{-(p-1)/2}$ . This follows from adding up contributions to the specific flux at  $\nu$  from those electrons with LF larger than

$$\gamma_\nu \sim \left( \frac{2\pi \nu m_e c}{qB} \right)^{1/2}, \quad (20)$$

and that leads to

$$f_\nu = \int_{\gamma_\nu}^{\infty} d\gamma_e \frac{dn_e}{d\gamma_e} P_{\text{syn}}(\nu) \propto \nu^{-(p-1)/2}, \quad (21)$$

where we made use of  $P_{\text{syn}}(\nu) \propto (\nu/\nu_{\text{syn}})^{1/3}$  for  $\nu < \nu_{\text{syn}}$ , and Eq. (18) for  $\nu_{\text{syn}}$ .

### 2.2.1. Effect of synchrotron cooling on electron distribution

Another characteristic synchrotron frequency is associated with the cooling of electrons ( $\nu_c$ ). Let us consider that electrons are accelerated at some time, and then cool via synchrotron radiation for time duration  $t_0$ . Electrons with LF  $\gtrsim \gamma_c$  (defined below) lose a significant fraction of their energy during this time and their LF drops below  $\gamma_c$

$$\frac{dm_e c^2 \gamma_e}{dt} = -\frac{\sigma_T}{6\pi} B^2 \gamma_e^2 c \quad \text{or} \quad \gamma_c \sim \frac{6\pi m_e c}{\sigma_T B^2 t_0}. \quad (22)$$

The synchrotron frequency corresponding to this LF is defined as the synchrotron cooling frequency:

$$\nu_c \equiv \frac{3qB\gamma_c^2}{4\pi m_e c} \sim \frac{27\pi q m_e c}{\sigma_T^2 B^3 t_0^2}. \quad (23)$$

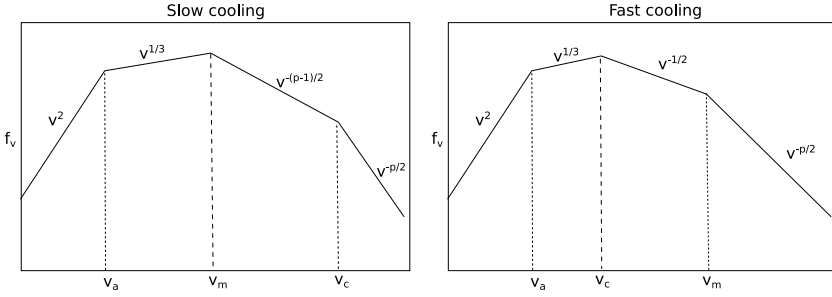


**Fig. 5.** Synchrotron spectrum for the case where  $v_a < v_m < v_c$  is shown in the left panel, and for the case  $v_a < v_c < v_m$  in the right panel, e.g. [131].

The power-law index of the synchrotron spectrum changes at  $v_c$  due to the fact that electron distribution function for  $\gamma_e > \gamma_c$  is modified as a result of loss of energy. This can be seen from the continuity equation for electrons in the energy space:

$$\frac{\partial}{\partial t} \frac{dn_e}{d\gamma_e} + \frac{\partial}{\partial \gamma_e} \left[ \dot{\gamma}_e \frac{dn_e}{d\gamma_e} \right] = S(\gamma_e), \quad (24)$$

where  $\dot{\gamma}_e = -\sigma_T B^2 \gamma_e^2 / (6\pi m_e c)$  is the rate of change of  $\gamma_e$  due to synchrotron loss, and  $S(\gamma_e)$  is the rate at which electrons with LF  $\gamma_e$  are injected into the system. The continuity equation has a steady state solution ( $\partial/\partial t = 0$ ) for time independent magnetic field which is:  $dn_e/d\gamma_e \propto \dot{\gamma}_e^{-1} \propto \gamma_e^{-2}$  for  $\gamma_c < \gamma_e < \gamma_m$ ; where  $\gamma_m$  is the minimum LF of injected electrons i.e.  $S(\gamma_e) = 0$  for  $\gamma_e < \gamma_m$ . The synchrotron spectrum corresponding to this segment of electron distribution function is  $f_v \propto v^{-1/2}$ . For a time dependent magnetic field the distribution function is not a power law function of  $\gamma_e$  with index 2, and in general its shape evolves with time [130].

For  $\gamma_e > \gamma_c > \gamma_m$ , the solution of the continuity equation is  $dn_e/d\gamma_e \propto \gamma_e^{-p-1}$  in the steady state (for constant  $B$ ). And the corresponding synchrotron spectrum is  $f_v \propto v^{-p/2}$ .

### 2.2.2. Synchrotron self-absorption frequency

Yet another characteristic frequency,  $v_a$ , corresponds to the case where absorption of photons by the inverse-synchrotron process becomes important. The easiest way to determine  $v_a$  is by the application of Kirchhoff's law — the emergent specific flux cannot exceed the black-body flux corresponding to the appropriate electron temperature which is

$$k_B T \approx \max(\gamma_a, \min[\gamma_m, \gamma_c]) m_e c^2 / 2.7 \quad (25)$$

where  $\gamma_m$ ,  $\gamma_c$  and  $\gamma_a$  are electron Lorentz factors corresponding to synchrotron frequencies  $v_m$ ,  $v_c$  and  $v_a$ , respectively, and  $k_B$  is Boltzmann constant. The synchrotron self-absorption frequency ( $v_a$ ) is the frequency where the emergent synchrotron flux is equal to the black-body flux:

$$\frac{2m_e c^2 \max(\gamma_a, \min[\gamma_m, \gamma_c]) v_a^2}{2.7 c^2} \approx \frac{\sigma_T B m_e c^2 N_>}{4\pi q} \quad (26)$$

where the left side of this equation is the Planck function in the Rayleigh-Jeans limit, and  $N_>$  is the column density of electrons with LF larger than  $\max(\gamma_a, \min[\gamma_m, \gamma_c])$ .

The emergent synchrotron spectrum for a distribution of electrons depends on the ordering of these characteristic frequencies. Spectra for two particular orderings are shown in Fig. 5.

### 2.2.3. Maximum energy of synchrotron photons

Charged articles are accelerated as they travel back and forth across a shock front via the first order Fermi process. They gain energy by a factor  $\sim 2$  each time they are scattered from one side to the other of a relativistic shock front. The maximum synchrotron frequency for an electron in this case turns out to be about  $50\Gamma$  MeV, and for a proton it is a factor  $m_p/m_e$  larger;  $\Gamma$  is the Lorentz factor of shocked plasma with respect to the observer, and  $m_p$  is proton mass.

The minimum time required for acceleration of a charged particle of mass  $m$  while crossing a shock front is of the order of the Larmor time  $t'_L = mc\gamma/(qB')$ ; where  $\gamma$  is LF of the particle in the shock comoving frame, and prime ('') refers to quantity measured in the rest frame of the shocked fluid. The particle should not lose more than half its energy to synchrotron radiation in time  $t'_L$ , otherwise it will never get accelerated to LF  $\gamma$ . This implies that  $4q^4 B'^2 \gamma^2 t'_L / (9m^2 c^3) < mc^2 \gamma / 2$  or  $qB'\gamma^2 / (2\pi mc) < 9mc^3 / (16\pi q^2)$ . The left side of the last inequality is the synchrotron frequency for the particle, and the right side depends on the particle's mass. So we find that the maximum synchrotron photon energy for an electron (proton) is  $\sim 50$  MeV (100 GeV) in shocked fluid comoving frame under the optimistic Bohm diffusion limit.

It is possible to violate this limit, by a factor of a few at least, when the magnetic field is highly inhomogeneous downstream of the shock front; synchrotron photons produced when a particle is passing through a region of much higher-than-average magnetic field can have energy larger than the limit described above, e.g. [132].

### 2.3. Inverse-Compton radiation

When a photon of frequency  $\nu$  is scattered by an electron of larger energy, the photon gains energy in this process on the average. If the electron Lorentz factor is  $\gamma_e$ , and  $h\nu\gamma_e \ll m_ec^2$ , then the average frequency of scattered photon is  $\nu_s \sim \nu\gamma_e^2$ . This is easy to see by viewing the process from the rest frame of the electron where the angle-averaged frequency of the incident photon is  $\nu' \sim \nu\gamma_e$  (see Eq. (5) for relativistic Doppler shift). For  $h\nu' \ll m_ec^2$  the scattering is elastic – the electron recoil can be neglected – so that the scattered photon has frequency  $\nu'$  (in electron rest frame) and its angular probability distribution is a dipole function. Transforming the frequency of the scattered photon back to the original frame introduces another Lorentz boost and that results in  $\nu_s \sim \nu\gamma_e^2$ .

Consider next an electron moving through a radiation field where the energy density in photons is  $u_\gamma$ . The power in IC-scattered photons,  $P_{ic}$ , follows from the energy boost by a factor  $\gamma_e^2$  for each photon (independent of photon energy for the case where  $h\nu\gamma_e \ll m_ec^2$  that we are considering here):

$$P_{ic} \sim \sigma_T \int d\nu \frac{u_\nu c}{h\nu} h\nu\gamma_e^2 \sim \sigma_T u_\gamma \gamma_e^2 c, \quad (27)$$

where  $u_\nu d\nu$  is energy density in photons of frequency between  $\nu$  and  $\nu + d\nu$ ;  $\int d\nu u_\nu = u_\gamma$ . We see from Eqs. (15) and (27) that the ratio of synchrotron and IC powers is  $u_B/u_\gamma$ ; where  $u_B = B^2/8\pi$  is the energy density in magnetic field.

A particularly important case of IC radiation is when seed photons are produced by the synchrotron process, i.e. electrons that produce seed photons also IC scatter them to typically much larger energies. This process – called synchrotron-self-Compton or SSC – could be important for GRBs and other relativistic sources. The relative importance of synchrotron and IC processes for extracting energy from a population of energetic electrons is specified by the Compton Y parameter. Energy density in photons for the synchrotron process is:

$$u_\gamma = \int dr \int d\gamma_e \frac{P_{syn}}{c} \frac{dn_e}{d\gamma_e} = \frac{\sigma_T(\delta R)B^2}{6\pi} \int d\gamma_e \gamma_e^2 \frac{dn_e}{d\gamma_e} = \frac{\sigma_T(\delta R)n_e B^2}{6\pi} \langle \gamma_e^2 \rangle, \quad (28)$$

where  $\delta R$  is the radial width of the source, and

$$\langle \gamma_e^2 \rangle \equiv \frac{1}{n_e} \int d\gamma_e \gamma_e^2 \frac{dn_e}{d\gamma_e}. \quad (29)$$

Making use of the expression for  $u_\gamma$  for synchrotron radiation we find the Compton-Y parameter to be

$$Y \sim P_{ic}/P_{syn} \sim \tau_e \langle \gamma_e^2 \rangle, \quad \text{where } \tau_e = \sigma_T(\delta R)n_e \quad (30)$$

is the optical depth of the source to Thomson scattering.

#### IC spectrum

The spectrum of IC radiation is obtained by convolving electron distribution with the seed photon spectrum [123]:

$$f_{ic}(\nu_{ic}) \approx \frac{3\sigma_T(\delta R)}{4} \int d\nu \frac{\nu_{ic}}{\nu^2} f_{syn}(\nu) \int \frac{d\gamma_e}{\gamma_e^2} \frac{dn_e}{d\gamma_e} F\left(\nu_{ic}/4\gamma_e^2\nu\right), \quad (31)$$

where

$$F(x) \approx \frac{2}{3}(1-x), \quad x \equiv \nu_{ic}/(4\gamma_e^2\nu). \quad (32)$$

It follows from these equations that the IC spectrum,  $f_{ic}(\nu_{ic})$ , for a  $\delta$ -function seed photon spectrum (where photons have frequency  $\nu_0$ ), and a power-law distribution of electrons with index  $p$  which is cutoff at the low energy end at  $\gamma_m$ , is proportional to  $\nu_{ic}$  for  $\nu_{ic} < 4\gamma_m^2\nu_0$ . Therefore, the low energy part of IC spectrum can be significantly harder than the hardest possible synchrotron spectrum ( $\nu^{1/3}$ ) when synchrotron-self-absorption is negligible. At higher photon energies,  $\nu_{ic} > 4\gamma_m^2\nu_0$ , the IC spectrum has an asymptotic power-law index  $\nu_{ic}^{-(p-1)/2}$ , same as the spectrum for the synchrotron process.

#### IC in Klein-Nishina regime

When photon energy in electron comoving frame approaches (or exceeds)  $m_ec^2$  two effects become important. One of which is that the electron recoil in the scattering can no longer be ignored. The other effect is that the cross-section is smaller than  $\sigma_T$  and it decreases with increasing photon energy as  $\sim\nu^{-1}$ . See [123] for appropriate equations. One simple consequence of the recoil effect is that the energy of the scattered photon is limited to  $\sim m_ec^2\gamma_e/2$  (and is no longer  $\sim\nu_0\gamma_e^2$ ) which is obvious from energy conservation.

## 2.4. Hadronic processes

Photo-pion process refers to the production of pions ( $\pi^0$ ,  $\pi^+$  and  $\pi^-$ ) in collisions of photons with protons; charge conservation requires that  $\pi^-$  is produced with at least one  $\pi^+$ . The decay of  $\pi^+$  produces positrons of very high LF which can then produce high energy photons via the synchrotron process. A neutral pion  $\pi^0$  can directly decay into two photons. The photo-pion process is likely to be important in those situations where electrons are unable to be accelerated efficiently to very high LFs whereas protons are. It also offers a way to beat the well known limit on the maximum synchrotron photon energy of about  $50\Gamma$  MeV for shock accelerated electrons (see Section 2.2.3).

The delta resonance for photon-proton interaction,  $p + \gamma \rightarrow \Delta^+$ , has the largest cross section,  $\sigma_{\gamma p} = 5 \times 10^{-28} \text{ cm}^2$ , and the lowest energy threshold –  $\sim 200$  MeV for photon in proton rest frame – of the photo-proton resonances, and is therefore the most important photo-pion interaction to consider for many astrophysical systems. The delta resonance has two main decay channels:  $\Delta^+ \rightarrow \pi^+ + n$  and  $\Delta^+ \rightarrow \pi^0 + p$ . The neutral pions quickly decay in  $8.4 \times 10^{-17} \text{ s}$  (in their rest frame) to two photons, and the outgoing  $\gamma$ -ray energy is at least 67 MeV (in pion rest frame).

The  $\pi^+$  decays in  $2.6 \times 10^{-8} \text{ s}$  to  $\mu^+ + \nu_\mu$ , and the anti-muon subsequently decays as  $\mu^+ \rightarrow e^+ + \bar{\nu}_\mu + \nu_e$ . The isospin conservation gives a branching ratio for  $\pi^+ : \pi^0$  decay channels of  $\Delta^+$  to be 1 : 2. However, when contributions from all the possible resonances as well as the direct pion production are included the ratio of charged pions to neutral pions is actually closer to 2 : 1 [133]. A detailed discussion of the photo-pion process in the context of high energy emission from GRBs is provided in Section 7.9.1, and its contribution to neutrinos is described in Section 10.

Another relevant process is the Bethe–Heitler pair production process  $p + \gamma \rightarrow p + e^+ + e^-$ . Its relative importance with respect to the photon pion process in contributing to radiation from GRBs is described in Section 7.9.2.

## 3. Afterglow theory

### 3.1. Relativistic shocks: basic scalings

One important piece of the GRB theory is a “generic” model that does not depend on the details of the central engine. This is a relativistic blastwave theory that describes interaction between the “fireball” – which moves with Lorentz factor  $\Gamma_0$  before deceleration & has total “isotropic equivalent” energy  $E$  – and the circumburst medium (CBM) described by the density profile,  $n(R) = (A/m_p)R^{-k}$ . Such a fireball–CBM interaction is inevitable for any type of energetic explosion. A power-law decaying multi-wavelength afterglow was in fact predicted by Paczynski and Rhoads [34], Mészáros and Rees [36] before the first observational detection of X-ray afterglow in 1997 by the BeppoSAX satellite. A relativistic shock theory was developed by Blandford and McKee [134] in the context of AGN jets which turned out to be well suited for interpreting GRB afterglows in X-ray, optical and radio bands when they were discovered in 1997 [17,19,20]. The self-similar nature of the blastwave solution naturally explains the power law behavior of the afterglow lightcurves.

The basic dynamics of blastwave is easy to understand using simple physical arguments, and the main results are sketched in Fig. 6. The emphasis is on trying to provide a physical understanding of the key concepts and not on rigorous derivations. For the latter we shall provide citations of the relevant literature.

It is best to work in the comoving frame of the shocked fluid which is traveling with Lorentz factor  $\Gamma$  with respect to unshocked fluid. The density of the unshocked medium in this frame is  $\Gamma n$ , and upstream particles are seen to be streaming toward the shocked fluid with a Lorentz factor  $\Gamma$ ; upstream particles have thermal energy much smaller than their rest mass. What a shock does is to randomize the orientation of particle velocity vectors, without changing their Lorentz factors, when they cross the shock front, and therefore the mean “thermal” energy of protons down-stream of the shock front is  $\Gamma m_p c^2$  (derivation provided below). As viewed from the lab frame, the average energy of each down-stream proton is  $\Gamma^2 m_p c^2$ , and hence for a blast wave at radius  $R$ , the total energy in the shocked plasma is

$$E \approx 4\pi AR^{3-k}c^2\Gamma^2/(3 - k), \quad (33)$$

where  $AR^{-k}$  is the density of the medium at radius  $R$  and  $4\pi AR^{3-k}/(3 - k)$  is the total swept up gas mass. This equation describes the basic dynamics of the blast wave. For instance, for a constant density CBM, and a non-radiative blast wave with constant total energy, the LF  $\Gamma \propto R^{-3/2}$ . The deceleration radius – the distance from the center of explosion (CoE) where the blast wave LF decreases by a factor 2 from its initial value of  $\Gamma_0$  and the energy imparted to the CBM is  $E/2$  – is obtained from the above equation which for a constant density medium is given by

$$R_d \approx (1.2 \times 10^{17} \text{ cm}) E_{53}^{1/3} n^{-1/3} \Gamma_{0.2}^{-2/3}. \quad (34)$$

Shocks also compress plasma – for highly relativistic shocks the compression factor is  $4\Gamma$ , i.e. the comoving frame density of the shocked plasma is  $4\Gamma n$  (quantitative expression is provided in Eq. (36)) – and accelerate particles to produce a power-law distribution function, and generate magnetic fields. These ingredients are all that one needs for calculating afterglow radiation from the interaction of a relativistic outflow with the surrounding medium.

We outline the derivation of the two results mentioned above, i.e. compression of plasma and entropy produced by a blast-wave, and then describe the dynamics for a number of different situations before taking up the radiation physics of GRB afterglows.

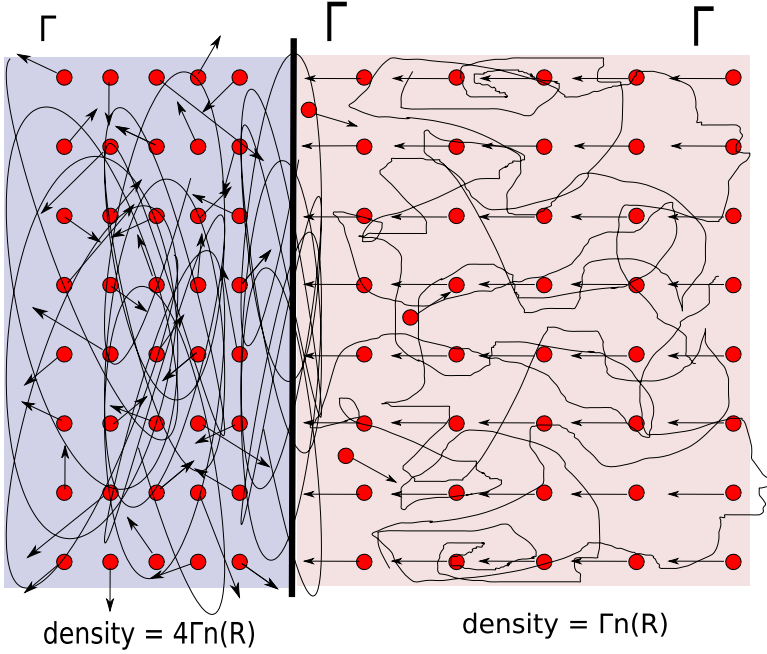


**Fig. 6.** A schematic sketch of highly relativistic shock as viewed from the mean rest frame of the shocked fluid; lines represent magnetic fields, and arrows show particle velocity with respect to the shocked plasma. The Lorentz factor of the unshocked medium (right hand part of the sketch) with respect to shocked plasma is  $\Gamma$ . Cold, upstream, particles stream toward the shocked plasma with Lorentz factor  $\Gamma$  as viewed in this frame, and after crossing the front their velocity direction is randomized but the magnitude of their proper-velocity is nearly unchanged. The shock also compresses plasma by a factor 4 (as viewed in the comoving frame of shocked plasma), and amplifies magnetic fields and accelerates particles.

For a relativistic shock propagating into a cold upstream medium, the physical condition of the shocked plasma is obtained from the conservation of baryon number, energy & momentum fluxes across the shock front; the baryon number flux is given by  $n' \Gamma c$ , and the momentum and energy fluxes are part of the energy-momentum tensor  $T^{\mu\nu} = (\rho' c^2 + p') u^\mu u^\nu + p' g^{\mu\nu}$ , where  $\rho' c^2$  &  $p'$  are the total energy density & pressure in the plasma rest frame,  $u^\mu$  is the 4-velocity, and  $g^{\mu\nu}$  is the metric tensor. These conservation equations can be reduced to the following three equations [134,135]:

$$\frac{e'_2}{n'_2} = (\gamma_{21} - 1)m_p c^2, \quad (35)$$

$$\frac{n'_2}{n'_1} = \frac{\hat{\gamma} \gamma_{21} + 1}{\hat{\gamma} - 1}, \quad (36)$$

$$\gamma_{1s}^2 = \frac{(\gamma_{21} + 1)[\hat{\gamma}(\gamma_{21} - 1) + 1]^2}{\hat{\gamma}(2 - \hat{\gamma})(\gamma_{21} - 1) + 2}. \quad (37)$$

Here  $m_p$  is proton mass,  $c$  is speed of light, subscript “2” and “1” denote downstream and upstream, respectively,  $e'$  &  $n'$  are internal energy density & proton number density (in local fluid rest frame),  $\gamma_{21}$  is the relative Lorentz factor of plasma in region 2 with respect to region 1,  $\gamma_{1s}$  is the relative Lorentz factor of plasma in region 1 with respect to the shock front, and  $\hat{\gamma}$  is the adiabatic index of the fluid. For ultra-relativistic shocks,  $\Gamma \gg 1$ , that describe the afterglow emission from GRB blastwave for a few days (e.g. [6]), one has  $\hat{\gamma} = 4/3$ , and it follows from the above conservation equations that  $e'_2/n'_2 \simeq \gamma_{21} m_p c^2$  (the average energy of protons down-stream of the shock front is  $\sim \gamma_{21} m_p c^2$ ),  $n'_2/n'_1 \simeq 4\gamma_{21}$  (downstream plasma is compressed by a factor of  $4\gamma_{21}$ ) and  $\gamma_{1s} \simeq \sqrt{2}\gamma_{21}$  (the shock front travels slightly faster than the downstream fluid).

Once the blastwave enters the self-similar deceleration phase, some simple scalings can be derived. Let us consider the case of a constant energy blastwave ( $E$ ) traveling in a constant density CBM ( $n$ ) as an example. Energy conservation can be written as

$$E = \frac{4\pi}{3} R^3 n m_p c^2 \cdot \Gamma^2 = \text{const}, \quad (38)$$

where  $\Gamma = \gamma_{21}$  is the bulk Lorentz factor of the blastwave (with respect to the unshocked medium),  $R$  is the distance of the shock front from the explosion center, and the factor  $\Gamma^2$  takes into account average proton thermal energy in the lab frame

(proton thermal energy in the shocked fluid comoving frame is  $m_p c^2 \Gamma$ ). One therefore finds  $\Gamma^2 R^3 = \text{constant}$ , or

$$\Gamma \propto R^{-3/2}. \quad (39)$$

The time duration for arrival of photons at the observer is smaller than the center-of-explosion (CoE) frame time by roughly a factor  $2\Gamma^2$  due to the blastwave and photons moving in more or less the same direction and the difference in their speed being  $\sim 1/2\Gamma^2$  (see Section 2.1). Therefore,

$$t_{\text{obs}} \sim \frac{R}{2\Gamma^2 c} \propto R^4 \propto \Gamma^{-8/3}, \quad (40)$$

and

$$\Gamma \propto R^{-3/2} \propto t_{\text{obs}}^{-3/8}, \quad R \propto t_{\text{obs}}^{1/4}. \quad (41)$$

More generally, one can consider a power-law stratified density profile

$$n = n_0 \left( \frac{R}{R_0} \right)^{-k}, \quad (42)$$

with  $k < 3$ . The energy conservation equation can be written as

$$E = \int n_0 \left( \frac{R}{R_0} \right)^{-k} m_p c^2 \Gamma^2 4\pi R^2 dR = \text{const}, \quad (43)$$

or  $R^{3-k} \Gamma^2 = \text{constant}$ . Carrying out the same exercise as above, one finds the observer frame time

$$t_{\text{obs}} \sim \frac{R}{2\Gamma^2 c} \propto R \Gamma^{-2} \propto \begin{cases} \Gamma^{\frac{2}{k-3}} \cdot \Gamma^{-2} \propto \Gamma^{\frac{8-2k}{k-3}} \\ R \cdot R^{3-k} \propto R^{4-k} \end{cases} \quad (44)$$

so that

$$\Gamma \propto R^{\frac{k-3}{2}} \propto t_{\text{obs}}^{\frac{k-3}{8-2k}}, \quad R \propto t_{\text{obs}}^{\frac{1}{4-k}}. \quad (45)$$

This reduces to (41) for  $k = 0$  (constant density). For a free wind with constant mass loss rate  $\dot{M}$  and wind speed  $v_w$ , one has  $\dot{M} = 4\pi R^2 n v_w = \text{constant}$ , or  $n \propto R^{-2}$  (or  $k = 2$ ). Plugging in  $k = 2$ , one gets the scaling for a wind medium [41,136,42,43]

$$\Gamma \propto R^{-1/2} \propto t_{\text{obs}}^{-1/4}, \quad R \propto t_{\text{obs}}^{1/2}. \quad (46)$$

It is possible that the blastwave energy continuously increases with time. This is the case for instance when a fireball is fed by a long lasting, Poynting-flux dominated, jet (so that the reverse shock, discussed in Section 3.3, does not exist or is very weak). Then, the dynamics of the blast wave is determined by taking into account the additional energy added to it by the outflow from the central engine [134,137]. This is particularly relevant when the central engine is a millisecond magnetar [138,109,139,140].

Consider a central engine with time dependent luminosity

$$L(t) = L_0 \left( \frac{t_{\text{obs}}}{t_0} \right)^{-q}. \quad (47)$$

For  $q \geq 1$  the injected energy does not grow appreciably with time, and the blastwave behavior is essentially same as the constant energy case. So in the following discussion we will consider the case of  $q < 1$ .

The total energy in the blastwave

$$E_{\text{tot}} = E_0 + E_{\text{inj}} = E_0 + \int_0^{t_{\text{obs}}} L(t) dt = E_0 + \frac{L_0 t_0^q}{1-q} \cdot t_{\text{obs}}^{1-q}, \quad (48)$$

where  $E_0$  is the initial energy in the blastwave, and  $E_{\text{inj}}$  is the injected energy into the blastwave from the long-lasting central engine.

The blastwave scaling becomes different when  $E_{\text{inj}} \gg E_0$  for  $q < 1$ . In this case, the total energy

$$E_{\text{tot}} \sim E_{\text{inj}} \propto t_{\text{obs}}^{1-q}. \quad (49)$$

For the constant density CBM case, one has

$$\Gamma^2 R^3 \propto t_{\text{obs}}^{1-q}. \quad (50)$$

Again taking  $t_{\text{obs}} \propto R/\Gamma^2$ , one can rewrite the above equation as

$$\Gamma^2 R^3 \propto R^{1-q} \Gamma^{2(q-1)}. \quad (51)$$

Regrouping the parameters, one finally has

$$\Gamma \propto R^{-\frac{2+q}{4-2q}} \propto t_{obs}^{-\frac{2+q}{8}}, \quad R \propto t_{obs}^{\frac{2-q}{4}}. \quad (52)$$

The limiting case of  $q \rightarrow 1$  reduces to the constant energy blastwave dynamics.

For the CBM with density falling off as  $R^{-2}$  (wind like medium), one has

$$\Gamma^2 R \propto t_{obs}^{1-q} \propto R^{1-q} \Gamma^{2q-2}. \quad (53)$$

This leads to the following time dependence for blastwave LF and radius

$$\Gamma \propto R^{\frac{q}{2q-4}} \propto t_{obs}^{-\frac{q}{4}}, \quad R \propto t_{obs}^{\frac{2-q}{2}}. \quad (54)$$

Again this is reduced to the constant energy wind medium when  $\rightarrow 1$ .

An alternative energy injection, or refreshed shock, mechanism is to consider a Lorentz factor stratification of the ejecta [141], e.g.

$$M(> \gamma) \propto \gamma^{-s}. \quad (55)$$

Mass (and therefore energy) is added to the blastwave when the blastwave progressively decelerates, so that

$$E \propto \gamma^{1-s} \propto \Gamma^{1-s}, \quad (56)$$

where  $\gamma$  is the Lorentz factor of the ejecta, and  $\Gamma$  is the Lorentz factor of the blastwave. Since energy is injected when  $\Gamma \sim \gamma$ , the reverse shock is very weak, one can again neglect the reverse shock contribution.

The two energy injection mechanisms can be considered equivalent, as far as the blast wave dynamics is considered, and one model can be related to the other by expressing the injection parameter  $s$  in terms of  $q$  [82]. For the constant density CBM one has

$$\Gamma \propto R^{-3/(1+s)} \propto t_{obs}^{-3/(7+s)}, \quad R \propto t_{obs}^{(1+s)/(7+s)}. \quad (57)$$

Therefore, the relation between  $s$  and  $q$  is obtained by comparing Eqs. (52) and (57), and requiring the dynamics for the two forms of energy injections to be the same:

$$s = \frac{10 - 7q}{2 + q}, \quad q = \frac{10 - 2s}{7 + s}. \quad (58)$$

For the wind like CBM one has

$$\Gamma \propto R^{-1/(1+s)} \propto t_{obs}^{-1/(3+s)}, \quad R \propto t_{obs}^{(1+s)/(3+s)}, \quad (59)$$

so that the equivalency relation between  $s$  &  $q$  for a wind-like CBM is

$$s = \frac{4 - 3q}{q}, \quad q = \frac{4}{3 + s}. \quad (60)$$

### 3.2. Afterglow synchrotron spectrum and lightcurve

An instantaneous afterglow spectrum can be characterized by a multi-segment broken power law [131], separated by three characteristic frequencies: the typical synchrotron frequency of the accelerated electrons with the minimum Lorentz factor  $\nu_m$ , the cooling frequency  $\nu_c$ , and the synchrotron self-absorption frequency  $\nu_a$ . In the afterglow phase,  $\nu_a$  is usually the smallest of these three frequencies at least for a few months after the explosion for a typical CBM density, and the spectrum falls into two broad categories depending on the ordering of  $\nu_m$  and  $\nu_c$ . The spectrum when  $\nu_m < \nu_c$ , classified as “slow cooling” case, is (see Section 2.2, Fig. 4, [131])

$$f_\nu = \begin{cases} f_{\nu,max} \left( \frac{\nu_a}{\nu_m} \right)^{1/3} \left( \frac{\nu}{\nu_a} \right)^2, & \nu < \nu_a \\ f_{\nu,max} \left( \frac{\nu}{\nu_m} \right)^{1/3}, & \nu_a < \nu < \nu_m \\ f_{\nu,max} \left( \frac{\nu}{\nu_m} \right)^{-(p-1)/2}, & \nu_m < \nu < \nu_c \\ f_{\nu,max} \left( \frac{\nu_c}{\nu_m} \right)^{-(p-1)/2} \left( \frac{\nu}{\nu_c} \right)^{-p/2}, & \nu > \nu_c \end{cases} \quad (61)$$

and for  $\nu_c < \nu_m$ , or “fast cooling” regime, the emergent spectrum is

$$f_\nu = \begin{cases} f_{\nu,\max} \left( \frac{\nu_a}{\nu_c} \right)^{1/3} \left( \frac{\nu}{\nu_a} \right)^2, & \nu < \nu_a \\ f_{\nu,\max} \left( \frac{\nu}{\nu_c} \right)^{1/3}, & \nu_a < \nu < \nu_c \\ f_{\nu,\max} \left( \frac{\nu}{\nu_c} \right)^{-1/2}, & \nu_c < \nu < \nu_m \\ f_{\nu,\max} \left( \frac{\nu_m}{\nu_c} \right)^{-1/2} \left( \frac{\nu}{\nu_m} \right)^{-p/2}. & \nu > \nu_m. \end{cases} \quad (62)$$

Here  $f_{\nu,\max}$  is the maximum flux density, which is  $f_\nu(\nu_m)$  for slow cooling and  $f_\nu(\nu_c)$  for fast cooling. These spectral functions are independent of blast-wave dynamics, although the ordering of  $\nu_m$ ,  $\nu_c$  and  $\nu_a$  and how they evolve with time are determined by the dynamics, CBM properties, and micro-physics parameters of shocked plasma.

The characteristic frequencies  $\nu_m$ ,  $\nu_c$  can be calculated from the synchrotron frequency formula (Section 2.2, Eq. (18))

$$\nu = \frac{3}{4\pi} \gamma^2 \frac{qB'}{m_e c} \quad (63)$$

by replacing  $\gamma$  with  $\gamma_m$  and  $\gamma_c$ , where  $\gamma_m$  is the minimum Lorentz factor of electrons in the shock heated plasma<sup>8</sup> which is given by

$$\gamma_m = g(p) \epsilon_e (\Gamma - 1) \frac{m_p n_p}{m_e n_e}, \quad (64)$$

$\Gamma$  is the Lorentz factor of the blast wave,  $\epsilon_e$  is the fraction of energy density of shocked fluid given to electrons,  $n_p$  &  $n_e$  are the number densities of protons and electrons, respectively, and the dimensionless factor  $g(p)$  when the maximum LF of electrons accelerated in the shock is  $\gamma_M$  is given by

$$g(p) \simeq \begin{cases} \frac{p-2}{p-1}, & p > 2 \\ \ln^{-1}(\gamma_M/\gamma_m), & p = 2. \end{cases} \quad (65)$$

The above expression for  $g$  follows from the requirement that the total electron energy – obtained by integrating the distribution function,  $dn/d\gamma \propto \gamma^{-p}$ , for  $\gamma > \gamma_m$  – is  $\epsilon_e$  times the energy density on the shocked fluid, i.e.  $\epsilon_e 4\Gamma(\Gamma-1)n_p m_p c^2$ . The Lorentz factor of electrons that cool on a dynamical time ( $t'$ ) is (see Section 2.2 for details)

$$\gamma_c = \frac{6\pi m_e c}{\sigma_t t' B'^2 (1+Y)}, \quad (66)$$

where  $Y = u_{\text{syn}}/u_B$  is the synchrotron self-Compton parameter,<sup>9</sup> which is the ratio of the synchrotron photon energy density  $u_{\text{syn}}$  and the magnetic energy density  $u_B = B^2/8\pi$ .

The self-absorption frequency  $\nu_a$  can be calculated by equating the emergent flux at  $\nu_a$  to the blackbody flux corresponding to the temperature of electrons with synchrotron characteristic frequency  $\nu_a$  (see Section 2.2 for details)

$$I_\nu^{\text{syn}}(\nu_a) = I_\nu^{\text{bb}}(\nu_a) \simeq 2k_B T \cdot \frac{\nu_a^2}{c^2}, \quad (67)$$

where

$$k_B T \simeq \max[\gamma_a, \min(\gamma_c, \gamma_m)] m_e c^2 / 3, \quad (68)$$

and  $\gamma_a$  is the Lorentz factor corresponding to  $\nu_a'$ , i.e.  $\gamma_a = (4\pi m_e c \nu_a'/3qB')^{1/2}$ . The comoving magnetic field strength is obtained by taking the energy density in magnetic field to be  $\epsilon_B$  times the energy density of shocked CBM:

$$B' \approx [32\pi m_p c^2 \epsilon_B n_p (\Gamma - 1) \Gamma]^{1/2}. \quad (69)$$

The time-dependence of spectral break frequencies  $\nu_m$ ,  $\nu_c$ , and  $\nu_a$  can be calculated from the shock dynamics, or in particular from the evolution of shock Lorentz factor  $\Gamma$ . For instance, for a constant density CBM,  $\Gamma \propto t_{\text{obs}}^{-3/8}$  (Eq. (41)), and

<sup>8</sup> The electron distribution function,  $dn/d\gamma$ , peaks at  $\gamma_m$ . For  $\gamma > \gamma_m$ ,  $dn/d\gamma \propto \gamma^{-p}$ , and for  $\gamma < \gamma_m$  the distribution function is uncertain but could be thermal.

<sup>9</sup> The expression for Compton Y parameter is different when photon-electron scatterings are in Klein-Nishina limit, i.e. when the energy of a typical photon in the rest frame of the electron is larger than  $m_e c^2$ .

therefore  $B' \propto \Gamma \propto t_{obs}^{-3/8}$ ,  $\gamma_m \propto \Gamma \propto t_{obs}^{-3/8}$ , and so  $v_m \propto B' \gamma_m^2 \Gamma \propto \Gamma^4 \propto t_{obs}^{-3/2}$ ; it is easy to show that  $v_m \propto t_{obs}^{-3/2}$  even when the CBM density is not constant but varies as a power-law function of distance. Similarly it can be shown that  $v_c \propto t_{obs}^{-1/2}$  and  $v_a$  is time independent for a constant density medium. The full expression for  $v_m$ ,  $v_c$  and  $v_a$  for a constant density medium is (e.g. [142, 143])

$$v_m = 3.3 \times 10^{14} \text{ Hz} (1+z)^{1/2} \epsilon_{B,-2}^{1/2} [\epsilon_e g(p)]^2 E_{52}^{1/2} t_{obs,d}^{-3/2}, \quad (70)$$

$$v_c = 6.3 \times 10^{15} \text{ Hz} (1+z)^{-1/2} \epsilon_{B,-2}^{-3/2} E_{52}^{-1/2} n_p^{-1} t_{obs,d}^{-1/2}, \quad (71)$$

$$v_a = 4.2 \times 10^8 \text{ Hz} (1+z)^{-1} \left[ \frac{(p+2)(p-1)}{(3p+2)} \right]^{0.6} [\epsilon_e g(p)]^{-1} \epsilon_{B,-2}^{1/5} E_{52}^{1/5} n_p^{3/5}, \quad (72)$$

whereas for a wind like CBM

$$v_m = 4.0 \times 10^{14} \text{ Hz} (p - 0.69)(1+z)^{1/2} \epsilon_{B,-2}^{1/2} [\epsilon_e g(p)]^2 E_{52}^{1/2} t_{obs,d}^{-3/2}; \quad (73)$$

$$v_c = 4.4 \times 10^{13} \text{ Hz} (3.45 - p) \exp(0.45p)(1+z)^{-3/2} \epsilon_{B,-2}^{-3/2} E_{52}^{1/2} A_*^{-2} t_{obs,d}^{1/2}; \quad (74)$$

$$v_a = 3.3 \times 10^9 \text{ Hz} (1+z)^{-2/5} \left( \frac{p-1}{3p+2} \right)^{3/5} [\epsilon_e g(p)]^{-1} \epsilon_{B,-2}^{1/5} E_{52}^{-2/5} A_*^{6/5} t_{obs,d}^{-3/5}; \quad (75)$$

where  $t_{obs,d}$  is time in observer frame in units of 1 day, and  $A_*$  is density parameter for a wind like CBM defined as  $n(R) = A_*(3 \times 10^{35})R^{-2} \text{ cm}^{-3}$  with the unit for R in cm;  $A_* = 1$  corresponds to mass loss rate in the wind of GRB progenitor star of  $10^{-5} M_\odot \text{ yr}^{-1}$  at wind speed of  $10^8 \text{ cm/s}$ .

The specific flux at the peak of the spectrum can be written as (see Section 2.2)

$$f_{v,max} = \frac{(1+z)L'_{\nu'} \Gamma}{4\pi D_L^2} \approx (1+z) \frac{N_{\text{tot}} P'_{\nu',max} \Gamma}{4\pi D_L^2}, \quad (76)$$

where  $L'_{\nu'}$  is specific luminosity in jet comoving frame,  $N_{\text{tot}}$  is the total number of electrons that contribute to radiation at frequency  $\nu$ ,

$$P'_{\nu',max} \approx \frac{\sqrt{3}q^3 B'}{m_e c^2}, \quad (77)$$

is the power radiated per unit frequency for one electron at the peak of the spectrum i.e. specific power for an electron with thermal LF  $\gamma \approx \min(\gamma_c, \gamma_m)$ ,  $z$  is the redshift of the burst, and

$$D_L = (1+z) \frac{c}{H_0} \int_0^z \frac{dz'}{\sqrt{\Omega_m(1+z')^3 + \Omega_\Lambda}} \quad (78)$$

is the luminosity distance of the burst,  $H_0$  is the Hubble's constant,  $\Omega_m$  and  $\Omega_\Lambda$  are density parameters for matter and dark energy, respectively.

We see from Eq. (76) that the peak specific flux,  $F_{v,max} \propto N_{\text{tot}} B' \Gamma \propto R^3 \Gamma^2$ , is time independent for a constant density medium – since  $R^3 \Gamma^2$  is the total energy in the blast wave which is constant for an adiabatic external shock. For a wind-like stratified medium  $F_{v,max} \propto R \Gamma B' \propto \Gamma^2 \propto t_{obs}^{-1/2}$ . The full expression for the peak specific flux for these two types of CBM media are (e.g. [142, 144])

$$f_{v,max} = 1.6 \text{ mJy} (1+z) \epsilon_{B,-2}^{1/2} E_{52} n_p^{1/2} D_{L,28}^{-2}, \quad n_p \propto R^0 \quad (79)$$

$$f_{v,max} = 7.7 \text{ mJy} (p + 0.12)(1+z)^{3/2} \epsilon_{B,-2}^{1/2} E_{52} A_* D_{L,28}^{-2} t_{obs,d}^{-1/2}, \quad n_p \propto R^{-2}. \quad (80)$$

Making use of these expressions for peak flux,  $v_m$ , and  $v_c$ , it can be shown that the observed specific flux for  $\nu > \max(v_m, v_c)$  is [145, 146]

$$f_\nu \propto E^{(p+2)/4} \epsilon_e^{p-1} \epsilon_B^{(p-2)/4} t_{obs}^{-(3p-2)/4} \nu^{-p/2}, \quad (81)$$

which is completely independent of CBM density and its stratification, and very weakly dependent on  $\epsilon_B$ , which are the two most uncertain parameters in afterglow modeling. This result turns out to be very useful for interpreting high energy GRB data ( $\nu \gtrsim 10^2 \text{ MeV}$ ) obtained by the Fermi/LAT as described in Section 4.3.

The synchrotron radiation mechanism in external shock provides a good description of late time ( $t \gtrsim 10 \text{ h}$ ) GRB afterglow radiation from radio to X-ray frequencies (see Fig. 7), as well as GeV emission of some GRBs at early times (see Section 4.3).

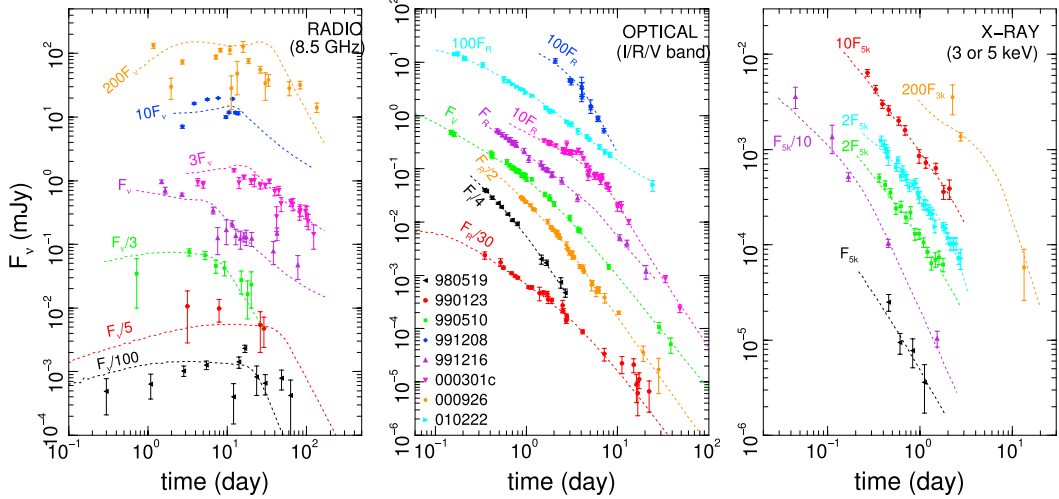


**Fig. 7.** Radio, optical, and X-ray model light-curves for eight GRB afterglows (legend of middle graph applies to all panels). The model light-curves were obtained by  $\chi^2$ -minimization using radio, millimeter, sub-millimeter, near infrared, optical, and X-ray data. The radio fluctuations are due to scatterings by inhomogeneities in the Galactic interstellar medium [48]. Fluxes have been multiplied by the indicated factors, for clarity.  
Source: Figure from [27].

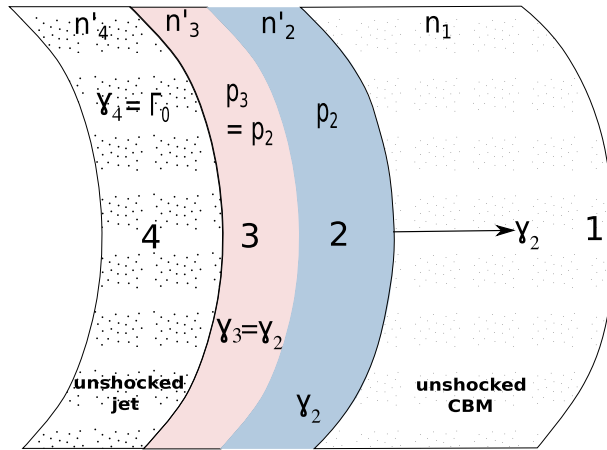


**Fig. 8.** This is a schematic sketch of a pair of shocks produced when a relativistic jet from a GRB collides with the circum-burst medium (CBM), as viewed from the rest frame of unshocked CBM. Regions 2 & 3 represent shocked CBM and GRB jet respectively. They move together with the same Lorentz factor ( $\gamma_2$ , as viewed by a stationary observer in the unshocked CBM), and have the same pressure but different densities.

### 3.3. Reverse shock

During the early afterglow phase, a strong reverse shock (RS) propagates across the GRB-ejecta to decelerate it if the magnetic field in the ejecta is dynamically unimportant, i.e. the magnetization parameter  $\sigma \equiv B'^2/(4\pi n'_p m_p c^2) \ll 1$ . The RS dynamics is more complicated than the self-similar solution for forward shock (FS) propagating into CBM. The RS-FS system can be separated in four regions (see Fig. 8): 1. the unshocked medium; 2. shocked medium; 3. shocked ejecta; 4. unshocked ejecta. These regions are separated by the forward shock front (FS, between 1 & 2), a surface of contact density-discontinuity (between 2 & 3), and the reverse shock front (RS, between 3 & 4). Radiation from RS-heated GRB ejecta was predicted [147,36,148] prior to its discovery in 1999 when a very bright optical flash was observed from GRB 990123 while  $\gamma$ -ray burst was still active [149–151].

A quick derivation of FS-RS system properties, for an unmagnetized GRB-jet, follows from the requirement of pressure equilibrium across the contact discontinuity surface (which separates regions 2 & 3). Let us take the Lorentz factors of the RS-heated GRB-jet with respect to unshocked jet to be  $\gamma_{34}$ , and the shocked CBM with respect to unshocked CBM to be  $\gamma_{21}$ . We know from previous discussions regarding relativistic shocks that the pressures of the shocked fluid in regions 2 & 3 are  $4\gamma_{21}^2 n_1$  &  $4\gamma_{34}^2 n'_4$ , respectively; density in region  $i$ , in the local comoving frame, is  $n'_i$ . The Lorentz factor of the unshocked jet (region 4) with respect to the unshocked CBM is the jet Lorentz factor  $\Gamma_0$  which is equal to  $2\gamma_{21}\gamma_{34}$  (this follows from the addition of 4-velocities). Combining this relation with pressure equilibrium across the contact discontinuity surface we

find:

$$\gamma_{34} \approx (n_1/4n'_4)^{1/4} \Gamma_0^{1/2}, \quad \text{and} \quad \gamma_{21} \approx (n'_4/4n_1)^{1/4} \Gamma_0^{1/2}. \quad (82)$$

These equations are only valid when both RS and FS are relativistic (similar relations are easy to obtain for a non-relativistic RS). We note that the Lorentz factor of the shocked jet with respect to CBM ( $\gamma_3$ ) is equal to  $\gamma_{21}$  since both shocked regions move together at the same speed. With RS/FS Lorentz factors in hand it is straightforward to determine various thermodynamical variables of the shocked plasma in regions 2 & 3. A more detailed derivation of these results can be found in [152].

The calculation of radiation from RS is similar to the FS emission described in Section 3.2. For the simplest model, one assumes a finite radial extent of the GRB-jet (related to the finite duration of the GRB) and a roughly constant Lorentz factor of the ejecta.<sup>10</sup> In this case the RS lightcurve declines rapidly ( $\sim t^{-2}$ ) due to adiabatic cooling of electrons, and a decrease of the magnetic field strength, after the RS reaches the back end of the jet [148]. A useful classification for RS is based on the dimensionless width of the ejecta defined below [152]

$$\xi \equiv (l/\Delta)^{1/2} \Gamma_0^{-4/3}, \quad (83)$$

where  $l$  is the Sedov radius (the radius at which the rest mass energy of the swept up CBM by the blastwave is equal to the initial energy of the GRB),  $\Delta = cT$  is the thickness of the GRB-ejecta in lab frame ( $T$  is the burst duration in CoE frame), and  $\Gamma_0$  is the initial Lorentz factor. The GRB-ejecta is considered a “thin shell” or a “thick shell” depending on whether  $\xi > 1$  or  $\xi < 1$ , respectively. The FS/RS dynamics for the two regimes are different, and so are the resulting lightcurves. A detailed study of the RS dynamics and emission signature can be found in [158]. A joint study of RS/FR emission signatures can be found in [159–163,143].

The shock solution for a jet with arbitrary magnetization  $\sigma$ , in the context of GRBs, can be found in e.g. [164–166]; [167] discuss the case of  $\sigma < 1$ . The shock solution of a continuous, relativistic magnetized jet is described in seminal papers of [168,169] in context of pulsar wind.

The relative importance of the RS and FS emissions depends on the ratio of microphysics parameters in these two shock regions, and on the Lorentz factors of reverse-shock & forward-shock fronts [159,160,170]. Radiation from the reverse-shock offers one of the few ways to determine the GRB jet composition, e.g. [171,170]. However, this requires separating FS and RS contributions to the afterglow data. A few different cases of RS/FS signatures are described below [160,172].

Type I: re-brightening. For standard microphysics parameters, i.e.  $\epsilon_e = 0.1$  and  $\epsilon_B = 0.01$ , for both FS and RS, the optical lightcurve usually shows a re-brightening signature. The first peak is dominated by the RS emission, while the second peak corresponds to the decline of  $\nu_m$  in the FS below the optical band. Such a pattern has been observed in some bursts (e.g. [159,173]), however, the color change at the second peak – associated with the passing of  $\nu_m$  through the optical band – has not been confirmed so far.

Type II: flattening. If the magnetization parameter for the unshocked GRB ejecta is not so large as to suppress the RS, and RS has larger magnetic field than the FS, then the emission from RS would dominate as was the case for GRB 990123. The early optical flare is RS dominated, and the flare peaks at the time when the reverse shock completes its passage through the GRB ejecta. The decay of the RS flux in a fixed observer frequency band after the peak is  $\sim t^{-2}$  [151,148]. This fast decline transitions to a more normal  $t^{-1}$  decay when emission from the FS takes over. There are quite a few cases of optical afterglows that show this behavior [174,175,160,161,176].

Type III: no RS component. In the Swift era, many early optical afterglow lightcurves have been obtained. To one’s surprise, many of these lightcurves show a smooth hump with the post-decay slope consistent with the FS emission, without the signature of a RS [177–179]. This can be due to a Poynting flux dominated GRB-jet that suppresses RS [164,165], or a very low  $\nu_m$  in the RS [172].

### 3.4. Jet break

Evidence suggests that GRB outflows are collimated as anticipated by Rhoads [180]. This is inferred from an achromatic break seen in many afterglow lightcurves which are known as “jet breaks”. The steepening of the lightcurve following the “jet break” is due to two effects (e.g. [24,25]).

The first is the so-called “edge” effect (e.g. [151,181,24,25]). For a jet moving relativistically with Lorentz factor  $\Gamma$ , photons emitted at any point on the jet are beamed, as seen in the lab frame, within a  $1/\Gamma$  cone. Thus, for a conical jet with opening angle  $\theta_j$ , initially when  $\Gamma > 1/\theta_j$ , an observer only sees radiation from a small fraction of the jet. He then has no knowledge about the finite collimation angle for the jet, and the jet dynamics resembles that of an isotropic fireball; the lightcurve during this phase is the “pre-jet-break” lightcurve. As the jet decelerates, the  $1/\Gamma$  cone increases, and the photon beaming angle becomes comparable to the opening angle of the jet-cone. Lightcurves display a “jet break” when this condition is satisfied. When  $\Gamma < 1/\theta_j$ , the observer becomes aware of a deficit of flux with respect to an isotropic fireball case, and the

<sup>10</sup> It is possible that the ejecta has a Lorentz factor stratification. If so, the RS is long-lived, and may give rise to interesting features in the RS lightcurve [141,153–157].

lightcurve starts to fall off more steeply than the pre-break, isotropic, phase. The edge effect involves no change to blastwave dynamics. It is a geometrical, plus special relativistic, effect, and its effect on the observed specific flux is to introduce an additional factor of  $\theta_j^2/(1/\Gamma)^2 \propto \Gamma^2$  to account for the deficit in the solid angle from which radiation is received compared with a spherical outflow. For a uniform density CSM case, one has  $\Gamma \propto t^{-3/8}$ , and therefore the post-jet-break lightcurve, for all different orderings of synchrotron characteristic frequencies, falls off faster than the isotropic case by a factor  $\Gamma^2 \propto t^{-3/4}$ ; the temporal behavior of synchrotron characteristic frequencies are unaffected by the edge effect.

For the case of a CBM with density stratification like that of a wind,  $\Gamma \propto t^{-1/4}$ , and post-jet-break lightcurve fall-off is steeper than the isotropic case by a factor  $t^{-1/2}$ . It is found that the jet break in the wind medium is very smooth, covering more than 2 orders of magnitude in time, when smearing due to integration over equal-arrival-time surface is taken into account [182–184]. However, numerical simulations of jet propagation find that lightcurves make a transition to a steeper fall-off, due to jet-break, on a shorter time scale of perhaps an order of magnitude (e.g. [185]).

The second effect of a finite jet angle on the lightcurve arises due to its sideways expansion. Rhoads [24] and Sari et al. [25] showed that the epoch when the edge effect kicks in is also the time when sound waves cross the jet in the transverse direction leading to its sideways expansion. The jet opening angle increases as  $\theta_j \sim \Gamma^{-1}$  when the sideways expansion speed in jet rest-frame is of order the sound speed which for a relativistic plasma is  $c/3^{1/2}$ ;  $\theta_j \sim \Gamma^{-1}$  is a consequence of time dilation plus transverse speed  $\sim c$  – the time elapsed in jet comoving frame is a factor  $\Gamma$  smaller than the lab frame time, and therefore the transverse size of the jet, when it expands with speed  $\sim c$  in its own rest frame, is approximately  $R/\Gamma$ . The transverse speed of the jet, in the lab frame, in this case is  $v_\theta \sim c/\Gamma$ . However, according to the momentum equation for a relativistic plasma  $\partial(\rho\Gamma^2 v_\theta)/\partial t \sim r^{-1}\partial p/\partial\theta$ , one has  $v_\theta \sim c/(\Gamma^2\theta_j)$ ; for a detailed discussion of this result see e.g. [186,184]. The jet evolution for these two different transverse speeds –  $c/\Gamma$  and  $c/(\Gamma^2\theta_j)$  – are found to be not too different [184].

Combining the energy conservation equation for a constant density CBM –  $E \propto R^3\Gamma^2\theta_j^2$  – with  $\theta_j \sim \Gamma^{-1}$  after the jet-break, we find that the jet radius increase slows down substantially after the jet-break. Therefore,  $\Gamma \propto (R/t_{obs})^{1/2} \propto t_{obs}^{-1/2}$  after the jet break. A more precise analytic derivation of jet radius and LF evolution is discussed in e.g. [24,25,183,184], and is given by:

$$\Gamma \approx \exp(-R/l_{jet}), \quad \rightarrow \quad \Gamma \propto t_{obs}^{-1/2}, \quad (84)$$

where

$$l_{jet} \equiv \left[ \frac{E_{jet}}{(4\pi/3)n_p m_p c^2} \right]^{1/3}. \quad (85)$$

Therefore, one has

$$v_m \propto \Gamma^4 \propto t_{obs}^{-2}, \quad (86)$$

$$v_c \propto \Gamma^{-1} t_{obs}^{-2} B^{-3} \propto t_{obs}^0; \quad (87)$$

$$F_{v,max} \propto R^3 B' \Gamma \propto R^3 \Gamma^2 \propto t_{obs}^{-1}, \quad (88)$$

so that the post jet-break afterglow lightcurve, in slow cooling regime, is given by

$$f_v \propto \begin{cases} v^{1/3} t_{obs}^{-1/3}, & v_a < v < v_m, \\ v^{-(p-1)/2} t_{obs}^{-p}, & v_m < v < v_c, \\ v^{-p/2} t_{obs}^{-p}, & v > v_c. \end{cases} \quad (89)$$

The flux decay in a band that lies above  $\min(v_c, v_m)$ ,  $\propto t^{-p}$ , is steeper than when the edge effect alone is considered.

Numerical simulations suggest that sideways expansion of a relativistic jet is unimportant until  $\Gamma$  drops below  $\sim 2$  [187,186,188,189,185,184,190,191]. Nevertheless, numerical simulations also show that a post-jet-break lightcurve is similar to the simple analytical model we have described with sideways expansion [189]. The light curve behavior also depends on observers' viewing direction. Fitting late time X-ray data with numerical jet models suggests that the line of sight for most GRBs is misaligned from the jet axis [192,193].

The GRB jets are expected to be structured, i.e. the luminosity per unit solid angle and Lorentz factor vary with angle across the jet. Several papers have analyzed jet properties varying with angle as a power-law function [136,194,195], or has a Gaussian distribution [195,186,196]. For an on-axis observer to a structured jet, the afterglow decay slope is steeper than the top hat jet case described above [136,197,198]. For an off-axis observer, the viewing angle becomes important for the lightcurve. For a power law jet, the “jet break” time for an off-axis observer is determined by the viewing angle  $\theta_v$  rather than the jet opening angle  $\theta_j$  as was the case for a “top hat” jet model [195,194,186,199]. For a Gaussian jet, the lightcurve is similar to a top hat jet if the line of sight is inside the Gaussian cone, while it is similar to the off-axis power-law case if the line of sight is outside (but not too much larger than) the Gaussian cone [186,199]. Structured jets make it possible to understand the GRB phenomenology within the framework of a “quasi-universal” [194–196] jet, i.e. GRB jets are similar to

each other, and different observed properties are due to different viewing angles of the observer.<sup>11</sup> Such models have well defined luminosity function [195,194] and distribution of the observed jet break time [201]. Even though the “universal” jet model is challenged by the data [202], a “quasi-universal” jet, with more free parameters, is perhaps consistent with various observational constraints [203,196,204].

Another widely discussed jet structure is the two-component jet model. According to which the GRB outflow is composed of a narrow jet, usually with higher  $L_{\gamma,\text{iso}}$  and  $\Gamma$ , which is surrounded by a wider, usually with lower  $L_{\gamma,\text{iso}}$  and  $\Gamma$ , jet component. Depending on the viewing angle, such a two-component jet can account for a variety of lightcurve features, including an early jet break and late time re-brightening [205–207]. The model has been applied to interpret the afterglow data for several bursts, such as GRB 030329 [208] and GRB 080319B [209]. The collapsar model of long-duration GRBs offers a natural mechanism for generating a two-component jet: a narrow, highly relativistic, jet emerging from a star is accompanied by a wider, less relativistic “cocoon” surrounding the jet [210,211]. Alternatively, the narrow jet may be related to a magnetically confined proton component, while the wide jet is related to a neutron component that is not subject to magnetic confinement [206].

The GRB jets can even be “patchy”, i.e. the emission comes from many bright patches or “mini-jets” within a broad jet cone [212,213]. Mechanisms to produce patchy jets include non-uniform shells within the internal shock scenario [212], localized Lorentz boosted emission regions associated with relativistic outflows in magnetic reconnections, or turbulence in a magnetically-dominated jet [107,214–216,108,217].

An interesting effect associated with relativistic jets of finite opening angle is the so-called “orphan afterglows”, namely, detection of afterglow events without the detection of prompt  $\gamma$ -ray emission itself. An observer lying outside the jet cone might not see  $\gamma$ -rays due to the strong relativistic beaming of photons in the direction of the jet and away from the observer line of sight. However, this observer will see the afterglow lightcurve rise initially as the Doppler beaming factor gradually increases when the  $1/\Gamma$  cone widens, and the flux will peak when  $1/\Gamma$  cone enters the line of sight. Subsequently, the lightcurve behaves like a normal (post jet-break) afterglow lightcurve [218]. An orphan afterglow is also possible for a dirty fireball, for which the prompt GRB is not detected due to its low Lorentz factor, while the afterglow radiation is produced when the outflow is decelerated [219]. Many authors have discussed the detectability of orphan afterglows over the years (e.g. [220–223]). However, thus far no positive detection has been made.<sup>12</sup> This is likely due to the combined effect of the faint nature of orphan afterglows and the difficulty of identifying them.

### 3.5. Other effects

In this sub-section we describe a number of effects that could modify the “standard” afterglow behavior of GRBs – which is based on an adiabatic, relativistic, blastwave dynamics – we have discussed thus far. The effects of radiative losses on the blastwave dynamics, and afterglow lightcurves, have been discussed by a number of authors (e.g. [141,225,151,226–228]), and we refer to these works for details. In the following subsections we describe a few selected effects that can leave a signature on afterglow lightcurves.

#### 3.5.1. Naked afterglow and high-latitude effect

When a blast wave encounters a void the observed flux does not drop abruptly even though the adiabatic cooling of electrons does indeed lead to a very sharp decline of emissivity in the absence of electron acceleration. The reason is that photons from parts of the jet lying at an angle larger than  $\Gamma^{-1}$  with respect to the line of sight (high latitudes) continue to contribute to the observed flux for some period of time – due to the larger path length they have to travel to get to the observer – after the jet has run into a void or the emission is turned off suddenly for some other reason. A characteristic signature of this “high latitude” radiation is that the temporal decay index ( $\alpha$ ) is related to the spectral index ( $\beta$ ) –  $f_\nu \propto t^{-\alpha} \nu^{-\beta}$  – as follows:

$$\alpha = \beta + 2. \quad (90)$$

A simple derivation of this result can be found in Section 2.1, and for a more complete discussion we refer to [47,129,229]. The “high latitude” emission contributes to the observed flux as the  $\gamma$ -ray emission winds down, and it probably accounts for the steeply declining X-ray lightcurve observed by the Swift satellite immediately following the prompt  $\gamma$ -ray phase for some GRBs [82]. It also provides a good model for the decay phase of X-ray flares when the “zero time point” is taken to be close to the start-time of the flare [230].

#### 3.5.2. Energy injection

Energy can be added to a decelerating blastwave, not only in a smooth, continuous way (for details of a continuously fed fireball, please see more extended discussion in Section 3.1, Eqs. (47)–(60)), but also in discrete steps when fast shells

<sup>11</sup> This suggestion arose from the rough anti-correlation between  $E_{\gamma,\text{iso}}$  and  $\theta_j$  [26,200], so the original suggestion was that GRB jets are quasi-universal (e.g. [195]), rather than strictly universal.

<sup>12</sup> One possible exception was PTF11agg [224], which is an optical transient with power law decay but without a  $\gamma$ -ray trigger. However, Cenko et al. [224] argued that it is unlikely an orphan afterglow seen off-axis.

ejected at late times from the central engine runs into the hot blastwave. This interaction can be described in terms of five [231] or six [232] different regions separated by three shocks and one or two contact continuities, and displays rich afterglow behavior. Some abrupt optical rebrightenings detected during the afterglow phase (e.g. [233]) might be related to such interactions [232].

### 3.5.3. Density bumps

A blastwave may run into regions of enhanced density in the circum-stellar medium. These may lead to bump features in afterglow lightcurves [234–237]. However, numerical calculations [238,89,154,157,239] suggest that this re-brightening feature is expected to be very smooth and its amplitude very small in most situations. The main reason is that due to the relativistic equal-arrival-time surface effect, the emission received at any observer time comes from different latitudes and different emission times. This poses some intrinsic constraint on  $\Delta L/L$  with respect to  $\Delta t/t$  (e.g. [238,88]), making the bumps very smooth. Furthermore, if the observed band (e.g. X-rays) is above the cooling frequency, then the observed flux is independent of the ambient density [145,146]. If there is a long-lasting reverse shock, the reverse shock lightcurve is more sensitive to the medium density fluctuations than the forward shock lightcurve [157]. A significant afterglow feature due to density fluctuation is expected only when the long-lasting reverse shock emission outshines the forward shock emission.

### 3.5.4. Synchrotron self-Compton

The synchrotron self-Compton (SSC) mechanism has two effects on the afterglow radiation. First, it introduces an extra cooling to electrons, so that the synchrotron cooling frequency is reduced by a factor  $(1 + Y)^2$  (e.g. [240–242]); where  $Y = u_{\text{syn}}/u_B$  is the ratio of synchrotron photon energy density and magnetic field energy density. Second, the SSC introduces an extra spectral component at high energies which could dominate in the GeV band, and might show up in the X-ray band at late time if the ambient density is large [147,243,242,244]. IC cooling of electrons in the Klein–Nishina regime can somewhat flatten the index of synchrotron spectrum in the cooling regime (e.g. [245–248]), and steepen the decay slope of GeV afterglows [249].

The GeV afterglows of most GRBs can be explained as synchrotron radiation from the forward shock (e.g. [104,250]). However, the GeV afterglow of GRB 130427A cannot be interpreted as the synchrotron radiation only [251], and a possible SSC contribution to the GeV afterglow has been suggested (e.g. [252,253]).

### 3.5.5. Hard electron spectrum

For  $p$  between 1 and 2, the minimum electron Lorentz factor ( $\gamma_m$ ) depends on the maximum Lorentz factor of shock accelerated electrons ( $\gamma_M$ ) and is given by

$$\gamma_m = \left( \frac{2-p}{p-1} \frac{m_p}{m_e} \epsilon_e \Gamma \gamma_M^{p-2} \right)^{1/(p-1)}, \quad (91)$$

cf. [254–256]. In this case the afterglow decay slopes are systematically shallower than when  $p > 2$ , which can be confused with injection of energy to the decelerating blastwave especially when spectral information is missing.

### 3.5.6. Effect of neutron decay

The immediate vicinity of the GRB central engine is likely to have high temperature for dissociation of nuclei. A baryonic jet launched from such a site, therefore, is expected to contain free neutrons along with protons. Neutrons decouple from protons when the proton–neutron elastic collision optical depth drops below unity, after which neutrons stream freely [257–260]. Free neutrons undergo  $\beta$ -decay

$$n \rightarrow p^+ + e^- + \bar{\nu}_e, \quad (92)$$

with a mean co-moving life time of just under 15 min

$$\tau'_n = 881.5 \pm 1.5 \text{ s}. \quad (93)$$

The typical radius of neutron decay is

$$R_\beta = c \tau'_n \Gamma_n \simeq (8 \times 10^{15} \text{ cm})(\Gamma_n/300), \quad (94)$$

which is below the deceleration radius for a uniform density CBM. Since neutron decay happens continuously in time (and in distance), neutron decay are expected to affect both prompt and early afterglow lightcurves.

The impact of neutron decay on the early afterglow has been studied by Beloborodov [261] and Fan et al. [262], who found that it can lead to a re-brightening feature in the otherwise power-law decay lightcurve. The signature is different for the ISM and wind cases [262].

### 3.5.7. Radiation front effect

Gamma-ray photons released during the prompt emission phase move ahead of the GRB ejecta and interact with the ambient medium before the ejecta drives a shock wave into the medium. The CBM profile is modified due to this interaction, and as a result the early afterglow emission is different from the case of a shock wave moving into an undisturbed medium [263–267]. The main effect of this interaction between  $\gamma$ -ray photons and the CBM is to enrich the medium ahead of the GRB ejecta with electron–positron pairs which are produced as a result of  $\gamma$ -rays scattered by electrons in the medium which then collide with outward moving  $\gamma$ -rays associated with the prompt radiation to produce  $e^\pm$ ; the newly created pairs further scatter  $\gamma$ -ray photons thereby leading to another generation of  $e^\pm$ , and so on. Thus, the blast-wave propagates through a medium loaded with pairs which is also moving away from the CoE due to momentum deposited to the CBM by outward moving radiation front. These effects are particularly important when the CBM density is large.

### 3.5.8. Transition to Newtonian phase

A decelerating, relativistic, blastwave becomes Newtonian when it has swept up mass from the CBM that is of order the rest mass of the GRB-ejecta times the initial Lorentz factor, or  $E/c^2$ ;  $E$  is the energy of the blastwave. For a uniform density CBM the radius where the shock becomes sub-relativistic is  $R_N \sim [3E/(4\pi c^2 n_0 m_p)]^{1/3} = 1.2 \times 10^{18} \text{ cm}(E_{52}/n_0)^{1/3}$ . The blastwave dynamics in the Newtonian phase, for a uniform density CBM, is described by the well known Sedov–van Neumann–Taylor solution:

$$v \propto R^{-3/2} \propto t_{obs}^{-3/5} \quad \text{and} \quad R \propto t_{obs}^{2/5}. \quad (95)$$

Therefore,  $B' \propto t_{obs}^{-3/5}$ ,  $\gamma_m \propto v^2 \propto t_{obs}^{-6/5}$ ,  $v_m \propto B' \gamma_m^2 \propto t_{obs}^{-3}$ ,  $v_c \propto t_{obs}^{-1/5}$ , and  $F_{v,max} \propto t_{obs}^{3/5}$ , so that

$$f_v \propto \begin{cases} v^{-(p-1)/2} t_{obs}^{(21-15p)/10}, & v_m < v < v_c, \\ v^{-p/2} t_{obs}^{(4-3p)/2}, & v > v_c. \end{cases} \quad (96)$$

For  $p = 2.3$ , the lightcurve decay slopes are  $-1.35$  and  $-1.45$  for  $v_m < v < v_c$  and  $v > v_c$ , respectively. This decay is steeper than the isotropic relativistic case but shallower than the post-jet break phase. So the lightcurve would show a steepening behavior if relativistic-to-Newtonian transition happens before the jet break [268,226], while it would become less steep if the transition happens after the jet break [269]. A generic dynamics model that connects the relativistic phase to non-relativistic phase was developed by Huang et al. [226] and improved by Pe'er [270] and Nava et al. [228]. The shock wave evolution in the deep Newtonian regime has been studied by Huang and Cheng [271] in the context of GRBs.

Due to host galaxy contamination, observing the Newtonian phase in the optical band is very difficult. This can be better accomplished in the radio band for nearby GRBs. For example, late time radio follow-up observations of GRB 030329 revealed a brightening of the decaying lightcurve which is consistent with the transition to the Newtonian phase when emission from the receding counter-jet becomes visible [272,189].

A complete compilation of characteristic frequencies and light curves of the analytical synchrotron external shock models in all spectral regimes (for different ordering of  $v_m$ ,  $v_c$  and  $v_a$ ) and all temporal phases (including the forward shock and reverse shock emission during and after the reverse shock crossing phase, the pre- and post-jet break self-similar phase, and Newtonian phase) can be found in an extended review article by Gao et al. [143].

## 4. Afterglow observations and interpretations

Broadband GRB afterglows were predicted before their discoveries [34,273,36]. Shortly after the publication of the seminal paper by Mészáros and Rees [36] which provided detailed predictions for the broad-band afterglow based on the external shock model, the first X-ray and optical afterglows were discovered for GRB 970228 [17,19], and the first radio afterglow was discovered for GRB 970508 [20]. Since then, regular follow-up observations of GRBs have been carried out, and a large amount of broad-band afterglow data have been collected. Before the launch of the NASA's dedicated GRB mission Swift [274], afterglow observations usually started several hours after the burst trigger. Swift (launched in 2004) has closed this gap, and provides continuous afterglow data in X-ray, optical and UV bands starting at  $\sim 1$  min after the  $\gamma$ -ray trigger. This opened a new window to the study of GRBs. The launch of the high energy mission Fermi has led to the discovery of an extended GeV afterglow emission for many bright GRBs. We discuss all these topics in this section.

### 4.1. Late time afterglow observations and interpretations

Before launch of the Swift satellite, broad-band, late time ( $t \gtrsim 10$  h) afterglow data had been collected for a moderate sample of GRBs. These observations were generally consistent with predictions of the external forward shock, synchrotron emission, model. The main observational properties of late time afterglow radiation are:

- In general the optical afterglow displays a power law decay behavior  $F_v \propto t^{-\alpha}$ , with a decay index  $\alpha \sim 1$  (e.g. [275,276]). This is consistent with the prediction of the standard external shock afterglow model (e.g. [36,131,27,37,144]), see Fig. 7;

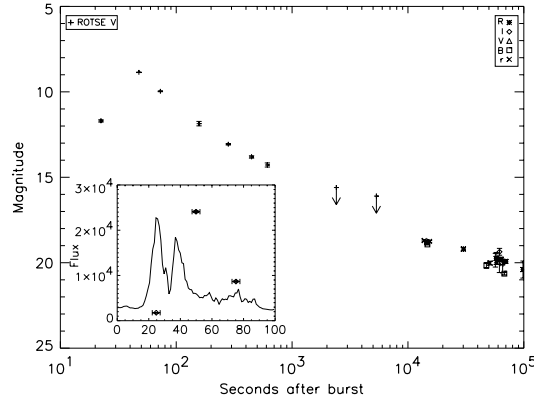


**Fig. 9.** The optical flash detected in GRB 990123 by ROTSE [149]. The peak flux was about 9th magnitude around 50 s after the trigger, which does not coincide with the  $\gamma$ -ray peaks.

- A temporal break in the optical afterglow light curve is usually detected for bright GRBs. The break time is typically around a day or so, which is followed by a steeper decay with slope  $\alpha \sim 2$  (e.g. [276]). This is consistent with the theoretical prediction of a “jet break” (e.g. [24,25]).
- The radio afterglow light curve initially rises and reaches a peak around 10 days, after which it starts to decline (e.g. [277]). The peak usually corresponds to passage of the synchrotron injection frequency  $\nu_m$ , or the synchrotron self-absorption frequency  $\nu_a$ , through the radio band.
- The broad-band afterglow spectrum can be fit with a broken power law, at a fixed observer time [278,276], as one expects for the synchrotron afterglow model.
- For bursts with high-quality data (e.g. GRB 021004 and GRB 030329), richer features in the optical light curves have been discovered, which include bumps and wiggles that deviate from the simple afterglow model predictions (e.g. [279,280]). Smooth bumps in afterglow lightcurves with duration  $\delta t_{obs} \sim t_{obs}$  may be interpreted as due to density bumps in the external medium [235,236,89] whereas sharper features in lightcurves might be due to energy injection from the central engine [281,231,232,282], angular fluctuations in energy per unit solid angle [212,283], or the existence of two-component jets [28,205,209].

Panaiteescu and Kumar [27,37] and Yost et al. [144] carried out detailed modeling of the broad-band afterglow data within the framework of the external shock model. They found that the late time afterglow data are in line with the predictions of this model (see Fig. 7), and they were able to derive the micro-physical shock parameters ( $\epsilon_e$ ,  $\epsilon_B$ ,  $p$ ) using the data which turned out to be different for different bursts; distribution of  $\epsilon_e$  and  $\epsilon_B$  are discussed in Section 5. Moreover, the afterglow data seem to favor a constant density medium (ISM) for most GRBs rather than the stratified density medium expected for a stellar wind. Another interesting result is that although the isotropic kinetic energy in the GRB blastwaves varies by more than 3 orders of magnitude the jet-corrected afterglow energy is clustered within about an order of magnitude. This, together with the same clustering of the jet-corrected  $\gamma$ -ray energy [26,200], point toward a roughly constant energy reservoir for GRBs that were detected before the *Swift* era.

#### 4.2. Early afterglow observations and interpretations

The Swift mission carries on board an X-ray telescope (XRT, [284]) and a UV-Optical Telescope (UVOT, [285]) besides the gamma-ray detector Burst Alert Telescope (BAT, [286]). The rapid slew of XRT and UVOT toward the GRB source allows detections of GRB early afterglows within less than 100 s after the  $\gamma$ -ray trigger. As a result, Swift has provided a rich trove of early afterglow data which revealed many, usually unexpected, interesting features. The early afterglow data and the ideas to interpret them are summarized below.

A bright optical flash was detected during the prompt emission of GRB 990123 which showed a distinct origin from the  $\gamma$ -ray emission. The flash was categorized by a sharp rise and a steep decay  $F_v \propto t^{-2}$  (Fig. 9) [149]. This is inconsistent with the external forward shock prediction, but is in accord with the theoretical expectation of emission from the reverse shock [36,151,150,148]. It was later realized that in order to produce a bright reverse shock optical flash such as GRB 990123 (and GRB 021211 and several others, [175,174,176]), the magnetic field in the reverse shock region should be stronger than in the external forward shock region [287,160,161], but not so strong that the magnetization parameter  $\gtrsim 0.1$  since in this case the magnetic fields would weaken the reverse shock and the emergent flux would be less than the observed value (e.g. [164–166]).

Radio flares, possibly associated with optical flashes, were also observed for some GRBs such as GRB 990123 and GRB 021004 [288]. These radio flares peak later (around 1 day), but can be interpreted as arising in the reverse shock (e.g. [150,159]).

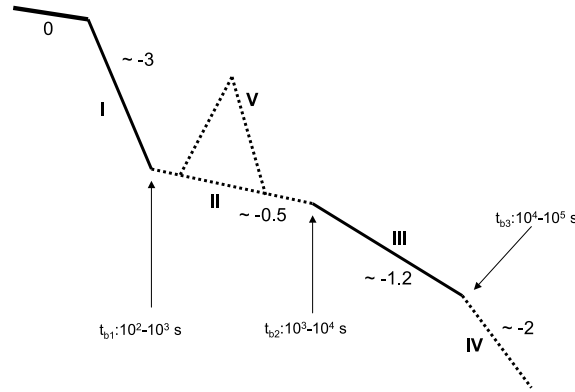


**Fig. 10.** The canonical X-ray afterglow light curve, which shows 5 distinct components: I. the steep decay phase which is the tail of prompt emission; II. the shallow decay phase (or plateau); III. the normal decay phase; IV. the late steepening phase; V. X-ray flares. The Numerical value provided for each segment of the lightcurve is the typical decay index for that segment, e.g. the lightcurve decays as  $t^{-3}$  during Phase I.

Source: From [82].

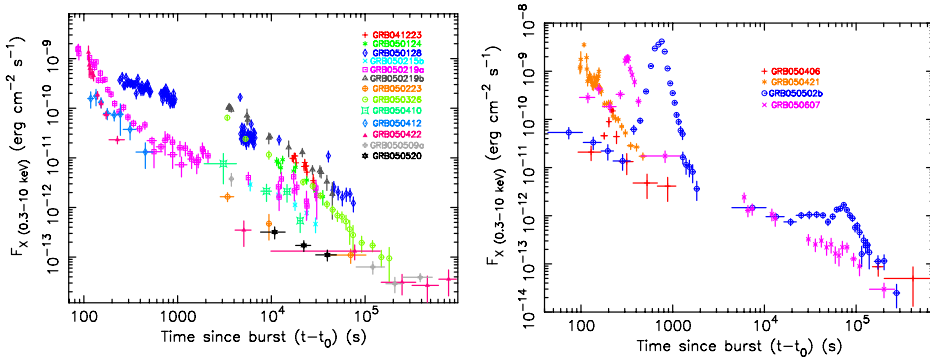


**Fig. 11.** Some examples of X-ray afterglow light curve detected by Swift XRT.  
Source: From [81].

Swift observations revealed several surprising emission components in early X-ray afterglow not predicted by the standard model. The data can be delineated as a canonical lightcurve, which generally includes 5 components ([82,81], see Figs. 10 and 11). Not all GRBs show all 5 components. The main properties of these 5 components, obtained for a large sample of Swift bursts [289,290], can be summarized as:

- I. An early time steep decay phase: it has a temporal decay index steeper than  $-2$ . When joint XRT/BAT observations were available, it is found that this phase is connected to the tail of the prompt emission [291]. This phase may be simply the high latitude emission (described in Section 2.1) associated with the prompt  $\gamma$ -ray source at  $R \gtrsim 10^{15}$  cm when the central engine turns off faster than the decline of the X-ray lightcurve [129,229,82,81,230]. On the other hand if the emission region is at a much smaller radius then the rapidly declining X-ray lightcurve reflects the time dependence of the central engine activity [92,292].
- II. Shallow decay phase (or plateau phase): the temporal decay of flux is shallow with slope  $-0.5$  or larger, sometimes flat or even slightly rising early on. In most GRBs, it is followed by a “normal” decay with flux decreasing with time as  $\sim t^{-1}$ . Such data can be incorporated within the external shock model, with the shallow decay phase being due to continuous energy injection into the blast wave [82,81,293]. Occasionally the plateau is followed by a very rapid drop (e.g. [294,96]), which demands an “internal” origin of the plateau.
- III. Normal decay phase: this is the typical decay ( $\sim t^{-1}$ ) expected in the standard forward shock model.
- IV. Late steep decay phase ( $\sim t^{-2}$  or steeper). Expected in the forward shock model as a jet break.
- V. X-ray flares<sup>13</sup>: one or more X-ray flares can be found in nearly half of GRB X-ray afterglows. These flares share many properties with prompt emission pulses. It is widely accepted that they are powered by late central engine activities [88,83,92,82,230,93,84,296,297].

An alternative way to describe the X-ray afterglow is a two-component phenomenological model [298–300]. According to this method, the X-ray afterglow can be decomposed into a “prompt” component (the prompt emission phase and

<sup>13</sup> One X-ray flare in each of the two GRBs 011211 and 011121 was detected by BeppoSAX [295], which was interpreted as onset of external shock afterglow.

the subsequent rapid decay phase), and an “afterglow” component (the plateau, normal decay and the late rapid decay). Although no theoretical model predicts the specific mathematical form of the two components, this phenomenological model seems to work well to fit the X-ray afterglow lightcurves of many Swift GRBs, and to identify X-ray flares or internal plateaus that demand central engine activities (e.g. [301]).

A puzzling feature seen in a fraction of GRBs is that the optical and X-ray afterglows are “chromatic” [95,302,54,30,303].<sup>14</sup> In some cases there is no temporal break in the optical lightcurve at the epoch when the X-ray lightcurve makes a transition from Segment II (plateau phase) to Segment III (normal decay phase) or from Segment III to IV (jet break phase). Within the external shock model, such a chromatic behavior is allowed if there is a significant spectral change across the temporal break due to, e.g. crossing of a spectral break in the X-ray band. The perplexing aspect of the phenomenon is that the X-ray spectral index almost never changes across the break. This suggests a hydrodynamical or geometrical origin for the break in the X-ray lightcurve, but in that case a simultaneous break must also be seen in the optical lightcurve. The non-detection of such a break in the optical band in some GRBs rules out the one-component forward shock model for the broadband afterglow emission observed from these bursts, and suggests at least two emission sites to account for the optical and X-ray emissions, respectively.

The unexpected, rich, X-ray lightcurve features detected by Swift and the puzzling chromatic behavior of afterglow stimulated a wave of intense modeling of early afterglow. We provide a brief summary of various different ideas proposed for explaining the prominent features in afterglow light-curves.

#### 4.2.1. Steep decay of early X-ray light-curve

The standard interpretation of the steep decay (I) phase is that it is the tail of prompt emission. The distinct separation between prompt emission and late afterglow settled down the pre-Swift debate regarding internal vs. external origin of prompt emission (e.g. [305,106]), and established the internal origin of prompt emission. It is not settled whether the X-ray flux during the steep decline is simply the high latitude emission associated with the rapid cessation of the prompt radiation [129,82] or emission from a somewhat less rapidly dying central engine [92,292]. It is quite common to find a strong spectral softening during the steep decay phase [306]. Such a spectral evolution is not expected in the simplest version of the high-latitude emission models but can be accounted for if the instantaneous spectrum at the end of prompt emission is characterized by a power law spectrum with an exponential cutoff [307]. Detailed analysis of a sample of GRBs suggests that the high-latitude “curvature effect” model can explain the steep decay phase of at least a sample of GRBs [307–310].

Other models of the steep decay phase include emission from a rapidly expanding cocoon [311],<sup>15</sup> rapid discharge of hadronic energy of the blastwave [312],<sup>16</sup> high-latitude emission in the external reverse shock [154,156],<sup>17</sup> and sweeping of the external forward shock synchrotron spectrum with a low maximum frequency across the X-ray band [313].<sup>18</sup> The latter three models have the underlying assumption that the prompt emission itself is also of an external shock origin, since observationally the steep decay phase is simply the tail of prompt emission, and hence are strongly disfavored by the rapid variability seen in  $\gamma$ -ray lightcurves.

#### 4.2.2. Sudden increase in X-ray flux (flares)

The X-ray flares are usually interpreted as due to re-start of GRB central engine because of their short rise time of  $\delta t_{obs}/t_{obs} \ll 1$  [83,82,92]. Such an interpretation is directly supported by data analysis. Liang et al. [230] assumed that the decay phase of X-ray flares is dominated by the high-latitude emission, and searched for the zero point of time ( $T_0$ ) to allow for the simple prediction  $\alpha = 2 + \beta$  [129] to be satisfied. They found that the required  $T_0$  usually corresponds to the beginning of X-ray flare. This is a good evidence for “re-starting the clock” when the central engine comes back to life. Further, more detailed, modeling [314,93,296] and data analysis [85,297,86] support this interpretation. Other ideas for the origin of X-ray flares include delayed magnetic dissipation activity as the ejecta decelerates [315] and anisotropic emission in the blast wave comoving frame [316]; however, these models do not account for the  $T_0$  effect found by Liang et al. [230].

#### 4.2.3. Plateaus in X-ray light-curves

The shallow decay (or plateau) phase (II) and the subsequent segments (III and IV) are more challenging to interpret. The plausible interpretation for the plateau phase is that it arises when energy is injected to the decelerating external shock thereby slowing down the decay of the lightcurve, and a transition to phase III occurs when energy injection is terminated [82,317,318,81,293]. This model predicts that the shape of lightcurves in the X-ray & optical bands should be similar where

<sup>14</sup> A recent detailed study suggests that about half of GRB afterglows are consistent with the achromatic hypothesis and the external shock model, while the others either do not comply with the external shock closure relations, or show clear “chromatic” behavior [304].

<sup>15</sup> This model predicts a quasi-thermal spectrum, which may interpret spectral softening during the X-ray tails. However, one needs to introduce coincidence to account for the smooth connection between the prompt emission and the X-ray tails as observed in many GRBs.

<sup>16</sup> This model requires both prompt and afterglow emissions to be produced in the external shock, which is highly unlikely as discussed in Section 7.

<sup>17</sup> This model requires significant suppression of forward shock emission to make the reverse shock feature to show up, and that is disfavored by the extensive afterglow data.

<sup>18</sup> This model also requires both prompt and afterglow radiation to arise in the external shock, which is inconsistent with GRB data.

breaks occur at the same time in these bands, i.e. an achromatic behavior across the EM spectrum. This model indeed works for all those bursts that display the expected achromatic behavior, e.g. GRB 060614 [319] and GRB 060729 [320]. However, this model cannot explain the data for chromatic afterglows, and another mechanism or emission component has to be invoked. The most straightforward extension of the external shock model is to introduce a two-component jet, with the narrow jet dominating the X-ray band emission while the wide jet dominating the optical emission (e.g. [209]). Some GRBs can be modeled this way at the price of introducing several additional parameters that vary significantly from burst to burst [321]. A further extension of the external shock model is to include emission from the reverse shock (RS). Uhm and Beloborodov [154] and Genet et al. [155] assumed that the external forward shock (FS) does not contribute much to the observed afterglow radiation, and that a long-lasting RS emission is responsible for the chromatic lightcurves observed in X-rays and optical bands. Indeed, the RS is more sensitive than the FS to the ejecta stratification and circumburst medium density inhomogeneity, and is capable of producing a wider variety of lightcurves [156,157]. One drawback of this proposal is a lack of good reason for suppressing the FS emission which is in fact expected to be brighter than the RS emission in the X-ray band (for the same microphysics parameters in FS & RS) by at least an order of magnitude, and has been very successful for interpreting the broad band afterglow data of many GRBs (e.g. [27,37,144]). A more reasonable possibility might be that the observed lightcurves are a superposition of the FS and RS emission, and that sometimes RS outshines FS emission in certain band. Evolving microphysics parameters of the external shock ( $\epsilon_e$  &  $\epsilon_B$ ) has also been suggested as a possible explanation for the chromatic X-ray plateau [322,73].

Shen and Matzner [323] interpreted the shallow decay phase as forward shock synchrotron radiation during the pre-deceleration, coasting phase in a wind medium. This model demands a relatively small Lorentz factor  $\Gamma$ , which might be at odds with the higher value for  $\Gamma$  obtained from the prompt emission data using the pair opacity argument. Moreover, this model predicts achromatic afterglows, and therefore can only explain a sub-sample of GRBs which have a shallow decay phase in both X-ray and optical bands at the same time. Shao and Dai [324] proposed that the X-ray plateau results from the contribution of prompt X-ray emission scattered by dust in the host galaxy. However, it predicts strong spectral evolution in X-rays which is not detected [325]. Ioka et al. [322] invoked a pre- $\gamma$ -ray-trigger outflow to modify the ambient medium profile in order to account for the shallow decay phase. Yamazaki [326] assumed a powerful outburst episode that preceded the GRB trigger, and suggested that the shallow decay phase is simply due to a mis-identification of the zero time point. This scenario predicts an optical flux, which is already ruled out by the prompt optical data [327]. In general, the scenarios of Ioka et al. [322] and Yamazaki [326] invoked a “prior explosion” episode, preceding the observed  $\gamma$ -ray burst by thousands of seconds, which no known central engine model can account for.

#### 4.2.4. Steep decay following the plateau in X-ray light-curve

Besides X-ray flares, there are a small fraction of GRBs which have plateaus in the X-ray lightcurve that are followed by a very steep decay that is more rapid than a  $f_v \propto t_{obs}^{-3}$  decline (e.g. GRB 070110 [294]), see Fig. 12. These cases of steep decline following a plateau are rare [96], and are not included in Fig. 10. They cannot be explained by the external shock model, and can only have an “internal” origin involving direct dissipation of a long-lasting jet. The existence of flares and these “internal plateaus” [83,84,328,294,301] suggest that the GRB central engine is long-lived. A more extreme opinion is that the entire X-ray emission is powered by a continuous jet from a long-lasting central engine, and that the X-ray flux from the external shock is buried beneath this emission [329]. Indeed, the canonical X-ray lightcurve can be matched with the accretion history in the collapsar GRB model [330–333] or with the spindown power of a magnetar central engine [334,335]. These models assume that the X-ray luminosity is proportional to the accretion power or the spindown power of the central engine. It is attractive to interpret GRB afterglows that display chromatic behavior as due to X-ray emission produced via some process internal to a continuous jet, and optical flux produced in the external shock. GRBs with achromatic lightcurves are cases where the standard forward shock emission dominates in both X-ray and optical bands.

Overall, the current data seem to suggest at least three emission sites: the erratic component (flares), the broken power-law X-ray component, and the broken power-law optical component (if chromatic). It is interesting to note that theoretically, one also naturally has three emission sites: the FS and RS of the blastwave, and an internal dissipation site within the relativistic outflow before it encounters the CBM. In a messy system that invokes late central engine activity, the RS is likely long-lived since late ejecta would continuously pile up onto the blastwave. The ejecta may also have a wide distribution of Lorentz factor, so that layers with different Lorentz factors may pile up onto the blastwave at different times. The internal dissipation site can be either the photosphere of the outflow, internal shocks, or magnetic dissipation site in a high  $\sigma$  (magnetization parameter) jet.

Unlike the late time afterglows ( $t_{obs} \gtrsim 7$  h) observed before the Swift mission, which had simple morphology, the afterglow modeling in the Swift era is much more complicated due to the complex behavior we see in the lightcurves for the first few hours following the  $\gamma$ -ray trigger. The first step is to disentangle various components, and decide which components likely have an external shock origin and which do not. The traditional modeling can be only applied to a sample of “well-behaved” afterglows that show clean achromatic behaviors. More detailed studies are needed to address following questions: What fraction of afterglows can be interpreted within the standard external shock model? Are the differences between the two categories (afterglows that are due to FS and those that are not) due to intrinsic differences in the central engine properties or these due to external factors such as variations in CBM from one burst to another? For those bursts that can be interpreted with the standard FS model, what are the shock microphysics parameters, and why do they vary from one burst to another?

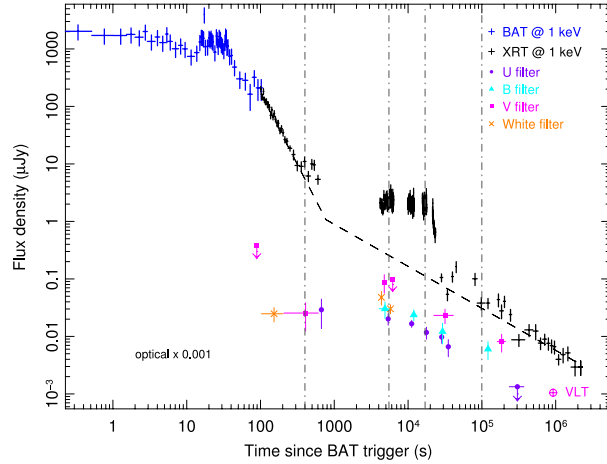


**Fig. 12.** The “internal” X-ray plateau observed in GRB 070110, which suggests that the central engine launches a long-lasting outflow with steady dissipation.

Source: From [294].

X.-G. Wang et al. (2014, in preparation) carried out a detailed study by confronting the joint X-ray and optical data of a large sample of Swift GRBs with the external shock models. They found that at least half of the GRBs are consistent with the external shock models in both bands and the lightcurves are achromatic. Only less than 15% of GRBs in the sample are chromatic, which demand two different emission components to account for the X-ray and optical data, respectively.

It is worth pointing out that short GRBs typically have fainter afterglows due to their lower energies and probably lower circumburst densities [336]. Comparing with the prompt emission properties, one finds that both long and short GRBs follow some similar correlations among prompt emission and afterglow properties [337–339]. This suggests a similar radiative efficiency and probably also a similar circumburst environment for both long and short GRBs [340,338].

In summary, Swift observations have led to the following modified understanding of afterglows: *The so-called “afterglow”, at least for the initial few hours, is no longer simply the external forward shock emission; instead, it is a superposition of multiple components, including emission powered by a long-lasting central engine.*

#### 4.3. High energy ( $>10^2$ MeV) afterglow radiation

Back in the Compton-Gamma-Ray-Observatory (CGRO) era, one burst detected by BATSE, GRB 941017, also triggered the high energy detector EGRET [91]. In fact, strong GeV emission was still detectable 1.5 h after the trigger when the burst re-emerged from the earth limb.

We provide a brief summary of the theoretical models that were suggested for the delayed, long lasting, high energy photons from GRBs. These include internal shocks, e.g. [341], SSC process operating in the external shock [342,244] – while the reverse shock is passing through the GRB jet, two SSC processes (in FS and RS, respectively) as well as two cross IC processes (FS photons up-scattered by RS electrons and vice versa) could also contribute to the observed high energy flux [343–349]. Moreover, prompt gamma-rays can be upscattered by electrons in the external FS or RS and produce high energy emission [350–352]. Yet another process for delayed GeV photons from GRBs is up-scattered CMB photons by high Lorentz factor electron–positron pairs in the inter-galactic medium [353]; these pairs are produced when TeV photons from a GRB interact with the cosmic infrared background radiation. This mechanism can only work when intergalactic magnetic field strength is very small, of order  $\lesssim 10^{-15}$  G, so that electron deflection angle is small and a collimated GeV front traveling toward Earth is produced [234,354–356].

The Fermi satellite, with the Large Area Telescope (LAT, [357]) and Gamma-ray Burst Monitor (GBM, [358]) on board, opened a new window in 2009 to systematically study GRBs above 100 MeV, and to finally settle the question as to which of the above mentioned mechanisms might be responsible for producing high energy  $\gamma$ -ray photons in GRBs.

About 10 GRBs per year are jointly detected by LAT and GBM, allowing a time-dependent broad-band spectral analysis of these GRBs. This led to two interesting observational discoveries, viz. the first photons of energy  $>10^2$  MeV typically arrive a few seconds after the GBM trigger (or arrival of photons of energy  $\lesssim 10$  MeV), and the emission in the LAT band ( $\gtrsim 10^2$  MeV) lasts for  $\sim 10^3$  s which is much longer than the typical burst duration in the GBM band ( $\sim 5$  keV–10 MeV) of 10–30 s. Moreover, the LAT lightcurve usually shows a simple power law decay with time for almost the entire duration of LAT observation [359,99,105,103].

It was realized soon after Fermi discovered these properties of high energy emission from GRBs that photons of energy  $>10^2$  MeV, after the prompt phase that lasts for  $\sim 30$  s, are produced via the synchrotron process in the external forward-shock [104,250,105]. The reasons for arriving at this conclusion are discussed below.

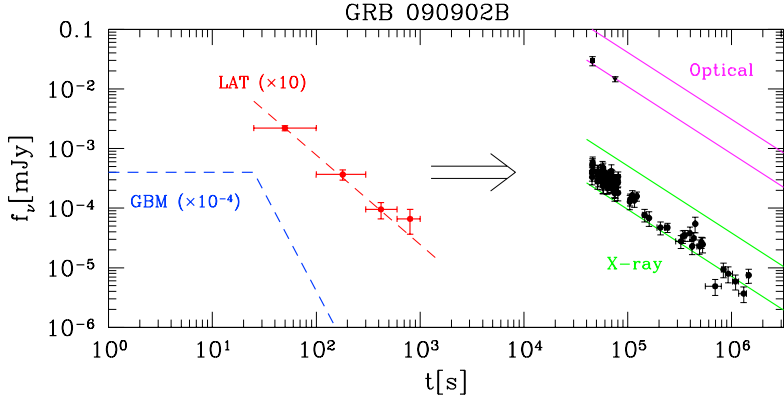


**Fig. 13.** The optical and X-ray fluxes of GRB 090902B predicted at late times using only the high energy data (photon energy  $\gtrsim 10^2$  MeV) at 50s (assuming synchrotron emission from external forward shock) are shown on the right half of this figure (diagonal bands). The predicted flux are compared with the observed data (discrete points with error bars).

Source: From [250].

**Table 1**

Comparison of observed flux at 100 MeV and the expected flux from external forward shock. The 4th column is time in observer frame when flux at 100 MeV due to synchrotron radiation in the external forward shock is calculated (which is reported in column 5) and that is compared with the Fermi/LAT measurements (column 6). For the flux calculation we took the energy in the blast wave to be  $E_{ES} = 3E_\gamma$ , and other parameters were  $\epsilon_e = 0.2$ ,  $\epsilon_B = 10^{-5}$  &  $p = 2.4$ ; the uncertainty in the predicted flux is about a factor 2 due to the uncertainty in  $\epsilon_e E_{ES}$  which is the energy carried by electrons in the external shock; we note that the predicted flux is independent of CSM density, and scales as  $\epsilon_B^{(p-2)/4} = \epsilon_B^{1/10}$  and hence is almost independent of  $\epsilon_B$  as long as the Fermi band lies above the synchrotron cooling frequency. Burst duration in 10 keV–10 MeV band is provided in the column marked  $T_{MeV}$ , and the time duration that  $> 100$  MeV photons were detected by Fermi/LAT is given in the 2nd last column ( $T_{LAT}$ ). Fermi/LAT lightcurves for all these bursts for  $T_{MeV} < t \leq T_{LAT}$  show a simple power-law decline. Considering that  $T_{LAT}/T_{MeV} \gg 3$  (the last column) models such as those where prompt MeV photons are IC scattered by  $e^\pm$  s in the external medium to produce these very long lasting LAT lightcurves e.g. [360] are ruled out.

	$z$	$E_\gamma$ ( $10^{54}$ erg)	$t_{obs}$ (s)	Exp. flux (nJy)	Obs. flux (nJy)	$T_{MeV}$ (s)	$T_{LAT}$ (s)	$T_{LAT}/T_{MeV}$
080916C	4.3	8.8	150	50	67	60	>400	>7
090510	0.9	0.11	100	9	14	0.3	120	360
090902B	1.8	3.6	50	300	220	30	700	23
110731A	2.83	0.6	100	8	~5	7.3	550	75
130427A	0.34	0.78	600	48	~40	138	>4300	>30

It is striking that the spectral index and the decay of the LAT lightcurve [ $f_\nu(t) \propto \nu^{-1.1} t^{-1.3}$ ] satisfy the closure relationship almost perfectly for synchrotron radiation from the shock heated circum-burst medium (CBM) by the relativistic jet of a GRB<sup>19</sup> when  $\nu > \nu_c$  (see Fig. 13).<sup>20</sup> It was shown by Kumar [145] that when the observation band is above the synchrotron cooling frequency ( $\nu > \nu_c$ ) then the specific flux from external forward shock is dependent only on the blast wave energy and the energy fraction in electrons (see Eq. (81)); the flux is completely independent of the highly uncertain CBM density, and is insensitive to  $\epsilon_B$  ( $f_\nu \propto \epsilon_B^{0.1}$ ). Therefore, one can confidently predict the flux in the Fermi/LAT band, to within a factor of a few, from the knowledge of energy in the prompt  $\gamma$ -ray radiation for a burst. And remarkably, it turns out that this predicted flux is consistent with Fermi/LAT observations for several well studied bursts [250] – Table 1 provides a comparison of the expected synchrotron flux from external forward-shock at 100 MeV and the Fermi/LAT data for five well studied bursts.

Furthermore, one can determine external shock parameters from early time ( $t \sim 10^2$  s) Fermi data and use that to predict late time optical and X-ray flux. Fig. 13 shows the result of this exercise for Fermi burst GRB 090902B; it shows the comparison between the predicted and the observed late time afterglow data, which are found to be in good agreement.

This exercise can also be carried out in the reverse direction, i.e. one can determine the external shock parameters from the late time ( $t \gtrsim 0.5$  day) X-ray, optical and radio data, and use these parameters to calculate the flux at 100 MeV at early times ( $t \lesssim 10^3$  s). We show in Fig. 14 that this “predicted flux” is in excellent agreement with the data obtained by Fermi/LAT. These results lend strong support to the suggestion that high energy photons from GRBs detected by Fermi/LAT, for  $t \gtrsim 30$  s, are produced via the synchrotron process in the external shock.

<sup>19</sup> See Section 3.1 for lightcurve scalings, and in particular Eq. (81).

<sup>20</sup> For a few GRBs, the temporal decline of the LAT lightcurve is just slightly steeper (the decay index,  $\alpha$ , larger by about 0.1 or 10%) than what one might expect from the LAT band spectral index in the regime  $\nu > \nu_c$ . Ghisellini et al. [105] suggested that this is due to radiative losses affecting the external shock dynamics. However, Wang et al. [249] showed that the decline of the LAT lightcurve is fine for an adiabatic blastwave, and the slightly steeper than expected decline can be understood as the result of IC cooling of high energy electrons (those that produce  $> 10^2$  MeV photons) which becomes more effective at later time; IC cooling of high energy electrons is suppressed at early times because scatterings are deeper in the Klein–Nishina regime at earlier times.

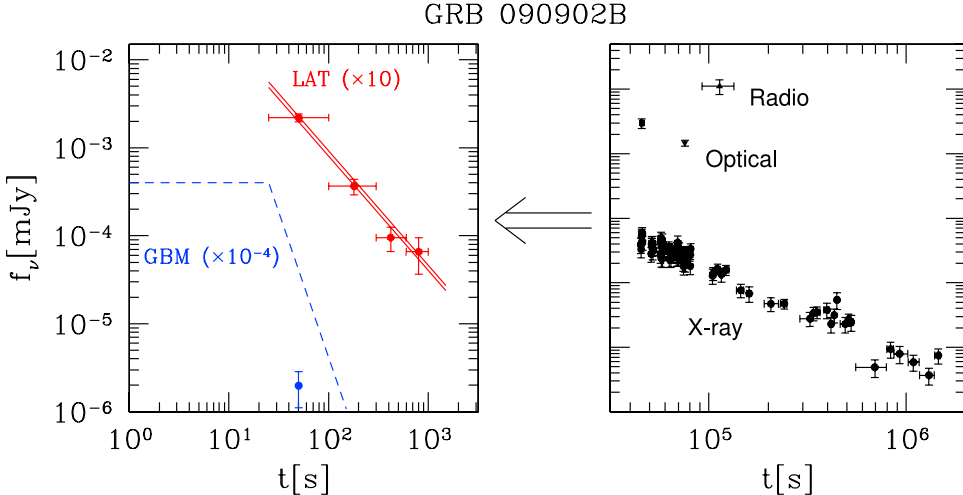


**Fig. 14.** Using the X-ray, optical and radio data of GRB 090902B at late times (right panel) we constrain the external forward shock parameters, and then use these parameters to predict the 100MeV flux at early times (left panel). The region between the red lines shows the range for the predicted flux at 100MeV; note the remarkably narrow range for the predicted 100 MeV flux and an excellent agreement with the Fermi/LAT data. The blue point (left panel) indicates the flux at 100 keV and 50 s that we expect from the external-shock model; note that the external-shock flux at 100 keV falls well below the observed Fermi/GBM flux shown schematically by the dashed line in the left panel, and that is why the GBM light curve undergoes a rapid decline with time ( $\sim t^{-3}$ ) at the end of the prompt burst phase.

Source: From [250].

One thing to point out though is that it is not easy to produce photons with energy more than  $\sim 50\Gamma$  MeV–5 GeV via the synchrotron process as described in Section 2.2 (but see [132], for a way around the maximum energy constraint). It is possible that the highest energy photons ( $\gtrsim 5$  GeV) detected by Fermi LAT from GRBs are produced via IC scattering of synchrotron photons. Zhang and Mészáros [244] considered a range of shock micro-physics parameters, and identified regimes where synchrotron and SSC dominate in the GeV–TeV energy range.

Kumar [104] and Barniol Duran [250] found that  $\epsilon_B$  should be small<sup>21</sup> in the highly relativistic external shock for Fermi bursts in order that the flux at  $\lesssim 1$  MeV produced in the external shock not exceed the observed value; Fermi/GBM lightcurves (10 keV–10 MeV) fall off very rapidly after the prompt phase ( $t^{-3}$  or faster), and so the contribution of the forward shock flux in this band – which declines with time as  $\sim t^{-1.2}$  – at the end of the prompt phase has to be well below the observed value in order to make it possible for the GBM lightcurve to fall off steeply.

It can be shown that this small magnetic field is sufficient for confining high energy electrons of thermal Lorentz factor  $\sim 10^8$  (that produce  $\sim 10$  GeV photons), both upstream and down-stream of the shock front, and for their efficient acceleration by the first order Fermi mechanism as long as these electrons are not exposed to a large flux of a few eV photons ( $\gtrsim 10$  mJy in our frame) to cause severe IC losses [361,362].

Measurements of  $\epsilon_B$  for a large sample of GRBs and its implications are discussed in Section 5.

It is interesting that GeV afterglows almost always follow a simple power law “normal” decay, while only 5% of X-ray afterglows are a single power law function [363,290] – most X-ray lightcurves show a steep-shallow-normal-steep decay behavior. Only a few GRBs have jointly triggered both Swift/LAT and Fermi/LAT. The currently available two cases,<sup>22</sup> i.e. GRB 090510 [367] and GRB 110731A [368], both show GeV and X-ray lightcurves to be power law functions of time for almost the entire duration of observations starting at  $\sim 5$  s for Fermi/LAT and  $\sim 10^2$  s for Swift/XRT.<sup>23</sup> The optical, X-ray and GeV data for these bursts are consistent with the external forward shock model. It would be interesting to find out whether all GRBs with GeV afterglows are just those rare cases that display a single power law decay X-ray lightcurve.<sup>24</sup>

Detailed data analysis [103] and theoretical modeling [369–372] suggest that the GeV emission during the prompt phase (when GBM emission is still on) is likely not dominated by the external shock component, and that the external shock emission starts to dominate after the prompt phase. This is because energy is still being added to the blastwave during the prompt phase [370], and observationally, LAT lightcurve spikes track those in the GBM lightcurves [99,103] which is very

<sup>21</sup>  $\epsilon_B \sim 10^{-6}$  if the CBM particle number density is  $0.1 \text{ cm}^{-3}$ , and it is smaller for higher densities.

<sup>22</sup> A third case of GRB100728A also has simultaneous Swift/XRT and Fermi/LAT observations. However, for this burst photons of energy  $> 10^2$  MeV were not detected during the prompt  $\gamma$ -ray phase but LAT saw emission during the X-ray flares [364] which perhaps were due to IC scatterings of X-ray flare photons by electrons in the external shock [365,366].

<sup>23</sup> The X-ray data for GRB 090510 shows a jet break at  $\sim 10^3$  s.

<sup>24</sup> If future Fermi/LAT observations find a burst that has a power-law decay lightcurve, but a complex X-ray afterglow lightcurve typical for GRBs, then that would constitute yet another evidence that the X-ray afterglow emission for at least a fraction of bursts is produced not by the FS but by some process internal to the relativistic jet.

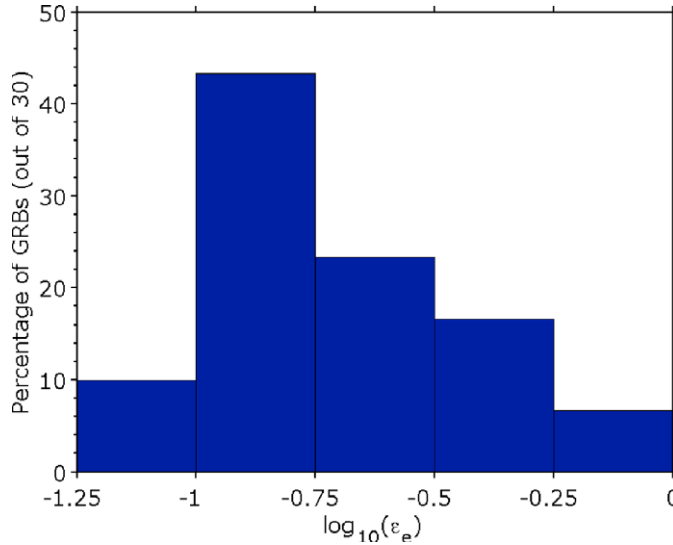


**Fig. 15.** Distribution of  $\epsilon_e$  for 30 GRBs from published literature; [208,376,377,32,378–380,369,381,27,37,382–385,144]. Source: This figure is taken from [386].

difficult to produce in external shocks [305]. According to recent observations, some GRBs show a steep to shallow transition in the GeV lightcurve, which suggests that the radiation mechanism might be switching from prompt emission to afterglow [373]. When the contribution of the early, steep, phase is subtracted from the Fermi/LAT lightcurve the temporal slope of the remaining afterglow data is found to be “normal” and consistent with synchrotron radiation from an adiabatic external shock [373].

## 5. Collisionless shock properties from GRB afterglow observations

GRB afterglows provide a good laboratory for the study of relativistic collisionless shocks. In spite of many years of theoretical work several basic questions regarding collisionless shock remain unanswered. Perhaps foremost amongst these questions are generation of magnetic fields down/up stream of the shock front ( $\epsilon_B$ ), particle acceleration ( $p$ ) and the fraction of energy of shocked plasma that is given to electrons ( $\epsilon_e$ ). The calculation of synchrotron radiation from shocked fluid requires these three quantities, and hence multi-wavelength GRB afterglow data can be exploited for their measurement, and that should shed light on the basic plasma physics of collisionless shocks.

The GRB afterglow flux at any given time is dependent on at least four parameters when the underlying radiation mechanism is the synchrotron process –  $E$  (energy in explosion),  $n$  (CBM density),  $\epsilon_e$  and  $\epsilon_B$  – even for the simplest, spherical, blastwave; there is a fifth parameter  $p$  (electron distribution index) that is readily determined from the X-ray spectrum, and so can be dropped from the list of unknown parameters. Therefore, at least four independent observations are needed to determine these four parameters. One might think that observing in four different energy bands, e.g. radio, mm, infrared and X-ray, would provide sufficient data to uniquely determine  $E$ ,  $n$  etc. However, this is incorrect. Observations at two different frequencies provide independent pieces of information only when these frequencies fall on different segments of the synchrotron spectrum, such as when one frequency band is below the synchrotron peak ( $\nu_m$ ) and the other is above it. Or when one frequency band is in the synchrotron-self-absorption regime whereas the other is not. Another way to emphasize this point is to consider an example where someone carries out observations of GRB afterglows in two different frequency bands, say mm and optical, for time periods of hours and days. This entire observational effort might provide just one independent piece of information – equivalent to an observation carried out at one frequency and at one single snap-shot in time – if the spectrum between mm and optical frequencies for the burst is a single power-law function for the entire time duration of the observation. Therefore, measurement of these four different parameters uniquely is not possible except for a small number of GRBs that have been followed up for a long time in X-ray, optical and radio bands.

The value of  $\epsilon_e$  is set by the micro-physics of relativistic shocks. And if magnetic fields in the shocked fluid is generated by the Weibel instability [374,375], or another instability based on the local physical condition of the plasma, then  $\epsilon_B$  is also determined by shock micro-physics. Therefore, based on basic physics considerations, it is expected that  $\epsilon_e$  &  $\epsilon_B$  should be functions of those variables that characterize a relativistic shock, viz.  $E$ ,  $n$  and  $\Gamma$  (Lorentz factor of shock front).

The afterglow flux at a frequency that lies above  $\nu_m$  is proportional to  $\epsilon_e^{p-1}$ , and due to this fairly strong dependence  $\epsilon_e$  is perhaps one of the most reliably measured parameters. Fig. 15 shows  $\epsilon_e$  distribution for a sample of 30 GRBs drawn from the published literature. Note that the mean value for  $\epsilon_e$  for these 30 bursts is 0.2 and the dispersion about the mean is a

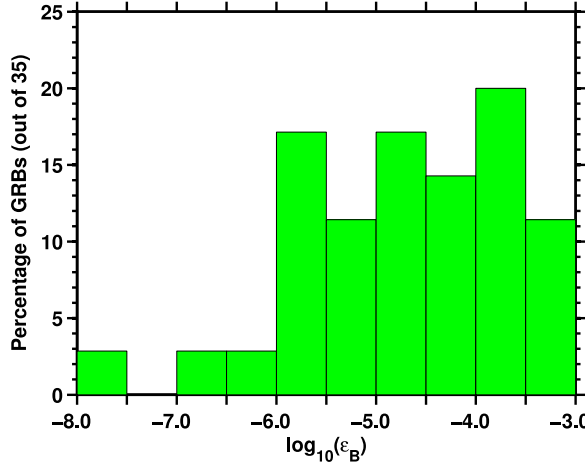


**Fig. 16.** Distribution of  $\epsilon_B$  for 35 GRBs detected by the Swift satellite. These  $\epsilon_B$  were determined from the optical afterglow data (see [386] for details) assuming that  $\epsilon_e = 0.2$ ,  $n = 1 \text{ cm}^{-3}$ , and energy in the external shock is 4 times the energy in prompt  $\gamma$ -ray radiation.  $p$  is determined from the temporal decay of the lightcurve. The effect of any error in  $n$ ,  $\epsilon_e$  and  $E$  on  $\epsilon_B$  determination can be estimated from the relation  $\epsilon_B \propto E^{-1.6} \epsilon_e^{-1.6} n^{-0.6}$  [386]. Source: This figure is taken from [386].

factor 2;  $\epsilon_e \sim 0.2$  is consistent with recent simulations of relativistic collisionless electron-ion shocks (e.g. [387]<sup>25</sup>). These bursts cover a wide range of  $E$  and  $n$ . So, to the lowest approximation,  $\epsilon_e$  is independent of shock strength, and it takes on a nearly universal value that varies by a factor  $\sim 2$  from one burst to another.

Assuming that the radiative efficiency for producing prompt  $\gamma$ -ray emission is 20% for GRBs (so that the energy in blast wave is 4 times the energy in prompt  $\gamma$ -rays), and  $\epsilon_e = 0.2$  for the external shock, one can find  $\epsilon_B/n$  from optical afterglow data alone. Fig. 16 shows a histogram for  $\epsilon_B$  for 35 GRBs detected by the Swift satellite [386]. This distribution is very wide – the median value of  $\epsilon_B$  is about  $3 \times 10^{-5}$ , and the distribution spans more than four orders of magnitude.

There is no evidence that  $\epsilon_B$  depends on shock Lorentz factor. For a couple of Fermi/LAT bursts one can determine  $\epsilon_B$  from early time  $\gamma$ -ray data when the blast wave Lorentz factor was larger than  $\sim 10^2$  (left panel of Fig. 17), and from late time X-ray and optical data when the Lorentz factor had dropped to  $\sim 10$  (result shown in Fig. 17 right panel). And it is found that the values of  $\epsilon_B$  at early and late times are entirely consistent with each other. Collisionless shock simulations also find no dependence of  $\epsilon_B$  on  $\Gamma$ , e.g. [387].

A wide distribution of  $\epsilon_B$ , which is independent of shock Lorentz factor, suggests that magnetic field is unlikely to be determined by micro-physics of relativistic collisionless shock alone.

For an upstream magnetic field of strength  $B_0$  (in CBM frame), the down stream field, due to shock compression alone, is  $4B_0\Gamma$  (in shock comoving frame). The ratio of energy density in this shock compressed field and the energy density of shocked plasma is:

$$\epsilon_B^{(sc)} = \frac{B_0^2}{2\pi nm_p c^2}. \quad (97)$$

The factor by which magnetic field is amplified in GRB external shock is given by,  $AF = [\epsilon_B/\epsilon_B^{(sc)}]^{1/2}$ . The amplification factor is very insensitive to the uncertain CBM density,  $AF \propto n^{0.2} B_0^{-1}$ , since  $\epsilon_B \propto n^{-0.6}$  and  $\epsilon_B^{(sc)} \propto n^{-1}$ . Hence  $B_0 \times AF$  can be determined quite accurately for the sample of 35 bursts in Fig. 16, and its distribution is shown in Fig. 18. The field amplification determined from the afterglow data corresponds to the average value of magnetic field for the entire volume of the shocked plasma that contributes to the observed radiation. Note that a modest amplification of CBM field, by a factor  $\sim 30$ , down-stream of shock front is all that is required by GRB afterglows;  $AF \sim 10^4$  for equipartition magnetic field.

If magnetic fields were to be generated down-stream by the Weibel mechanism then we expect  $\epsilon_B \sim 0.1$  near the shock-front [375]. This field, however, has small coherence length scale of order the plasma skin depth, and likely decays by a large factor over the width of the shocked plasma which is of order  $10^8$  skin depth for GRB external shocks. This might be the reason for the small average  $AF$  inferred from afterglow observations; numerical simulations [388,389,387], and analysis of GRB afterglow data [390] support this general picture of strong field near the shock front and their decay down-stream.<sup>26</sup>

<sup>25</sup> The simulations by Sironi and Spitkovsky [387] also find the down-stream particle distribution to have a prominent thermal peak at electron energy of  $\sim m_p \Gamma c^2$  which is not observed in GRB spectra; where  $\Gamma$  is the shock-front Lorentz factor.

<sup>26</sup> An earlier suggestion was made by Rossi and Ress [391] that strong magnetic fields only pervade a few percent of the total thickness of the shocked region. They did not derive detailed constraints from the data. A similar suggestion was made by Pe'er and Zhang [392] for internal shocks.

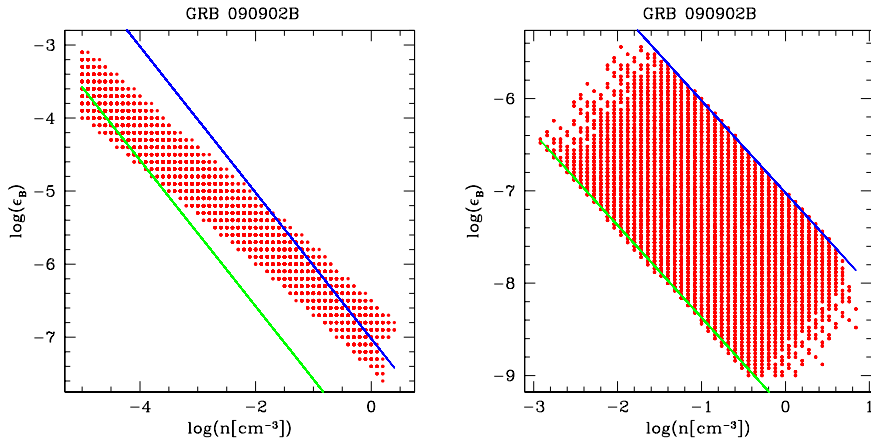


**Fig. 17.** The left panel shows  $\epsilon_B$ - $n$  space (for the forward external forward shock going into a uniform density CBM) allowed by the high energy data for GRB 090902B at  $t = 50$  s when the shock front Lorentz factor was  $\sim 300$  (see [250]); the discrete points reflect the numerical resolution of the calculation. Also shown is the expected  $\epsilon_B$  for a shock compressed CBM magnetic field of 5 and 30  $\mu\text{-Gauss}$  as the green and blue lines respectively; for a CBM field of strength  $B_0$ , the value of  $\epsilon_B$  downstream of the shock-front resulting from the shock compressed CBM field is  $\approx B_0^2/(2\pi n m_p c^2)$ , where  $n m_p$  is the CBM mass density, and  $c$  is the speed of light. The right panel shows  $\epsilon_B$ - $n$  space allowed by the late time ( $t > 0.5$  day) X-ray, optical and radio data for GRB 090902B when the shock front Lorentz factor had dropped to  $\sim 10$ . Also plotted is the expected  $\epsilon_B$  for a shock compressed CBM magnetic field of 2 and 30  $\mu\text{-Gauss}$  as the green and blue lines, respectively.

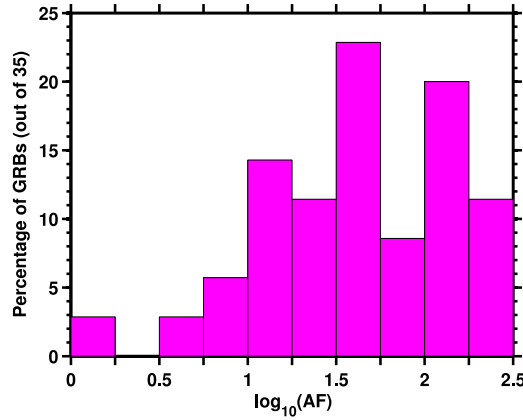


**Fig. 18.** Results for the magnetic field amplification factor (AF) for the optical sample shown in Fig. 16. A fixed  $n = 1 \text{ cm}^3$  and  $B_0 = 10 \mu\text{G}$  were assumed;  $AF \propto n^{0.2} B_0^{-1}$ .  
Source: This figure is taken from [386].

Another possible mechanism for magnetic field generation is shear across the GRB-jet, or density inhomogeneity of the ISM, which generates turbulence down-stream and leads to a modest field amplification by about an order of magnitude e.g. [393–397]. In this case the coherence length of the field is large – of order the shear length scale or the size of the system – and such a field persists throughout the down-stream volume.

Lemoine et al. [390] have suggested from the analysis of X-ray and GeV afterglow data for four different GRBs that the turbulent magnetic field generated in shocks is strong near the shock front ( $\epsilon_B \sim 10^{-2}$ ) where GeV photons are generated by the synchrotron process, and that the field decays with distance ( $d'$ ) from the shock-front so that the value of  $\epsilon_B$  further down-stream where X-rays are produced is  $\sim 10^{-6}$ ; Lemoine et al. [390] find that the X-ray data is consistent with  $\epsilon_B \propto d'^{-0.5}$ .

The maximum photon energy detected from a burst is  $\sim 94 \text{ GeV}$  (GRB 130427A), and  $> 1 \text{ GeV}$  photons have been observed by Fermi/LAT from more than 20 GRBs [373]. These high energy photons provide a lower limit on the upstream magnetic field in the external forward shock. A minimum CBM field strength is required to ensure that high energy electrons (those that produce GeV photons via the synchrotron process down-stream and have LF  $\sim 10^8$  in shock comoving frame) are confined to the shock, and that these electrons could be turned around on a short time scale while upstream before losing a good fraction of their energy to IC scatterings. Barniol Duran and Kumar [361] showed that a CBM magnetic field of  $10 \mu\text{G}$  is sufficient for accelerating electrons to an energy so that they produce  $\sim 10 \text{ GeV}$  synchrotron photons.

The distribution function for electron energy, just behind the shock front, is a power-law function of energy with index  $p$ . A number of calculations suggest that  $p$  should be about 2.2 for collisionless relativistic shocks independent of shock LF

e.g. [398–401]. This expectation is not supported by GRB afterglow spectra which show that  $p$  varies considerably from one burst to another [402–404]. One possible way out of this discrepancy is that  $p$  calculated from X-ray afterglow spectrum has nothing to do with shocks; considering the complexity of X-ray lightcurves it is possible that the radiation is not produced in external shocks but rather by some other dissipative process internal to the jet [329,331]. The other possibility is that something is missing in theoretical calculations of  $p$  in relativistic shocks, and in that case the observed distribution should guide us to the correct model.

## 6. Observational properties of GRB prompt radiation

### 6.1. Temporal properties

Observationally, the prompt emission phase of a GRB is conventionally defined as the temporal phase during which sub-MeV emission is detected by the GRB triggering detectors above the background level. Quantitatively, the duration of a burst is defined by the so-called “ $T_{90}$ ”: the time interval between the epochs when 5% and 95% of the total fluence is registered by the detector. Such an observation-based definition has some limitations: 1. It depends on the energy band of the detector. A detector with a lower energy bandpass typically gets a longer  $T_{90}$  for the same GRB. 2. It is sensitivity-dependent. A more sensitive detector (e.g. due to a larger collection area) would detect a longer duration of a same burst above the background level, and hence, has a longer  $T_{90}$ . 3. Some GRBs have clearly separated emission episodes with long quiescent gaps in between. The parameter  $T_{90}$  therefore may over-estimate the duration of GRB central engine in these cases. 4. Physically, the emission registered within  $T_{90}$  may include contributions from different sites (e.g. internal dissipation regions and external shocks). Modelers tend to attribute “prompt emission” and “afterglow” as emissions from the internal dissipation sites and the external shock, respectively. Although emission during  $T_{90}$  for most GRBs seems to be consistent with an internal origin, the differentiation between an internal and an external origin of emission is not straightforward. Throughout this review we stick to the observation-defined  $T_{90}$  as the duration of “prompt emission”, but limit ourselves to discuss internal dissipation models for prompt emission.

The temporal properties of GRBs may be summarized as the following:

- The duration  $T_{90}$  ranges from milliseconds to thousands of seconds. The  $T_{90}$  distribution includes at least two log-normal components with a separation line around 2 s in the observer frame in the BATSE energy band (25–350 keV) [3]: a long-duration class with  $T_{90}$  peaking at 20–30 s, and a short-duration class with  $T_{90}$  peaking at 0.2–0.3 s. Several papers have suggested that the  $T_{90}$  distribution may include a third, intermediate-duration group e.g. [405–409]. However, the recent analysis of [410] finds little support for a third class of GRBs.

Statistically, the long-duration group is “softer” than the short-duration group, which means that the ratio between the photon numbers in the detector’s low-energy and high-energy bands is larger for long GRBs than short GRBs (Fig. 19). The duration distribution is energy-band-dependent and sensitivity-dependent, so that different detectors give different distributions [3,411–415]. Qin et al. [415] show that when breaking the Fermi bandpass to different sub-bandpasses of the previous detectors, similar  $T_{90}$  distributions as previous detectors can be reproduced.

- The GRB lightcurves are notoriously irregular. Some are extremely variable, with detectable minimum variability time scale reaching millisecond range, while some others have smooth lightcurves with relatively simple temporal structures [5]. Some GRBs have distinct emission episodes separated by long gaps in between. Some sample lightcurves are presented in Fig. 20.
- A fraction of GRBs have a typically softer and weaker “precursor” emission well separated from the main burst by 10s to 100s of seconds. Subject to definition, the fraction of GRBs with a precursor emission ranges from 3% [416] to 12% [417]. Statistical studies suggest that the characteristics of the main episode emission are independent of the existence of the precursor emission, and the properties of the precursors in some GRBs are similar to those of the main-episode emission [418,419,417,420].
- Power density spectrum (PDS) analysis of GRB lightcurves reveals null periodicity. The PDSs of individual GRBs can be noisy. However, averaging the PDS of several bright GRBs leads to a power law with index  $-5/3$  and a sharp break around 1 Hz [421].
- There is evidence that GRB lightcurves are the superposition of a slower component and a faster component. This is evidenced by a gradual depletion of the fast component at low energies [422], and the existence of a distinct low frequency component in a stepwise low-pass filter correlation analysis [423].
- The shape of individual pulses in the lightcurves is typically asymmetric, with a sharp rising phase and a shallower decay phase. It can be fit by a variety of function forms. For some bright, isolated pulses, the pulse shape is often modeled by a “FRED” (fast-rising exponential-decay) function.
- There are quiescent episodes during a burst. The distribution of the separation times between pulses also satisfies a lognormal distribution e.g. [424–426].
- Lightcurves vary with energy band. Pulses tend to be narrower in harder bands (e.g. Figs. 21 and 22). The width  $w$  of individual pulses is a function of energy  $E$ :  $w(E) \propto E^{-\alpha}$  with  $\alpha \sim 0.3–0.4$  [427,230].
- A “spectral lag”, namely, pulses with a lower energy being systematically lagged behind those with a high energy, is observed in the keV–MeV regime for many long GRBs [428,429,427]. Short GRBs do not show significant spectral lags [430]. A fraction of short GRBs show “negative” lags, i.e. high energy pulses are lagged behind low energy pulses [431].

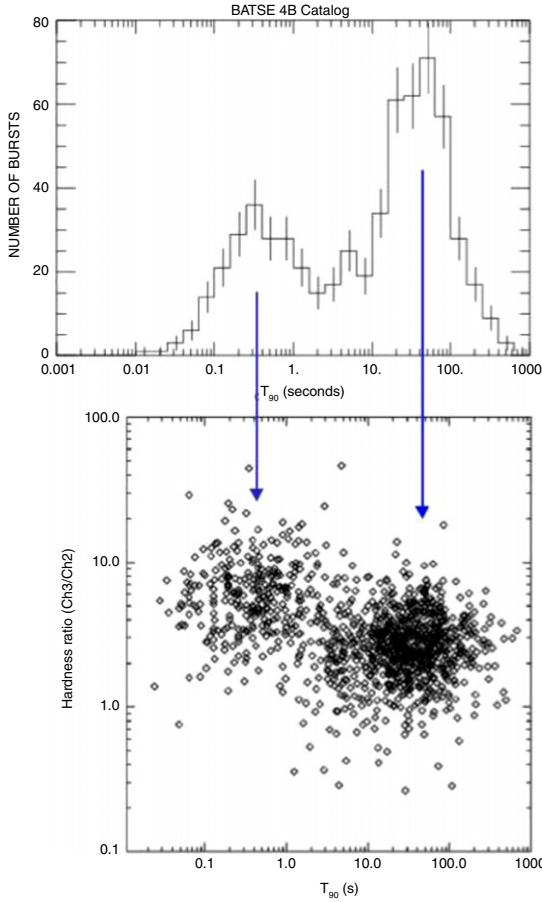


**Fig. 19.** Duration and duration/hardness ratio distribution of GRBs detected by BATSE on board CGRO. Adapted from the BATSE GRB Catalogs (<http://gammaray.msfc.nasa.gov/batse/grb/catalog/>).

## 6.2. Spectral properties

### 6.2.1. Spectral shapes and functions

The GRB spectra are non-thermal. Spectra are often extracted over the entire duration of the bursts. This is the time integrated spectrum of a GRB. Strong spectral evolution in some GRBs is observed. Therefore time resolved spectral information is more essential to understand GRB physics. Technically, the time bin size cannot be infinitely small, which is limited by the requirement that there are enough photons within each time bin to allow reasonable spectral fitting to test several plausible spectral models. Therefore, a time-resolved spectral analysis can be carried out only for bright GRBs.

When the detector's energy band is wide enough, a typical GRB spectrum can be fit with a smoothly-joined broken power law known as the “Band-function” [2]. The photon number spectrum in this model reads

$$N(E) = \begin{cases} A \left( \frac{E}{100 \text{ keV}} \right)^\alpha \exp\left(-\frac{E}{E_0}\right), & E < (\alpha - \beta)E_0, \\ A \left[ \frac{(\alpha - \beta)E_0}{100 \text{ keV}} \right]^{\alpha-\beta} \exp(\beta - \alpha) \left( \frac{E}{100 \text{ keV}} \right)^\beta, & E \geq (\alpha - \beta)E_0, \end{cases} \quad (98)$$

where  $N(E)dE$  is the number of photons in the energy bin  $dE$ ,  $\alpha$  and  $\beta$  (both negative) are the photon spectral indices<sup>27</sup> below and above the break energy  $E_0$ . The flux density spectrum ( $F_\nu$ ) usually used in low-energy (optical, IR, and radio) astronomy corresponds to  $EN(E)$ , and the spectral energy distribution (SED) corresponds to  $E^2N(E)$  or  $\nu F_\nu$ . The peak of the  $E^2N(E)$  spectrum is called the “E peak”, which is given by

$$E_p = (2 + \alpha)E_0. \quad (99)$$

<sup>27</sup> Within the GRB afterglow context, the notation  $\alpha$  and  $\beta$  are also used to define the temporal decay index and flux density spectral index of the afterglow, with the convention  $F_\nu \propto t^{-\alpha} \nu^{-\beta}$ . In this review, we do not differentiate these notations and keep the convention in the community, but just alert the readers to pay attention to the possible confusion. The physical meaning of these notations are usually self-evident within the context of the review.

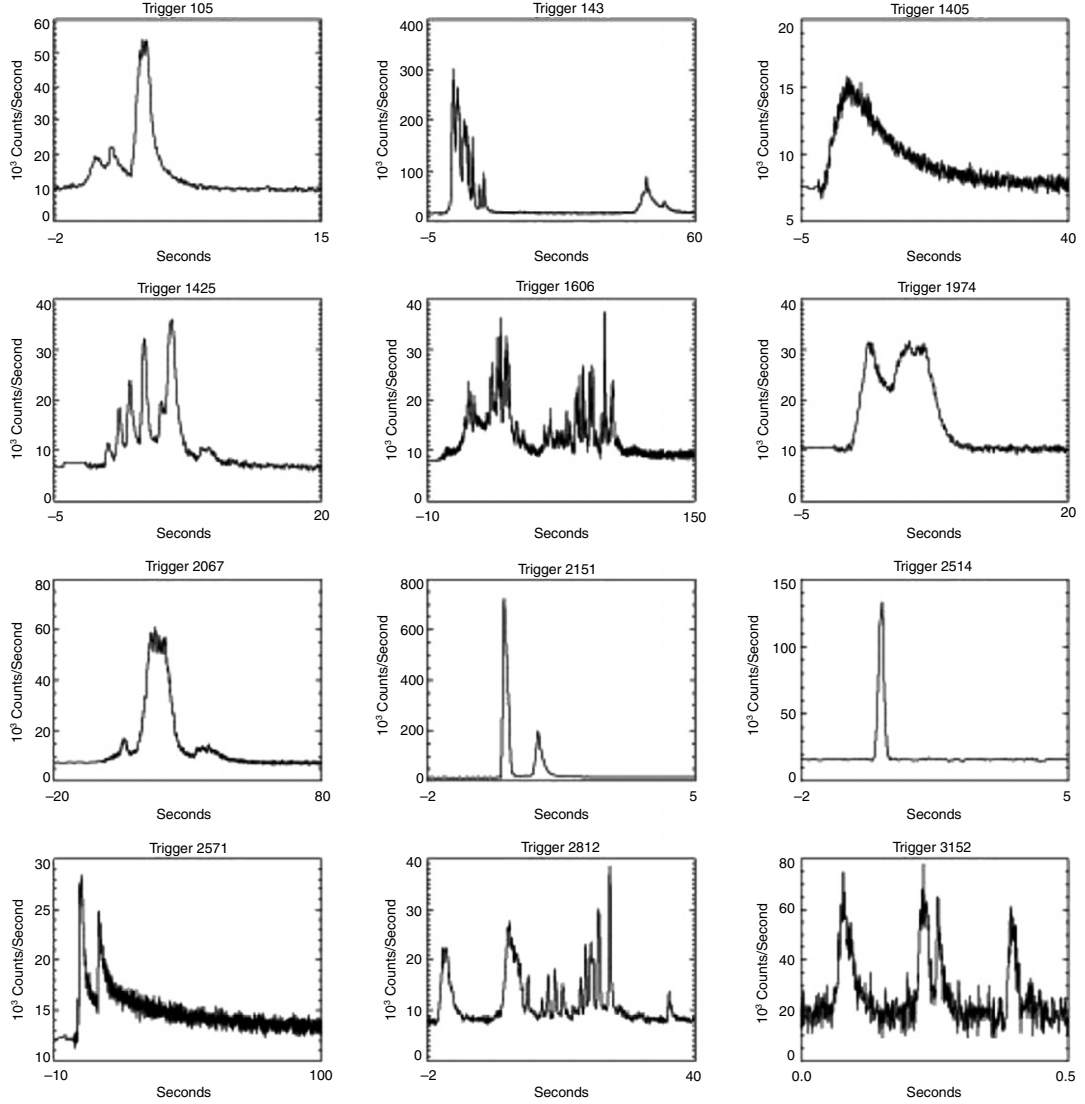


**Fig. 20.** Sample lightcurves of GRBs.  
Source: [5].

Fig. 23 gives an example of GRB 990123 whose time integrated spectrum is well fit by the Band function [432].

The  $E_p$  distribution of GRBs is wide. While bright BATSE GRBs (a sample of 156 bursts with 5500 spectra) have  $E_p$  clustered around 200–300 keV range [433], lower  $E_p$  bursts are found by softer detectors such as *HETE-2* and *Swift*. The distribution of  $E_p$  seems to form a continuum from several keV to the MeV range, e.g. [434]. From hard to soft, bursts are sometimes also vaguely classified as gamma-ray bursts (GRBs,  $E_p > 50$  keV), X-ray rich GRBs (XGRBs,  $30$  keV  $< E_p < 50$  keV), and X-ray flashes (XRFs,  $E_p < 30$  keV), with no clear boundaries in between [435]. For the bright BATSE sample, the two spectral indices have a distribution of  $\alpha \sim -1 \pm 1$  and  $\beta \sim -2^{+1}_{-2}$  [433]. Such a distribution is also confirmed for the *Fermi* and INTEGRAL bursts [103,436,434].

Spectra for some GRBs can be fitted with a cutoff power-law spectrum, in the form

$$N(E) = A \left( \frac{E}{100 \text{ keV}} \right)^{-\hat{\Gamma}} \exp \left( -\frac{E}{E_c} \right) \quad (100)$$

This is essentially the first portion of the Band-function, with  $\alpha$  replaced by  $-\hat{\Gamma}$  ( $\hat{\Gamma}$  is positive). This function has been used to fit the prompt spectrum of many *HETE-2*, *Swift*, and GBM GRBs [437,411,413]. However, this is mainly due to the narrow bandpass of the detectors, so that the high energy photon index  $\beta$  of the Band-function is not well-constrained. In fact, in most cases when a *Swift* burst was co-detected by another detector with high-energy band coverage (e.g. *Konus-Wind*, *Fermi-GBM*), the global spectrum can be still fit by a Band function.

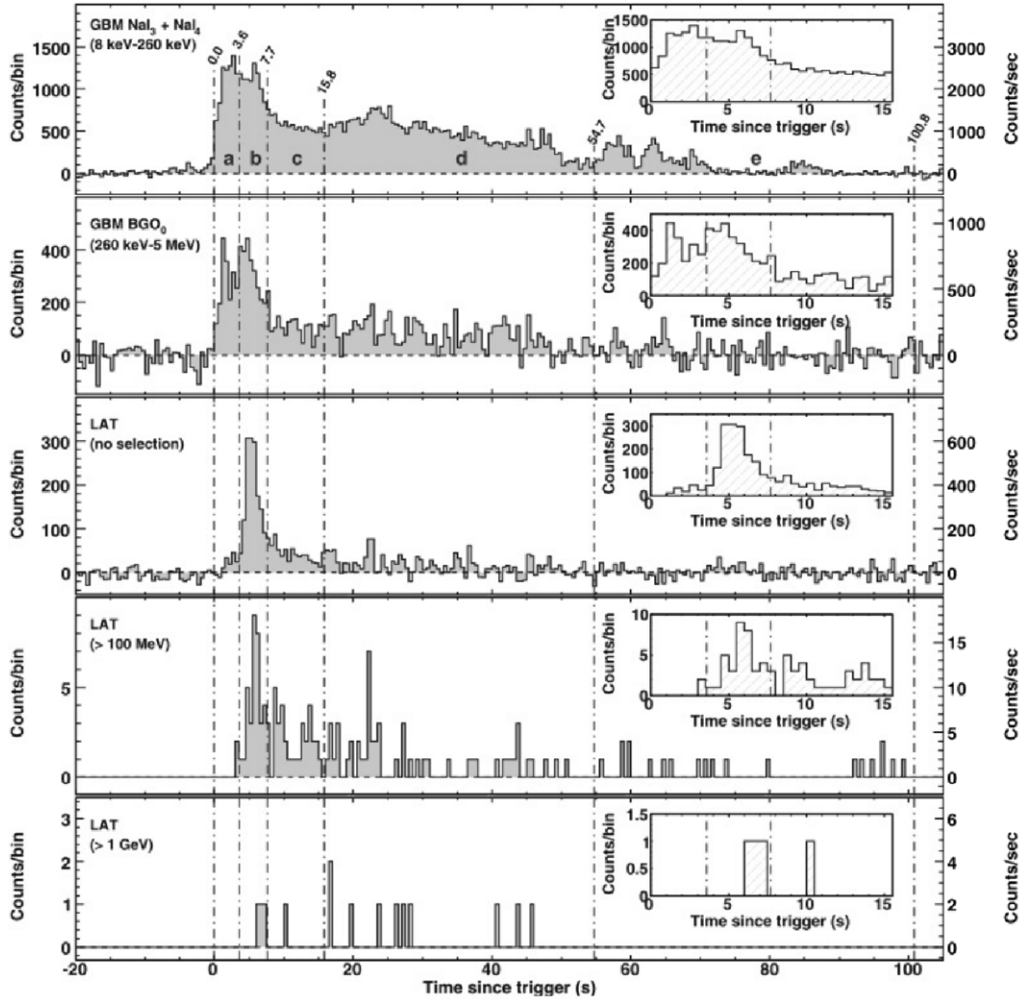


**Fig. 21.** Multi-wavelength lightcurves of GRB 080916C as detected by Fermi.  
Source: From [99].

In the pre-*Fermi* era, it was suggested [438,439] that the observed prompt GRB spectrum is the superposition of a thermal (blackbody) component and a non-thermal (power law) component. The traditional  $E_p$  is interpreted as the peak of the thermal component in this model. The spectra of some BATSE GRBs could be fit with such a “hybrid” model, which within the BATSE window may mimic a Band-like spectrum. This model however over-predicts the flux in the X-ray range for most GRBs, which violates the observational constraints by Beppo-SAX for some BATSE bursts [440,441]. A spectral break below the gamma-ray band is needed for such a model. *Fermi*, with both GBM and LAT on board, significantly extended the observational spectral window. It is clear now that there are (at least) two types of prompt emission spectra. The first type, exemplified by GRB 080916C, has a Band component covering 6–7 orders of magnitude [99]. There is essentially no evidence of superposition between a thermal and non-thermal component.<sup>28</sup> A second type – the prototype of which is GRB 090902B [359] – shows superposition of a thermal-like spectrum and a non-thermal power law spectrum extending both to low- and high-energy regimes [443,103]. The difference between the two types becomes evident when one zooms in the lightcurve and study the time-resolved spectra [103] (Fig. 24). GRB 080916C shows Band-function spectra with essentially no change of spectral indices as one reduces the time bin. GRB 090902B, on the other hand, shows narrowing of the Band component as one goes to smaller time bins, and eventually can be fit with a quasi-thermal component superposed with a power law component. A systematic analysis of 17 Fermi/LAT GRBs suggest that the first type is very common (14/17), while the second type is relatively rare (2/17) [103].

A synthesized prompt emission spectrum may include three components [103]: (I) a non-thermal “Band” component; (II) a quasi-thermal component; and (III) another non-thermal component that can be fit as a power law extending to high

<sup>28</sup> A latest study by S. Guiriec et al. (2014, in preparation) claims that there is a thermal component in GRB 080916C. In any case, the amplitude of the blackbody component is low, which requires significant suppression due to a Poynting flux dominated flow [442].

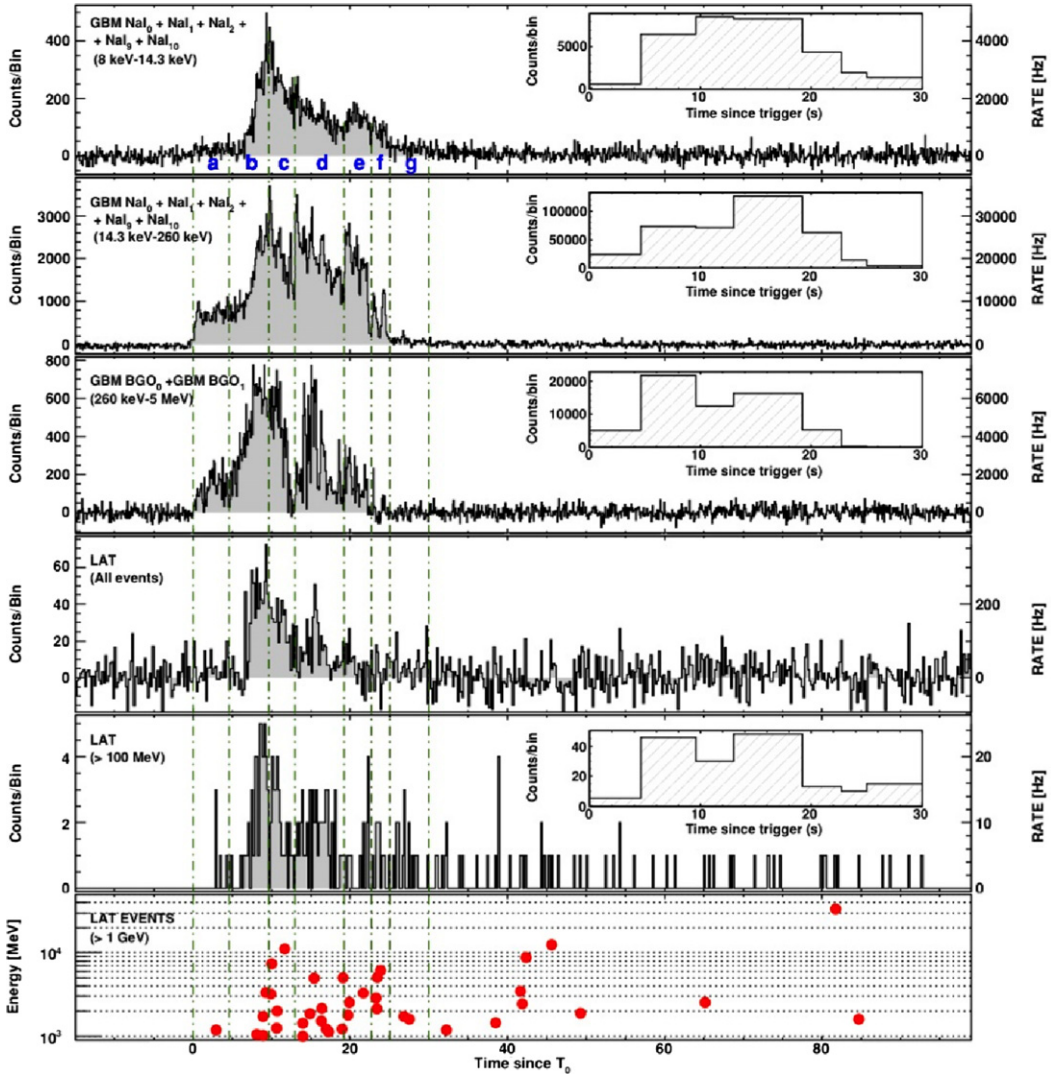


**Fig. 22.** Multi-wavelength lightcurves of GRB 090902B as detected by Fermi.  
Source: From [100].

energies (Fig. 25). This last component may have been detected in the EGRET burst GRB 941017 [444], and has been clearly detected in GRB 090510 and GRB 090902B [359,101,103]. Another *Fermi* burst GRB 090926A [102,103] shows late emergence of a high energy component with a potential high energy cutoff [102], which might have the same origin as the component III. The superposition of the first two components (I and II) have been seen in several GRBs: 100724B [445], 110721A [446], and 120323A [447]. In all these cases, the quasi-thermal component is sub-dominant. A tentative correlation between the peak energies of the thermal and non-thermal components was reported [448].

It is interesting to note that at least some low-luminosity GRBs seem to have a somewhat different prompt emission spectrum. An intrinsic cutoff power law spectrum is found to correctly describe the joint *Swift* BAT/XRT prompt emission spectra of the low-luminosity GRB 060218 [60]. The  $E_p$  of this burst rapidly evolves with time from  $\sim 80$  keV to 5 keV, with an exponential tail or very steep power law above  $E_p$ . Since GRB 060218 is special in many aspects (e.g. nearby, low luminosity, supernova association, extremely long duration, existence of a thermal component that might be related to shock breakout), the prompt emission of this burst (and probably also of other nearby low-luminosity GRBs (e.g. [449]).

### 6.2.2. Spectral evolution

For bright bursts, time resolved spectral analysis give more clues about GRB prompt emission. We summarize several interesting features:

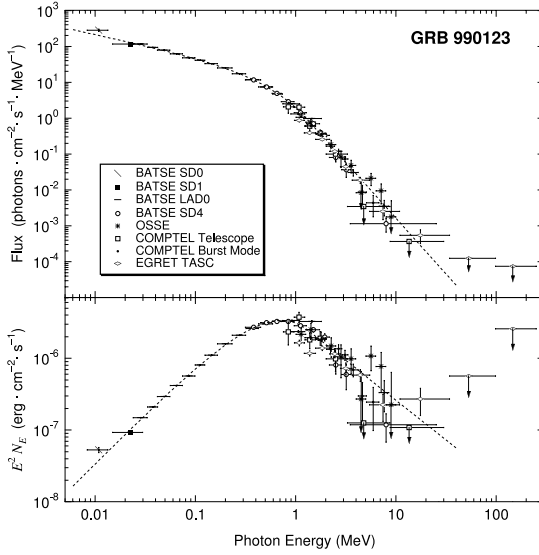


**Fig. 23.** A typical Band-function spectrum of GRB 990123.  
Source: From [432].

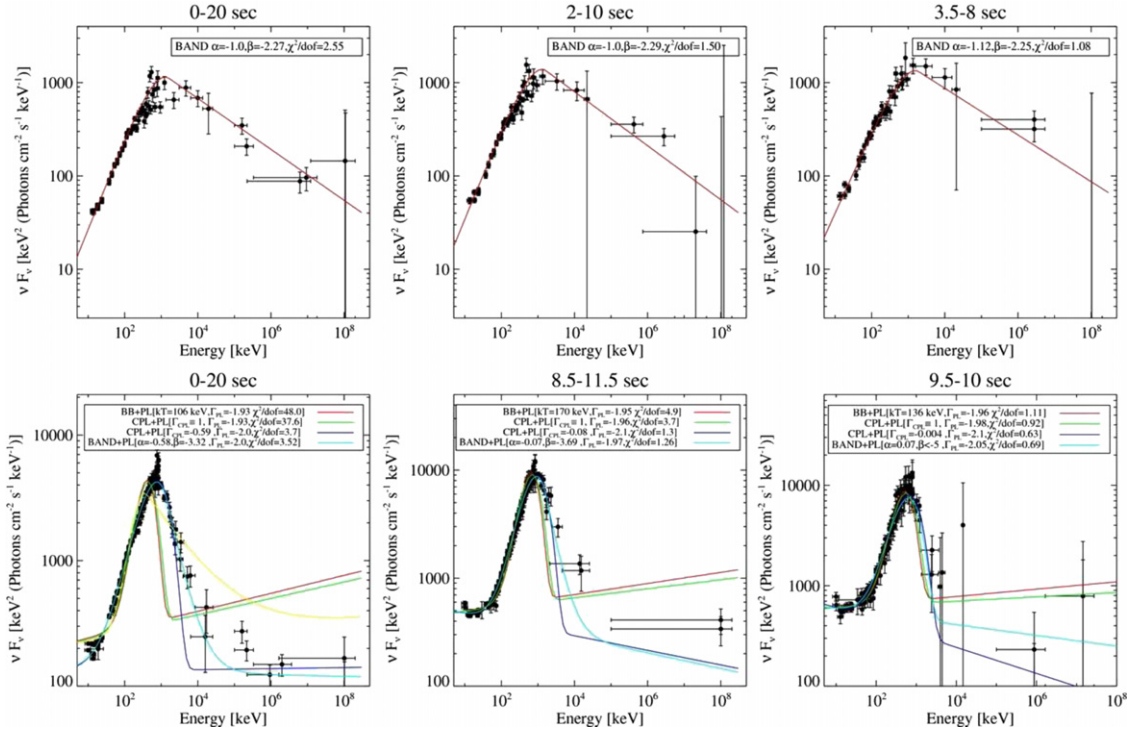


**Fig. 24.** Comparison between GRB 080916C that shows no evidence of spectral narrowing with reducing time bin, and GRB 090902B that shows clear spectral narrowing with reducing time bin.  
Source: From [103].

- Regarding the correlation between  $E_p$  and flux, it is found that in general there are two types of behaviors of GRB pulses. The first type shows a pattern of “hard-to-soft” evolution, which means that  $E_p$  is decreasing from the very beginning of the pulse (even during the rising phase of the pulse) [450]. The second type shows a “tracking” behavior: spectral hardness well tracks intensity ( $E_p$  increases during the rising phase of the pulse) [451]. Observationally, both types of behavior can be seen in a same burst [452,453], but see [454]. Considering a superposition effect, it is suggested that all pulses are consistent with having a “hard-to-soft” evolution [455].

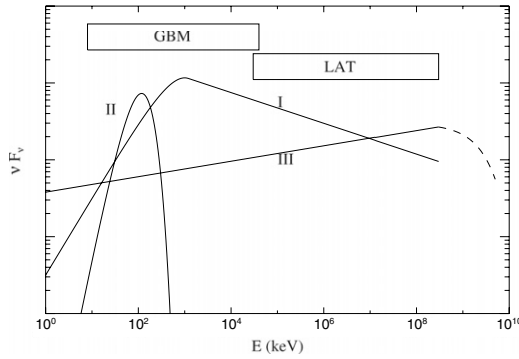


**Fig. 25.** The three possible elemental spectrum components that shape the observed time-resolved spectra of GRBs. Some components can be suppressed in some GRBs.

Source: Adapted from [103].

- In some bursts, e.g. GRB 080916C [99,103], there exists a trend of “opening” of the “Band” spectra. Initially, the spectrum is narrow with a relatively large  $\alpha$  and a relatively small  $\beta$ . However, this behavior is not representative in the 17 LAT GRB sample [103]. Most bursts do not show a clear pattern of evolution trend.
- A good fraction (but not all) of LAT GRBs show a delayed onset of GeV emission with respect to MeV emission as shown in Figs. 21 and 22 [99,359,101,103]. For GRB 080916C, the delayed onset may be related to hardening of  $\beta$  or the existence of a spectral cutoff early on [103]. For GRB 090902B and 090510, it may be related to the delayed onset of the power law component extending to high energies (component III). Several models have been suggested for the delayed onset of GeV emission [104,456,457,103,458,361,459–461], but it is unclear which of these mechanisms operates in GRBs.

### 6.3. Broad-band prompt emission

During the prompt phase, it is believed that there should be emission outside the triggering detectors’ bandpass window. Observationally it is very challenging to obtain a broad-band prompt emission spectrum. Nonetheless, current observations revealed a sparse picture.

In the high energy regime, Fermi/LAT observations so far suggest that most GRBs do not have significant emission beyond 100 MeV (e.g. [462,463]). Their prompt spectra are consistent with the extension of a Band-function spectrum to the GeV regime [103], sometimes with a possible spectral cutoff [102]. On the other hand, occasionally one does have bursts with a second component extending to high energies (e.g. GRB 090902B and GRB 090510, [100,101,103]). The hard component of these GRBs have a rising slope in their spectral energy distribution, suggesting that there could be more energy emitted above the LAT band. These sources can be ideal targets for ground-based 100 GeV–TeV detectors (e.g. [464,465]).

In the low energy regime, broad-band (optical to sub-MeV gamma-ray) spectra are available for several GRBs that had a precursor or a very long duration. Swift XRT and UVOT were able to slew to the source before the main burst arrives. Examples include GRB 060124 [466], GRB 060218 [60], and GRB 061121 [467]. For some other bursts, early optical observations were carried out by ground-based robotic telescopes during the prompt phase, which revealed interesting features. Examples include GRB 990123 [149], GRB 041219A [468,469], GRB 050820 [470], GRB 080319B [209,471], and GRB 110205A [472–474].

So far no burst, with the exception of GRB 130427A [475], has been simultaneously detected from optical all the way to GeV during the prompt phase.

Regarding the relation between the prompt optical and gamma-ray emissions, there are at least three patterns. The first pattern shows a clear offset between the optical flux peak and gamma-ray flux peaks. An example is GRB 990123, which showed an optical peak after all the gamma-ray peaks [149]. This suggests different physical origins of the two components. The standard interpretation is that gamma-rays come from the internal dissipation region (internal shocks or magnetic dissipation), while optical comes from the external reverse shock during the early deceleration of the ejecta by the ambient medium [150,151]. The second pattern shows a tracking behavior between the optical and gamma-ray lightcurves. It was seen in GRB 041219B with sparse time resolution in the optical data [469], and in the “naked-eye” GRB 080319B with high-quality optical and gamma-ray data [209,471] – see Fig. 26. Spectroscopically, although the optical fluxes are consistent with spectral extension of the gamma/X-ray fluxes in GRB 041219B [476], the optical fluxes in GRB 080319B clearly stand above the spectral extension of the gamma/X-ray fluxes, suggesting a distinct origin [209]. Leading models include attributing optical and gamma-ray emission to synchrotron and synchrotron self-Compton emission components, respectively [477,209], invoking two different emission sites [349,478], or two (reverse and forward) shocks in a pair of internal shocks [151,479]. The third pattern shows a mix of both (offset and tracking) components, as evidenced in GRB 050820 [470] and GRB 110205A [472]. Multiple emission sites have to be invoked to generate these components.

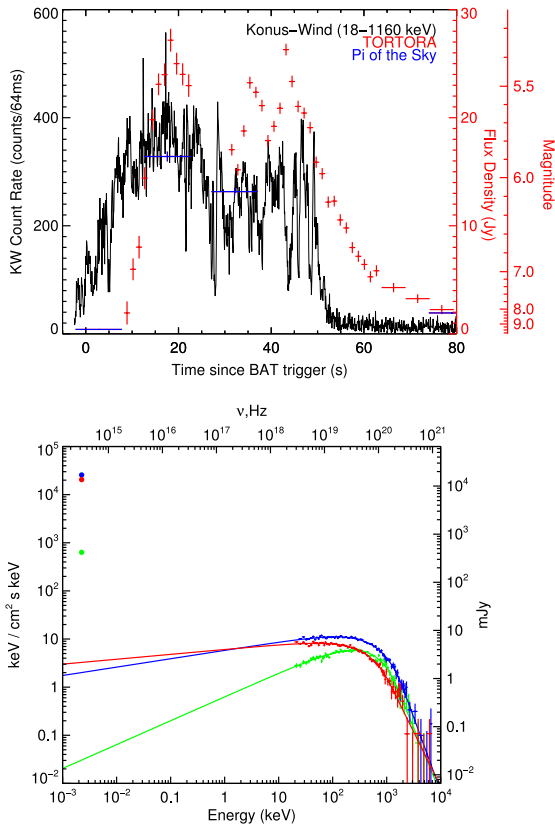


**Fig. 26.** Prompt optical and  $\gamma$ -ray lightcurves and spectra of the “naked-eye” GRB 080319B.  
Source: From [209].

#### 6.4. Polarization

Several claims have been made suggesting that the prompt  $\gamma$ -ray emission is linearly polarized with a large degree of polarization. An analysis of RHESSI data of GRB 021206 suggested a polarization degree  $\Pi = (80 \pm 20)\%$  [480], but the conclusion was refuted by an independent study [481]. Using the BATSE Albedo Polarimetry System (BAPS) data, [482] claimed of linear polarization degree  $\Pi > 35\%$  and  $\Pi > 50\%$  for GRB 930131 and GRB 960924, respectively. Two analysis of the INTEGRAL data of GRB 041219A led to evidence of linear polarization, but the significance is only marginal [483,484]. Recently, Yonetoku et al. [485] claimed detection of  $\Pi = (27 \pm 11)\%$  with  $2.9\sigma$  significance during the prompt emission of GRB 100826A using a GRB polarimeter on board a small solar-power-sail demonstrator IKAROS. They also reported strong polarization for two other bright GRBs [486].

Early polarization measurements were made for a handful of bursts in the optical band. Using a ring polarimeter on the robotic Liverpool Telescope, Mundell et al. [487] placed a  $2\sigma$  upper limit on  $\Pi$  of 8% for GRB 060418 at 203 s after trigger. The epoch coincides with the peak of the forward shock emission. The non-detection is consistent with the theoretical expectation, since the shocked ambient medium is not expected to carry significant ordered magnetic fields. Observation of another burst GRB 090102 by the same group [488] revealed a  $\Pi = (10 \pm 1)\%$  polarization around 160 s after trigger, and Uehara et al. [489] report a polarization of  $10.4 \pm 2.5\%$  for GRB 091208B between 149 s & 706 s after the burst trigger. These measurements suggest a possibly ordered magnetic field configuration. The polarization measurement for GRB 090102 was during the phase with relatively steep decay ( $F \propto t^{-\alpha}$  with  $\alpha = 1.50 \pm 0.06$ ) before breaking to a more normal decay phase ( $\alpha = 0.97 \pm 0.03$ ) after around 1000 s. The steep decay phase of the optical lightcurve is believed to be powered by the reverse shock heating of GRB ejecta, which could carry an ordered magnetic field, and that could account for the polarization measurement of Steele et al. [488]. The polarization measurement for GRB 091208B, however, was carried out during the phase when the lightcurve decayed with  $\alpha = 0.75 \pm 0.02$  and that suggests that the optical emission was probably produced in the external forward shock. Optical polarization for GRB 091208B has important implications for the generation of magnetic fields in relativistic shocks if FS origin is confirmed, e.g. [489]. Recently, Mundell et al. [490] reported evolution (decrease) of linear polarization degree in the early optical afterglow of GRB 120308A. This is consistent with the theoretical expectation of an early RS-dominated (with ordered magnetic field in the emission region) lightcurve which makes a transition to a FS-dominated lightcurve (which has a much lower polarization degree). Wiersema et al. [491] reported a circular polarization signature 0.15 days after GRB 121024, whose physical origin is unclear.

So far, no optical polarization observation is carried out during the prompt emission phase.

### 6.5. Isotropic luminosity function

The bolometric isotropic  $\gamma$ -ray energy of GRBs (usually  $1\text{--}10^4$  keV in the rest frame of the GRB), ranges from  $\sim 10^{49}$  to  $\sim 10^{55}$  erg. At the peak of the lightcurve, the isotropic  $\gamma$ -ray luminosity ranges from  $\sim 10^{47}$  to  $\sim 10^{54}$  erg s $^{-1}$ . For high-luminosity long-GRBs (typical ones), the luminosity function can be characterized as a broken power law of the following form

$$\Phi(L)dL = \Phi_0 \left[ \left( \frac{L}{L_b} \right)^{\alpha_1} + \left( \frac{L}{L_b} \right)^{\alpha_2} \right]^{-1} dL, \quad (101)$$

where the break luminosity  $L_b$  is  $\sim 10^{52.2}$  erg s $^{-1}$ . Several studies agree that the high-luminosity slope is steep:  $\alpha_2 \sim 2.5$  (e.g. [54,492,493]). The value of  $\alpha_1$  depends on whether one introduces a two-component (low-luminosity vs. high-luminosity) model. If one considers low-luminosity GRBs (those with luminosity below  $\sim 10^{48}\text{--}10^{49}$  erg s $^{-1}$ , typically with long durations, soft spectra, and single-peaked smooth lightcurves) as a separate population, which has a distinct bump in the luminosity function, then it is found that  $\alpha_1 \sim 0.5$  for the high-luminosity GRB component (e.g. [54,492]). On the other hand, if we include low-luminosity bursts to the GRB sample, then for the combined luminosity function  $\alpha_1 \sim 1.2$  [493].<sup>29</sup> The normalization  $\Phi_0$  depends on the local rate of GRBs per unit volume, which is constrained to be around  $1 \text{ Gpc}^{-3} \text{ yr}^{-1}$ .

Low-luminosity (LL) GRBs have a higher local event rate [494,54] which is inconsistent with a simple extrapolation of the high-luminosity GRB luminosity function to low luminosities, and they constitute a distinct class of objects [54,492,55,495]. The exact form of the LL-GRB luminosity function is not well constrained due to the limit of detectors' sensitivity.

The luminosity function of short-GRBs is also not well constrained because of the small sample size with redshift measurements. In order to be able to use short-GRBs with unknown redshifts to constrain the luminosity function, one needs to introduce an intrinsic redshift distribution of short GRBs, which is unknown. In practice, one can adopt the NS-NS or NS-BH merger model to provide an approximate  $z$ -distribution which can then be used to constrain the luminosity function [496,497]. Virgili et al. [497] show that compact binary star merger models cannot simultaneously reproduce all the observational data of short GRBs for both the  $z$ -known (Swift) and  $z$ -unknown samples. In these simulations, the short GRB luminosity function was assumed to take a form similar to the long-GRBs (broken power law), but the indices are left free parameters to be constrained by the data. The sample with known redshift demands a shallow luminosity function for short-GRBs with  $\alpha_1 < 0.4$ . This shallow luminosity function in turn usually translates to a shallow flux distribution, which is inconsistent with the BATSE data [497]. There are two possibilities to reconcile the inconsistency between theory and data. One is that there is a significant contribution of massive star bursts to the short-GRB sample. And the other is that the delay time scale since star formation for short GRBs to occur has a typical value of about 2 Gyr. Both conclusions are confirmed recently by Wanderman and Piran [498], who suggested that the typical delay time scale is closer to 3 Gyr.

### 6.6. Correlations between different observed parameters

Several observed parameters of the prompt  $\gamma$ -ray radiation are claimed to be correlated. In this section we summarize these correlations and comment on the ongoing debate of their validity.

#### 6.6.1. $E_{p,z}$ – $E_{\gamma,\text{iso}}$ (Amati) and $E_{p,z}$ – $L_{\gamma,\text{iso}}$ (Yonetoku) relations

Amati et al. [499] discovered that  $E_{p,z} \propto E_{\gamma,\text{iso}}^{1/2}$ , where  $E_{p,z} = E_p(1+z)$  is photon energy at the peak of the prompt spectrum in the rest frame of the GRB, and  $E_{\gamma,\text{iso}}$  is the isotropic gamma-ray energy spectrally extrapolated to a standard energy band in the GRB rest frame (usually 1 keV–10,000 keV). Numerically, this relation can be written as

$$\frac{E_{p,z}}{100 \text{ keV}} = C \left( \frac{E_{\gamma,\text{iso}}}{10^{52} \text{ erg}} \right)^m \quad (102)$$

with  $C \sim (0.8\text{--}1)$  and  $m \sim (0.4\text{--}0.6)$  [500]. This relation is found for long GRBs with known redshifts [499–501], which covers a wide range of  $E_{\gamma,\text{iso}}$  and  $E_{p,z}$  (from hard GRBs to low luminosity X-ray flashes) [502]. GRB 980425, a low luminosity GRB with supernova association (SN 1998bw), is a significant outlier of this relation.

Several groups have argued that the Amati-relation is an artifact of observational selection effects (e.g. [503–506]). Counter arguments suggest that selection effects cannot completely destroy the correlation [507]. In general, a positive correlation between  $E_{p,z}$  and  $E_{\gamma,\text{iso}}$  seems real, although the scatter may be wide.

<sup>29</sup> Notice that Wanderman and Piran [493] defined luminosity function as  $\Phi(L)d \log L$  instead of  $\Phi(L)dL$ . As a result, the two indices reported in that paper are systematically smaller by 1 than quoted here.

Similarly, a positive correlation between  $E_{p,z}$  and  $L_{\gamma,p,iso}$  has been reported [508,509]; where  $L_{\gamma,p,iso}$  is the isotropic gamma-ray luminosity of a burst at its peak flux. Adapted from the original form [509], this relation reads

$$\frac{E_{p,z}}{100 \text{ keV}} \simeq 1.8 \left( \frac{L_{\gamma,p,iso}}{10^{52} \text{ erg s}^{-1}} \right)^{0.52}. \quad (103)$$

This is also a correlation with broad scatter.

A  $E_p$ - $L_\gamma$  correlation also exists for the time resolved lightcurve of an individual GRB [510,501,453,447]. This behavior, at least partially, can be explained by the behavior of the falling phase of GRB pulses, during which emission clearly softens as flux decreases (e.g. [453,511]).

Short-GRBs do not fall onto long-GRB Amati-relation. They seem to form a parallel track above it. In other words, given the same  $E_{p,z}$ , short GRBs are systematically less energetic. This can be attributed to their shorter durations, which hints that luminosity may be more intrinsically related to  $E_{p,z}$ . Indeed, in the  $E_{p,z}$ - $L_{\gamma,p,iso}$  space, short and long GRBs are no longer clearly separated, suggesting that their radiation processes are similar [512,513,447,514].

#### 6.6.2. $E_{p,z}$ - $E_\gamma$ (Ghirlanda) relation

Assuming that the afterglow temporal breaks discovered in the pre-Swift era are jet breaks [24,25], Ghirlanda et al. [515] found a correlation between  $E_{p,z}$  and the geometrically-corrected gamma-ray energy

$$E_\gamma = \frac{E_{\gamma,iso}}{4\pi} \int_0^{\theta_j} 2 \times 2\pi \sin \theta d\theta = (1 - \cos \theta_j) E_{\gamma,iso} \simeq (\theta_j^2/2) E_{\gamma,iso}, \quad (104)$$

where  $\theta_j$  is the jet opening angle inferred from the afterglow temporal break time  $t_{obs,j}$ . The correlation (Ghirlanda relation), in its original form [515], reads

$$\frac{E_{p,z}}{100 \text{ keV}} \simeq 4.8 \left( \frac{E_\gamma}{10^{51} \text{ erg}} \right)^{0.7}, \quad (105)$$

which was claimed to be tighter than the Amati relation. In the Swift era, interpreting all the afterglow lightcurve breaks as jet breaks has been questioned. First, the jet-like breaks in X-ray lightcurves are either systematically earlier than the jet-like breaks in optical data [30,516] or no jet-break is detected in XRT observations [97,31]. Second, achromaticity, a required feature of jet breaks, is not commonly observed for these late time jet-like breaks [30]. Growing evidence suggests that the X-ray afterglow of a good fraction of GRBs might not originate from the external shock, and is likely powered by a long-lasting central engine [329,331,330,332,333,335]. The optical lightcurve may be still related to the external shock. So jet break time may be obtained for optically-identified breaks only.

#### 6.6.3. $E_{p,z}$ - $E_{\gamma,iso}$ - $t_{b,z}$ (Liang-Zhang) relation

Regardless of the interpretation of afterglow temporal breaks, Liang and Zhang [517] discovered a fundamental-plane correlation among  $E_{p,z}$ ,  $E_{\gamma,iso}$  and  $t_{b,z}$ , where  $t_{b,z} = t_{obs,b}/(1+z)$  is the afterglow lightcurve break time in the rest frame of the burst as measured in the *optical* band. In its original form, this relation reads

$$\frac{E_{p,z}}{100 \text{ keV}} \simeq 1.09 \left( \frac{E_{\gamma,iso}}{10^{52} \text{ erg}} \right)^{0.52} \left( \frac{t_{b,z}}{\text{day}} \right)^{0.64}. \quad (106)$$

Such an empirical correlation is not dependent on interpreting the break in the lightcurve to be jet-break.

#### 6.6.4. $E_{p,z}$ - $L_{\gamma,iso}$ - $T_{0.45}$ (Fermani) relation

With prompt emission parameters only, [518] discovered another three-parameter correlation

$$\frac{E_{p,z}}{100 \text{ keV}} \simeq 1.37 \left( \frac{L_{\gamma,iso}}{10^{52} \text{ erg s}^{-1}} \right)^{0.62} \left( \frac{T_{0.45,z}}{10 \text{ s}} \right)^{-0.30}. \quad (107)$$

Here  $T_{0.45,z} = T_{0.45}/(1+z)$ , and  $T_{0.45}$  is the time spanned by the brightest 45% of the total counts above the background. Traditionally, the burst duration is defined by  $T_{90}$  (or  $T_{50}$ ), the time interval within which 90% (or 50%) of the burst fluence is detected. The main difference between  $T_{0.45}$  and  $T_{90}$  ( $T_{50}$ ) is that the former deducts any quiescent period that may exist during the burst, and therefore better represents the duration of the emission episode of a burst. The 45% percentage has no physical significance, which was adopted to achieve the most significant correlation.

### 6.6.5. $E_{\gamma,\text{iso}}-\theta_j$ (Frail) relation: constant energy reservoir

Frail et al. [26] found that the measured jet opening angle  $\theta_j$  of early GRBs seem to be anti-correlated to  $E_{\gamma,\text{iso}}$  through  $E_{\gamma,\text{iso}} \propto \theta_j^{-2}$ . This led to an interesting conclusion that the jet corrected gamma-ray energy  $E_{\gamma} \simeq (\theta_j^2/2)E_{\gamma,\text{iso}}$  is roughly constant for all GRBs. The correlation was confirmed by a later study [200], with  $E_{\gamma}$  tightly clustered around  $\sim 10^{51}$  erg. Replacing  $E_{\gamma,\text{iso}}$  by isotropic kinetic energy of the afterglow, Panaitescu and Kumar [37] and [28] found that  $E_K \simeq (\theta_j^2/2)E_{\gamma,\text{iso}}$  is also roughly constant. The implication is that long GRBs have a standard energy reservoir. Wider jets have low energy concentration, while narrow jets have high energy concentration. Alternatively, this may be understood as a universal [195,194] or quasi-universal [196] jet for all GRBs, with the measured jet break defined by observers' viewing angle wrt the jet-axis.

In the Swift era, the Frail relation is found no longer tightly clustered. Both  $E_{\gamma}$  and  $E_K$  are found to have a much wider distribution than the pre-Swift sample [30,516,31]. The Ghirlanda relation discussed above is in conflict with the Frail relation: instead of having  $E_{\gamma}$  as a constant, the former relation suggests a correlation between  $E_{\gamma}$  and  $E_{p,z}$ .

### 6.6.6. Luminosity-spectral lag ( $L-\tau$ ), Norris relation

Norris et al. [428] discovered an anti-correlation between GRB peak luminosity and the delay time (lag),  $\tau$ , for the arrival of low energy photons (25–50 keV) compared with photons of higher energies (100–300 keV and  $>300$  keV) for a sample of BATSE GRBs. In its original form, it is written as

$$\frac{L_{\gamma,p,\text{iso}}}{10^{53} \text{ erg s}^{-1}} \simeq 1.3 \left( \frac{\tau}{0.01 \text{ s}} \right)^{-1.14}, \quad (108)$$

where  $\tau$  is measured in the observed frame. Several groups have later investigated this correlation by considering the lags in the burst rest frame. One way is to correlate  $L_{\gamma,p,\text{iso}}$  with  $\tau/(1+z) \times (1+z)^{0.33} = \tau/(1+z)^{0.67}$  [519,512]. By doing so, one has assumed that spectral lag is proportional to the pulse width  $w$  (which has an energy dependence of  $\sim 0.33$  power). This is valid for individual pulses. For complex bursts with overlapping pulses, Ukwatta et al. [520] argued that it is more appropriate to investigate a correlation between  $L_{\gamma,p,\text{iso}}$  and  $\tau_z = \tau/(1+z)$ . They gave

$$\log \left( \frac{L_{\gamma,p,\text{iso}}}{\text{erg s}^{-1}} \right) = (54.7 \pm 0.4) - (1.2 \pm 0.2) \log \frac{\tau_z}{\text{ms}} \quad (109)$$

for the lag defined between 100–150 keV and 200–250 keV energy bands in the rest frame of the GRB source.

There are significant outliers in the luminosity-spectral lag correlation. It seems that even though the low-luminosity GRB 060218 may be moderately accommodated within the correlation [521], several other low luminosity GRBs (e.g. GRB 980425, GRB 031203) and the supernova-less long GRBs (060614 and 060505) all lie well below the correlation [519,522,512]. All short-GRBs have negligible lags [431], and do not follow the correlation.

### 6.6.7. Luminosity-variability ( $L-V$ ) relation

Fenimore and Ramirez-Ruiz [523] and Reichart et al. [524] proposed a correlation between the GRB luminosity and the complexity of GRB lightcurves which they parametrize as “variability”  $V$ . The definition of variability depends on how the smoothed background lightcurve is defined, and can be technically very different among authors. In any case, a positive correlation  $L_{\gamma,p,\text{iso}} \propto V^m$  with large scatter was found, although the index  $m$  ranges from 3.3 [524] to 1.1 [525].

### 6.6.8. $E_{\gamma,\text{iso}}-\Gamma$ and $L_{\gamma,\text{iso}}-\Gamma$ relations

A sample of GRBs has high-quality early optical afterglow data collected. A good fraction of them show an early hump in the lightcurve, which is consistent with being due to deceleration of the blastwave. Assuming such an interpretation, the Lorentz factor  $\Gamma$  of a moderate sample of GRBs was measured. Liang et al. [179] discovered a positive correlation between  $\Gamma$  and the isotropic gamma-ray energy  $\Gamma \propto E_{\gamma,\text{iso}}^a$ , with  $a \sim 1/4$ . The positive correlation was verified by Ghirlanda et al. [454] and Lü et al. [526]. Lü et al. [526] further discovered a similar correlation between  $\Gamma$  and mean isotropic gamma-ray luminosity  $L_{\gamma,\text{iso}}$ , i.e.  $\Gamma \propto L_{\gamma,\text{iso}}^b$ , with  $b$  also close to 1/4. Lei et al. [527] interpret the correlation within the framework of both a neutrino-cooling dominated accretion flow model and a Blandford-Znajek model for GRB central engine, whereas Fan et al. [528] and Lazzati et al. [529] suggest that the photospheric model for prompt  $\gamma$ -ray radiation can explain this and other correlations.

## 6.7. GRB cosmography

An exciting prospect of having a tight GRB correlation is to apply it to measure the geometry of the universe. Since GRBs are typically observed at a much higher redshift than the “standard candle” SN Ia, they can potentially extend the Hubble diagram to higher redshifts. This would lead to improvements in the determination of cosmological parameters, and in particular help explore the nature of dark energy. The difficulty has been to find a tight enough GRB correlation to conduct such an exercise.

Early efforts in this direction made use of some not-too-tight correlations (e.g. the  $L - \tau$  and  $L - V$  correlations by [530] and the Frail correlation by Schaefer [200]) to construct the GRB Hubble diagram. Since these correlations have large scatter,

the data cannot place meaningful constraints on cosmological parameters. A step forward was after the tight Ghirlanda-relation [515] was discovered. Dai et al. [531], Ghirlanda et al. [532] and Xu et al. [533] show that GRBs can serve as a tool to conduct cosmography, and the constrained cosmological parameters (even if with large errors) are broadly consistent with the  $\Lambda$ CDM model supported by the combined SN Ia and WMAP-CMB data. Another correlation with claimed similar tightness is the Liang-Zhang relation. Applying this relation to the cosmography study, Liang and Zhang [517] found constraints on cosmological parameters similar to the one obtained using the Ghirlanda relation. Later, Amati and collaborators suggested that the Amati-relation can also be used for the purpose of constraining cosmological parameters (e.g. [534]); see [535] for a review.

We would like to point out two serious limitations we face today when using GRBs for cosmography. First, due to the *intrinsic* dispersion of the GRB correlations (no clean physics behind the correlations unlike the Chandrasekhar limit behind the SNe Ia physics), the GRB candle is much less standard than the SN Ia candle. The efforts using GRB data alone have so far led to much poorer constraints on the cosmological parameters than other well known methods (e.g. SNe Ia and CMB). On the other hand, the advantage of GRBs is that they can be detected at much higher redshifts than SNe Ia, so they can potentially be used to measure how the dark energy evolves with redshift. For example, Schaefer [536] applied multiple correlations to construct the Hubble diagram of 69 GRBs in the redshift range from 0.17 to  $>6$ , and obtained consistency with the concordance  $\Lambda$ CDM model without invoking dark energy evolution. Second, it is not easy to calibrate GRB candles using GRB data alone. A robust calibration (e.g. for SNe Ia) requires a low- $z$  sample. However, the nearby GRBs tend to have a much lower luminosity than their cosmological cousins [56,60], and likely form a distinct population [54]. Their detected number is also low. One suggested method is to consider bursts in a narrow redshift bin to partially calibrate the correlation [537,538]. This can well calibrate the indices of the correlation, but the normalization parameter still depends on the adopted cosmological parameters, and can be only “marginalized”. A more practical method of calibration is to make use of the SN Ia data [539,540]. Taking GRBs in the same redshift range as SN Ia, one can use the distance moduli of SNe Ia and assign them to GRBs at the same redshifts, and then give a cosmology-independent calibration to the GRB candles. The derived cosmological parameters using the calibrated candles are again found consistent with the concordance model [539].

## 7. Progress toward understanding GRB prompt radiation

The origin of the prompt  $\gamma$ -ray emission from GRBs is not well understood. This is due in large part to our lack of knowledge of jet composition, energy dissipation and particle acceleration mechanisms. A widely used model is the matter-dominated “fireball”, which consists of baryons (primarily protons and neutrons), electron & positron pairs, and photons. A fireball could be produced in cataclysmic events such as mergers of binary neutron stars [78] or collapses of massive stars [38]. The energy in radiation is initially larger than in baryons (including baryon rest mass) by a factor of about  $10^2$ , and as the fireball expands, baryons get accelerated to a high Lorentz factor. According to this model, a fraction of the initial thermal energy of the fireball is radiated away at the photosphere, and at a larger radius internal shocks tap into the kinetic energy of the jet to accelerate electrons which produce non-thermal  $\gamma$ -rays via the synchrotron and inverse-Compton processes.

Alternatively, the outflow launched from the GRB central engine might be Poynting-flux-dominated (e.g. [541–543, 107,108]). In this case, jet acceleration, dissipation and particle acceleration are harder to calculate, and the model lacks predictive power due to our limited understanding of these processes.

This section provides an overview of GRB prompt emission models. The structure of the section is as follows:

- We begin with a quantitative description of the standard hot fireball model for GRBs (Section 7.1). We discuss the dynamics of fireball evolution as well as the photospheric radiation properties. Observational constraints on the distance of the  $\gamma$ -ray emission region from the center of explosion are presented in Section 7.2.
- Next, the internal shock model is discussed in detail. The topics include conversion of the kinetic energy of the outflow to thermal energy and the efficiency for producing radiation (Section 7.3), the difficulty of reproducing the observed spectrum (Sections 7.4 and 7.5) as well as a critical assessment of several recent models that have been proposed to explain the nearly flat spectrum ( $f_\nu \propto \nu^0$ ) below the peak.
- For a GRB jet consisting of protons and neutrons, a fraction of the outflow kinetic energy is converted to thermal energy and radiation when these particles undergo collisions near the photosphere. Whether this process can explain the GRB prompt radiation is taken up in Section 7.7.
- A more general discussion of photospheric radiation, including multiple IC scatterings and its application to GRBs is discussed in Section 7.8. The hadronic model for the generation of prompt  $\gamma$ -ray radiation is analyzed in Section 7.9.
- Finally, analytical calculations for the acceleration and dissipation of Poynting jets are discussed in Section 7.10. Numerical simulations on magnetic reconnection and particle acceleration are also reviewed in that section.

Our emphasis is on providing physical insights, and not on rigorous mathematical derivations, and thus we will make numerous approximations that simplify calculations while focusing on the important physical concepts underlying various derivations and estimates throughout this section.

## 7.1. Hot fireball model

One of the widely discussed models for GRBs is the so called hot fireball model. This model was suggested in its currently used form<sup>30</sup> by Paczynski [45] and Goodman [46] when Paczynski realized that GRBs might be at cosmological distances and therefore have luminosity of  $\sim 10^{51}$  erg s $^{-1}$  produced within a small volume of radius  $\lesssim 10^7$  cm (from lightcurve variability) and hence a temperature of  $\sim 10^{10}$  K so that electron–positron pairs coexist with photons in thermal equilibrium. The energy per proton according to the hot fireball model is of order 10<sup>2</sup> GeV; much of this energy is initially in photons, relativistic  $e^\pm$  pairs, and neutrinos. The radius where the fireball is produced is set by the size of the compact object formed in these explosions which is believed to be either a black hole or a millisecond magnetar.<sup>31</sup> As the fireball undergoes adiabatic expansion, the energy of photons and  $e^\pm$ s is transferred to protons which are accelerated to a high Lorentz factor [545]. The kinetic energy of the outflow is converted back to thermal energy and radiated away as  $\gamma$ -ray photons at some large distances from the place where the fireball is produced [33,35,98].

The dynamical evolution of a fireball during the acceleration phase has been studied analytically [545–547,111,548], as well as numerically [549].

We describe in this subsection the fireball dynamics and the conversion of kinetic energy to radiation via collision between fast and slow parts of the outflow. The main results for the fireball dynamics are shown in Fig. 28.

### 7.1.1. Dynamics of a hot fireball

Consider an outflow of luminosity  $L$  and initial radius  $R_0$  that is related to the size of the compact object (black hole or a rapidly rotating neutron star) formed in these explosions. The initial temperature of the fireball is

$$k_B T_0 \approx k_B \left[ \frac{L}{4\pi R_0^2 g_0 \sigma_B} \right]^{1/4} = (1.3 \text{ MeV}) L_{52}^{1/4} R_{0.7}^{-1/2}, \quad (110)$$

where  $k_B$  &  $\sigma_B$  are Boltzmann and Stefan–Boltzmann constants, and  $g_0 = 2.75$  is half of the effective degrees of freedom for a plasma consisting of photons, electrons & positrons in thermal equilibrium<sup>32</sup>; we are continuing to use the notation  $X_n \equiv X/10^n$ .

The Lorentz factor of the fireball undergoing adiabatic expansion increases linearly with radius as long as the energy in radiation per baryon is larger than  $\sim m_p c^2$ , and the fireball is optically thick to Thomson scattering.

The fireball dynamics is described by conservation of energy flux and entropy. We describe the process as viewed in an inertial frame at rest in the GRB host galaxy. Hereafter we call this rest frame as the “CoE frame”, sometimes also called the “lab frame” or “cosmic proper frame”. Let us consider a spherical shell of radius  $r$  and width  $\delta r$  in the CoE frame (the width in the comoving frame is  $\delta r'$ ; see Fig. 27). The comoving temperature of the shell is  $T'(r)$ , and its Lorentz factor is  $\Gamma(r)$ . Its luminosity in the CoE frame does not change as the shell expands to larger radius, and is given by

$$L = 4\pi r^2 g(r) \sigma_B T'^4(r) \Gamma^2(r). \quad (111)$$

Moreover, the entropy contained in the shell is

$$s = 4\pi r^2 (\delta r') g(r) T'^3 \quad (112)$$

which is a frame independent, and a conserved quantity for an adiabatically expanding shell (ignoring the initial decrease due to neutrino loss).

The width of the shell in the CoE frame does not change much with  $r$  since the front and the back surfaces of the shell move close to the speed of light and their relative speed is small. However, the shell-width in the comoving frame, which is given by  $\delta r' = \Gamma \delta r$ , does change with radius as the shell expands and its LF increases.

The equation for the conservation of entropy (Eq. (112)) can be solved for comoving temperature

$$T' = T_0 (R_0/r)^{2/3} (g_0/g)^{1/3} \Gamma^{-1/3}, \quad (113)$$

where  $g_0 \equiv g(R_0)$ . Substituting this into Eq. (111) we find

$$\Gamma(r) = (r/R_0)(g/g_0)^{1/2}, \quad (114)$$

and we can solve for  $T'$  by eliminating  $\Gamma$  from Eq. (113)

$$T'(r) = T_0 (r/R_0)^{-1} (g_0/g)^{1/2}. \quad (115)$$

<sup>30</sup> The fireball model in the context of GRBs and some consequences of high opacity due to electron–positron pairs produced by MeV photon collisions were described by Cavallo and Rees [544] well before the work of Paczynski [45] and Goodman [46].

<sup>31</sup> A magnetar is a neutron star with magnetic field of strength much larger than a typical pulsar. The surface field of a magnetar is of order 10<sup>14</sup> G or larger.

<sup>32</sup> Initially, at radius  $R_0$ , the temperature is larger than 1 MeV so that electrons, positrons, and electron neutrinos are readily created. However, neutrinos fall out of thermal equilibrium when the fireball radius is just a little larger than  $R_0$  and hence are not counted toward the effective degree of freedom for particles in thermal equilibrium. Each Fermion internal degree of freedom – spin state – contributes 7/8 of a Bosonic degree of freedom, so the total for a  $e^\pm$  and photon plasma comes out to be 5.5. The 2 degree of freedom for photons is already included in the radiation constant  $\sigma_B$ , hence  $g_0 = 5.5/2 = 2.75$ .

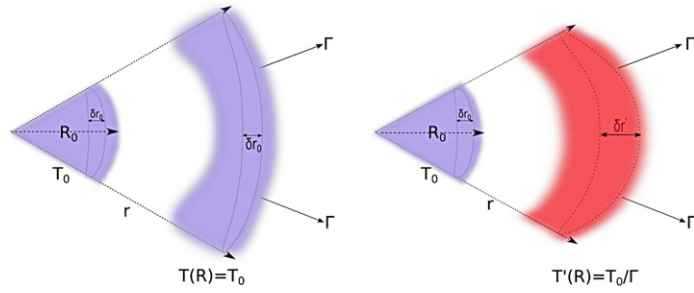


**Fig. 27.** Fireball dynamics in lab frame is shown in the left panel and in the shell comoving frame (right panel). Shown here is a small section of the fireball of initial radial width  $\delta R_0$  at two different times when it was at radius  $R_0$  and  $r$ . Its LF when at radius  $R_0$  was  $\sim 1$ , and hence its radial widths in the lab and comoving frames were the same. At a later time when at radius  $r$  its LF increased to  $\Gamma$  and its comoving temperature decreased by a factor  $\Gamma$ .

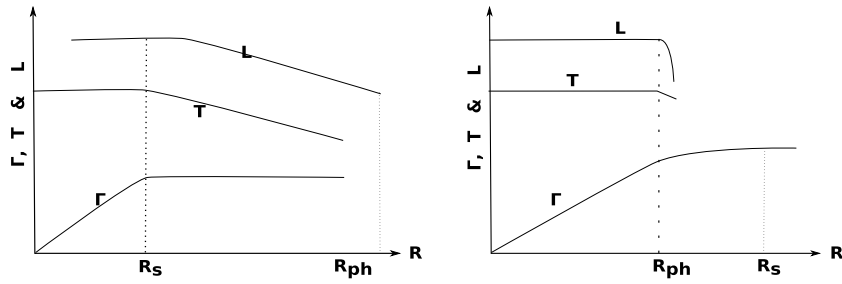


**Fig. 28.** Lorentz factor ( $\Gamma$ ), temperature ( $T$ ) and thermal luminosity  $L$  (in observer frame) are shown schematically as a function of fireball radius for the case where  $\eta \lesssim 10^3$  so that the photosphere ( $R_{ph}$ ) lies above the saturation radius  $R_s = \eta R_0$  (left panel).  $\Gamma$ ,  $T$  &  $L$  for the case where  $\eta \gtrsim 10^3$ , so that  $R_{ph} < R_s$ , is shown in the right panel;  $\Gamma$ ,  $T$  &  $L$  in this case have the same dependence on  $R$  for  $R < R_{ph}$  as shown in the first segment of the left panel, however, the outflow fails to attain the asymptotic LF of  $\eta$  in this case (the slight increase of  $\Gamma$  for  $R > R_{ph}$  is due to Compton drag on electrons by photons streaming to larger radius). The time dependence of the observed thermal luminosity and temperature, after a brief transient period, mirrors temporal fluctuations of the thermal fireball (or outflow) at its base at  $R_0$ .

The Lorentz factor continues to increase as  $\Gamma \propto r$  as long as energy in photons per baryon in the comoving frame ( $3k_B T' n_\gamma$ ) is larger than  $mc^2$  & the system is optically thick to Thomson scattering so that photons and particles are coupled. The terminal value of the Lorentz factor is

$$\Gamma_s = \frac{L}{\dot{M}c^2} \equiv \eta, \quad (116)$$

which is attained at the radius

$$R_s \sim R_0 \Gamma_s \quad (117)$$

provided that the fireball remains optically thick to Thomson scattering at  $R_s$ ;  $\dot{M}$  is the baryonic mass flux associated with the outflow. We will see toward the end of this sub-section that for  $\eta \gtrsim 10^3$  the fireball becomes optically thin before attaining  $\Gamma_s \sim \eta$ .

The optical depth is dominated by  $e^\pm$  when  $\eta \gtrsim 10^6$ , and in this case the system becomes transparent to photons when  $T'$  drops to about 20 keV and pairs annihilate. The number density of electron–positron pairs, in the comoving frame of the outflow, at temperature  $T'$  is

$$n'_\pm = \frac{2(2\pi k_B m_e T')^{3/2}}{h^3} \exp(-m_e c^2/k_B T'), \quad (118)$$

where  $m_e$  is electron mass &  $h$  is Planck's constant. The cross-section for pair annihilation is

$$\sigma_{e^\pm \rightarrow 2\gamma} = \frac{\sigma_T}{\langle v/c \rangle} \quad (119)$$

where  $\langle v \rangle$  is the mean speed of  $e^\pm$ , and  $\sigma_T$  is Thomson scattering cross-section. Thus, the comoving frame time for a positron to annihilate with an electron is

$$t'_{e^\pm \rightarrow 2\gamma} = \frac{2}{\sigma_{e^\pm \rightarrow 2\gamma} n'_\pm \langle v \rangle} \approx \frac{2}{\sigma_T n'_\pm c}, \quad (120)$$

where the factor 2 in the numerator is due to the fact that the number density of electrons =  $n'_\pm/2$  (ignoring the contribution of electrons associated with baryons). The process of pair annihilation/creation freezes when  $t'_{e^\pm \rightarrow 2\gamma}$  becomes of order the

dynamical time  $\sim r/c\Gamma(r)$ . From the above equation we see that the  $e^\pm$  freeze-out radius is the same as the Thomson-photospheric radius when the baryon loading is negligible, i.e. when the electron density is not much larger than  $n'_\pm/2$  given by Eq. (118). If the freeze-out were to occur during the acceleration phase of the jet then  $\Gamma(r)/r \sim 1/R_0$ , and in that case

$$\sigma_T n'_\pm R_0 \sim 2, \quad \text{or} \quad n'_\pm \sim 2/(\sigma_T R_0). \quad (121)$$

Substituting for  $n'_\pm$  from Eq. (118) we find

$$T'^{3/2} e^{-\frac{5.9 \times 10^9}{T'}} \approx 62 R_{0.7}^{-1}. \quad (122)$$

The solution of this equation is  $T'_{\text{freeze}} \approx 20.5$  keV. The fireball Lorentz-factor at the freeze-out can be obtained using Eqs. (115) and (114) and is

$$\Gamma_{\text{freeze}} \sim T(R_0)/T'_{\text{freeze}} \sim 64, \quad (123)$$

independent of the  $g$ -value, and the radius where the freeze-out occurs is

$$R_{\text{freeze}} \sim R_0 \Gamma_{\text{freeze}} (g_0/g)^{1/2} \sim 1.7 R_0 \Gamma_{\text{freeze}}. \quad (124)$$

For the last part of the above equation we took  $g = 1$  since at this radius the entropy is dominated by photons. The Lorentz factor of the fireball can continue to increase by another factor of  $\sim 2$  due to Compton drag [546].

Let us next consider the effect of a non-zero baryon component on the jet dynamics, and determine the criterion when the fireball dynamics is significantly affected by baryon contamination.

The number density of electrons associated with protons can be obtained from the equation for mass outflow,  $\dot{M}$ ,

$$n'_p = \frac{\dot{M}}{4\pi r^2 m_p c \Gamma} = \frac{L}{4\pi r^2 m_p c^3 \eta \Gamma} \quad \text{where } \eta \equiv \frac{L}{\dot{M} c^2}. \quad (125)$$

Therefore, the number density at  $R_{\text{freeze}}$  is

$$n'_p = \frac{L}{4\pi R_0^2 m_p c^3 \eta \Gamma_{\text{freeze}}^3}. \quad (126)$$

The fireball dynamics beyond  $R_{\text{freeze}}$  is dominated by electrons associated with protons when

$$n'_p(R_{\text{freeze}}) > n'_\pm(R_{\text{freeze}}) \sim \frac{2}{\sigma_T R_0}. \quad (127)$$

Or using Eqs. (126), (127), (110) and (123) we find

$$\eta < \frac{L \sigma_T}{8\pi R_0 m_p c^3 \Gamma_{\text{freeze}}^3} \sim 2 \times 10^6 L_{52}^{1/4} R_{0.7}^{1/2}. \quad (128)$$

Whenever this condition is satisfied – which is likely for most GRBs – the jet continues to accelerate for  $r > R_{\text{freeze}}$  until  $\Gamma(r) \sim \eta$  or the outflow reaches the Thomson photospheric radius (whichever comes first).

The Thomson scattering optical depth for a photon at radius  $r$  is

$$\tau_T = \int \frac{dr_1}{c} (c - v) \sigma_T n_p \approx \int \frac{dr_1}{2\Gamma^2} \sigma_T n_e \approx \sigma_T n'_p(r/2\Gamma) \approx \frac{L \sigma_T}{8\pi r m_p c^3 \eta \Gamma^2}, \quad (129)$$

where we made use of Eq. (125) for electron density. Therefore, the photospheric radius, where  $\tau_T = 1$ , is

$$R_{ph} \approx (5.5 \times 10^{12} \text{ cm}) L_{52} \eta_2^{-1} \Gamma_2^{-2}. \quad (130)$$

The Lorentz factor stops increasing when the outflow reaches the photosphere, if not before, since at this radius photons decouple from electrons and start streaming freely.<sup>33</sup> Thus, the maximum possible value for Lorentz factor that can be attained in a hot-fireball is when  $R_{ph} \sim \eta R_0$  or

$$\eta_* \equiv \Gamma_{\text{max}} \sim 8.5 \times 10^2 L_{52}^{1/4} R_{0.7}^{-1/4}. \quad (131)$$

The most energetic Fermi bursts from which >GeV photons have been detected approach this theoretical limit on Lorentz factor.<sup>34</sup> For  $\eta > \eta_*$  only a fraction of the initial photon energy of the fireball is imparted to baryons.

<sup>33</sup> Some additional acceleration above the photosphere can occur by outward streaming photons dragging electrons along for a while [546].

<sup>34</sup> The Fermi LAT team published lower limits of  $\Gamma$  for a few bright LAT GRBs, which approach 1000 [99–101], and are much larger than the constrained  $\Gamma$  from other GRBs using other methods [550]. However, these constraints were based on a simple one-zone model with the emission site defined at the internal shock radius  $R_{IS} \sim \Gamma^2 c \Delta t_{\text{min}}$ , which could be an over-estimate if the emission region is not at  $R_{IS}$  [551,442], or when more sophisticated analysis are carried out [552–555].

### 7.1.2. Photospheric radiation

When  $\eta > \eta_* \sim 10^3$  – the limit given by Eq. (131) – the Thomson photosphere lies within the acceleration zone of the outflow, and the emergent thermal radiation from the photosphere is

$$L_{th} = 4\pi R_{ph}^2 \sigma_B T'(R_{ph})^4 \Gamma(R_{ph})^2 \sim 4\pi R_0^2 \sigma_B T_0^4 \sim L, \quad (132)$$

which is of order the central engine luminosity ( $L$ ); in deriving this result we made use of the scalings  $\Gamma(R_{ph}) \sim R_{ph}/R_0$  (Eq. (114)) and  $T'(R_{ph}) \sim T_0 R_0/R_{ph}$  (Eq. (115)). The observed peak of the thermal flash is at a temperature  $T'(R_{ph}) \Gamma(R_{ph})/(1+z) \sim T_0/(1+z) \sim [1.3/(1+z)\text{MeV}] L_{52}^{1/4} R_{0.7}^{-1/2}$  (see Eq. (110)). This radiation lasts for as long as the central engine is active.

For  $\eta \lesssim 10^3$ , the Thomson photosphere lies outside the acceleration zone of the outflow, and the emergent thermal luminosity is smaller than  $L$ . The temperature continues to decrease, due to adiabatic cooling, beyond the saturation radius as

$$T(r) \sim T_0 (R_s/r)^{2/3}, \quad (133)$$

since the comoving volume of a shell increases with radius as  $r^2$  when the Lorentz factor of the shell stops increasing with distance;  $R_s$  is the saturation radius given by Eq. (117). The observed thermal luminosity while the jet head is between  $R_s$  &  $R_{ph}$  varies as  $r^{-2/3}$  (Fig. 28). Once the jet crosses  $R_{ph}$ , the photospheric luminosity is given by (e.g. [111,556])

$$L_{th} = 4\pi R_{ph}^2 \sigma_B T'(R_{ph})^4 \Gamma(R_{ph})^2 \sim L (R_s/R_{ph})^{2/3} \sim L R_{0.7}^{2/3} L_{52}^{-2/3} \eta_3^{8/3}. \quad (134)$$

This equation is valid only when  $\eta < \eta_*$ ; for  $\eta > \eta_*$ ,  $L_{th} \sim L$ . The strong dependence of thermal luminosity on  $\eta$  is due to the fact that the photospheric radius scales as  $\eta^{-3}$  and the saturation radius ( $R_s$ ) increases as  $\eta$ , and therefore the thermal luminosity – which scales as  $(R_{ph}/R_s)^{-2/3}$  – decreases rapidly with decreasing  $\eta$ . The peak of the thermal spectrum in the observer frame, when the jet becomes optically thin at  $r = R_{ph}$ , for  $\eta < \eta_*$ , is

$$\hbar v_{th} \sim 3k_B T'(R_{ph}) \Gamma(R_{ph})/(1+z) \sim \left( \frac{4\text{MeV}}{1+z} \right) L_{52}^{-5/12} R_{0.7}^{1/6} \eta_3^{8/3}, \quad (135)$$

which was obtained by making use of  $T'(R_s) \Gamma(R_s) \sim T_0$ ,  $T(R_{ph}) \sim T(R_s) (R_s/R_{ph})^{-2/3}$  and Eq. (110) for  $T_0$ . For  $\eta > \eta_*$ , the observed peak is at  $\sim 3k_B T_0$ . The observed specific flux at the peak of the spectrum is obtained from Eqs. (134) and (135), and is given by,

$$f_p^{th} \sim \frac{L_{th}}{4\pi d_L^2 v_{th}} \sim \frac{L(1+z)}{4\pi d_L^2 (3k_B T_0/h)} \sim [1 \text{ mJy}] (1+z) L_{52}^{3/4} d_{L28}^{-2} R_{0.7}^{1/2}. \quad (136)$$

The emergent specific flux at the peak of the thermal spectrum is approximately 1 mJy, which is independent of the highly uncertain value of  $\eta$  and weakly dependent on jet luminosity  $L$ , and should be detectable by a telescope observing in a band that includes  $v_{th}$ ; we should point out that the observed non-thermal emission between 10 keV and  $\sim 1$  MeV for a typical GRB is also of order 1 mJy. An observational campaign designed to look for this thermal component<sup>35</sup> between optical and  $\gamma$ -ray frequencies would help determine the baryonic content of GRB jets. For instance, if a thermal component with peak flux of a few mJy is not found between 1 eV and 1 MeV, then that would suggest that  $\eta < 5$ . Since this would contradict a vast amount of data that suggests  $\Gamma \gtrsim 10^2$  [148,559,160,177,99,100,179] – and therefore  $\eta \gtrsim 10^2$  – the non-detection of a thermal component would imply that the GRB jet was launched with a relatively small radiation component thereby strengthening the case for a Poynting outflow (e.g. [560,442]). On the other hand, a detection of thermal signal and measurement of  $v_{th}$  would help us determine the amount of baryonic matter in GRB jets;  $v_{th}$  depends primarily on  $\eta$  (Eq. (135)) and has a weak dependence on  $L$  and  $R_0$  as long as photons are not created or processed between  $R_0$  and the photosphere.

## 7.2. Distance from the central engine where $\gamma$ -rays are produced

We describe in this sub-section various constraints on the distance from the center of explosion,  $R_\gamma$ , where  $\gamma$ -ray emission is generated. Four different ideas have been used to get a handle on  $R_\gamma$ : optical depth to Thomson scattering should be less than  $\sim 1$ ; detection of high-energy  $\gamma$ -rays suggests that  $e^\pm$  production optical depth should also be less than one; detection of a bright optical transient during the prompt  $\gamma$ -ray phase implies that the synchrotron-self absorption frequency is below the optical band; the rapid decay of X-ray lightcurves at the end of prompt radiation phase signals a rapid turn-off of the central engine and this can be used to determine  $R_\gamma$ . The first three methods provide a lower limit for  $R_\gamma$ . The last two techniques assume a one zone model where the lower frequency photons (optical or X-rays) and  $\gamma$ -rays are produced at the same location – results described below are invalid if this assumption were to turn out to be incorrect.

<sup>35</sup> The observed spectrum is expected to deviate from the Planck function due to the fact that photons arriving at any given time at the observer in fact originated at different radii and time. Hence, the observed spectrum is a superposition of Planck functions of different temperatures. In particular, the observed spectrum below the peak is likely flattened to  $f_v \propto v^{1.4}$  from the original  $f_v \propto v^2$  shape [118,557]. And if the LF of the jet has an angular dependence such that it peaks at the jet axis and decreases with angle then the observed spectrum is flattened even further and can become  $f_v \propto v^0$  [558].

The  $\gamma$ -ray source distance ( $R_\gamma$ ) should be smaller than the deceleration radius for the jet, which is of order  $10^{17}$  cm for a uniform density circum-stellar medium (see Eq. (34)), otherwise much of the energy of the GRB-jet is imparted to the surrounding medium and not available for  $\gamma$ -ray radiation.<sup>36</sup>

The initially highly opaque fireball becomes optically thin at a distance  $\sim 5 \times 10^{12} L_{52} \Gamma_2^{-3}$  cm (Eq. (130)) – if baryonic – and so we expect the observed radiation to originate at  $R_\gamma \gtrsim 10^{12}$  cm.

The detection of high energy  $\gamma$ -ray photons provides a constraint on GRB-jet LF ( $\Gamma$ ), which combined with the variability time for GRB prompt lightcurve ( $\delta t$ ) gives a rough estimate for the radius where  $\gamma$ -rays are produced –  $R_\gamma \sim 2c(1+z)\delta t \Gamma^2 \sim 10^{14}(\delta t)^{-1}$  cm (e.g. [98]); where we used  $\Gamma \sim 10^2$  obtained from pair opacity argument described in the next two paragraphs.

Consider that we see a photon of energy  $\epsilon_0 \gg m_e c^2$ , that lies on a power-law spectrum with photon index  $\alpha$ , from a GRB at redshift  $z$ . The isotropic equivalent luminosity for this burst is  $L_\gamma$ , the jet LF is  $\Gamma$ , and consider that  $\gamma$ -ray photons are produced at a distance  $R_\gamma$  from the center of explosion. The photon energy in the jet comoving frame is  $\epsilon_0(1+z)/\Gamma$ , which we assume is larger than  $m_e c^2$ , otherwise there is little chance for it to be converted to a  $e^\pm$ -pair.<sup>37</sup> This photon can interact with a photon of jet-comoving frame energy  $>(m_e c^2)^2 \Gamma/(1+z)\epsilon_0 \equiv \epsilon'_1$  and produce  $e^\pm$ ; the observer frame photon energy is  $\epsilon_1 = \epsilon'_1 \Gamma/(1+z)$ .

The number density of photons of energy  $\geq \epsilon'_1$  in the jet comoving frame is  $n'_\gamma \sim L_\gamma (h\nu_p/\epsilon_1)^{\beta-2}/(4\pi R_\gamma^2 \Gamma^2 \epsilon'_1 c)$ ; where  $\nu_p$  is frequency at the peak of the spectrum in observer frame, and  $\beta \sim 2.2$  is the photon index of the spectrum ( $f_\nu \propto \nu^{-\beta+1}$ ) for  $\nu > \nu_p$ . The probability that the photon of energy  $\epsilon_0$  will get converted to  $e^\pm$  as it tries to escape the jet is  $\sigma_{\gamma\gamma \rightarrow e^\pm} n'_\gamma R_\gamma/\Gamma$ ; where the pair production cross-section  $\sigma_{\gamma\gamma \rightarrow e^\pm} = 1.2 \times 10^{-25}$  cm<sup>2</sup> at the optimal photon energy. Therefore, a lower limit to the LF of jet in order to avoid pair production is

$$\Gamma > \left[ \frac{\sigma_{\gamma\gamma \rightarrow e^\pm} L_\gamma (1+z)\epsilon_0}{4\pi R_\gamma m_e^2 c^5} \right]^{1/2\beta} \left( \frac{h\nu_p (1+z)^2 \epsilon_0}{m_e^2 c^4} \right)^{(\beta-2)/2\beta}. \quad (137)$$

If we detect a 100 MeV photon from a typical long-duration-GRB at  $z = 2$ , with  $\beta = 2$  and  $\gamma$ -ray luminosity  $L_\gamma \sim 10^{52}$  erg s<sup>-1</sup>, then that suggests  $\Gamma \gtrsim 200$ . Combining this with the 0.1 s variability time for the prompt  $\gamma$ -ray lightcurve implies  $R_\gamma \sim 3 \times 10^{14}$  cm (see, e.g. [16,559,561,551,442]).

Optical photons have been detected during the prompt  $\gamma$ -ray burst for a number of GRBs [149,469,470,562,209,472,563]. If optical and  $\gamma$ -ray photons are produced at the same location – which is likely the case whenever correlated fluctuations are seen in optical and  $\gamma$ -ray lightcurves or when optical flux declines rapidly (faster than  $t^{-2}$ ) at the end of the prompt phase – then that suggests that the synchrotron-self-absorption frequency is below the optical band. This provides a lower limit on  $R_\gamma$  since for a given  $\gamma$ -ray flux and spectral peak frequency, the electron column density increases with decreasing  $R_\gamma$ , which leads to a larger self-absorption frequency. This method was used by Shen and Zhang (2009) for a sample of 4 GRBs and they found  $R_\gamma \gtrsim 10^{14}$  cm.

One of the major discoveries made by the Swift satellite in regards to GRBs was the detection of a rapidly declining X-ray lightcurve at the end of the prompt phase, when the flux declines as  $t^{-3}$  or faster for a duration of a few minutes, and before a slowly declining “afterglow” phase sets in [79]. This rapid decline is seen in the majority of GRBs [290,363] and heralds the winding down of central engine activity.<sup>38</sup> Considering that there is no discontinuous change in X-ray flux between the prompt phase and the rapidly declining X-ray phase [291], the radiation during the latter phase should have the same origin as the prompt GRB radiation. As long as the opening angle of a GRB-jet is larger than  $\Gamma^{-1}$  (which seems to be the case from observations of achromatic breaks in optical & X-ray lightcurves several days after the explosion) it is expected that we will continue to see a tail of prompt radiation coming from parts of the jet lying at angles ( $\theta$ ) larger than  $\Gamma^{-1}$  with respect to the observer line of sight. Radiation from larger  $\theta$  arrives at a later time due to the larger path length the light has to travel to get to the observer, and it is also subject to a much smaller Doppler boosting, thereby leading to a rapidly declining flux. In fact, this “large angle radiation”, or the tail of the prompt phase, has a well defined, unique signature, that relates the temporal decline during the steep phase with the spectral slope at the end of the prompt phase [128,129,229,307,308]:  $f_\nu(t) \propto t^{-2-\beta} \nu^{-\beta}$  (see Section 2.1 for a derivation of this result)<sup>39</sup>; so the steeper the flux density spectral index ( $\beta$ ), the steeper is the temporal decline during the steep phase. The time when the steep decline begins (time measured from the peak of the last pulse in  $\gamma$ -ray lightcurve) is set by the radius where the prompt radiation is produced and the jet Lorentz factor:  $t_{\text{decline}} \sim R_\gamma/(2c\Gamma^2)$ . And the steep decline lasts for a duration that is related to the

<sup>36</sup> The  $\gamma$ -ray radiation during the prompt phase cannot be produced by the shock heated GRB circumstellar medium (the so called external shock) since the resulting lightcurve would vary on timescale of  $R_\gamma/(2c\Gamma^2) \sim 10$  s [305] – instead of 0.1s or less as observed – and the X-ray lightcurve would not show a sharp drop-off at the end of the prompt phase as is seen for a good fraction of bursts [79] – but see also [106].

<sup>37</sup> If the comoving energy were to be less than  $m_e c^2$ , then most of photons of energy  $\epsilon_0$  can escape conversion to  $e^\pm$  since they will have to interact with photons of larger energy for pair production. And such photons are much smaller in number since  $\beta \sim 2$  for GRBs.

<sup>38</sup> The central engine can continue to operate, sporadically, as evidenced by sudden increases in X-ray flux or flaring events, for a period of hours to days, e.g. [284] Chincarini et al. (2011).

<sup>39</sup> The decay index  $\alpha$  depends on the choice of the zero time. It is usually set to the trigger time, but can be later for the cases with distinct emission episodes [82,230].

jet opening angle  $\theta_j$ :  $t_{\text{tail}} \sim (R_\gamma/c)\theta_j^2/2$ . Hence, the timescale for steep decline, and a measurement of  $\Gamma$  from the onset of “afterglow” radiation (or the jet deceleration time) enable the determination of  $R_\gamma$ . This idea for the determination of  $R_\gamma$  was suggested by Lyutikov [564], and Lazzati and Begelman [565], soon after the discovery of the steep decline of X-ray light-curves by the Swift satellite, and was recently re-emphasized by Hascoët et al. [566].

A number of GRBs satisfy the “large angle radiation” relation,  $\alpha = 2 + \beta$ , between the temporal decay index ( $\alpha$ ) and spectral index ( $\beta$ ) during the steep decline phase of X-ray afterglow lightcurve, e.g. [298,567]. Kumar et al. [568] analyzed the data for a sample of 10 of these GRBs that satisfy this “closure relation”, and found  $R_\gamma \gtrsim 10^{16}$  cm using the method described above.

### 7.3. Internal shocks: conversion of outflow kinetic energy to radiation

We describe in this section the widely used internal shock model for converting the kinetic energy of a baryonic jet to  $\gamma$ -rays [78,98]. Consider a relativistic, baryonic outflow, where the LF is time dependent. In this case, the faster part of the outflow will catch up with a slower moving part ahead of it. The resulting collision produces a pair of shock waves that propagate into the fast and slow shells, and a fraction of jet kinetic energy is converted to thermal energy. The thermal energy is radiated away via synchrotron and the inverse-Compton processes. This model is called the *internal shock model* since shocks are produced within the jet due to non-zero gradient of velocity.

The main strength of this model lies in its simplicity and its ability to account for short time scale variability, of order milli-seconds, seen in prompt GRB lightcurves. One of its main weaknesses is the inability to explain the observed spectrum – in particular, the spectral index below the peak – and possibly its low efficiency. We expand on these points below.

For simplicity, let us consider two shells of masses  $m_1$  &  $m_2$  ejected from the central engine moving with terminal LFs  $\Gamma_1$  and  $\Gamma_2$ . The slower moving shell-1 was launched  $\delta t$  time before the other shell. The distance from the center of explosion where these shells collide, when  $\Gamma_2 \gtrsim 2\Gamma_1$ , is

$$R_{\text{coll}} = \frac{v_1 v_2 \delta t}{v_2 - v_1} \approx 2c\Gamma_1^2 \delta t. \quad (138)$$

Therefore, the time when the radiation produced in this collision will arrive at the observer is given by

$$t_{\text{obs}} \sim t_0 + R_{\text{coll}}/(2c\Gamma_f^2) \sim t_0 + (\delta t)\Gamma_1/\Gamma_2, \quad (139)$$

where  $t_0$  is the time when shell-2 was ejected from the central engine,  $\Gamma_f$  is the final Lorentz factor of merged shells, which is given by

$$\Gamma_f = \frac{m_1\Gamma_1 + m_2\Gamma_2}{(m_1^2 + m_2^2 + 2m_1m_2\Gamma_r)^{1/2}}, \quad (140)$$

and

$$\Gamma_r = \Gamma_1\Gamma_2(1 - v_1v_2/c^2) \quad (141)$$

is the relative LF of the two shells before collision. We see from Eq. (139) that the variability time of the GRB lightcurve roughly tracks the engine variability time according to this model (assuming that  $\Gamma_2/\Gamma_1$  does not fluctuate wildly during the course of engine activity). Therefore, the internal shock model is capable of explaining the observed short time scale variability (milli-seconds) by linking it to the central engine time-scale, whereas external shocks occurring at a much larger radius cannot account for this without sacrificing the efficiency for producing  $\gamma$ -ray emission [305]; efficiency is somewhat problematic for internal shocks as well (as discussed below), but it is a much more severe problem for external shocks when the requirement of milli-second (or even 100 ms) time variability is imposed.

The 4-momenta of the two shells before the collision are  $\Gamma_i m_i(1, v_i, 0, 0)$ ;  $i = 1, 2$ . And the momentum after the collision of the merged shells moving together =  $\Gamma_f m(1, v_f, 0, 0)$ . It is straightforward to show using the conservation of 4-momentum that the thermal energy produced in this collision, where the two shells merge and move together, is

$$\Delta E = \Gamma_f(m - m_1 - m_2) = \Gamma_f \left[ (m_1^2 + m_2^2 + 2m_1m_2\Gamma_r)^{1/2} - (m_1 + m_2) \right] c^2. \quad (142)$$

Therefore, the efficiency for producing thermal energy in the collision is given by

$$\epsilon_t = \frac{\Delta E}{(m_1\Gamma_1 + m_2\Gamma_2)c^2} = \left[ 1 - \frac{m_1 + m_2}{(m_1^2 + m_2^2 + 2m_1m_2\Gamma_r)^{1/2}} \right]. \quad (143)$$

It is easy to see that for a fixed  $\Gamma_r$ , the highest efficiency is achieved when equal mass shells collide, and in that case the efficiency is  $\epsilon_{\text{max}} = [1 - 2^{1/2}/(1 + \Gamma_r)^{1/2}]$ . Only a fraction of the thermal energy produced in collisions is likely deposited in electrons, the rest is taken up by protons and magnetic fields. Since protons are very inefficient radiators – the synchrotron and the IC power for a proton is smaller than an electron of similar energy by a factor  $(m_p/m_e)^4$  – the maximum radiative efficiency one might hope to get in colliding shells is  $\sim \epsilon_{\text{max}}/2$  when electrons carry 50% of the total thermal energy produced

in the collision.<sup>40</sup> Therefore, the maximum possible radiative efficiency when two shells of  $\Gamma_2/\Gamma_1 = 20$ , or  $\Gamma_r = 10$ , collide is 28.7%. However, even in this case of extreme LF contrast between colliding shells, and the highly idealized situation of equal shell mass, the radiative efficiency in the energy band for a typical GRB instrument (10 keV–10 MeV) is smaller than the bolometric efficiency calculated above by a factor of a few (IC scatterings produce much higher energy photons in internal shocks that carry away a good fraction of electron energy). More detailed calculations find the radiative efficiency for internal shocks in the observer band – by considering an ensemble of colliding shells with various LF distributions – to be between 1 and 10 percent [569–572,296]. By contrast, the observed efficiency for prompt  $\gamma$ -ray emission is reported to be much higher – approaching, or possibly exceeding 50% [340,94].

Beloborodov [421] suggested that internal shocks can be efficient. However, that is based on the assumption that  $\Gamma_2/\Gamma_1 \gg 10$  for almost all collisions, which is unlikely to be realistic, and he does not take into account the fact that only a fraction of thermal energy is radiated in the observing energy band of 10 keV–10 MeV.

We next discuss whether synchrotron radiation in internal-shocks can account for the observed  $\gamma$ -ray spectrum.

#### 7.4. Viability of Synchrotron radiation mechanism for GRBs for shock heated plasma

We provide in this section some constraints on properties of  $\gamma$ -ray sources – such as the magnetic field strength, Lorentz factor of electrons associated with their random motion in the source comoving frame ( $\gamma_e$ ) and the Compton-Y parameter – using general theoretical arguments when the radiation mechanism is synchrotron. We assume that electrons are accelerated on a time scale short compared with the dynamical time, and subsequent to the phase of acceleration they have vanishingly small rate of energy gain, which is the case for the Fermi acceleration mechanism in internal and external shocks.

The  $\gamma$ -ray source might be highly inhomogeneous where magnetic fields might occupy a small fraction of the source volume, and only a fraction of electrons (and positrons) might be accelerated to high enough Lorentz factor to radiate in the observed  $\gamma$ -ray band. The calculations in this section circumvent these complications by focusing only on those electrons that radiate in the observer band, and we consider only that part of the source region where the magnetic field is strong enough for these electrons to produce  $\gamma$ -ray photons. If there are a large number of regions with very different values of ( $\gamma_e$ ,  $B'$ ) contributing roughly equally to the observed flux, then the simplified calculation presented here is invalid; however, it would require quite a coincidence for different pairs of ( $\gamma_e$ ,  $B'$ ) to have the same synchrotron frequency.

Let us consider the isotropic equivalent of  $\gamma$ -ray luminosity for a burst to be  $L_\gamma$ , and the frequency at the peak of the  $\nu f_\nu$  spectrum to be  $\nu_p$  in the observer frame.

If we associate the peak of the spectrum,  $\nu_p \equiv \nu_{p,5} \times 100$  keV, with the synchrotron frequency of electrons with Lorentz factor  $\sim \gamma_e$ , then that gives

$$\frac{qB'\gamma_e^2\Gamma}{2\pi m_e c(1+z)} = 2.4 \times 10^{19} \nu_{p,5} \text{ Hz} \implies B'\gamma_e^2\Gamma_2 = 8.5 \times 10^{10} (1+z)\nu_{p,5}, \quad (144)$$

where  $B'$  is the magnetic field in the source comoving frame, and  $\Gamma$  is the Lorentz factor of the source.

The radiative cooling time for electrons, in the observer frame, is (e.g. [573])

$$t_c = \frac{3\pi m_e c(1+z)}{\sigma_T B'^2 \gamma_e \Gamma (1+Y)} \sim (5 \times 10^{-16} \text{ s}) (1+z)^{-1} \gamma_e^3 \nu_{p,5}^{-2} \Gamma_2 (1+Y)^{-1}, \quad (145)$$

where  $Y$  is the Compton-Y parameter, and the second part of the equation was obtained by substituting for  $B'$  using Eq. (144). If  $t_c$  is much smaller than the dynamical time,  $t_d \sim R(1+z)/(2c\Gamma^2)$ , then the rapid cooling of electrons leads to the spectrum below  $\nu_p$  to be  $f_\nu \propto \nu^{-1/2}$  [131], which is much softer than the spectrum for most GRBs; the observed low energy spectrum is often close to  $\nu^0$  (see Section 6.2 for detailed information regarding observations). The condition that  $t_c \gtrsim t_d$  implies

$$\gamma_e \Gamma_2 \gtrsim 1.5 \times 10^5 R_{15}^{1/3} (1+z)^{2/3} \nu_{p,5}^{2/3} (1+Y)^{1/3}. \quad (146)$$

Thus, for the synchrotron radiation mechanism to be able to explain the GRB peak frequency, and the spectrum below the peak, a very high LF of electrons is required<sup>41</sup>:  $\gamma_e \gg 10^4$ . This large  $\gamma_e$  might be a problem for the internal shock model (where the LF of the shock front is of order a few) unless just one in  $\sim 10^2$  electrons crossing the shock front are accelerated carrying away  $\sim 10\%$  of the energy of the shocked fluid as suggested by e.g. Daigne et al. [247]. Numerical simulations of collisionless ion-electron shocks find that these requirement might be satisfied as long as magnetic fields in the unshocked GRB jet carry less than  $\sim 0.1\%$  of the luminosity [387]; the parameters of these simulations, however, fall far short of GRB jet conditions, and therefore one needs to be careful applying simulation results to GRBs.

<sup>40</sup> The radiative efficiency can exceed  $\epsilon_{max}/2$  if energy could be transferred from protons to electrons on a dynamical time. However, considering that the Coulomb interaction cross-section for relativistic electrons is smaller than the Thomson cross-section this energy transfer will have to involve some kind of a collective plasma process.

<sup>41</sup> This condition on  $\gamma_e$  is basically equivalent to the problem discussed in [574], where they showed that the synchrotron cooling time for electrons in internal shock with  $\gamma_e \sim 10^2$  is much smaller than the dynamical time.

A large value for  $\gamma_e$  implies a small magnetic field (in order for  $v_p \sim 10^2$  keV) and in that case IC losses might dominate. The maximum magnetic field strength (corresponding to the minimum value for  $\gamma_e \Gamma$ ) can be calculated using Eqs. (144) and (146):

$$B' \sim (4 \text{ Gauss}) R_{15}^{-2/3} (1+z)^{-1/3} \Gamma_2 v_{p,5}^{-1/3} (1+Y)^{-2/3}, \quad (147)$$

and therefore the energy in magnetic fields is

$$E_B = \frac{\Gamma^2 B'^2}{8\pi} \frac{4\pi R^3}{\Gamma^2} \lesssim (7 \times 10^{45} \text{ ergs}) R_{15}^{5/3} (1+z)^{-2/3} \Gamma_2^2 v_{p,5}^{-2/3} (1+Y)^{-4/3}. \quad (148)$$

The energy in electrons can be calculated from the observed flux at the peak of the spectrum. The synchrotron flux at  $v_p$  depends on the total number of electrons (isotropic equivalent),  $N_e$ , that radiate at  $v_p$ , i.e. electrons that have LF  $\geq \gamma_e$ . The synchrotron specific luminosity in the jet comoving frame can be obtained by dividing the total synchrotron power for  $N_e$  electrons by  $v_p$ . Multiplying this with  $\Gamma$  gives the luminosity in observer frame. Thus,

$$f_p^{\text{syn}} = \frac{N_e (1+z)}{4\pi d_L^2} \frac{\sqrt{3} q^3 B' \Gamma}{m_e c^2} = \frac{(1.8 \times 10^{-3} \text{ mJy}) N_{e,50} B' \Gamma}{(1+z)^{-1} d_{L,28}^2}, \quad (149)$$

or

$$N_{e,50} B' \Gamma_2 \sim 5 f_{p,\text{mJy}}^{\text{syn}} (1+z)^{-1} d_{L,28}^2, \quad (150)$$

where  $d_L$  is the luminosity distance, and  $f_{p,\text{mJy}}^{\text{syn}}$  is the observed flux at the peak of spectrum in mJy. The total number of electrons that contribute to the observed flux at  $v_p$  is obtained by making use of Eqs. (147) and (150):

$$N_e \sim 1.2 \times 10^{50} f_{p,\text{mJy}}^{\text{syn}} d_{L,28}^2 v_{p,5}^{1/3} R_{15}^{2/3} (1+z)^{-2/3} \Gamma_2^{-2} (1+Y)^{2/3}, \quad (151)$$

and therefore the energy in electrons is

$$E_e \sim \Gamma N_e \gamma_e m_e c^2 \gtrsim (1.5 \times 10^{51} \text{ ergs}) f_{p,\text{mJy}}^{\text{syn}} d_{L,28}^2 R_{15} \Gamma_2^{-2} v_{p,5} (1+Y). \quad (152)$$

The second part of the equation was obtained by making use of (146) and (151), and the lower limit to electron energy is due to the fact that we only have a lower bound on  $\gamma_e$  through Eq. (146).

The ratio  $E_e/E_B \propto \Gamma^{-4}$  is much larger than 1 even when we consider an extreme value for GRB jet LF of  $\sim 10^3$ , and this suggests that IC scatterings might carry away a large fraction of electron energy to produce very high energy  $\gamma$ -rays ( $\gtrsim$  TeV) thereby significantly increasing the total energy budget for GRBs. To address this concern we calculate the Compton-Y parameter.

The optical depth to Thomson scattering can be calculated using Eq. (151) for  $N_e$

$$\tau_e = \frac{\sigma_T N_e}{4\pi R^2} \sim 6 \times 10^{-6} f_{p,\text{mJy}}^{\text{syn}} v_{p,5}^{1/3} d_{L,28}^2 (1+z)^{-2/3} R_{15}^{-4/3} \Gamma_2^{-2} (1+Y)^{2/3}, \quad (153)$$

and with this we can now estimate Compton-Y parameter, which for a typical GRB with  $f_{p,\text{mJy}}^{\text{syn}} = 1$ ,  $v_{p,5} = 1$ ,  $d_{L,28} = 1$  and  $z = 1$  is given by:

$$Y \sim \frac{\tau_e \gamma_e^2}{[h v_p (1+z)/m_e c^2] (\gamma_e/\Gamma)} \sim \tau_e \gamma_e \Gamma \sim 10^2 R_{15}^{-1} (1+Y) \Gamma_2^{-2}, \quad (154)$$

where we have included the Klein–Nishina (K–N) reduction to the photon–electron scattering cross-section, since the photon energy in the electron-rest frame exceeds  $m_e c^2$ ; the factor in the denominator,  $(h v_p [1+z]/m_e c^2)(\gamma_e/\Gamma)$ , is the ratio of photon energy in electron rest frame divided by electron rest-mass energy which is the factor by which the scattering cross-section in the K–N regime is smaller than the Thomson cross-section.

Eq. (154) has no solution for  $Y$  unless  $R_{15} \Gamma_2^2 \gtrsim 10^2$ . If we take  $\Gamma \sim 100$  as is inferred for an average GRB jet, then  $R \gtrsim 10^{17} \text{ cm}$ , which is equal to or larger than the deceleration radius for GRB jets. Thus, there is no synchrotron solution for the case where the spectrum below the observed peak ( $v_p$ ) is  $\propto v^0$ , unless the source lies at a distance from the central engine that is close to the deceleration radius and assuming that electrons are not continuously accelerated [575,576]. The solution corresponding to  $R \sim 10^{17} \text{ cm}$ , has  $\gamma_e \sim 7 \times 10^5$ ,  $Y \lesssim 1$  (Eqs. (153) and (154)), and the total energy in electrons that are responsible for producing one pulse in a GRB lightcurve is  $\sim N_e m_e c^2 \gamma_e \Gamma \gtrsim 10^{53} \text{ erg}$ , and the energy in magnetic field is  $\sim B'^2 R^3 / 2 \lesssim 10^{50} \text{ erg}$ ; moreover, the lightcurve variability time is  $\sim R/(2c\Gamma^2) \sim 10^2 R_{17}/\Gamma_2^2 \text{ s}$ , which is much longer than what observations find for most GRBs.

It is very difficult to get around the low-energy spectrum problem for the synchrotron model as was pointed out by Ghisellini et al. [574] more than a decade ago. One possible solution is that electrons are continuously accelerated (as opposed to acceleration while crossing the shock front multiple times but no further energy gain while traveling downstream of the shock front). In this case  $B'$  can be larger and  $\gamma_e$  smaller – so that the radiation can be produced at a smaller  $R$  while keeping  $Y \lesssim 1$  – and the radiative loss of energy for electrons is balanced by energy gain due to continuous acceleration

thereby maintaining the low energy spectrum to be  $f_v \propto v^0$  Asano and Terasawa [575]; see also Murase et al. [116] and [577], who invoked continued acceleration due to MHD turbulence down-stream of the shock front. Alternatively, the electron cooling problem can be alleviated if magnetic fields were to decay rapidly downstream of the shock front [392]. However, a likely serious problem for this model is the excessive energy requirement, since the luminosity in the IC component might be much larger than the synchrotron emission.

Uhm and Zhang [130] have suggested that the decrease of the magnetic field with distance from the center of explosion offers another way to explain the low energy spectral index for GRB prompt emission. The idea is that the synchrotron loss rate for  $\gamma$ -ray emitting electrons decreases rapidly with time as these electrons move to larger distances where the magnetic field is weaker. Therefore, these electrons do not cool much to give rise to a  $f_v \propto v^{-1/2}$  spectrum. This mechanism works well as long as the magnetic field strength at the radius where electrons are accelerated is such that the synchrotron cooling time is not much smaller than the dynamical time. This suggests, using Eqs. (144) and (145), that  $\gamma_e \sim 10^5$  and the magnetic field strength is relatively small (Poynting luminosity  $\sim 10^{46} R_{15}^2$  ergs $^{-1}$ ) for this mechanism to be effective at explaining the low energy spectral index. While the required large emission radius is consistent with constraints of a large  $R_\gamma$  (Section 7.2), it is unclear how a small magnetization parameter could be achieved in the emission region.

Yet another solution to the low-energy spectrum problem is for electron cooling to be dominated by IC scatterings in K-N regime. In this case, the low energy electron spectrum is  $dn_e/d\gamma_e \propto \gamma_e^{-1}$  – in the limit of large  $\gamma_e$  and IC scatterings in K-N regime as the dominant energy loss mechanism for electrons [245–247] – and consequently  $f_v \propto v^0$ . One of the drawbacks with this solution is the extreme value for  $\gamma_e$  required ( $\gtrsim 10^6$ ), and even then the low energy spectrum is found to be no harder than  $v^{-0.1}$ , which fails to account for the observed spectrum for a substantial number of GRBs [248].

The bottom line is that the GRB prompt emission can be produced by the synchrotron process provided that electrons are either continuously accelerated, or that there is some mechanism that prevents their rapid radiative cooling to ensure that the spectrum below the peak is consistent with observations.

### 7.5. Constraints on Synchrotron-self-Compton mechanism for GRBs

The peak frequency and flux at the peak for the SSC case are  $\nu_{syn}\gamma_e^2$  and  $f_p^{syn}\tau_e$  respectively; where  $\nu_{syn}$  and  $f_p^{syn}$  are the synchrotron peak frequency and the peak flux,  $\tau_e$  is the optical depth of the source to Thomson scattering and  $\gamma_e$  is LF of electrons with characteristic synchrotron frequency of  $\nu_{syn}$ . Equating the IC frequency to the observed peak frequency  $\nu_p$ , and the IC flux to the observed peak flux  $f_{p,mJy}$  (in milli-Jansky) provides the following constraints:

$$B'\gamma_e^4\Gamma_2 \sim 8.5 \times 10^{10}(1+z)\nu_{p,5} \quad (155)$$

$$\tau_e N_{e,55} B' \Gamma_2 \sim 5 \times 10^{-5} f_{p,mJy}(1+z)^{-1} d_{L,28}^2 \quad (156)$$

$$\text{or } \tau_e^2 R_{15}^2 B' \Gamma_2 \sim 2.5 \times 10^{-5} f_{p,mJy}(1+z)^{-1} d_{L,28}^2, \quad (157)$$

where we made use of Eqs. (144) and (150) for synchrotron frequency and flux, and substituted for  $N_e = 4\pi R^2 \tau_e/\sigma_T$  in the last part. Moreover, taking the radiative cooling time for electrons of LF  $\gamma_e$  to be of order the dynamical time, for an efficient production of  $\gamma$ -rays, and to ensure that the low energy spectrum does not become cooling dominated ( $f_v \propto v^{-1/2}$ ) as suggested by data for most GRBs, requires

$$B'^2 \gamma_e R_{15} (1+Y) \sim 2.3 \times 10^6 \Gamma_2. \quad (158)$$

These equations can be solved for  $\gamma_e$ ,  $B'$ ,  $\tau_e$  &  $Y$  to yield:

$$\gamma_e \sim 164 R_{15}^{1/7} \Gamma_2^{-3/7} (1+Y)^{1/7} (1+z)^{2/7} \nu_{p,5}^{2/7}, \quad (159)$$

$$B' \sim (120 \text{ Gauss}) R_{15}^{-4/7} \Gamma_2^{5/7} (1+Y)^{-4/7} (1+z)^{-1/7} \nu_{p,5}^{-1/7}, \quad (160)$$

$$\tau_e \sim 5 \times 10^{-4} R_{15}^{-5/7} \Gamma_2^{-6/7} (1+Y)^{2/7} (1+z)^{-3/7} \nu_{p,5}^{1/14} f_{p,mJy}^{1/2} d_{L,28}, \quad (161)$$

$$Y \sim \gamma_e^2 \tau_e \sim 300 R_{15}^{-1} \Gamma_2^{-4} (1+z)^{1/3} \nu_{p,5}^{3/2} f_{p,mJy}^{7/6} d_{L,28}^{7/3}. \quad (162)$$

Thus, for a solution with  $Y \sim 1$  (so that the second IC-scattering does not carry away too much energy), we require  $R \sim 10^{16}$  cm (if we take  $\Gamma \sim 200$ );  $\tau_e \sim 5 \times 10^{-5}$  at this distance. For most bursts that have optical data available during the prompt gamma-ray phase, it is found that the specific flux at the optical band is just a factor 10 or so larger than the  $\gamma$ -ray flux, and not a factor  $1/\tau_e \sim 10^4$  as one would expect if  $\gamma$ -rays are produced via the SSC process. For the SSC peak to be at 100 keV,  $\nu_p^{syn} \sim 10^5/\gamma_e^2 \sim (3.7 \text{ eV}) R_{15}^{-2/7} \Gamma_2^{6/7} (1+Y)^{-2/7}$  – see Eq. (159) for  $\gamma_e$  – and that has a very weak dependence on  $R$  and  $Y$ , and a not particularly strong dependence on  $\Gamma$ . So it is unlikely that  $\nu_p^{syn}$  could be far below or above 2 eV, and therefore it is not possible to suppress the optical flux associated with the synchrotron seed field by a factor  $\sim 10^3$ , in order for that to be compatible with the observed optical data (or upper limit). Another drawback of the SSC mechanism is that the second order SSC would carry more energy, which greatly increases the total energy budget of the burst [245]. This point was recently emphasized by Piran et al. [578] who concluded that the SSC mechanism is not viable for a typical GRB as the energy in seed

photons or the second IC component is excessive. One other difficulty with the SSC mechanism is that its  $E_p$  is very sensitive to the electron injection Lorentz factor ( $\propto \gamma_{\text{inj}}^4$ ), so that it requires fine tuning to obtain the typical  $E_p \sim 10^2$  keV [579].

The same conclusion can be obtained from the Fermi/LAT data alone. The lack of an excess flux at high energies – there is no evidence for departure from a Band function fit for most GRBs e.g. [373] – means that the IC scattering of photons near the peak ( $\nu_p$ ) into the LAT band should have a flux small compared with the Band-function flux. Let us consider the case where  $\gamma_e \lesssim \Gamma$  (IC scatterings take place in the Thomson regime in this case). The lack of a bump in Fermi/LAT band requires  $\tau_e \lesssim \gamma_e^{2(\beta+1)} / 5 \sim \gamma_e^{-2.5} / 5$ ; where  $\beta \sim -2.2$  is high-energy photon index, and the factor 5 takes into account the fact that any departure from a Band-function-fit for most bursts detected by Fermi/LAT is less than  $\sim 20\%$ . The implication of this is that  $\tau_e \lesssim 10^{-3}$  for  $\gamma_e \gtrsim 5$ , and thus one expects a bright optical flash ( $\gtrsim 1$  Jy or 9-mag) whenever  $\gamma$ -rays are produced via the SSC process; we note that  $\gamma_e^2 \gg 20$  since the spectrum between 10 keV and  $\nu_p$  is a flat, single power law, function. A similar result is obtained for  $\gamma_e \gtrsim \Gamma$ .

We close this sub-section with a brief discussion of an exceptional burst, GRB 080319B (the “naked-eye” GRB), which was detected to have a very bright optical counterpart during the prompt phase – it reached a peak apparent magnitude of  $5.8 \sim 30$  s after the GRB trigger – that roughly tracked the  $\gamma$ -ray lightcurve [209]. An attractive possibility for this burst is that the optical emission was produced by the synchrotron process, while  $\gamma$ -rays were due to the SSC mechanism [477,209]. However, the  $\gamma$ -ray light curve for this GRB varied more rapidly than the optical flux, which poses problems for the simplest SSC model [580], but is consistent with the relativistic turbulence model [215]. People have also invoked a two zone model to interpret  $\gamma$ -ray and optical emissions from this burst [581,479,478,582].

## 7.6. General constraints on electron Lorentz factor ( $\gamma_e$ )

The calculation below, based on very general considerations, shows that the Lorentz factor of electrons associated with their random motion ( $\gamma_e$ ) in GRB jets, at the site of  $\gamma$ -ray generation, is either less than 2 or larger than  $\sim 10^2$ .

Let us consider the isotropic  $\gamma$ -ray luminosity in the CoE frame to be  $L_\gamma$ . We assume that  $\gamma$ -rays are produced by electrons (and positrons) by some combination of synchrotron and IC processes.

We will consider two cases separately.

- (1) Short lived acceleration phase: when electrons in the jet are accelerated to a typical LF  $\gamma_e$  on a timescale much smaller than the dynamical time (for instance, while crossing the shock front back and forth multiple times), and subsequently they radiate a part of their energy to produce  $\gamma$ -ray photons of frequency  $\nu_p$ , but this loss of their energy is not compensated by any further acceleration (such is the case for electrons moving down-stream after crossing the shock-front for the last time); a more accurate calculation should consider a distribution of electron LF, however this changes the result by a factor of a few, which is of little concern here. The energy-luminosity carried by electrons (and positrons) at the end of the acceleration phase,  $L_e$ , in this case should be at least as large as  $L_\gamma$ , and so we take

$$L_e = \zeta L_\gamma, \quad (163)$$

where  $\zeta \geq 1$  is a dimensionless parameter of order no larger than a few so that the GRB radiative efficiency is roughly of order the observed value.

- (2) Continuous acceleration: when electrons in the jet are continuously, or repeatedly, accelerated while they are producing  $\gamma$ -rays, so that the energy they loose to radiation is balanced by the gain from the acceleration mechanism (the details of this process are unimportant, but such a scenario could operate in magnetic reconnections inside a current sheet). The luminosity carried by  $e^\pm$ s in this case can be much smaller than  $L_\gamma$ .

### 7.6.1. Short lived acceleration phase for electrons

The comoving number density of electrons & positrons,  $n_e$ , is related to the luminosity,  $L_e$ , carried by  $e^\pm$  as follows –

$$L_e = 4\pi R^2 m_e c^3 (\gamma_e - 1) \Gamma^2 n_e = \zeta L_\gamma, \quad (164)$$

or

$$n_e = \frac{\zeta L_\gamma}{4\pi R^2 m_e c^3 (\gamma_e - 1) \Gamma^2}, \quad (165)$$

where  $R$  is the distance from the center of explosion,  $\Gamma$  is the jet LF and  $\gamma_e$  is the average LF of electrons (in jet comoving frame) that emit photons of frequency  $\nu_p$  (peak of the  $\gamma$ -ray spectrum).

The optical depth to Thomson scattering for electrons of LF  $\gamma_e$  is given by

$$\tau_e = \sigma_T n_e \min\{ct'_c, R/\Gamma\}, \quad (166)$$

where  $t'_c$  is the radiative cooling time for electrons of LF  $\gamma_e$  in the jet comoving frame. The upper bound on the cooling time is provided by the IC loss of energy, and is given by

$$t'_{ic} = \frac{4\pi R^2 \Gamma^2 m_e c^2}{(\gamma_e + 1) \sigma_T L_\gamma} = (150 \text{ s}) \frac{R_{15}^2 \Gamma_2^2}{(\gamma_e + 1) L_{\gamma,51}}. \quad (167)$$

The ratio of the cooling and the dynamical time,  $t'_d = R/c\Gamma$ , is

$$\frac{t'_{ic}}{t'_d} = \frac{0.5R_{15}\Gamma_2^3}{(\gamma_e + 1)L_{\gamma,51}}. \quad (168)$$

Let us assume that the ratio of energy loss rate for an electron of LF  $\gamma_e$  due to IC scatterings (considered above) and the loss rate associated with the radiation mechanism that produced photons of frequency  $\sim\nu_p$  is  $Y$ . The electron cooling time,  $t'_c$ , can then be written as  $t'_c \sim t'_{ic}Y/(Y + 1)$ . Making use of this relation, and Eqs. (165)–(167) we find the optical depth to Thomson scattering of electrons responsible for the observed  $\gamma$ -rays to be

$$\tau_e \sim \frac{\zeta}{\gamma_e^2 - 1} \frac{Y}{Y + 1}, \quad (169)$$

as long as  $t'_c < t'_d$ ; the optical depth is smaller than given by the above equation by a factor  $t'_c/t'_d$  when  $t'_c > t'_d$ . We note that  $Y$  cannot be much smaller than 1 since that would imply the energy in magnetic fields (or seed photons that get IC scattered to  $\nu_p$ ) to be much larger than the energy in prompt  $\gamma$ -ray radiation, and hence a low efficiency for producing prompt radiation, which is not supported by the data.

We can now obtain limits on  $\gamma_e$  using Eq. (169) by requiring that IC scatterings of sub-MeV photons should not produce a bump in the observed spectrum above  $\nu_p$  since *Fermi* finds no evidence for such a bump.

Electrons that produce  $\gamma$ -rays near the peak of the spectrum ( $\nu_p$ ) also IC scatter these photons to a frequency  $\nu_{ic} \sim \gamma_e^2 \nu_p$ . The specific flux at  $\nu_{ic}$  is  $\sim \tau_e f_p$ ; where  $f_p$  is the flux at  $\nu_p$ . From Eq. (169), we see that the IC flux exceeds the underlying seed photon flux at  $\nu_{ic}$  as long as the observed  $\gamma$ -ray spectrum above  $\nu_p$  is not shallower than  $\nu^{-1}$  (which is never the case by the definition of the spectral peak), and  $\zeta Y$  is not much less than 1 (which is unlikely due to radiative efficiency considerations). Therefore, IC scatterings of sub-MeV photons by electrons would produce a prominent second peak in the spectrum above  $\nu_p$  that could lie in the *Fermi*/GBM or LAT energy band (1 MeV–300 GeV) depending on the value of  $\gamma_e$ .

One way to avoid this second peak (which is not found in GRB spectra) is if  $\gamma_e$  is less than  $\sim 1.5$  so that the IC and the seed photon peaks merge together to produce a single peak in the emergent spectrum. Another possibility is that  $\gamma_e \gtrsim \Gamma \sim 10^2$  so that the IC scattering cross-section is reduced due to Klein–Nishina effect, thereby suppressing the bump in the spectrum above  $\sim 10$  MeV. It could be that the IC scattered photons are converted to electron–positron pairs by interacting with lower energy photons as they make their way out of the source region, and therefore do not contribute to the observed flux at high energies [347]; however, this is not so likely for  $\Gamma \gtrsim 200$  when the pair production optical depth is small (Section 7.2).

The bottom line is that  $1.5 \lesssim \gamma_e \lesssim 10^2$  can be ruled out due to the fact that it gives rise to an IC bump above the peak of the observed spectrum in the *Fermi* energy band. Solutions with  $\gamma_e \lesssim 1.5$  have  $\tau_e \sim 1$ , which can be identified as photospheric radiation with possibly multiple IC-scatterings accounting for a power law spectrum above  $\nu_p$ .

### 7.6.2. Continuous/repeated acceleration of electrons

When electrons are continuously, or repeatedly, accelerated while losing energy to radiation, their average Lorentz factor in the jet comoving frame ( $\gamma_e$ ) is such that the energy gain and loss rates are balanced. The observed luminosity in this case is:

$$L_\gamma = 4\pi R^2 n_e m_e c^3 (\gamma_e - 1) \Gamma^2 \frac{R}{c\Gamma} \frac{1}{t'_c}. \quad (170)$$

Therefore, the optical depth to Thomson scattering is

$$\tau_e = \sigma_T n_e R / \Gamma = \sigma_T \frac{L_\gamma}{4\pi R^2 \Gamma^2 c} \frac{t'_c}{m_e c (\gamma_e - 1)} = \frac{Y}{(Y + 1)(\gamma_e^2 - 1)}. \quad (171)$$

This optical depth is basically the same as that in Eq. (169), and the constraint on  $\gamma_e$  obtained in the previous subsection holds, i.e.  $1.5 \lesssim \gamma_e \lesssim 10^2$  is ruled out.

## 7.7. Effects of neutrons on jet dynamics and radiation

GRB jets might be produced by some hydrodynamic processes in an accretion disk around a black hole or a neutron star. In this case, the jet composition could include free neutrons that are produced by the dissociation of nuclei by  $\gamma$ -ray photons in the inner regions of the disk. These neutrons decouple from protons at a radius smaller than the Thomson photosphere (e.g. [257,258]) – due to a smaller cross-section for neutron–proton scattering – and their collisions below the photosphere can significantly affect the jet dynamics, e.g. [583], and produce positrons (by the decay of pions) that IC scatter thermal photons and produce  $\gamma$ -ray radiation with peak at  $\sim 1$  MeV [118]. Neutrons that survive these collisions travel to larger distances before decaying and that could affect the afterglow radiation from GRBs [261,262].

Neutrons and protons in the GRB outflow move together as a single fluid as long as the timescale for a neutron to collide with a proton is smaller than the dynamical time. The collision time, in the jet comoving frame, is

$$t'_{np} = \frac{1}{\sigma_{np} n'_p v} \sim \frac{4\pi R^2 m_p c^2 \eta \Gamma}{L \sigma_{nuc}}, \quad (172)$$

where  $\sigma_{np} = \sigma_{nuc} c/v$  is the cross-section for neutron–proton scatterings,  $\sigma_{nuc} \approx 3 \times 10^{-26} \text{ cm}^2$ ; we made use of Eq. (125) for the proton density ( $n'_p$ ) to arrive at the second equality. The scattering is elastic when  $v \ll c$  and it becomes inelastic that produces pions when  $v \sim c$ . The dynamical time in the fluid comoving frame is

$$t'_d \sim R/(c \Gamma). \quad (173)$$

When  $t'_{np} > t'_d$ , neutrons and protons decouple, and the radius where this occurs is

$$R_{np} \sim \frac{\sigma_{nuc} L}{4\pi m_p c^3 \eta \Gamma^2}. \quad (174)$$

In deriving this equation we have assumed that the luminosity carried by neutrons is of the same order as protons, and the LF  $\Gamma$  is the smaller of proton and neutron LFs. We note that  $R_{np}$  is smaller than Thomson photosphere radius by a factor  $\sim 20$ , since  $\sigma_T/\sigma_{nuc} \sim 20$ . If  $R_{np}$  is smaller than  $R_s$  – the radius where protons attain their terminal speed – neutrons stop accelerating before protons do, and the free energy of neutron–proton differential motion is dissipated below the photosphere, and can be used for producing a non-thermal photon spectrum. The condition for non-zero differential velocity to arise is

$$R_{np} < R_s \quad \text{or} \quad \Gamma > \left[ \frac{\sigma_{nuc} L}{4\pi m_p c^3 R_0} \right]^{1/4} = 485 L_{52}^{1/4} R_{0.7}^{-1/4}. \quad (175)$$

Thus, a substantial fraction of the kinetic energy of those GRB jets that consist of neutrons and protons, and reach terminal LF larger than about 500, is dissipated below the Thomson photosphere. A fraction of this energy goes into producing  $e^\pm$ 's that can scatter photons to possibly produce the observed  $\gamma$ -ray spectrum [118].

Observational evidence does not point to many GRB jets having Lorentz factor larger than what is needed for this mechanism to operate (Eq. (175)). However, neutrons and protons can develop substantial differential velocity even when the condition in Eq. (175) is not satisfied. This can happen, for instance, in internal shocks where protons are slowed down (and accelerated) in the collision, whereas neutrons continue moving at the speed they had before the collision [118]. However, in this case only a small fraction of the energy of differential motion is dissipated, unless shell collisions were to take place close to  $R_{np}$ . If the variability time for the central engine is  $\delta t$ , and the Lorentz-factor of the slower part of the outflow is  $\Gamma$ , then the radius where collisions take place is  $R_{col} \sim 2c\Gamma^2\delta t = 6 \times 10^{12} \Gamma_2^2 (\delta t)_{-2} \text{ cm}$ ;  $(\delta t)_{-2}$  is variability time in units of  $10^{-2} \text{ s}$ . The radius where the probability for n-p collision drops below one-half is  $R_{np} \sim 5 \times 10^{11} L_{52} \Gamma_2^{-3} \text{ cm}$ . Thus,  $R_{col}/R_{np} \sim 10 L_{52}^{-1} \Gamma_2^5 (\delta t)_{-2}$ . For an efficient conversion of outflow kinetic energy to thermal energy via n-p collisions these radii should be approximately equal, i.e.  $R_{col} \sim R_{np}$ , and that requires  $50 \lesssim \Gamma < 10^2$ ; considering that  $R_{col}/R_{np} \propto \Gamma^5$ , these limits are quite firm, and the allowed range for  $\Gamma$  is uncomfortably narrow.<sup>42</sup> Moreover, given a random distribution of  $\delta t$  and  $\Gamma$ , and assuming that they are uncorrelated, there should be many collisions where  $R_{col} \gg R_{np}$  or  $R_{col} \ll R_{np}$  and the spectra produced in these collisions would be very different from those for which  $R_{col} \sim R_{np}$ . The problem is that observations do not find big variations of  $E_{\text{peak}}$  and photon indices for time resolved spectra. Nor do they find systematic differences in spectra for bursts that show fast variability and those that do not (including the extreme case of FRED bursts that have a single, smooth, pulse in the lightcurve).

Neutron–proton differential velocity could arise for a structured jet where neutrons from the outer, slower, part of the jet diffuse toward the middle region, where the plasma is moving at a higher speed [259]. We now assume that somehow neutron–proton differential velocity gets set up in a GRB jet, and look at the sequence of events leading to generation of  $\gamma$ -rays due to neutron–proton collisions for this GRB. The basic processes are sketched in Fig. 29, and the emergent radiation can be understood by using simple physical considerations described below; much of this discussion closely follows the work of Beloborodov [118].

The inelastic collision of a neutron with a proton produces a pion ( $n + p^+ \rightarrow \pi^+ + n + n$ ; it can also produce a  $\pi^-$  or a  $\pi^0$ ). The charged pion decays in 26 nano-seconds to a muon, and the muon decays in  $2.2 \mu\text{s}$  to a positron. If the relative LF of a collision between neutron and proton is  $\Gamma_r \sim 2$ , then the LF of the positron produced is  $\gamma_i \sim \Gamma_r m_\pi/(6m_e) \sim 100$ ; the factor 1/6 accounts for the fact that  $\mu^+$  carries away roughly half of the energy of  $\pi^+$  when it decays and the decay of a  $\mu^+$  imparts roughly equal energies to  $e^+$  and the two neutrinos.

<sup>42</sup> When  $R_{col}/R_{np} \ll 1$ , shell collisions affect both protons and neutrons since they are well coupled below  $R_{np}$ . Moreover, any radiation produced in such a collision would find itself in a medium of high optical depth and hence, the emergent spectrum is nearly thermal, which is inconsistent with observed spectra of most GRBs. For  $R_{col}/R_{np} \gg 1$ , neutrons have a small probability for collision and the radiative efficiency is low.

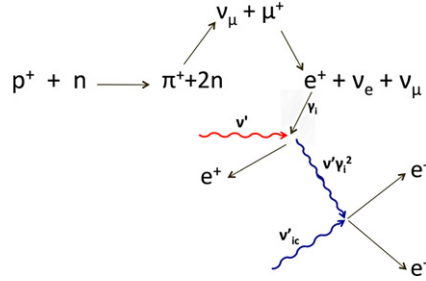


**Fig. 29.** This figure provides a quick overview of the p-n collision process that produces a pion ( $\pi^+$ ), which decays to give a positron of LF  $\gamma_i \sim 10^2$ . This positron inverse Compton scatters thermal photons of frequency  $\nu'$  to energy  $\sim h\nu'\gamma_i^2 > m_e c^2$  (see Eq. (176)), which in turn collides with another IC photon to produce  $e^\pm$  pair. This cascade to more and more pairs continues until  $e^\pm$  LF drops below a few.

These positrons IC scatter thermal photons produced at the jet launch site, and carried by the outflow to larger radii, to an energy, in the jet comoving frame, that is

$$\epsilon_{th}^{ic} \sim 3k_B T_0 (R_s/R_{np})^{2/3} \gamma_i^2 / \Gamma \sim (40 \text{ MeV}) L_{52}^{-5/12} R_{0.7}^{1/6} \Gamma_3^{5/3}. \quad (176)$$

In deriving this equation, we made use of (110) and (133), (117) and (174), and we assumed that neutrons and protons carry roughly equal fractions of the jet luminosity, and also that the LF of neutron jet is  $\sim 4$  times smaller than the proton jet;  $\Gamma_3 \equiv \Gamma/10^3$  is proton jet LF.<sup>43</sup> The energy of these scattered photons is larger than  $m_e c^2$  and they get converted to  $e^\pm$  pairs since the optical depth for  $\gamma + \gamma \rightarrow e^\pm$  is larger than 1 below the photosphere.<sup>44</sup>

The ratio of IC loss time for  $e^\pm$  of LF  $\gamma_e$  and the dynamical time is very small at the photospheric radius ( $R_{ph} \sim 10^{12} \text{ cm}$  – Eq. (130)) even for  $\gamma_e \sim 1$  (see Eq. (168)), and thus the LF of pairs drops rapidly to order unity. Considering the high optical depth to IC scattering for  $R \sim R_{np}$ , photons are repeatedly scattered by  $e^\pm$  and a good fraction of energy of the first generation pairs is used up in producing more pairs. This process stops when pair LF drops below  $\sim 2$ , and IC energy loss rate for  $e^\pm$  is balanced by energy gain due to interactions with protons. The number of pairs created per n-p collision is of order the LF of the first  $e^\pm$  produced by muon decay. These secondary pairs dominate the Thomson scattering optical depth as they outnumber electrons associated with protons by a factor  $\sim 10^2$ . The nearly thermal population of  $e^\pm$  of mildly relativistic temperature ( $\gamma_e < 2$ ) scatter thermal photons multiple times to produce a non-thermal emergent spectrum that has a peak not far from the peak of the underlying seed-thermal-photons, and the low & high energy spectra are  $f_\nu \propto \nu \propto \nu^{-1}$  respectively (see Section 7.8 for a more detailed discussion of spectrum produced in multiple-IC scatterings). For the peak of the emergent spectrum to be of order a few  $10^2 \text{ keV}$ , n-p collisions should not take place far from  $R_s \sim 10^{10} R_{0.7} \Gamma_3 \text{ cm}$ , otherwise adiabatic expansion shifts the thermal peak to an energy below a typical GRB spectral peak. Thus, for a highly fluctuating central engine, where  $\delta t$  has a broad distribution, many collisions are expected to occur far away from the photosphere and these should produce  $\gamma$ -ray spectra with peaks at low energies. However, even though variations of  $E_p$  has been observed in individual GRBs, observations do not find large variations as expected from this model during the course of a burst.

If a GRB-jet has a non-zero magnetic field – which is very likely – then there can be significant synchrotron radiation produced by positrons from  $\pi^+$  decay, and that would modify the IC spectrum. We note, however, that if the synchrotron process were to be the dominant radiation mechanism below the peak of the spectrum, then the low energy spectral index should be  $\alpha = -1.5$  – since the radiative cooling time for  $e^\pm$  is very short at the photospheric radius – and that is too small (soft) for most GRBs. Vurm et al. [584] report that a combination of thermal and synchrotron radiations results in  $\alpha \sim -1$ , which is roughly where the observed  $\alpha$ -distribution peaks. However, it turns out that the addition of a synchrotron component also steepens the high energy photon index ( $\beta < -3$ ) and that is significantly smaller than the average observed value for  $\beta$ . Moreover, it is unclear how a combination of synchrotron and thermal spectra can produce a smooth, single peak, Band-function between 10 keV and  $10^2 \text{ MeV}$  without some fine tuning of parameters. Vurm et al. [584] also find a prominent bump in their spectra at 300 MeV (in the GRB host galaxy rest frame) due to annihilation of pairs of LF  $\gamma_e \sim 1.05$ . Such a feature has never been seen for any GRBs, perhaps because the bump is smeared out when data is integrated over a finite time interval. This bump disappears when the energy fraction in magnetic fields in the jet is taken to be larger than  $\sim 0.5$ . However, in this case the observed flux above the spectral-peak falls off extremely rapidly [584], which is inconsistent with observations.

<sup>43</sup> Beloborodov did not correct for the decrease of thermal photon energy – the factor  $(R_s/R_{np})^{2/3}$  – in his calculations, which has an effect on the emergent spectrum.

<sup>44</sup> The collision of thermal photons with IC scattered photons of energy a few MeV cannot produce pairs since the thermal photons have too little energy ( $\lesssim 1 \text{ keV}$ ) in the comoving frame. Instead, MeV photons must collide with other MeV, non-thermal, photons to produce pairs.

### 7.8. Prompt $\gamma$ -rays from photosphere: processed thermal photons

We consider the “photospheric” model for the generation of 10 keV–10 MeV  $\gamma$ -rays during the main burst in this subsection. According to this model a population of nearly thermal “seed” photons interact with electrons below the Thomson photosphere to produce GRB spectrum. It is assumed that the average seed photon energy is much smaller than the electron’s energy. In this case, photons typically gain energy by scattering off of electrons, and the energy continues to increase as they undergo multiple scatterings as long as their energy is less than the average electron energy. There are a number of excellent articles that discuss multiple-IC scatterings and the emergent spectrum at great depth [585,586,123,587,588]. Here we provide a simple physical picture of this process and its application to GRBs.

The average frequency of a photon scattered off of an electron ( $\nu_s$ ) is, e.g. [123]

$$\nu_s/\nu_i \equiv A_f = 1 + 4k_B T/m_e c^2 \quad (177)$$

for non-relativistic electron temperature  $T$ , and

$$\nu_s/\nu_i = 1 + 4\gamma_e^2/3 \quad (178)$$

for highly relativistic electrons of LF  $\gamma_e$  in Thomson scattering regime; where  $\nu_i$  is the photon frequency before scattering.

The number of scatterings it takes for the average photon energy to approach that of electrons is  $N \approx \ln(k_B T/h\nu_i)/\ln A_f$ , which for sub-relativistic electrons can be rewritten as  $N \approx (m_e c^2/4k_B T) \ln(k_B T/h\nu_i)$ . If these scatterings take place in a medium of Thomson optical depth  $\tau_T$ , then the average number of scatterings suffered by a photon before it escapes from the surface is  $\sim \max(\tau_T, \tau_T^2)$ , and in that case it is useful to define a parameter

$$Y \equiv \max(\tau_T, \tau_T^2) \max[(4k_B T/m_e c^2), 4\gamma_e^2/3], \quad (179)$$

called the Compton-Y, that captures the information regarding whether photons undergo sufficient number of scatterings while traveling through the medium to thermalize with electrons or not.

For  $Y \ll 1$ , the emergent photon spectrum is not too different from the seed photon spectrum except that it can develop a power law tail above the peak, which for  $\tau_T < 1$  has photon index  $\beta = \ln(\tau_T/A_f)/\ln(A_f)$ ; photon index is defined as:  $n(\nu) \propto \nu^\beta$ , where  $n(\nu)$  is the number of photons per unit frequency.

For  $Y \gg 1$  – called saturated Comptonization – it follows from the discussion above that an average seed photon undergoes sufficient number of inverse-Compton scatterings before escaping from the medium so that its energy is approximately equal to the average electron energy. If the electrons have a thermal distribution, then the emergent photon spectrum is Bose–Einstein distribution with a non-zero chemical potential, since the number of photons is conserved; the spectrum has a Wien shape where the specific flux below the peak scales as  $\nu^3$ , instead of  $\nu^2$  for a black-body spectrum.

For the intermediate case of  $Y \sim 1$  &  $\tau_T > 1$  – un-saturated or quasi-saturated Comptonization – the emergent spectrum is more complex and is obtained by solving the Kompaneets equation. However, the qualitative behavior of the spectrum can be understood using simple arguments described below.<sup>45</sup>

Consider a slab of optical depth  $\tau_T$  (measured from the mid plane of the slab to its surface) consisting of hot but non-relativistic electrons. Let us assume that photons of energy much smaller than the average electron thermal energy are injected at the mid-plane of the slab. These photons undergo a number of IC scatterings before arriving at the surface. For  $Y \sim 1$  &  $\tau_T > 1$ , the peak of the photon spectrum at the surface of the slab lies at a higher energy than the injected photons, but the mean number of scatterings is not sufficiently large for the emergent radiation to have attained thermal equilibrium with electrons. If the probability of scattering for a photon while crossing the medium is  $p$ , then the mean number of scatterings suffered before escape is  $\langle N \rangle \sim \sum_k kp^k(1-p) = p/(1-p)$ , or  $p \sim \langle N \rangle/(1 + \langle N \rangle)$ . The peak of the emergent photon spectrum in this case lies at frequency  $\nu_p^{ic} \sim A_f^{(N)} \nu_p$ , where  $\nu_p$  is the peak of the seed photon spectrum;  $\nu_p^{ic} \sim \nu_p \exp(Y)$  is within a factor of a few of  $\nu_p$  since  $Y \sim 1$ , and hence the photon energy at the peak of the emergent spectrum is likely to be much smaller than the mean electron energy. The photon spectral index above the peak is  $\beta \sim \ln(p/A_f)/\ln(A_f) \sim -1 - 1/[\langle N \rangle \ln(A_f)]$ . In the limit of a large optical depth, i.e.  $\langle N \rangle \sim \tau_T^2 \gg 1$ , and a small gain factor ( $k_B T/m_e c^2 \ll 1$ )  $\beta \sim -1 - 1/(\tau_T^2 4k_B T/m_e c^2) = -(1 + Y)/Y$ .

Another derivation for the photon index  $\beta$  (for  $\nu > \nu_p^{ic}$ ) for the case  $\tau_T \gg 1$  and  $Y \sim 1$  follows from photon escape probability  $P_N$ , which is probability that a seed photon released at the mid-plane of the slab is scattered  $N$  times before escaping at the surface. The probability function  $P_N$  is shown in Fig. 30 for a slab with Thomson scattering optical depth of  $\tau_T = 10$ . The escape probability increases for  $N \lesssim 20$  and then decreases exponentially for larger  $N$ ; the large  $N$  behavior is  $P_N \propto \exp(-2N/\tau_T^2)$ . A photon of initial frequency  $\nu$  after undergoing  $N$  scatterings with electrons at temperature  $T$  has frequency  $\nu_{ic} \sim \nu A_f^N \sim \nu \exp(4k_B TN/m_e c^2)$ . Using the conservation of photon numbers in scatterings, and the increase to frequency bandwidth after  $N$  scatterings by a factor  $A_f^N$ , we find  $\beta \sim d \ln(P_N/A_f^N)/d \ln(\nu_{ic}) \sim -1 - 2/Y$  as long as  $\nu_{ic}$  is well below the mean energy of electrons. The two expressions we have obtained for  $\beta$  differ by  $1/Y$  due to different approximations made in these two derivations. The exact result, obtained from solution of Kompaneets’ equation, is  $\beta = -1 - 4/(3Y)$ . The spectrum for  $\nu_{ic} > k_B T/h$  declines exponentially.

<sup>45</sup> This simple physical picture closely follows a discussion PK had with Lev Titarchuk in Ferrara, Italy, in summer 2011.

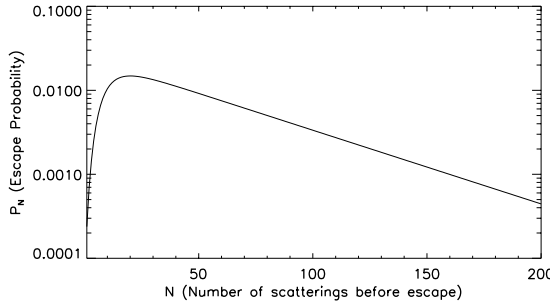


**Fig. 30.** The escape probability ( $P_N$ ) for a photon after undergoing  $N$  scatterings within a slab of optical depth  $\tau = 10$  ( $\tau$  is measured from the mid-plane of the slab to its surface). The function  $P_N$  peaks at  $N \sim 20$  and declines exponentially at larger  $N$ .

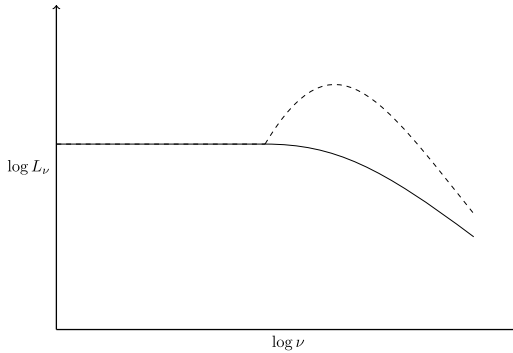


**Fig. 31.** Spectrum due to multiple Compton scattering of thermal seed photons (dotted line) which shows a sharp rise just below the peak and a flat shape corresponding to  $\alpha = -1$  far below the peak (it is a schematic drawing). The Band function spectrum (solid line) shows no such hump below the peak.

The spectrum far below the peak is a rising function of frequency since  $P_N$  increases for  $N \ll \tau_T^2$ . However, the emergent flux is nearly independent of frequency below the peak  $\nu_p^{ic}$ , i.e.  $\alpha \sim -1$ , when  $\tau_T \gg 1$ ,  $Y \sim 1$  and  $\nu_p \ll k_B T/h$ . This can be understood using a simple physical argument provided in [588]. Consider seed photons, and thermal electrons at temperature  $T$ , that populate a region of finite height but infinite length/width uniformly. The optical depth of the source to Thomson scattering from mid-plane to the surface ( $\tau_T$ ) is assumed to be much larger than unity. Photons escape from a thin surface layer of approximately unit optical depth, and the number of photons leaving the surface per unit time (integrated over frequency),  $\dot{n}_\gamma$ , is roughly constant until photons in the medium are depleted substantially; the depletion becomes severe only when photons from the mid-plane of the medium start arriving at the surface. However, the mean energy of emergent photons increases with time since later arriving photons come from deeper layers having undergone more scatterings. Let us take the spectrum of seed photons to peak at  $\nu_0$  and its width to be  $\Delta\nu_0$ . The emergent instantaneous spectrum at time  $t$  peaks at  $\nu(t)$  and its width is  $\Delta\nu(t)$ ;  $\Delta\nu/\nu$  is nearly independent of time for roughly the time it takes for photons to diffuse from the mid-plane to the surface. The instantaneous specific flux at the peak is  $\nu(t)(\dot{n}_\gamma/\Delta\nu)$ , which is time independent. And therefore the emergent specific flux averaged over the diffusion time across the layer is nearly independent of frequency between  $\sim\nu_0$  and  $\nu_p \sim \nu_0 \exp(Y)$  as  $\nu(t)$  sweeps across this band roughly linearly with time, i.e.  $\alpha \approx -1$ .

A straightforward prediction of this model is that the spectral-peak should shift to larger frequencies with time as photons emerging later have undergone more number of IC scatterings on average, and thus have gained more energy. Moreover, the flux should increase with time, at first, as the slab radius increases and its optical depth decreases, and later on the flux should decline due to the adiabatic cooling of electrons and photons.

The peak of the emergent spectrum moves closer to  $k_B T/h$  as the Compton-Y parameter increases. The specific flux has a sharp rise just below the peak when the peak frequency approaches  $k_B T/h$ . This rise arises, as shown by e.g. [588], due to accumulation of photons in the frequency space as their energies approach  $k_B T$  after multiple IC scatterings (see Fig. 31). Such a sharp rise, just below the peak, is never seen in GRB spectra, which suggests that Compton Y cannot be much greater than 1 (that is to say, if prompt  $\gamma$ -rays were to be produced as a result of multiple IC scatterings at the photosphere).

Energy gained by photons in multiple-IC scatterings at the photosphere has been suggested as a possible mechanism to explain the prompt  $\gamma$ -ray spectrum, e.g. [109–111, 589, 548, 590, 112, 315, 114, 115, 113, 116, 591, 117, 119–121, 55, 459, 592].

One of the drawbacks of this mechanism is the spectral shape below the peak. The observed specific flux for a typical GRB is nearly flat below the peak, i.e.  $\alpha \approx -1$  over an extended energy band covering more than an order of magnitude (from  $\sim 10$  keV to several hundred keV). The spectrum produced by multiple IC scatterings, on the other hand, in the unsaturated regime with  $Y \sim 1$  has  $\alpha \sim -1$  over a more limited bandwidth as described above.

Lundman et al. [558] find that photospheric radiation has a low energy spectral index  $\alpha \approx -1$  when the jet LF decreases with azimuthal angle  $\theta$  from the jet axis while the jet luminosity remains constant. This is because in such a configuration, more photons from larger angles with respect to the observer's line of sight can contribute to the low-energy flux to flatten the low energy spectrum. It is unclear whether such a specific jet structure applies to the majority of GRBs.

Another suggestion invoked integration over equal-arrival-time hypersurface to explain  $\gamma$ -ray spectra, i.e. photons arriving at any given observer time originated at different locations near the photosphere, with different temperatures, and this superposition makes the observed spectrum non-thermal. Deng and Zhang [557] investigated this scenario, and concluded that the low energy photon spectral index remains essentially intact, i.e. the spectrum below the peak is much harder than the observed GRB spectra. They also find that it is difficult to obtain the commonly observed "hard-to-soft"  $E_p$  evolution for GRB pulses in this model.

One commonly used argument in support of the photospheric origin of the GRB prompt spectrum is that the observed  $E_p$  is narrowly clustered around the sub-MeV range [433], which is consistent with the photosphere temperature (e.g. [593]). This corresponds to the  $Y \leq 1$  regime. For such cases, there is a maximum photosphere temperature (and hence  $E_p$ ) given an observed  $\gamma$ -ray luminosity (see Eq. (110)). This defines a "death line" of the model in the  $E_p$ - $L$  plane [594]. For GRB 110721A,  $E_p = 15$  MeV early on [446], which lies above the death line, and hence the thermal photospheric model is ruled out. The main spectral component of this burst is well fitted by a Band function, and that must come from a non-thermal emission process in the optically thin region [594,595]. Considering that the Band-function parameters of this burst are fairly typical for a GRB, this argument casts a doubt on the claim that Band spectra are quasi-thermal emission from the photosphere.

There is another issue with the photospheric radiation mechanism for prompt  $\gamma$ -ray emission: electrons need to be heated below the photosphere continuously while keeping their temperature sub-relativistic ( $\ll 1$  MeV). This requires some degree of fine tuning for this model as described below.

If the thermal Lorentz factor of electrons is of order unity – as it is the case for most photospheric models – then electrons carry a tiny fraction of the jet luminosity or the observed  $\gamma$ -ray luminosity of GRBs. Most of the jet energy is in protons (unless the jet has  $\gtrsim 10^3 e^\pm$  pairs per proton) or magnetic fields. Therefore, IC scatterings of seed photons off of electrons, to produce the observed  $\gamma$ -ray luminosity, requires dissipation of a substantial fraction of jet energy below the photosphere and transferring that energy to electrons while keeping the electron temperature sub-relativistic. The reason that electron temperature should be sub-relativistic (in the jet comoving frame) is to prevent IC peaks appearing in GRB spectra which we have never seen, and also to keep Compton-Y from becoming too large otherwise the peak of the emergent spectrum will appear at  $\sim 10^2$  MeV instead of  $\sim 10^2$  keV. For a baryonic jet with one electron per proton,  $\lesssim 1$  MeV per electron is a tiny fraction (of order  $10^{-3}$ ) of the jet luminosity. This means that electrons need to be heated rapidly and repeatedly, of order  $\gtrsim 10^3$  times in one dynamical time, at the photosphere, in order to transfer a good fraction of jet luminosity to electrons, which then is passed on to  $\gamma$ -rays via IC process. This requires a certain degree of fine tuning so that electrons receive a good fraction of jet energy while the temperature is kept sub-relativistic – if the jet energy is transferred to electrons on a time much shorter than the dynamical time then the temperature would become relativistic.

Vurm et al. [596] provide general constraints on energy dissipation processes, photon generation mechanisms, and jet LF, for a dissipative photospheric model to be able to explain the low energy spectral index for gamma-ray bursts. They claim that scattering of seed photons by electrons is not sufficient to be able to account for the observed GRB spectra, and that seed photons ought to be produced at a moderate to small Thomson optical depths which is a severe requirement for a dissipative photosphere model. Asano and Mészáros [597] have derived stringent constraints on the dissipation radius for the photosphere model to be able to reproduce the observed GRB spectra.

## 7.9. Hadronic model for prompt $\gamma$ -ray radiation

Thus far we have considered electrons that are accelerated in shocks or otherwise, and these electrons produce  $\gamma$ -rays via the synchrotron and inverse-Compton processes. Protons are also accelerated in shocks and attain energy much larger than electrons due to their smaller radiative loss rate, and they too could contribute to the observed  $\gamma$ -ray radiation from GRBs as described in a number of papers (e.g. [598–602,347,603,348,457,460,604]). This is taken up in Section 7.9.3, where we show that for the proton-synchrotron process to account for the observed flux, particularly at photon energies of  $\sim$ GeV, one requires the total energy in GRB explosions to be several orders of magnitude larger than the energy we see in  $\gamma$ -rays.

High energy protons can contribute to  $\gamma$ -ray generation in another, indirect, way. They can produce positrons of very large Lorentz factor by the photo-pion and Bethe-Heitler processes. Both of these processes involve collisions between energetic protons and photons to produce  $e^\pm$  directly (Bethe-Heitler process) or via generation of pions (photo-pion process) which decay to positrons and neutrinos. Photo-pion and Bethe-Heitler processes, although inefficient for producing high energy electrons compared with the Fermi acceleration process operating in shocks, can be important in those situations where we need electrons of energy larger than the maximum that a shock can deliver. These processes and the radiation they produce are described in the next two sub-sections.

### 7.9.1. Photo-pion process for producing high energy photons

The basics of photo-pion process is described in Section 2.4. In this section, we provide an estimate of the energy required in protons for producing a certain observed flux in photons of  $> 100$  MeV via the photo-pion process. We consider

photons at the peak of the prompt GRB spectrum ( $\nu_p$ ) colliding with high energy protons to produce pions, and positrons produced by the decay of these pions emitting high energy photons by the synchrotron process; a more precise numerical calculation (e.g. [603,460]) that takes into account photon and proton spectra gives results for the energy requirement that is within an order of magnitude of the estimate provided below.

The photon energy at the peak of the spectrum, in the jet comoving frame, is  $\nu'_p = \nu_p(1+z)/\Gamma$ , if the observed peak is at  $\nu_p$  for a burst located at redshift  $z$ , and the jet is moving with LF  $\Gamma$ . The threshold photon energy, in the proton rest frame, for photo-pion production is approximately 200 MeV. Therefore, the Lorentz factor of a proton for pion production, when interacting with photons of energy  $\nu'_p$ , must satisfy

$$\gamma'_p \gtrsim 2 \times 10^4 \nu_{p,6}^{-1} (1+z)^{-1} \Gamma_2, \quad (180)$$

where  $\nu_{p,6}$  is the observed spectral peak in MeV.

At the threshold energy, the pion LF in the jet frame is also equal to  $\gamma'_p$ , since it is more or less at rest in the proton-rest frame. The decay of a  $\pi^+$  (half life 26 ns) produces  $\mu^+$  and  $\nu_\mu$ , and the muon decays to  $e^+$  and neutrinos in 2.2  $\mu$ s on average. The positron carries roughly 1/4 the energy of the pion, and therefore, the Lorentz factor of the  $e^+$  in the jet rest frame is

$$\gamma'_e \sim 50 \gamma'_p \sim 10^6 \Gamma_2 \nu_{p,6}^{-1} (1+z)^{-1}. \quad (181)$$

For a GRB of observed isotropic luminosity  $L_\gamma$  (integrated over Band function spectrum), the number density of photons in the comoving frame of the jet is

$$n'_\gamma \sim \frac{L_\gamma (1+z)^{-1}}{4\pi R^2 \Gamma c h \nu_p} \approx 2 \times 10^{14} L_{\gamma,52} R_{15}^{-2} \Gamma_2^{-1} \nu_{p,6}^{-1} (1+z)^{-1} \text{ cm}^{-3}, \quad (182)$$

where  $R$  is the distance from the center of the explosion in centimeters.

Given the cross-section for the delta resonance,  $\sigma_{\gamma p} = 5 \times 10^{-28} \text{ cm}^2$ , the optical depth for pion production for a photon of frequency  $\sim \nu'_p$  interacting with a proton of LF given by Eq. (180) is

$$\tau_{\gamma p} \approx \sigma_{\gamma p} n'_\gamma \frac{R}{\Gamma} \approx 0.8 L_{\gamma,52} R_{15}^{-1} \Gamma_2^{-2} \nu_{p,6}^{-1} (1+z)^{-1}. \quad (183)$$

The magnetic field in the source comoving frame can be constrained by the requirement that the synchrotron frequency for positrons produced by the photo-pion process has some desired frequency  $\nu$ . Using Eq. (181), this condition leads to:

$$\frac{qB' \gamma_e'^2 \Gamma}{2\pi m_e c (1+z)} \sim 1.6 \times 10^{-4} \nu_8 \implies B' \sim (10^2 \text{ G}) \nu_8 \nu_{p,6}^2 (1+z)^3 \Gamma_2^{-3}, \quad (184)$$

where  $\nu_8$  is frequency in unit of  $10^8$  eV.

We now use this magnetic field to determine the total energy in protons so that the photo-pion process results in a desired level of flux at  $\nu_8$ . The observed synchrotron flux at  $\nu$  is related to the number of positrons,  $N_{e^+}$ , that radiate at that frequency –

$$f_\nu = 1.2 \mu\text{Jy} N_{e,50} B' \Gamma d_{L,28}^{-2} (1+z). \quad (185)$$

Thus, the number of  $e^+$  needed to produce the observed flux at  $\nu$  is

$$N_{e^+} \approx 8 \times 10^{47} \frac{f_{\nu, \mu\text{Jy}} d_{L,28}^2}{B' \Gamma_2 (1+z)}, \quad (186)$$

where  $f_{\nu, \mu\text{Jy}}$  is observed specific flux in  $\mu\text{Jy}$ .

The number of protons with energy above the pion production threshold required to produce the necessary number of positrons (Eq. (186)) is given by

$$N_p \approx \frac{N_{e^+}}{\tau_{\gamma p}} \approx 10^{48} f_{\nu, \mu\text{Jy}} d_{L,28}^2 \Gamma_2 R_{15} \nu_{p,6} B'^{-1} L_{\gamma,52}^{-1}, \quad (187)$$

and the energy in these protons is

$$E_p \approx N_p (\gamma'_p m_p c^2) \Gamma \approx 3.0 \times 10^{51} \frac{\Gamma_2^3 f_{\nu, \mu\text{Jy}} d_{L,28}^2 R_{15}}{B' L_{\gamma,52} (1+z)} \text{ erg}. \quad (188)$$

It is more useful to consider the luminosity carried by these protons ( $L_p$ ) for determining the efficiency of the photo-pion process for high energy  $\gamma$ -ray production. The proton-luminosity is related to  $E_p$  via

$$L_p = E_p \Gamma \times \max\{t_{dyn}'^{-1}, t_{cool}'^{-1}\}, \quad (189)$$

where  $t'_{dyn}$  is the dynamical time in the jet comoving frame

$$t'_{dyn} = \frac{R}{2c\Gamma} \approx (170 \text{ s}) R_{15} \Gamma_2^{-1}, \quad (190)$$

and  $t'_{cool}$  is the synchrotron cooling time<sup>46</sup> for a positron with LF  $\gamma'_e$  (Eq. (181)) that is moving in a magnetic field given by Eq. (184),

$$t'_{cool} = \frac{6\pi m_e c}{\sigma_T B'^2 \gamma'_e} \approx (8 \times 10^{-2} \text{ s}) \frac{\Gamma_2^5}{v_8^2 v_{p,6}^3 (1+z)^5}. \quad (191)$$

Substituting, Eqs. (184), (188), (190) and (191) into (189), we find the proton luminosity to be [604]

$$L_p = \begin{cases} 2 \times 10^{49} \Gamma_2^8 f_{v,\mu\text{Jy}} d_{L,28}^2 L_{\gamma,52}^{-1} v_8^{-1} v_{p,6}^{-2} (1+z)^{-4} \text{ erg s}^{-1} & t'_{cool} > t'_{dyn} \\ \Gamma_2^2 f_{v,\mu\text{Jy}} d_{L,28}^2 v_8 v_{p,6} L_{\gamma,52}^{-1} (1+z) R_{15} \text{ erg s}^{-1} & t'_{cool} < t'_{dyn}. \end{cases} \quad (192)$$

This proton luminosity is based on taking the magnetic field strength as given in Eq. (184). It might be tempting to think that a larger magnetic field might reduce  $L_p$ . However, that turns out not to be the case because even though a larger  $B'$  means that  $e^+$  LF ( $\gamma'_e$ ) needed for producing a photon of a desired synchrotron frequency is smaller ( $\gamma'_e \propto B'^{-1/2}$ ), it also means that a smaller fraction of particles produced by the photo-pion process can radiate at this frequency at any given time since the synchrotron cooling time decreases as  $B'^{-2} \gamma'^{-1} \propto B'^{-3/2}$ ; the latter effect overwhelms the net gain of the former as can be readily seen by the dependence of  $L_p$  on  $v_8$  in Eq. (192).<sup>47</sup>

We can assess the viability of the photo-pion process for producing  $> 10^2$  MeV photons detected by the Fermi satellite from a number of highly luminous GRBs. Let us consider the data for a particular burst, GRB 080916C, as an example. This burst was at a redshift of 4.3,  $d_{L,28} = 12$ , the peak of the observed spectrum was at 400 keV, and the flux at 100 MeV during the burst was  $f_v \sim 3 \mu\text{Jy}$ . The  $\gamma$ -ray isotropic luminosity for GRB 080916C was  $L_{\gamma,52} \sim 20$ , and the jet LF is estimated to be  $\Gamma_2 \sim 9$  (e.g. [99,605]). For these parameters we find  $t'_{cool} < t'_{dyn}$  as long as  $R > 10^{15}$  cm, and in that case the required luminosity in protons of LF  $\gtrsim 10^5$  is  $L_p \sim 1.5 \times 10^{56} R_{15}$  erg/s. This is larger than the  $\gamma$ -ray luminosity by a factor  $\sim 700$ , if the radiation is produced at  $R = 10^{15}$  cm. For  $R < 10^{15}$  cm,  $t'_{dyn} < t'_{cool}$  and the proton luminosity is independent of  $R$ . The total luminosity carried by protons, if their distribution function extends down to LF  $\sim 10$  with  $p = 2.4$ , is another factor of  $\sim 40$  larger, and that makes the photo-pion process unacceptably inefficient for this burst. Moreover, the high proton luminosity required for the photo-pion process is inconsistent with the upper limit on high-energy neutrino flux from GRBs provided by the IceCube observations [606].

### 7.9.2. Bethe–Heitler process

We assess the viability of the Bethe–Heitler process in this sub-section for producing high energy  $\gamma$ -rays detected by Fermi/LAT from a number of bursts.

The cross-section for Bethe–Heitler pair production process –  $p + \gamma \rightarrow p + e^+ + e^-$  – has a strong dependence on the angle between the outgoing electron and the incident photon in the nuclear rest frame. Assuming that the protons and photons are isotropic in the jet's rest frame, and using the head on approximation, i.e. the angle between the photon and proton is zero in the nuclear rest frame,  $\epsilon'' = 2\gamma'_p \epsilon'$  [where  $\epsilon' = h\nu'/(m_e c^2)$ ], the equation for the rate of production of secondary electrons is:

$$\frac{d\dot{N}_e}{d\gamma'_e} = 2c \int_0^\infty d\epsilon' n'(\epsilon') \int_1^\infty d\gamma'_p N_p(\gamma'_p) \frac{d\sigma_{BH}(\epsilon', \gamma'_p)}{d\gamma'_e}, \quad (193)$$

where  $N_p$  is the number of protons in the shell with LF  $\gamma'_p$ , and  $n'(\epsilon')$  is the number density of photons in the jet comoving frame with dimensionless energy  $\epsilon'$  defined above. The differential cross section in the Born approximation integrated over angles, in the highly relativistic regime, was derived by Bethe & Maximon [608] (see [609], for a recent review)

$$\frac{d\sigma_{BH}}{d\gamma''_+} = \frac{3\alpha_f \sigma_T}{2\pi \epsilon''^3} \left( \gamma''_+^2 + \gamma''_-^2 + \frac{2}{3} \gamma''_+ \gamma''_- \right) \left( \log \frac{2\gamma''_+ \gamma''_-}{\epsilon''} - \frac{1}{2} \right) \quad (194)$$

where  $\gamma''_+$ ,  $\gamma''_-$  are the Lorentz factors of the positron and electron, respectively, in the nuclear rest frame, as are all other variables in the above equation, and  $\alpha_f \approx 1/137$  is the fine-structure constant. The differential cross-section peaks sharply

<sup>46</sup> To be more precise,  $t'_{cool}$  is the radiative cooling time which includes inverse-Compton and synchrotron contributions. However, for positrons of LF  $\gtrsim 10^6$  considered here, the IC scattering lies in the Klein–Nishina regime, and so for a large part of the GRB parameter space, synchrotron losses dominate.

<sup>47</sup> If the synchrotron cooling time for  $e^\pm$  radiating at  $v_8$  is larger than the dynamical time, then a magnetic field of strength higher than that given by Eq. (184) does reduce the energy requirement for protons; the dependence on  $B$  is weak though. However, for the vast majority of allowed GRB parameter space, the cooling time is smaller than the dynamical time.

when the angle between the incoming photon and the outgoing  $e^\pm$  in the nuclear rest frame ( $\theta_\pm''$ ) is  $\sim 1/\gamma_\pm''$ . So, for  $\gamma_p' \gg \gamma_\pm''$ , the Lorentz factor of  $e^\pm$  in the jet rest frame is

$$\gamma_\pm' = \gamma_p' \gamma_\pm'' (1 - \beta_p' \beta_\pm'' \cos \theta_\pm'') \approx \frac{\gamma_p' \gamma_\pm''}{2} (\gamma_p'^{-2} + \gamma_\pm''^{-2} + \theta_\pm''^{-2}) \approx \frac{\gamma_p'}{\gamma_\pm''}. \quad (195)$$

Therefore, pairs produced via the Bethe–Heitler process have LF (in jet comoving frame) that is smaller than the proton LF most of the time.

If  $\epsilon'' \ll m_p/m_e \sim 10^3$ , the proton recoil can be neglected and the following equality holds

$$\gamma_+'' + \gamma_-'' = \epsilon''. \quad (196)$$

For large  $\epsilon''$ , the differential cross-section decreases extremely rapidly when  $\gamma_\pm'' < 2$ . Therefore, we restrict ourselves to  $\gamma_\pm'' \geq 2$ . In this regime, the differential cross section simplifies as follows

$$\frac{d\sigma_{BH}}{d\gamma_+''} \approx \frac{\alpha_f \sigma_T}{\epsilon''}, \quad \text{if } 2 \leq \gamma_+'' \leq \epsilon'' - 2. \quad (197)$$

Or writing Eq. (197) in terms of quantities in the jet comoving frame, using  $\epsilon'' \approx 2\gamma_p'\epsilon'$ , we find:

$$\frac{d\sigma_{BH}}{d\gamma'_+} \approx \frac{\alpha_f \sigma_T}{2\epsilon' \gamma_+'^2}, \quad \text{if } \frac{1}{2\epsilon'} \leq \gamma'_+ \leq \frac{\gamma_p'}{2}. \quad (198)$$

The integral in Eq. (193) can be simplified when we exclude the part of the  $\gamma'_p$ - $\epsilon'$  plane where the cross-section,  $\sigma_{BH}$ , is small, i.e.  $\epsilon' \lesssim \gamma_e'^{-1}$  and  $\gamma_p' \lesssim 2\gamma_e'$ . The cross-section in the remainder of the plane is given by Eq. (198). With these approximations, and taking the photon spectrum to be Band function with indices  $\alpha$  &  $\beta$ , the integral in Eq. (193) is straightforward to calculate and the result is [604]

$$\frac{dN_e}{d\gamma'_e} \approx \begin{cases} \frac{2c\alpha_f \sigma_T}{\beta(p+1)\gamma'_e} n'(\epsilon'_p) N_p(\gamma'_i) \left(\frac{\gamma'_e \epsilon'_p}{5}\right)^{-\beta} \left(\frac{2\gamma'_e}{\gamma'_i}\right)^{-p} & \text{for } \frac{\gamma'_i}{2} \leq \gamma'_e \leq 5/\epsilon'_p \\ \frac{2c\alpha_f \sigma_T \epsilon'_p}{5\beta(p+1)} n'(\epsilon'_p) N_p(\gamma'_i) \left(\frac{10}{\epsilon'_p \gamma'_i}\right)^{-p} \left(\frac{\epsilon'_p \gamma'_e}{5}\right)^{-\alpha-p-1} & \text{for } 5/\epsilon'_p \leq \gamma'_e \leq 5/\epsilon'_{\min} \end{cases} \quad (199)$$

where  $\epsilon'_p = h\nu_p(1+z)/(\Gamma m_e c^2)$  is the dimensionless photon energy at the peak of the spectrum in the jet comoving frame (which is of order  $10^{-2}$  for a typical long-GRB),  $\gamma'_i$  is the minimum LF of protons in the jet comoving frame, and  $\epsilon'_{\min}$  is the dimensionless photon energy (jet comoving frame) below which the source becomes opaque due to synchrotron absorption and the spectrum declines rapidly; the value of  $\epsilon'_{\min}$  is poorly constrained by GRB observations, but theoretical calculations suggest it is likely of order  $10^{-7}$ , which corresponds to a synchrotron self-absorption frequency of a few eV in the observer frame.

The peak cross-section for the Bethe–Heitler process is roughly 10 times larger than the cross section for the photo–pion  $\Delta$ -resonance. For any given proton LF, the photon energy required for the former process is roughly 50 times smaller than the photo–pion process. Moreover, protons of LF  $\gamma'_p$  produce  $e^\pm$  with an average Lorentz factor  $\sim \gamma'_p/4$  via the Bethe–Heitler process (Eqs. (195) and (197)), whereas  $\gamma'_e \sim 50\gamma'_p$  for the  $\Delta$ -resonance of the photo–pion process (Eq. (181)).

Therefore, the ratio of the rate of generation of  $e^\pm$  with LF  $\gtrsim \gamma'_e$  by the Bethe–Heitler and photo–pion processes is  $\sim 10 \times (10^4)^{-\alpha-1} \times (200)^{-p+1}$ ; where the first factor is the ratio of the cross-sections for the two processes, the second factor accounts for the larger number of photons that participate in the Bethe–Heitler process – the dimensionless photon threshold energy for producing  $e^\pm$  of LF  $\gamma'_e$  by the B–H process is  $\epsilon' \sim \gamma_e'^{-1}$  and for the photo–pion it is  $10^4 \gamma_e'^{-1}$  – and the third factor is due to the fewer number of protons that are capable of producing positrons of LF  $\gtrsim \gamma'_e$  via the Bethe–Heitler process. For  $\gamma'_e \gtrsim 10^6$ , the threshold photon energy for both processes lies below the peak of the spectrum, and in that case  $\alpha \sim -1$ . Thus, for these high energy positrons, the Bethe–Heitler is less efficient than the photo–pion process by a factor  $\sim 10^2$ . However, for  $\gamma'_e \lesssim 10^3$ , the threshold photon energy lies above the peak of the spectrum, and the Bethe–Heitler process is a lot more efficient than the photo–pion process [604]. Whether the Bethe–Heitler or photo–pion process are more important for the intermediate regime,  $10^3 \lesssim \gamma'_e \lesssim 10^6$ , depends on the spectral indices, proton distribution index  $p$ , and  $\epsilon'_p$ .

Relativistic shocks are believed to accelerate electrons to  $\gamma'_e \gg 10^3$  efficiently via the Fermi mechanism, and that might suggest that the Bethe–Heitler process cannot compete with it and play an important role for GRBs. However, Bethe–Heitler might be important for those GRBs where the number of  $e^\pm$ s produced by this process is larger than the number of electrons that came with protons in GRB jets. We quantify this condition below.

Let us consider the isotropic luminosity carried by protons in a GRB jet to be  $L_p$ , which is a factor  $\eta_p$  larger than the  $\gamma$ -ray luminosity:  $L_p = \eta_p L_\gamma$ . The co-moving number density of electrons associated with protons is

$$n'_e = n'_p \approx 2 \times 10^9 \eta_p L_{\gamma,52} \Gamma_2^{-2} R_{15}^{-2}. \quad (200)$$

The number density of  $e^\pm$  produced by the Bethe–Heitler process is [604]

$$n'_{BH} \approx \alpha_f \sigma_T n'_\gamma n'_p R / \Gamma \Rightarrow \frac{n'_{BH}}{n'_e} < \alpha_f \sigma_T n'_\gamma R / \Gamma, \quad (201)$$

where  $\alpha_f \approx 1/137$  is the fine-structure constant, and the inequality is due to the fact that only a fraction of protons have sufficient energy for pair production. Since the optical depth to Thomson scattering associated with proton–electrons is  $\tau_T = \sigma_T n'_e R / \Gamma$ , we find

$$\frac{n'_{BH}}{n'_e} < \alpha_f \frac{n'_\gamma \tau_T}{n'_e} \sim 10^3 \tau_T \eta_p^{-1} \Gamma_2 v_{p,6}^{-1} (1+z)^{-1} \quad (202)$$

where we used Eq. (182) for  $n'_\gamma$ . The Bethe–Heitler process is likely important whenever  $n'_{BH}/n'_e > 1$ .

### 7.9.3. Proton synchrotron model for producing $>10^2$ MeV photons

Protons are easier to accelerate in shocks due to their lower rate of radiative losses, and the Lorentz factor that protons can attain is much larger than the maximum LF electrons can be accelerated to. It is easy to show that the maximum synchrotron photon energy for protons (accelerated in shocks) is a factor  $m_p/m_e$  larger than that for electrons, i.e. instead of a maximum energy of  $\sim 50$  MeV for electron-synchrotron photons (see Section 2.2.3), the proton synchrotron process can produce photons of energy  $10^2$  GeV (in the jet comoving frame). For this reason, whenever photons of energy larger than  $\sim 10^2 \Gamma$  MeV are detected from a source, proton synchrotron process is suggested as a possible radiation mechanism for the generation of these photons (e.g. [598–602,457,604]).

However, due to the low radiative efficiency of the proton-synchrotron process, the energy requirement to produce  $\gtrsim$ GeV photon flux at the level observed by the Fermi satellite, for a number of GRBs, is found to be highly excessive [604].

Let us consider protons of LF  $\gamma_i$  in the GRB-jet comoving frame. The synchrotron frequency for these protons is

$$\nu_i = \frac{qB' \Gamma \gamma_i^2}{2\pi m_p c (1+z)} \approx 6.3 \times 10^{-10} B' \Gamma_2 \gamma_i^2 (1+z)^{-1} \text{ eV.} \quad (203)$$

A reasonable upper limit for  $B'$  is obtained by requiring that the luminosity carried by magnetic fields is not much larger than the  $\gamma$ -ray luminosity,  $L_\gamma$ , in order to avoid low radiative efficiency of GRBs ( $\lesssim 10\%$ ) which is not supported by observations. The luminosity carried by magnetic fields is  $R^2 B'^2 c \Gamma^2$ . Therefore,  $B' \lesssim 2 \times 10^3 L_{51}^{1/2} R_{15}^{-1} \Gamma_2^{-1}$  Gauss. Substituting this into Eq. (203), we find  $\gamma_i \gtrsim 2 \times 10^7 L_{51}^{-1/4} R_{15}^{1/2}$  in order to produce photons of energy  $\sim 1$  GeV.

The typical proton Lorentz factor associated with the random component of velocity, in a relativistic shock, is approximately equal to the LF of the shock front with respect to unshocked fluid if every proton crossing the shock front is accelerated; proton LF is proportionally larger if only a small fraction of protons are accelerated and the remaining ones are “cold” downstream of the shock front. Considering that the LF for GRB internal shocks is of order a few to perhaps a few tens, the typical proton LF should be  $\sim 10$ – $10^3$  (the larger value corresponds to when only 1 in  $\sim 10^2$  protons are accelerated as suggested by some simulations, e.g. [387]). Considering that  $\gamma_i \gg 10^3$ , the proton synchrotron spectrum should extend down to photon energies of  $\sim 10$  eV, and the spectrum between 10 eV and 1 GeV should be  $f_\nu \propto \nu^{-(p-1)/2}$ ; where  $p \gtrsim 2.2$  is the power law index for the proton distribution function. Thus, if the proton synchrotron flux at 1 GeV matches the observed value, then this process would overproduce the flux below MeV.<sup>48</sup> Another problem with this process is the excessive energy requirement described below.

The synchrotron flux  $f_{\nu_i}$  at  $\nu_i$  is

$$f_{\nu_i} \approx 7B' N_{52} \Gamma_2 (1+z) d_{L,28}^{-2} \mu\text{Jy}, \quad (204)$$

where  $N$  is the total number of protons (assuming an isotropic source), in a region of comoving radial width  $\delta R' = R/\Gamma$ , from which radiation at  $\nu_i$  is received at a fixed observer time. In order to account for  $\sim 0.1$   $\mu\text{Jy}$  flux at 1 GeV observed for several GRBs at  $z \approx 2$  &  $d_{L,28} \approx 4.5$  (e.g. [99,359,101,102]), it is required that  $N \gtrsim 5 \times 10^{47} R_{15} L_{51}^{-1/2}$ . Therefore, the energy in protons in the shell of thickness  $\delta R'$ , responsible for the GeV emission, is:

$$E_{\text{proton}} = m_p c^2 N \Gamma \gamma_i \gtrsim 10^{54} R_{15}^{3/2} L_{51}^{-3/4} \Gamma_2 \text{ erg,} \quad (205)$$

and the luminosity carried by these very high LF protons is [604]:

$$L_{\text{proton}} \sim \frac{E_{\text{proton}} c}{R/\Gamma^2} \gtrsim 10^{54} R_{15}^{1/2} L_{51}^{-3/4} \Gamma_2^3 \text{ erg s}^{-1}. \quad (206)$$

---

<sup>48</sup> The observed spectra are often  $f_\nu \propto \nu^0$  below the peak of the spectrum which lies at a few hundred keV. The proton-synchrotron spectrum, as we have discussed, is  $\nu^{-0.6}$  or steeper between  $\sim 10$  eV and GeV, and therefore it would dominate below  $\sim 1$  MeV, in clear conflict with data.

GRBs from which GeV photons are detected have  $200 \lesssim \Gamma \lesssim 10^3$  [99,359,553,555]. For these bursts, the requirement on luminosity carried by protons of  $\text{LF} \gtrsim 10^7$  is  $L_p \gtrsim 10^{55} \text{ erg s}^{-1}$ , and the total proton luminosity – most of which is in protons of  $\text{LF} \ll 10^7$  – is at least  $10^{56} \text{ erg s}^{-1}$ . This makes the energy requirement for the proton-synchrotron process a factor  $\sim 10^3$  larger than the energy in  $\gamma$ -rays, and therefore this process is too inefficient to account for the observed GeV emission from GRBs.

### 7.10. Magnetic jet model

Magnetic outflows in the astrophysical context have been extensively investigated for decades in order to understand properties of jets associated with active galactic nuclei (AGNs), micro-quasars, pulsars and relatively more recently GRBs.

We consider in this section an outflow where magnetic fields carry a substantial fraction of the luminosity at the base of the jet where it is launched. We describe how such a Poynting jet can be accelerated by converting the magnetic field energy to bulk kinetic energy of the jet, and how radiation might be produced.

A class of magnetic jet models has been developed that is based on the force-free electrodynamics approximation (or “magnetodynamics”) in which the plasma inertia is ignored e.g. [610]. This approach has limited application because the neglect of the inertia term means that these models cannot account for the transformation of magnetic energy to jet kinetic energy, which is an important process of interest to many astrophysical systems.

The acceleration of a magnetic jet can proceed either by dissipation of field (if the magnetic field has the right geometry and scale, such as the stripped configuration of a pulsar wind) or by adiabatic expansion of the outflow.

Analytical and semi-analytical solutions have been found for a limited class of configurations that are characterized by steady-state, axisymmetric, dissipation-less flows. For instance, Li et al. [611] described a self-similar solution for a cold magnetic outflow. They find that the jet acceleration takes place over a very extended range of distance, well past the fast magnetosonic surface – the surface where the magnetosonic wave speed is equal to the flow speed – until the magnetization parameter ( $\sigma$ ) drops to order unity (for comparison, for a radial wind, the outflow LF saturates at  $\sim \sigma_0^{1/3}$  and  $\sigma$  does not decrease below  $\sim \sigma_0^{2/3}$ );  $\sigma \equiv B^2/[4\pi(\rho'c^2 + p')]$ , and  $\sigma_0$  is the initial magnetization parameter of the outflow. Vlahakis and königl [612], Vlahakis et al. [613] and Beskin and Nokhrina [614] extended this work and found an exact self-similar solution for an initially hot, axisymmetric, magnetic jet.<sup>49</sup>

Recent advances in numerical solutions for relativistic MHD have led to significant progress in our understanding of the magnetic jet launching mechanism, propagation and acceleration (e.g. [617–627]).

The plan for this sub-section is that we first discuss a steady state, axisymmetric outflow, and show that the asymptotic Lorentz factor is limited to  $\sim \sigma_0^{1/3}$  for spherically symmetric systems, as pointed out by Goldreich and Julian [628]. For an outflow of a finite opening angle ( $\theta_j$ ), the asymptotic value of LF is larger by a factor  $\theta_j^{-2/3}$  provided that it is collimated by the pressure of an external medium and causal contact across the jet in the transverse direction is maintained.

Next, we drop the assumption of steady state and describe the acceleration of an impulsive outflow of finite radial extent due to adiabatic expansion. Jet acceleration when ideal-MHD approximation breaks down, magnetic field is dissipated, and its energy is converted to the bulk kinetic energy of plasma is taken up last.

#### 7.10.1. Adiabatic expansion and acceleration of a Poynting jet

We consider in this sub-section an axisymmetric, highly magnetized, time independent outflow. The magnetization parameter of the outflow,  $\sigma$ , is defined as the ratio of Poynting flux and energy flux carried by particles,

$$\sigma = \frac{B^2}{4\pi(\rho'c^2 + p')\Gamma^2} = \frac{B'^2}{4\pi(\rho'c^2 + p')}, \quad (207)$$

where  $B'$ ,  $\rho'$  and  $p'$  are magnetic field strength, internal plus rest mass energy density, and pressure as measured in the local plasma comoving frame;  $B$  and  $\Gamma$  are magnetic field strength and outflow LF as measured in the CoE frame. The base of the outflow is at  $R = R_0$ , where the magnetization parameter is  $\sigma_0 \equiv \sigma(R_0)$  and the Lorentz factor is  $\Gamma_0$ ;  $\sigma_0 \gg 1$ .

The conservation of energy flux for a cold magnetized outflows governed by the non-dissipative ideal MHD equations is

$$R^2 [\pi\rho'c^2\Gamma^2v + B'^2\Gamma^2v/4]\theta_j(R)^2 = L, \quad (208)$$

where  $\theta_j(R)$  is half-angular-size of the jet at radius  $R$ ,  $v$  is the proper velocity of the jet corresponding to  $\Gamma$ , and the second term is the Poynting luminosity (electric field in the outflow comoving frame vanishes). The equation for the conservation of mass flux is

$$\pi R^2\theta_j(R)^2\rho'\Gamma v = \dot{M}. \quad (209)$$

These two equations can be combined to give

$$\Gamma(1 + \sigma) = L/\dot{M}c^2 = \Gamma_0(1 + \sigma_0). \quad (210)$$

<sup>49</sup> A non-axisymmetric jet is typically subject to instabilities [615,616], and that can substantially increase the efficiency of jet acceleration.

As the outflow moves to larger distances,  $\sigma$  decreases and  $\Gamma$  increases and their product remains constant. According to these conservation laws, it is allowed for the magnetic energy to be entirely converted to outflow kinetic energy, and in that case the outflow LF attains a value of  $(1 + \sigma_0)\Gamma_0 \approx \sigma_0$ . For a steady, spherical, outflow, however, the LF stops increasing when  $\Gamma \approx \sigma_0^{1/3}$  [628]. The reason for this is that when  $\Gamma \gtrsim \sigma_0^{1/3}$ , causal contact is only maintained in a narrow region of the outflow and magnetic pressure gradients can no longer accelerate the flow. To see this, let us consider a signal propagating at a speed  $c'_s$  and at an angle  $\theta'$  with respect to the radial direction in the comoving frame. The signal speed and direction in the CoE frame are  $c_s$  and  $\theta$ . The 4-velocity in the outflow frame is  $\Gamma'_s(1, c'_s \cos \theta', c'_s \sin \theta', 0)$ , and in the CoE frame  $\Gamma_s(1, c_s \cos \theta, c_s \sin \theta, 0)$ . Taking the outflow velocity and LF to be  $v$  and  $\Gamma$ , and Lorentz transforming the CoE frame 4-velocity for signal propagation to the comoving frame, we find

$$\Gamma'_s = \Gamma \Gamma_s (1 - vc_s \cos \theta/c^2), \quad (211)$$

which can be solved to determine the signal speed,  $c_s$ , in CoE frame

$$\frac{c_s}{c} = \frac{v \cos \theta/c + [v^2 \cos^2 \theta/c^2 + (\Gamma'_s/\Gamma)^2 - 1]^{1/2} (\Gamma'_s/\Gamma)}{v^2 \cos^2 \theta/c^2 + \Gamma_s'^2/\Gamma^2}. \quad (212)$$

The signal propagation in the CoE frame is confined to a narrow cone of half-opening angle,  $\theta_s$ , with axis along the direction of outflow velocity, when  $\Gamma'_s/\Gamma < 1$ . This angle can be obtained by setting the discriminant to zero in the above equation. We thus find,

$$\sin \theta_s = \frac{\Gamma'_s c'_s}{\Gamma v}, \quad (213)$$

which is a relativistic generalization of the familiar expression for “Mach cone” opening angle when an object moves at a speed faster than the signal speed in the medium. Points outside the “Mach cone” are not in causal contact with the apex of the cone.

The fast-magnetosonic wave proper-velocity in the jet comoving frame is

$$\Gamma'_s c'_s = (B^2/4\pi\rho')^{1/2} = c \sigma^{1/2} \approx c(\sigma_0/\Gamma)^{1/2}. \quad (214)$$

We used Eqs. (207) and (210) for deriving the last two relations. Thus,  $\theta_s < \pi/2$  when  $\Gamma > \sigma_0^{1/3}$ , and only part of the outflow is causally connected in the lateral direction (see Fig. 32). For a collimated outflow with opening angle  $\theta_j$ , lateral causal contact can be maintained as long as  $\Gamma \lesssim \sigma_0^{1/3} \theta_j^{-2/3}$ . During this phase, the acceleration of the magnetic jet is governed by pressure stratification of the surrounding medium.

Far away from the CoE, magnetic fields are predominantly toroidal (transverse to the radial direction), and the field falls off as  $1/R$  if the jet diameter increases linearly with  $R$ . In this case,  $\sigma \propto B^2/\rho$  has no explicit dependence on  $R$ , and therefore  $\Gamma$  does not increase with distance (see Eq. (210)). In order for  $\Gamma$  to increase with  $R$ , the separation between neighboring magnetic field lines must increase faster than  $R^1$ . This can only be done if different parts of the jet are in causal contact so that as the pressure of the ambient medium (e.g. GRB progenitor star) decreases with radius, a signal can propagate from the outer to the inner part of the jet and field lines can fan outward in response.

If the pressure of the ambient medium decreases as  $p \propto R^{-a}$ , then the transverse size of the jet and the jet Lorentz factor both increase as  $R^{a/4}$  for  $a \leq 2$  [624].<sup>50</sup> Thus, the radius where the jet Lorentz factor is equal to the fast-magnetosonic wave Lorentz factor is given by  $R_{ms} \sim R_0 \sigma_0^{4/3a}$ ; where  $R_0$  is the radius where the jet is launched. For  $a \gtrsim 2$ , the central region of the jet ceases to be in causal contact with the external medium at radius  $R_{ncc} \sim R_0 \sigma_0^{4/3a} \theta_j(R)^{-8/3a}$ , and consequently the jet acceleration is more or less terminated at  $R \sim R_{ncc}$ .

A steady state collimated outflow, with a small opening angle  $\theta_j(R)$ , confined by the pressure of an external medium, can accelerate to a terminal LF  $\Gamma \sim \min \left\{ \sigma_0, \sigma_0^{1/3} \theta_j^{-2/3} \right\}$  while causal contact with the external medium is maintained. This suggests that for an efficient acceleration of jet to LF  $\Gamma \sim \sigma_0, \theta_j \sigma_0$  should be less than 1, whereas GRB afterglow observations suggest  $\theta_j \Gamma \sim 10$  [37]. MHD simulations of high magnetization jets carried out by Komissarov et al. [629] and Tchekhovskoy et al. [627] find that magnetic field lines fan outward rapidly when the jet emerges from the surface of the progenitor star into the surrounding vacuum. This leads to a sudden increase to the jet LF by a factor of a few to  $\sim 10$  for long duration GRBs

<sup>50</sup> The result  $\Gamma \propto R^{a/4}$  is easy to understand. To maintain pressure equilibrium, the magnetic field in the jet comoving frame falls off as  $R^{-a/2}$  since the pressure on the sideways surface of the jet, which is perpendicular to the jet velocity, is same in the jet comoving frame and the star's rest frame. Let us take the jet transverse radius to increase with  $R$  as  $R_\perp(R)$ . The transverse and the radial components of the magnetic field, in the rest frame of the star, scale as  $B_\phi \propto R_\perp^{-1}$  and  $B_r \propto R_\perp^{-2}$  respectively. These field components in the jet rest frame vary as  $R_\perp^{-1}/\Gamma(R)$  and  $R_\perp^{-2} B'_\phi$  (jet comoving frame transverse field) should not be much stronger than  $B_r$ , otherwise the jet becomes unstable and constricted. And it is difficult to have  $B'_r > B'_\phi$  over an extended interval of  $R$  since that requires the jet to continue to flare up rapidly in the transverse direction, which is prevented by the pressure of the external medium. Taking  $B'_\phi \sim B'_r$  (for a jet in lateral pressure balance with the external medium) we find  $\Gamma \propto R_\perp$ , and therefore the magnetic pressure falls off as  $\Gamma^{-4}$ . Equating the magnetic pressure with the external pressure, we finally obtain  $\Gamma \propto R^{a/4}$ . We are grateful to Jonathan Granot, for pointing out the simple, physical, arguments in this footnote.

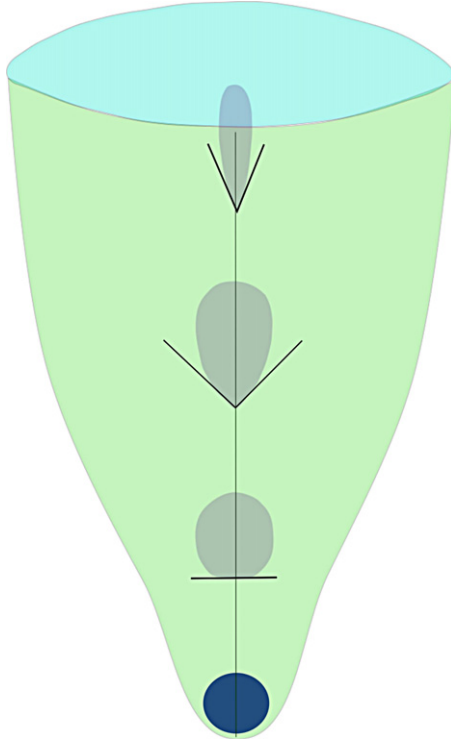


**Fig. 32.** The darker shaded regions show the causally connected part of the jet at different distances from the jet launching site as seen by a lab frame observer. Fast magnetosonic signal propagation is confined to cones of decreasing opening angle as the jet accelerates with distance. When the opening angle of the “causal cone” becomes smaller than the jet opening angle then the jet is no longer in causal contact with the external medium in the direction normal to the jet axis and its acceleration cannot be influenced by the pressure stratification of the GRB progenitor star.

while their jet opening angle remains essentially unchanged. The rapid acceleration phase ceases when the rarefaction wave crosses the jet in the transverse direction. This short lived phase of sudden acceleration could be responsible for  $\theta_j \Gamma \sim 10$  as GRB observations suggest. However, jets produced by short duration GRBs, which are not collimated by the envelope of a star, are unlikely to undergo this sudden acceleration phase, and yet for these bursts  $\theta_j \Gamma \gtrsim 10$ . This poses an interesting puzzle regarding jet acceleration mechanism for a Poynting flux dominated jet.

We now drop the steady state assumption, and consider the acceleration of a magnetic outflow of a finite, short, duration. An outflow of a short spatial extent can undergo efficient acceleration while traveling in vacuum as a result of adiabatic expansion, e.g. Contopoulos [630] who considered adiabatic expansion and acceleration of a Newtonian jet, and Granot et al. [631] showed that a relativistic outflow can attain the limiting LF of  $\sigma_0$  while traveling in vacuum and its  $\sigma$  can decrease well below unity as a result of continued adiabatic expansion. The adiabatic expansion and acceleration of a spherical, relativistic, outflow of short spatial extent with  $\sigma_0 \gg 1$  is described next.

Consider a thin shell of magnetized plasma undergoing adiabatic expansion in vacuum driven by magnetic pressure. For simplicity, we will consider the magnetic field in the shell to be uniform and of strength  $B(R)$  in the CoE frame when the shell is at radius  $R$ . The field orientation is transverse to the radial vector. Consider two spherical surfaces within this magnetized shell, one of which lies close to the front end of the shell and the other somewhere in the middle. These surfaces are frozen into the shell plasma and move with them as the shell expands. The separation between the surfaces is  $\xi(R)$  in the CoE frame when the shell is at a distance  $R$  from the center. The difference in speed between these surfaces, in the CoE frame, is  $\sim c/[2\Gamma(R)^2]$ ; the front end of the shell is moving faster. The plasma in the shell is in causal contact in the radial direction (the causal contact in the transverse direction extends only to distance  $\sim R/\Gamma$ ).

The separation between the surfaces increases with  $R$  as

$$\xi(R) = \xi(R_i) + \int_{R_i}^R \frac{dr}{2\Gamma^2(r)}. \quad (215)$$

The magnetic field strength can be obtained by flux conservation across a planar annulus of width  $\xi$  that is perpendicular to the two spherical surfaces

$$B(R) = B_i \frac{\xi_i R_i}{\xi(R) R}, \quad (216)$$

where  $B_i \equiv B(R_i)$  &  $\xi_i \equiv \xi(R_i)$ .

The total electro-magnetic energy contained in between the two spherical surfaces, in the CoE frame, is

$$E_B = B^2 R^2 \xi(R) = B_i^2 R_i^2 \xi_i^2 / \xi(R) \sim \frac{L \xi_i}{c} \left[ 1 - \int_{R_i}^R \frac{dr}{2 \Gamma^2(r) \xi_i} \right]. \quad (217)$$

The last step in the above equation was obtained by assuming that  $[\xi(R)/\xi_i - 1] \ll 1$ , which is a fine approximation to describe the dynamics of the shell because when  $\xi(R) \sim 2\xi_i$ , the electro-magnetic energy drops by a factor 2 and  $\Gamma \sim \sigma_i/2$ , i.e. the shell LF is close to attaining its terminal value.

The rate of increase of the kinetic energy of the plasma contained between the two spherical surfaces should be equal to the rate of decrease of electro-magnetic energy, i.e.

$$\frac{d}{dR} [4\pi R^2 \xi \rho c^2 \Gamma] = -\frac{dE_B}{dR} \sim \frac{L}{2c \Gamma^2}, \quad (218)$$

or

$$\frac{d(Mc^2 \Gamma)}{dR} \sim \frac{L}{2c \Gamma^2}, \quad (219)$$

where  $M = 4\pi R^2 \xi \rho$  is the plasma mass contained within the shell of thickness  $\xi$ , which does not change with time for a cold outflow undergoing adiabatic expansion. The solution of the above equation is straight forward to obtain and is given by

$$\Gamma(R) \sim \Gamma_i \left[ 1 + \frac{3\sigma_i}{2\Gamma_i^2} \frac{(R - R_i)}{\xi_i} \right]^{1/3}, \quad (220)$$

where  $\Gamma_i = \Gamma(R_i)$  and  $\sigma_i = \sigma(R_i)$ . Note that  $\Gamma$  attains a value  $\sim \Gamma_i \sigma_i^{1/3}$  when the jet has traveled a distance  $\sim \xi_i \Gamma_i^2$  [631]; for an outflow of a finite opening angle,  $\Gamma_i \sim \sigma_0^{1/3} \theta_j^{-2/3}$  is the LF at the time when the central part of the jet loses causal contact with the surrounding medium, so that any further acceleration of the jet results from its radial expansion.

The LF increases with radius as  $R^{1/3}$  until it approaches  $\Gamma_i \sigma_i \sim \sigma_0$  at  $R_s \sim \xi_i \sigma_0^2$  (Eq. (220) is not valid beyond this radius). The overall momentum conservation of the outflow is maintained by the back-end of the shell slowing down to a LF order unity, while the outer part of the shell, which contains most of the energy and momentum, accelerates to  $\Gamma \sim \sigma_0$ .

For  $R \gg R_s$ , the LF is approximately constant, and therefore  $\xi \propto R$  (the radial width of the jet increases linearly with  $R$ ),  $B \propto R^{-2}$  and  $\sigma \propto R^{-1}$ , e.g. [631]. So the shell magnetization can drop to well below unity at large distances, and shell collisions can then in principle convert the jet kinetic energy to internal energy efficiently.

### 7.10.2. Magnetic dissipation and jet acceleration

If the magnetic field geometry in a high  $\sigma_0$  outflow is such as to promote reconnection and dissipation, then a fraction of the magnetic energy can be converted to jet kinetic energy (Eq. (210)) and a fraction goes into accelerating electrons & protons by the electric field in the current sheet. Magnetic field reversing directions on short length scales, such as the stripped wind from a fast rotating pulsar, or scrambled field lines that result from repeated internal collisions of ordered, magnetized, outflow [108], are examples where reconnection is expected to take place. In the former case, the dissipation of magnetic energy and jet acceleration are gradual processes that take place over an extended range of radius, and is discussed below. In the latter case, the dissipation can be sudden, which is triggered by an instability when the magnetic geometry becomes sufficiently tangled.

The dissipation of magnetic energy, and jet acceleration, for a reversing magnetic field geometry, or any similar configuration that is conducive to reconnection, is described using a simplified picture that should capture the basic physics of a rather complex process.

Two effects control the acceleration of a jet when magnetic field is dissipated. One of which is a drop in thermal plus magnetic pressure when magnetic field is dissipated which can speed up magnetic reconnections (conversion of magnetic energy to thermal energy of particles and photons, even in the absence of any radiative loss, leads to a drop in the total pressure because the magnetic pressure is equal to the energy density, whereas the pressure for a relativistic fluid is one-third its energy density). The other process is the conversion of thermal energy (from magnetic dissipation) to jet kinetic energy as a result of adiabatic expansion. For the simplified calculations presented below, we will ignore radiative losses and assume that a good fraction of the magnetic energy dissipated is converted to bulk kinetic energy of the jet.

Let us consider an outflow which has a uniform magnetic field of strength  $B$  whose direction reverses on a length scale  $\ell_0$  (these quantities are in the CoE frame). The magnetic field is toroidal, and thus  $B(R) \propto R^{-1}$ . We assume that there is no differential velocity across stripes of radial width  $\sim \ell_0$ , and therefore the length scale over which the magnetic field reverses direction ( $\ell_0$ ) does not change with  $R$ .

Let us consider a highly simplified model for reconnection where we assume, following Drenkhahn and Spruit [632] and Drenkhahn [633], that the reconnection speed in the comoving frame of the jet is a fraction of the Alfvén speed, i.e. the speed at which plasma from outside the current sheet flows into it is  $v'_{in} = \epsilon V'_A$  (see Figs. 33 and 34 for schematic sketches

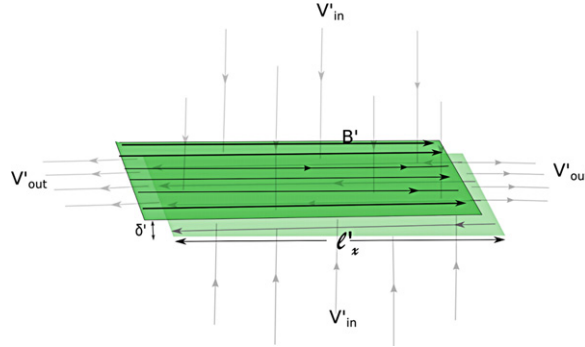


**Fig. 33.** A schematic sketch of current-sheet, and plasma from outside the sheet flowing toward it, for Sweet–Parker magnetic reconnection. The sketch only shows the region in the immediate vicinity of the current sheet. Magnetic field lines outside of the sheet are curved away from the center of the current sheet.

of possible reconnection scenarios). For a high  $\sigma$  plasma, the LF corresponding to the Alfvén speed is  $\sigma^{1/2} \gg 1$ , and thus we take  $v'_m = \epsilon c$ .

The radial width of the region where the magnetic field has been dissipated when the jet has traveled a distance  $R$  from the center of explosion is

$$w(R) \sim v'_m \left[ \frac{R}{c\Gamma(R)} \right] \frac{1}{\Gamma(R)} = \frac{\epsilon R}{\Gamma^2(R)}, \quad (221)$$

where the factor  $R/(c\Gamma)$  is time elapsed in the jet comoving frame, and  $\Gamma^{-1}$  transforms the comoving length to the CoE frame.

The total energy – magnetic, thermal and jet kinetic energies – contained within a segment of jet of radial width  $\ell_0$  should not change as the jet propagates to larger radii since the net energy flux across the segment is zero for a uniform system. Thus, any loss of magnetic energy should show up as an increase to the kinetic energy of the jet when the thermal energy share can be ignored. Therefore,

$$4\pi R^2 \rho \Gamma c^2 \ell_0 \sim w r^2 B^2 \sim w L/c, \quad (222)$$

where  $L$  is the total luminosity carried by the jet (which is a conserved quantity in absence of radiative losses). Since the mass flux associated with the jet is  $\dot{M} = 4\pi R^2 \rho c$ , we can rewrite the above equation as

$$\dot{M} \Gamma c^2 \sim \frac{L w}{\ell_0}, \quad \text{or} \quad \Gamma \sim \frac{L}{\dot{M} c^2} \frac{\epsilon R}{\Gamma^2 \ell_0}. \quad (223)$$

From Eq. (210)  $L/(\dot{M} c^2) = \sigma_0$ , and thus we arrive at the desired scaling for jet LF with  $R$

$$\Gamma(R) \sim (\epsilon \sigma_0)^{1/3} (R/\ell_0)^{1/3}. \quad (224)$$

It should be noted that the increase of  $\Gamma$  with distance for the magnetic dissipation model (Eq. (224)) is same as that for the adiabatic expansion case given by Eq. (220), even though the underlying physical processes are very different. The reason for the identical scaling is that the increase of  $\Gamma$  with  $R$  is ultimately set by the speed of rarefaction waves for the adiabatic expansion model and the reconnection speed (for magnetic dissipation) which are both of order  $c$ .

The jet LF attains its terminal value,  $\sim \sigma_0$ , when  $w(R_s) \sim \ell_0$ , i.e. when the magnetic field in the entire slab of width  $\ell_0$  has undergone reconnection. The radius where this occurs,  $R_s$ , is estimated from the above expression for  $w$  and is given by

$$R_s \sim \ell_0 \sigma_0^2 / \epsilon. \quad (225)$$

If the magnetic field in the outflow reverses direction on the length scale of light-cylinder radius for a millisecond pulsar, or the Schwarzschild radius for a  $\sim 10 M_\odot$  black hole, believed to be likely central engines for long-GRBs, then  $\ell_0 \sim 10^7$  cm. Numerical simulations for relativistic reconnection find  $\epsilon \sim 10^{-2}$  (e.g. [634]). Therefore,  $R_s \sim 10^{15} \sigma_{0,3}^2$  cm, which is much larger than the LF saturation radius for a thermal fireball ( $10^{10}$  cm).

McKinney and Uzdensky [635] studied the reconnection process of GRBs in a striped wind in detail. They found a transition from collisional reconnection to collisionless reconnection at a radius around  $10^{13}$ – $10^{14}$  cm, and they identify this as the GRB prompt emission site.

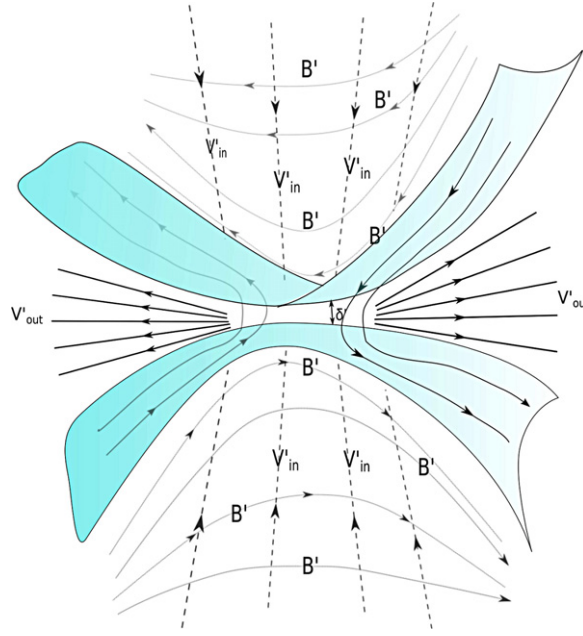


**Fig. 34.** A schematic sketch of plasma inflow, and current-sheet, for Petschek magnetic reconnection. Much of the plasma flowing toward the current sheet does not pass through it, but instead is redirected by standing shock waves; the inflow and outflow regions are separated by stationary slow mode shocks.

#### 7.10.3. Basic reconnection physics

A general discussion of magnetic field dissipation and jet acceleration when the direction reverses on a short distance scale is described in the previous subsection. In this subsection, we describe some aspects of the physics of magnetic dissipation in a reconnection layer, or current sheet, for an electron–proton plasma.

According to Sweet [636] and Parker [637], plasma consisting of oppositely oriented magnetic field can undergo forced reconnection where the magnetic field is dissipated on a time scale much shorter than the diffusion time. The basic configuration is a thin current sheet of width  $\delta'$ , and length,  $\ell'_x$ , where magnetic field is dissipated due to its large gradient across this region. Plasma carrying magnetic fields of strength  $B'$  flows into this region at speed  $v'_{in}$ , and is squirted out of the thin current sheet at proper-velocity  $v'_{out} \gamma'_{out}$  (see Fig. 33). The basic features of Sweet–Parker reconnection for a relativistic plasma – with magnetization parameter  $\sigma \gg 1$  – can be obtained from the conservation of mass and energy flux at the surface of the current sheet, and the pressure balance. The mass and energy flux conservation equations are

$$n''_1 \ell'_x v'_{in} = n''_2 \delta' v'_{out} \gamma'_{out}, \quad (226)$$

$$(B'^2 / 4\pi) \ell'_x v'_{in} = n''_2 \delta' m_p c^2 v'_{out} \gamma'_{out} \gamma_t', \quad (227)$$

where  $n''_1$  &  $n''_2$  are plasma densities outside and inside the current sheet, respectively, as measured in the local plasma rest frame, and  $\gamma_t'$  is the Lorentz factor associated with the random velocity component of protons, in the mean rest frame of plasma, inside the current sheet. The ratio of these equations give

$$\frac{B'^2}{4\pi n''_1 m_p c^2} \equiv \sigma = \gamma_A'^2 = \gamma'_{out} \gamma_t', \quad (228)$$

where  $V'_{A'} = B' / (4\pi n''_1 m_p)^{1/2}$  is the Alfvén wave proper-velocity outside the current sheet. If  $\gamma_t'$  were to be of order unity, then the Lorentz factor of the plasma leaving the current-sheet is  $\sim \gamma_A'^2$  [638]. Lyubarsky [639] has suggested that  $\gamma'_{out} \sim 1$ , however, his argument is based on making ad hoc assumptions regarding the length scale over which  $\gamma'_{out}$  changes and the strength of the magnetic field component perpendicular to the current sheet, which might not apply to GRB jets.

The magnetic pressure outside the current sheet should roughly equal the pressure inside the sheet provided by the transverse “thermal” motion of protons. This yields

$$\frac{B'^2}{8\pi} \sim n''_2 \gamma_t' m_p c^2 \quad \text{or} \quad \frac{n''_2}{n''_1} \sim \frac{\sigma}{\gamma_t'} \sim \gamma'_{out}, \quad (229)$$

where we used Eq. (228) to obtain the last equality.

The plasma inflow velocity toward the current sheet ( $v'_{in}$ ), which is the speed at which forced reconnection can proceed, is regulated by the requirement that the rate at which magnetic flux flows into the current sheet should not exceed the

rate at which magnetic field is dissipated inside the sheet (otherwise magnetic field will build up and prevent plasma from entering the sheet). Let us assume that the diffusion coefficient for magnetic field dissipation is  $\eta$ , which could be microscopic or turbulent in origin. The time scale for magnetic field dissipation in the current sheet is

$$t'_{B,\text{dissi}} \approx \frac{\delta'^2}{\eta}. \quad (230)$$

Therefore, the effective speed at which magnetic field dissipation proceeds inside the current sheet is given by

$$\frac{\delta'}{t'_{B,\text{dissi}}} \sim \frac{\eta}{\delta'}. \quad (231)$$

The speed for plasma flowing into the current sheet,  $v'_{in}$ , should be roughly this speed, i.e.  $v'_{in} \sim \eta/\delta'$ . Using Eqs. (226) and (229) we find

$$v'_{in} \sim (V'_A v'_{out})^{1/2} \gamma'_{out} s^{-1/2}, \quad (232)$$

where  $s$  is the Lundquist number, defined as

$$s \equiv \frac{\ell'_x V'_A}{\eta}. \quad (233)$$

For a typical GRB jet with  $\Gamma \sim 10^2$ ,  $\ell'_x \sim R/\Gamma$  (size of causally connected region in the jet comoving frame), isotropic jet luminosity of  $10^{52}$  erg s $^{-1}$  carried by magnetic fields ( $B' \sim 10^4 R_{15}^{-1}$  Gauss), &  $V'_A \sim c$ , we find  $s \sim 10^{11}$  in the Bohm diffusion limit, i.e. when  $\eta = cR'_L$  ( $R'_L$  is the proton Larmor radius), and hence the speed at which reconnection is expected to proceed according to Sweet–Parker mechanism is  $\sim 10^{-5}$  c, which is much too slow to be of practical interest. A fast steady-state reconnection scenario was proposed by Petschek [640], which invokes a much shorter length for the resistive layer, thereby significantly increasing the speed at which reconnection can proceed (see Fig. 34). However, according to resistive MHD simulations the Petschek model is unstable, unless the magnetic diffusivity increases near the X-point (e.g. [641]). Simulations also find that the Alfvénic tearing instability of Sweet–Parker current sheet (e.g. [642,643]) could increase the reconnection rate significantly.

Lazarian and Vishniac [644] proposed that reconnection in magnetic fields with stochastic geometry can proceed rapidly, thanks to the turbulent nature of the magnetized fluid that both broadens the reconnection zone and allows many independent reconnection events to occur simultaneously. Moreover, once reconnection gets started in one localized region, it can trigger many other reconnection events as a result of the plasma squirting out of the current sheet at speed  $V'_A$  and stirring up magnetic fields in neighboring regions. Three-dimensional numerical simulations of reconnection carried out by [645] provide support for this turbulence model.

In the presence of turbulence, magnetic fields reconnect on the length scale  $\lambda_{||}$  for magnetic field fluctuation, rather than the much larger global scale  $\ell'_x$ . Accordingly, it is the effective Lundquist number

$$s = \frac{\lambda_{||} V'_A}{\eta}, \quad (234)$$

that determines the speed at which reconnection proceeds.

In turbulent reconnection, the global reconnection rate is larger by a factor  $\sim \ell'_x/\lambda_{||}$ , since there are  $\sim \ell'_x/\lambda_{||}$  reconnection sites along any random direction cutting across the outflow [108]. As a result, the small local reconnection speed  $V'_{in} \sim V'_A/s^{1/2}$  is adequate to power a GRB as long as  $(\ell'_x/\lambda_{||})s^{1/2} \sim 1$ , or

$$\lambda'_{||} \sim \ell'^{2/3}_x (\eta/c)^{1/3}. \quad (235)$$

We note that the effective speed at which magnetic field needs to be dissipated should be of order the speed of light (comoving frame) in order to obtain the large luminosity of GRBs at a reasonable efficiency of  $\gtrsim 10\%$  [108].

#### 7.10.4. Forced reconnection of magnetic fields for a high- $\sigma$ GRB jet and prompt $\gamma$ -ray radiation

The magnetic field geometry for a black hole central engine is likely to have a non-alternating toroidal configuration, which is less amenable to dissipation via reconnection. Zhang and Yan [108] have suggested the possibility that if the Lorentz factor of the outflow varies with time, then multiple internal collisions can scramble magnetic fields and ignite reconnections, thereby converting a fraction of magnetic energy to thermal energy and radiation, and named it the ICMART model (Internal Collision-induced MAgnetic Reconnection and Turbulence). Since magnetic fields are stretched in the transverse direction, thereby straightening out field lines in between episodes of collisions when the shell undergoes adiabatic expansion, frequent collisions with large relative LF are required in order to sufficiently tangle up the magnetic fields for efficient reconnection.

According to the ICMART model,  $\gamma$ -rays are produced in highly localized reconnection regions via the synchrotron process. The Lorentz factor of the outflow in these regions could be relativistic, say, of the order of the Alfvén wave LF;

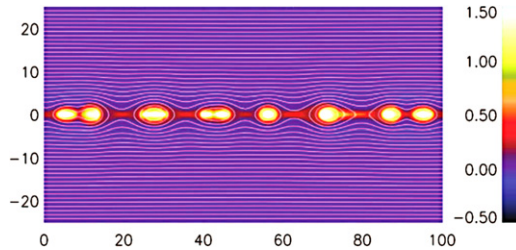


**Fig. 35.** Formation of magnetic islands due to tearing instability is shown in this numerical simulation result taken from Hesse & Zenitani (2007). Plotted are magnetic field lines and the component of current density perpendicular to the figure plane with color coded strength (color bar to the right).

$\gamma'_t \sim \gamma'_A = (1 + \sigma)^{1/2}$ . Therefore, the observed radiation is dominated by those regions where the outflow velocity is pointing in our direction, and the observed duration of a  $\gamma$ -ray pulse from one of these regions is at most  $\sim R/(c\Gamma^2\sigma)$ ; where  $R$  is the distance from the center of explosion where the magnetic energy is being dissipated, and  $\Gamma$  is the LF of the jet associated with its mean bulk velocity. A  $\gamma$ -ray pulse can be of even shorter duration if the size of the reconnection region is much smaller than the transverse size of the jet. This idea of producing rapid variability of  $\gamma$ -ray lightcurves even when radiation is produced at a large distance ( $R \gtrsim 10^{15}$  cm) – as suggested by a number of observations discussed in Section 7.2 – is a generic feature of relativistic turbulence models described by Lyutikov and Blandford [107], Narayan and Kumar [214], Kumar and Narayan [215], Lazar et al. [216], and the ICMART model of [108].

One of the positive features of the relativistic turbulence model is its high radiative efficiency,<sup>51</sup> and unlike the internal-shock model, it is capable of explaining the observed GRB spectra [215]. Since the model invokes synchrotron emission of particles in an ordered magnetic field (which is being rapidly distorted), the observed emission is expected to be highly polarized, with the polarization degree decreasing with time during the course of a broad pulse [108]. According to the model, only a small amount of energy should come out in the IC component, which is consistent with Fermi observations [215].

Lazar et al. [216] criticized the relativistic turbulence model by suggesting that it tends to produce too spiky light curves, with each pulse being symmetric. The ICMART model invokes an exponential growth of the number of mini-jets due to the reconnection-turbulence “avalanche”, which abruptly discharges the magnetic field energy. As a result, at any instant, an observer would receive emission from many mini-jets that beam in random directions. While those beaming toward the observer make rapid spikes, the other off-beam jets contribute to the broad component [217]. The rising wing of a broad pulse is defined by this exponential growth of the number of mini-jets, while the decaying wing is controlled by the high-latitude curvature effect. As a result, this model produces an asymmetric broad pulse for each ICMART event. A GRB is composed of multiple ICMART events, and the simulated light curves are roughly in line with observed lightcurves (e.g. [423]). However, full numerical simulations invoking a high- $\sigma$ , high- $\Gamma$  outflow with strong (cascade) magnetic dissipation are not available. Recent numerical simulations of relativistic magnetohydrodynamical turbulence, e.g. [646], shed some light on the power spectrum of velocity field, but we are far from being able to simulate anything close to the parameters expected for GRB jets.

It is expected that a Poynting jet would suffer rapid dissipation of magnetic energy at the deceleration radius – the distance from the CoE where roughly half of the jet energy is transferred to the circum-stellar medium – if it were to be able to travel to this radius with its high magnetization parameter intact. This is because a collision with the circum-stellar medium sends a strong magneto-sonic wave into the outflow. This can lead to development of a large gradient in the magnetic field, and trigger current driven instabilities that dissipate magnetic fields [107]. The ensuing acceleration of particles then produces  $\gamma$ -rays via the synchrotron mechanism. A signature of this mechanism is that  $\gamma$ -rays are generated close to the deceleration radius.

#### 7.10.5. Particle acceleration

Particles are accelerated in current sheets, where magnetic field dissipation takes place, via a number of different processes. These sheets have regions where the electric field is larger than the local magnetic field and where particles can be accelerated to relativistic speeds by the electric field. Tearing instability of the current sheet, in the non-linear phase, produces a number of magnetic islands (plasmoids) moving close to the Alfvén speed (see Fig. 35). Particles are also accelerated via the Fermi mechanism by scattering off of these plasmoids. Moreover, converging inflow of plasma toward the current sheet provides another venue for particle acceleration via the first-order Fermi process (e.g. [647]). These processes together produce a hard spectrum for accelerated particles that cuts-off steeply at some LF to ensure overall energy conservation.

The minimum electric field inside the current sheet is  $E' = \mathbf{v}'_{in} \times \mathbf{B}'/c$  (where  $\mathbf{v}'_{in}$  is the speed with which plasma flows into the sheet). This follows from the induction equation for time independent reconnection, i.e.  $\nabla \times \mathbf{E}' = 0$ , according to which the electric field parallel to the current sheet inside the sheet has the same magnitude as the outside field. The electric field inside the sheet can be significantly larger than this due to particle inertia and non-zero divergence of anisotropic pressure tensor (terms in the generalized Ohm's law equation), (e.g. [648]).

<sup>51</sup> The internal shock model seems incapable of explaining the observed GRB spectrum and has low radiative efficiency in the MeV band as discussed in Section 7.4.

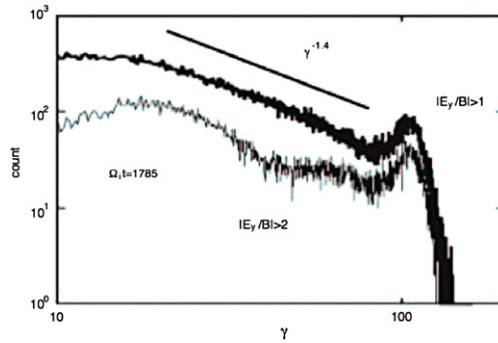


**Fig. 36.** Spectrum of particles accelerated in a current sheet according to recent numerical simulations of [650].

This field can rapidly accelerate particles to high LFs, provided that the particle trajectory passes through the region where the electric field is larger than the magnetic field. A number of people have calculated particle acceleration and their distribution function by following particle trajectory in the combined electric and magnetic fields inside current sheets (e.g. [647,649,650]). A number of groups have carried out numerical Particle-In-Cell (PIC) studies of reconnection and particle acceleration (e.g. [651–655,650,656,657,387,658,659]) – see [660] for a more complete discussion of the extensive literature. According to several of these simulations, much of the particle acceleration takes place near X-points, which are located in between magnetic islands, due to the reconnection electric field (e.g. [651,654,658]), and some acceleration occurs due to first-order Fermi process as particles are reflected back and forth between converging islands (e.g. [661,658]). However, little acceleration takes place while particles are trapped to an island. Presence of a non-zero guide field does not change the acceleration process significantly unless its strength becomes of order the reversing magnetic field (the field undergoing reconnection) in which case fewer particle pass through X-points and hence fewer particles are accelerated by the reconnection electric field and the mean thermal LF of accelerated particles is lower [653,658].

The power-law index for the non-thermal electron distribution in magnetic dissipation,  $p \equiv -d \ln n / d \ln \gamma$ , is reported to be about 1 [662,651,663]. The distribution function must steepen at some LF in order to keep the total energy finite. In fact, several papers claim that the distribution function in reconnection layer falls off exponentially at high LF ([650] find the fall off to be proportional to  $\exp(-\gamma^{1/2})$  – see Fig. 36 – and [659] find the particle spectrum to be a superposition of two thermal peaks); in contrast,  $p < 3$  for particles accelerated in shocks almost up to the LF where particles are no longer confined to the system. Although numerical simulations do not offer a precise answer as to the dependence of the particle terminal LF – where the distribution function begins its steep decline – on parameters such as  $\sigma$ , guide field strength, and relevant length scale of the system, energy conservation suggests that the average thermal LF of particles should be of order  $\sigma$  as long as most of the particles flowing into the current sheet undergo acceleration (which is expected, since the reconnection electric field is fairly wide-spread in the sheet). Results of the recent PIC simulations of [658] for a relativistic striped wind are consistent with this expectation.

Cerutti et al. [664,665] report strong, energy dependent, anisotropy in the distribution of accelerated particles such that higher energy particles are more concentrated along the electric field in the current sheet, which is perpendicular to the plasma inflow direction and the outside alternating-magnetic field, i.e. more high energy particles are found along the guide field; according to their simulations the anisotropy increases with increasing energy, and similar beaming effect is also found in simulations of [659]. This result, if correct, has important implications for lightcurve variability for relativistic outflows associated with neutron stars and black holes.

### 7.11. Some off-the-beaten-track ideas for GRB prompt radiation mechanism

The models we have described thus far as to how  $\gamma$ -ray prompt radiation is produced in GRBs are ideas widely discussed in the published literature and are popular amongst active researchers in this field. Since our understanding of the  $\gamma$ -ray generation mechanism remains elusive, there is a possibility that none of these models survive a closer scrutiny and more detailed future investigations. Therefore, we briefly discuss several other proposals put forward for the origin of GRB prompt radiation which have received somewhat limited attention but might contribute toward our eventual understanding of these enigmatic bursts. All of these models have strengths and weaknesses, but we are going to have to let the reader decide this for herself by reading the original papers since this section is already very long.

Lazzati et al. [666] proposed that photons from the GRB progenitor star, or from the cocoon produced by the passage of the jet through the star, undergo IC scattering by cold electrons in the highly relativistic jet to produce the prompt  $\gamma$ -ray radiation. Many variations of the general idea of converting the kinetic energy of a relativistic jet to  $\gamma$ -ray radiation by inverse-Compton scatterings have been published. For instance, Broderick [667] considered IC scattering of supernova light by a relativistic jet which is produced by accretion of supernova ejecta onto a neutron star companion; the system just prior to the supernova was a helium star–neutron star binary system.

Dar, de Rújula and Dado have spent a huge amount of effort in developing a model for GRBs they refer to as the cannon-ball model. They have written numerous papers analyzing different aspects of this model, and carried out detailed comparisons with GRB data. We refer the interested person to their review article that describes the cannon-ball model and its application to GRB observations [668]. The basic idea is that small packets of plasma, or “cannon-balls”, are shot out from the GRB central engine moving at close to the speed of light (LF of these “cannon balls” is  $\sim 10^3$ ), and cold electrons in these objects IC scatter ambient radiation – which was either produced by the supernova that preceded the launch of these bullets by several hours, or it resulted from episodes of intense stellar activity just prior to the death of the progenitor star, and then scattered by the dense wind of the star, resulting in a nearly isotropic radiation field – to produce the prompt  $\gamma$ -ray lightcurve. The absence of diffractive scintillation in the VLBI data of a relatively nearby burst, GRB 030329 at  $z = 0.168$ , is at odds with the expectation of the cannonball model, and so is the smaller than expected proper motion [49]; but see [669] for an interpretation of the Taylor et al. observations according to the cannonball model.

Another model, developed extensively by Ruffini and his collaborators, is the so called “fireshell” model for GRBs, which suggests a unified picture for long- and short- GRBs ([670,671], and references therein). According to this model, a spherically symmetric  $e^\pm$  shell is ejected when a charged black-hole is formed in a catastrophic collapse [672]. This model is characterized by the energy in this shell (related to the black-hole charge and mass) and the amount of baryonic matter: fireshells of low baryonic loading (fractional rest-mass energy in baryons less than  $10^{-5}$ ) produce short GRBs, whereas a larger baryon loading leads to long-GRBs. Ruffini et al. suggest that a radiation pulse is produced when the fireshell becomes transparent (they call it P-GRB), which could be either the precursor to a GRB or the first pulse of the main burst. The fireshell interacting with blobs in the circum-stellar medium produces more pulses of radiation in the prompt  $\gamma$ -ray lightcurve [673]. The basic physical processes at work in the generation of  $e^\pm$  shell are described in an extensive review article [674]. The question of astrophysical processes responsible for the formation of a charged black-hole – a central element of the fireshell model – however, is unclear to us. It is also unclear how a spherical fireshell gives rise to a jet break, and how to explain the association of long GRBs with supernovae but not short GRBs, and the different distribution for the location of these two classes of GRBs in their host galaxies.

A number of people have invoked a precessing jet to explain the complex  $\gamma$ -ray lightcurve of GRBs, e.g. [675–678]. However, it is difficult to avoid high baryon loading for a precessing jet, which instead of moving straight through an evacuated polar cavity, is likely to collide with the cavity wall and entrain a lot of baryonic matter, and therefore might not attain the high LF inferred for GRBs.

Ioka et al. [679] suggested a model where a jet of very low baryonic content and low magnetization undergoes internal shocks while still radiation dominated; it is suggested that the jet is confined by the external pressure of the progenitor star so that its cross-section increases more slowly than a conical jet, and therefore it continues to be radiation dominated out to a much larger radius. In such radiation dominated shocks, thermal photons cross the shock front multiple times and their energy increases as a result of the first order Fermi process, i.e. energy is transferred from the bulk kinetic energy of the jet to photons, when the photons are scattered by the converging outflow associated with the shock. The emergent photon spectrum in this case has a non-thermal power-law shape above the peak.

Titarchuk et al. [680] have proposed a two step process for the generation of  $\gamma$ -rays by inverse-Compton scatterings. The first step involves Compton scattering of low energy photons from the GRB progenitor star, in the high Compton-Y parameter regime, by electrons of energy  $\sim 10^2$  keV in the radiation dominated sub-relativistic outflow produced in the explosion. The outflow subsequently expands and becomes relativistic, and relatively cold electrons in the jet inverse-Compton scatter photons produced in step 1 that results in a non-thermal, Band, Spectrum. Titarchuk et al. [680] have provided a detailed fit to the observed GRB data using this model.

Kazanas et al. [681] proposed a “supercritical pile” model for GRBs. The idea is that as a relativistic GRB blastwave propagates in the interstellar medium, the Bethe-Heitler process ( $p\gamma \rightarrow pe^+e^-$ ) may reach resonance, namely, the typical energy of synchrotron radiation of the pairs is just the one to ensure Bethe-Heitler kinetic condition, and the column density of the photons also satisfy runaway production of  $e^+e^-$  pairs. Similar to the external shock model, this model invokes an “external” site to discharge the kinetic energy of the blastwave, which has difficulties to account for the GRB variability data.

## 8. GRB central engine

Although the progenitors of long- and short- GRBs might be very different objects, the basic nature of the central engine – the mechanism by which highly luminous relativistic jet is produced – is expected to be similar for these bursts. The details of the process can be somewhat different. The discussion below mostly focuses on long duration GRBs, but short GRBs will be discussed whenever noticeable differences with long GRBs exist. For a more detailed discussions of short GRB central engine, please see e.g. [682–685,686,687,13,688] and references therein.

The central engine of GRBs has not been positively identified, however, observations have narrowed down candidates to a small number of possibilities. Any successful GRB central engine model should be able to satisfy the following requirements: (1) Ability to launch an extremely energetic and luminous jet whose luminosity greatly exceeds the Eddington luminosity; (2) The jet must be clean, i.e. energy per baryon  $\gg m_p c^2$ , so that the outflow can reach ultra-relativistic speed with Lorentz

factor greater than  $\sim 10^2$ ; (3) The engine should be intermittent as suggested by the erratic rapidly variable light curves<sup>52</sup>; (4) The central engine should be able to re-activate at later times to power softer flares.<sup>53</sup>

Two types of widely discussed central engines satisfy these requirements: a hyper-accreting stellar-mass black hole [38,689–697,527,698–700], and a rapidly spinning, highly magnetized, neutron star or “fast magnetar” [138,109,139,701,702,140,703–705,335]. We describe these models in the following subsections.

### 8.1. Hyper-accreting black holes

If a GRB is powered by accretion onto a stellar mass black hole, a very high accretion rate is required. In general, one can write

$$L_{\text{GRB}} = \zeta \dot{M} c^2 = 1.8 \times 10^{51} \text{ erg s}^{-1} \zeta_{-3} \left( \frac{\dot{M}}{1 M_{\odot} \text{ s}^{-1}} \right), \quad (236)$$

where  $\zeta$  is a dimensionless number that represents the efficiency of converting accretion power to radiation power. For reasonable values, the accretion rate for a typical cosmological GRB is  $(0.01 - \text{several}) M_{\odot} \text{ s}^{-1}$ .

At these high accretion rates the plasma is extremely hot and forms a thick disk or torus around the central black hole/neutron-star. Photons are trapped in the accretion flow, and neutrino cooling might be effective only for a fraction of the burst duration close to the central engine, so that the accretion flow is advection dominated (ADAF) or convective (CDAF) throughout much of the volume. Close to the inner disk radius, the temperature is so high that neutrino cooling does become effective for at least some time, and in that case the disk temperature drops, density increases, and the geometrical shape of the flow is that of a thin disk; this is called neutrino-dominated accretion flow (NDAF).

The accreting BH likely carries large angular momentum. This is naturally formed in a rapidly rotating core. Due to the large accretion rate, the BH can spin up further rather quickly. If a strong magnetic field threads the spinning BH and is connected with an external astrophysical load, BH spin energy can be tapped via the Blandford–Znajek mechanism [706].

In general, a GRB jet can be launched from a hyper-accreting BH via three possible mechanisms:

- Neutrino annihilation along the spin axis of a NDAF can drive a hot jet with properties similar to what is conjectured in the hot fireball model;
- Blandford–Znajek mechanism can launch a Poynting-flux-dominated outflow from the central engine;
- The accretion disk can be also highly magnetized. A plausible, but less well studied, mechanism is that differential accretion would lead to accumulation of vorticity and energy within the accretion disk, leading to eruption of magnetic blobs.

We discuss these mechanisms in the following subsections.

#### 8.1.1. Neutrino-dominated accretion flow (NDAF) and advection-dominated accretion flow (ADAF)

The structure of the GRB accretion disk depends on the mass of the black hole  $M$ , accretion rate  $\dot{M}$ , radius  $r$  from the central engine, and the poorly known viscosity (usually parametrized by a dimensionless parameter  $\alpha$ ). At the high accretion rate required for GRBs, the disk temperature is very high. Above a critical accretion rate, the disk is cooled by significant neutrino emission and is in the NDAF regime. Below the critical rate, neutrino cooling is not important. The disk becomes much thicker, significant thermal energy is “adverted” into the black hole, and the disk is in the ADAF regime. For a given GRB accretion disk, there is a characteristic radius below and above which the disk is approximately in the NDAF and ADAF regimes, respectively (e.g. [696]).

To derive the structure of a GRB accretion disk, one needs to solve a set of equations [689], including mass conservation equation, energy equation, radial momentum equation, angular momentum conservation equation, equation of state, and cooling and heating of plasma. In general, numerical calculations are needed to precisely solve the GRB accretion disk problems. An approximate solution to the disk structure in the NDAF and ADAF regimes can be written in the following forms using results of numerical calculations [689,691,707,708,696,698]:

NDAF:

$$\rho = 1.2 \times 10^{14} \text{ g cm}^{-3} \alpha_{-2}^{-1.3} \dot{M}_{-1} \left( \frac{M}{3M_{\odot}} \right)^{-1.7} \left( \frac{r}{r_g} \right)^{-2.55} \quad (237)$$

$$T = 3 \times 10^{10} \text{ K} \alpha_{-2}^{0.2} \left( \frac{M}{3M_{\odot}} \right)^{-0.2} \left( \frac{r}{r_g} \right)^{-0.3} \quad (238)$$

$$V_r = 2 \times 10^6 \text{ cm s}^{-1} \alpha_{-2}^{1.2} \left( \frac{M}{3M_{\odot}} \right)^{-0.2} \left( \frac{r}{r_g} \right)^{0.2} \quad (239)$$

<sup>52</sup> It is possible that the variability observed in prompt  $\gamma$ -ray lightcurves is due to relativistic turbulence at the location where  $\gamma$ -rays are produced, and in that case the jet luminosity from the GRB central engine might be a smooth function of time. It is also possible that variability is introduced by the interaction of jet with the stellar envelope. See Section 7.10.4 for detailed discussion.

<sup>53</sup> Some ideas to interpret X-ray flares without invoking a re-activation of central engine have been proposed, but these proposals are not well developed to interpret the entire X-ray flare phenomenology. See Section 4.2.2 for a detailed discussion.

ADAF:

$$\rho = 6 \times 10^{11} \text{ g cm}^{-3} \alpha_{-2}^{-1} \dot{M}_{-1} \left( \frac{M}{3M_\odot} \right)^{-2} \left( \frac{r}{r_g} \right)^{-1.5} \quad (240)$$

$$T = 3 \times 10^{11} \text{ K} \alpha_{-2}^{-1/4} \left( \frac{M}{3M_\odot} \right)^{-0.5} \left( \frac{r}{r_g} \right)^{-5/8} \quad (241)$$

$$V_r = 10^8 \text{ cm s}^{-1} \alpha_{-2} \left( \frac{r}{r_g} \right)^{-0.5}. \quad (242)$$

Here  $\rho$ ,  $T$ , and  $V_r$  are the density, temperature, and radial velocity of the accretion flow,  $\alpha$  is the viscosity parameter,  $M$  is the black hole mass,  $\dot{M}_{-1} = \dot{M}/0.1M_\odot \text{ s}^{-1}$  is accretion rate, and  $r_g = 2GM/c^2$  is the Schwarzschild radius of the black hole. It is possible that for a given accretion rate, different parts of an accretion disk (different  $r$  ranges) belong to different regimes, i.e. ADAF or CDAF, (e.g. [696]).

Neutrino and anti-neutrino emission from an NDAF with power  $\dot{E}_\nu$  would lead to  $\nu\bar{\nu}$  annihilation, and generate a hot photon and electron-positron gas, which expands under its thermal pressure as a fireball. The annihilation power [709,527]

$$\dot{E}_{\nu\bar{\nu}} \simeq 1.1 \times 10^{52} \text{ erg s}^{-1} \left( \frac{M}{M_\odot} \right)^{-3/2} \left( \frac{\dot{M}}{M_\odot/\text{s}} \right)^{9/4} \quad (243)$$

launches an outflow with luminosity of order given by the above equation.

Neutrinos can also interact with protons through weak interaction and transfer momentum to protons. This gives rise to a neutrino-driven baryon wind. The baryon-loading rate is [710,527]

$$\dot{M}_v = 10^{-6} M_\odot \text{ s}^{-1} \dot{E}_{\nu,52}^{5/3} \left( \left( \frac{\epsilon_\nu}{10 \text{ MeV}} \right)^2 \right)^{5/3} r_6^{5/3} \left( \frac{M}{3M_\odot} \right)^{-2} \left( \frac{h}{r} \right)^{-1}. \quad (244)$$

One can then calculate the amount of baryon loading in a  $\nu\bar{\nu}$  annihilation jet [527]:

$$\eta = \frac{\dot{E}_{\nu\bar{\nu}}}{\dot{M}_v c^2}, \quad (245)$$

where  $\eta$  is the “dimensionless entropy” of the fireball, which is essentially the terminal Lorentz factor of the baryon loaded fireball at the end of its acceleration phase. Given a range of black hole mass, accretion rate, and spin rate, one can simulate the distribution of  $\eta$  and  $\dot{E}_{\nu\bar{\nu}}$ .

### 8.1.2. Blandford-Znajek mechanism

The rotational energy of a BH with angular momentum  $J$  can be written as:

$$E_{\text{rot}} = 1.8 \times 10^{54} f_{\text{rot}}(a_*) \frac{M}{M_\odot} \text{ erg}, \quad (246)$$

where

$$f_{\text{rot}}(a_*) = 1 - \sqrt{(1 + q)/2}, \quad (247)$$

$q = \sqrt{1 - a_*^2}$  and  $a_* = Jc/GM^2$  is the BH spin parameter. For a maximally rotating BH ( $a_* = 1$ ), one has  $f(1) = 0.29$ .

Then the total power of Poynting flux from the BZ process can be estimated as [690,711,693,694,527]

$$\dot{E}_{\text{BZ}} = 1.7 \times 10^{50} \text{ erg s}^{-1} a_*^2 \left( \frac{M}{M_\odot} \right)^2 B_{15}^2 F(a_*). \quad (248)$$

The spin-dependent function  $F(a_*)$  needs full general relativity to solve [706]. An analytical approximation gives [690,693]

$$F(a_*) = \left[ \frac{1 + h^2}{h^2} \right] \left[ \left( h + \frac{1}{h} \right) \arctan h - 1 \right], \quad (249)$$

where

$$h = \frac{a_*}{1 + q}, \quad (250)$$

and so  $F(0) = 2/3$ , and  $F(1) = \pi - 2$ . Tchekhovskoy et al. [627], Tchekhovskoy and McKinney [712] investigated this function numerically and obtained an analytical fit to the numerical model. The results are similar to Eq. (249) at most  $a_*$  values and only slightly deviates from (becomes lower than) Eq. (249) when  $a_*$  is close to 1.

A major uncertainty in estimating the BZ power is the strength of magnetic fields. Depending on how  $B$  is estimated (e.g. magnetic pressure vs. ram pressure balance or equipartition with the gas pressure), the BZ power is different. Numerically, Tchekhovskoy and McKinney [712] estimated the BZ power by feeding a spinning black hole with high magnetic flux. The BZ efficiency (defined as  $\eta_{\text{BZ}} \equiv \langle \dot{E}_{\text{BZ}} \rangle / \langle \dot{M} \rangle c^2 \times 100\%$ ) was found to exceed 100% under certain conditions. This suggests that the jet power indeed comes from the BH spin, not from accretion. Evidence for BZ mechanism at work in long-GRB central engines is also found in 2-D general-relativistic MHD simulations (e.g. [699,700]).

In any case, to maintain a high BZ power, accretion rate should be still very high. Neutrino emission/annihilation, and neutrino-driven wind still occur from the disk. This has two implications [527]: First, the total jet power should be the sum of the BZ power and the neutrino-annihilation power, so that the jet launched from the base has both a “hot” (neutrino annihilation) and “cold” (Poynting flux) component. Second, due to the magnetic barrier, protons cannot drift into the central magnetically dominated jet. Baryon loading, however, may proceed through neutron drift [713]. This results in much cleaner jets.

### 8.1.3. Magnetic jets launched from the accretion disk

A less well studied, yet plausible, mechanism invokes magnetic blobs launched from the accretion disk. [695] applied the “magnetic tower” mechanism (self-collimated toroidal magnetic jet structure produced by a differentially-rotating central disk or a magnetar) suggested by Lynden-Bell [714] for producing AGN jets to the collapsar model of GRBs. The magnetic fields in the disk tend to twist, wind up, and erupt, forming episodic magnetic bubbles. This gives rise to an intrinsically episodic magnetically launched jet even if the accretion rate is not episodic. Baryon loading in such a model is however not easy to estimate. Besides the neutrino-driven baryon load, corona materials can be trapped in magnetic blobs, the amount of which is difficult to estimate.

### 8.1.4. Effects of the stellar envelope in long GRBs

For a long GRB formed from the collapse of a massive star, the jet has to propagate through the stellar envelope. For a matter-dominated jet, Kelvin-Helmholtz instability develops at the lateral-surface of the jet where there is substantial differential motion wrt the star. This induces variability in a jet even when the central engine has little fluctuation [715]. The envelope also collimates the jet so that it has an opening angle of a few degrees when it emerges at the stellar surface. The propagation of the jet through the envelope of the star, outside the iron core, produces a hot cocoon which can be very effective in collimating the jet (e.g. [716,717,210,718,719]). When the cocoon erupts at the stellar surface it makes a wider, weaker, and less relativistic jet surrounding the central narrow, stronger, and highly relativistic jet [210,718,720,211].

For a highly-magnetized jet, the strong magnetic pressure prevents ambient material from entering the jet. The hot cocoon surrounding the jet also helps in its collimation and acceleration, and magnetic jets require less expenditure of energy to punch through the star than baryonic jets of same luminosity and cross-section at the launching site [626,627,721,722].

### 8.1.5. Black hole engine in short GRBs

For NS-NS or NS-BH mergers, the material in the accretion torus has high density and total mass of order  $0.1 M_{\odot}$ . The duration of accretion is short, which is suitable for producing short GRBs (e.g. [683,684]). Lacking a heavy envelope, the jet is expected to be less collimated. In any case, the black hole vicinity is permeated by tidal debris launched during the merger and baryons launched from a neutrino wind from the hot accretion flow. These materials can collimate the GRB jet to  $\sim 10-20^\circ$  (e.g. [688,723]).

## 8.2. Millisecond magnetars

An alternative possibility for the GRB central engine is a rapidly spinning (period  $P \sim 1$  ms), highly magnetized (surface magnetic field  $B_s \sim 10^{15}$  G) neutron star known as a millisecond magnetar. Such a magnetar, when spinning down, has the right parameters to power a GRB [138,702]. The total spin energy (which is the main power source of a millisecond magnetar) for a magnetar with initial spin period  $P_0 \sim 1$  ms is

$$E_{\text{rot}} \simeq \frac{1}{2} I \Omega^2 \simeq 2 \times 10^{52} \text{ erg} \frac{M}{1.4 M_{\odot}} R_b^2 P_{0,-3}^{-2}. \quad (251)$$

This equation gives an upper limit to GRB energy when the central engine is a magnetar. If a GRB violates this constraint, then the magnetar model is ruled out for that GRB. A systematic study of GRB prompt emission and afterglow data suggests that all the magnetar-candidate GRBs appear to have collimation-corrected energy in electromagnetic radiation that is smaller than this limit, while some other GRBs (presumably having a black hole central engine) do violate such a limit [724].

Making the simplest assumption of dipolar spindown, the total luminosity for a magnetar is given by

$$L(t) = L_0 \frac{1}{(1 + t/t_0)^2} \simeq \begin{cases} L_0, & t \ll t_0, \\ L_0(t/t_0)^{-2}, & t \gg t_0, \end{cases} \quad (252)$$

where

$$t_0 = \frac{3c^3 I}{B_p^2 R^6 \Omega_0^2} \simeq 20.5 \text{ s} (I_{45} B_{p,16}^{-2} P_{0,-3}^2 R_6^{-6}) \quad (253)$$

is the characteristic spindown time scale, and

$$L_0 = \frac{I \Omega_0^2}{2 t_0} = \frac{B_p^2 R^6 \Omega^4}{6 c^3} \simeq 1.0 \times 10^{51} \text{ erg s}^{-1} (B_{p,16}^2 P_{0,-3}^{-4} R_6^6) \quad (254)$$

is the typical spindown luminosity. For  $P \sim 1$  ms, and  $B_p \gtrsim 10^{16}$  G, the typical spindown luminosity and time scale coincide with the typical luminosity and duration of a GRB [138].

The mechanism by which a new-born magnetar might power a GRB has been studied in detail in recent years [704,705,335,725,726]. During the early phase of evolution, the simple dipole spindown formula is not adequate to describe the relevant physics. The evolution of a magnetar-powered GRB is well summarized by Metzger et al. [335]: a new born neutron star is initially very hot which leads to a heavy baryon loading of the wind from magnetar due to neutrino driven mass loss from the surface, and such an outflow has too small a terminal Lorentz factor to power a GRB. After  $\sim 10$  s or so, the neutron star cools down, the neutrino driven baryonic wind diminishes, and a jet with  $\sigma > 100$  is produced. This phase lasts for about half a minute when  $\sigma$  increases rapidly due to an abrupt drop in neutrino wind and that according to Metzger et al. [335] terminates the prompt GRB phase. During the prompt phase, erratic lightcurves can be powered by magnetic dissipation instabilities [701,727]. The energy budget during the prompt emission phase is from the differential rotation of the neutron star, which generates magnetic energy via a dynamo mechanism. After this phase, the magnetar continuously spins down and injects energy as a Poynting flux. Late magnetic activities arising from the residual differential rotation of the neutron star can power X-ray flares after the prompt phase [703].

The spin down power of a magnetar can leave an interesting signature in the GRB afterglow lightcurve [140]; see also [139] for the case of a millisecond neutron star central engine with a normal ( $\sim 10^{12}$  G) magnetic field. The basic feature is that Poynting flux from the neutron star spin down can be directly injected into the blastwave. If the injected energy exceeds the energy deposited during the prompt phase, the external forward shock afterglow lightcurve would show a shallow decay phase. The shallow decay phase of GRB afterglow lightcurves requires such an energy injection mechanism, and a magnetar central engine could perhaps offer a plausible explanation for this behavior [728,82,335,729]. On the other hand, another model that invokes stratification of ejecta Lorentz factor [141,730,156] could also explain these plateaus.

The discovery of an “internal plateau” for GRB 070110 [294] which was followed by a very rapid decay ( $t^{-9}$ ) of the X-ray flux rules out an external shock origin for the X-ray emission, and requires internal dissipation of a long-lived jet to account for this steep decline. A smooth lightcurve during the plateau is easier to understand when the power source is the spin down of a neutron star. From the observed luminosity and duration of the plateau, one can infer the parameters of the neutron star which turns out to be consistent with a fast magnetar:  $P_0 \sim 1$  ms, and  $B_p \gtrsim 3 \times 10^{14}$  G when the jet opening angle is assumed to be a large angle ( $\sim 18^\circ$ ) [301].

Such a magnetar signature also shows up in several short GRBs (e.g. [731,732]). This suggests that NS–NS mergers may also give rise to a supra-massive, likely highly magnetized, millisecond magnetar (e.g. [703,733–738]). Since the magnetar spindown time scale is typically 20s or more (Eq. (253)), one challenge of this model is to produce a short duration prompt emission. Mechanisms discussed in the literature include a brief accretion phase [735], a brief differential rotation phase (e.g. [739]), and phase transition [740,741].

Since the millisecond magnetar wind is essentially isotropic (data are consistent with such a hypothesis [724]), a post-merger supra-massive millisecond magnetar is expected to emit bright electromagnetic emission in the off-jet directions. [742] proposed that NS–NS merger-induced gravitational wave bursts can have a bright early X-ray afterglow powered by a supra-massive magnetar even if they are not associated with short GRBs (jet misses earth). Such a magnetar also powers a bright multi-wavelength afterglow [743] and a bright “merger” nova [744,745]. The collapse of the supra-massive neutron star into a black hole would give distinct observational signatures, such as a sharp decline in the X-ray lightcurve [731,732].

### 8.3. Models of late central engine activities

Shortly after the observations of the first afterglow Katz and Piran [746] and Katz et al. [281] suggested the possibility that some of the afterglow flux arises due to long lasting central engine activity, stressing that a strong variability in afterglow light curves cannot be produced via an external shocks. Swift observations indeed find that GRB central engine activity lasts for much longer than the duration of prompt emission. There are two types of extended engine activity. One is erratic, manifested as late X-ray flares [83,84,328]; the other is where the power output is steady for an extended period which we see as “internal X-ray plateaus” [294,54,301]. A successful central engine model should be able to interpret these diverse properties.

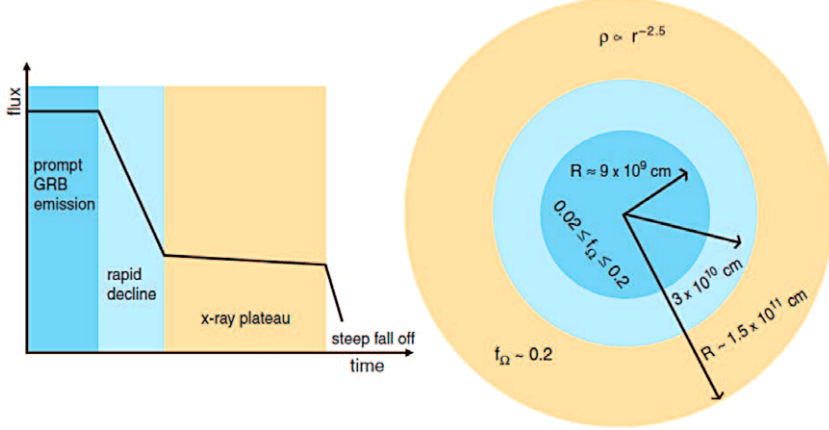


**Fig. 37.** The panel on the left shows a schematic X-ray lightcurve with the following four segments: a prompt emission phase, a steep decline phase, a plateau phase, and a post-plateau phase. The panel on the right shows how the different segments in the LC are related to the accretion of different parts of the progenitor star. The radii ( $r$ ) and spin parameters ( $f_\Omega \equiv \Omega/\Omega_k$ ) of the various zones can be estimated from the X-ray data [330];  $\omega_k(r)$  is Keplerian rotation rate at  $r$ .

### 8.3.1. X-ray flares

A number of different models have been suggested for X-ray flares:

- King et al. [747] proposed that a collapsing massive star may fragment into many blobs, which are accreted onto the central compact object at different times; blobs accreted at late times give rise to X-ray flares. Since short GRBs also have flares (e.g. GRB 050724 [291]), and a number of them are found in elliptical galaxies with very low star formation rates e.g. the host galaxy of GRB 050724, this suggests that the X-ray flare mechanism should also apply to progenitors that are not massive stars.
- Perna et al. [748] argued that the outer part of accretion disk, for long and short GRBS, is susceptible to gravitational instability and could fragment into clumps, and the accretion of these clumps produces X-ray flares; short GRBs require some extreme conditions for this mechanism to work.
- Proga and Zhang [749] argued that accumulation of magnetic flux near the black hole during accretion can temporarily build up a “magnetic barrier”, which shuts down accretion for some time. When accretion resumes after accumulating enough material, an X-ray flare is produced. Such a process may repeat itself to power multiple flares. A similar scenario was proposed by [750] to interpret extended emission of short GRBs.
- Dai et al. [703] invoked a post-merger differentially-rotating millisecond neutron star to power X-ray flares following short GRBs within the framework of the NS-NS merger progenitor.
- Lee et al. [751] suggested that post merger accretion disk may undergo “phase transition” triggered by He-synthesis, which would temporarily launch a powerful wind to shut down accretion. Accretion resumes later to power an X-ray flare.

### 8.3.2. X-ray “plateaus”

The “internal plateau” observed in X-ray afterglow lightcurves requires energy dissipation within the jet of a long-lasting central engine [294]. A plausible scenario is that it is due to continuous energy injection from a magnetar wind [335,726], and the abrupt decay of flux at the end of plateau may be related to collapse of the magnetar to a black hole after it has lost enough angular momentum that it can no longer support itself against the force of gravity [294,752].

Regular X-ray plateaus (those followed by a normal decay  $\propto t^{-1}$ ) may be interpreted as due to energy being added for a period of plateau duration to a decelerating external shock [82,81]. Some afterglows show achromatic behavior in both X-ray and optical bands, which can be easily explained by this model. However, some others show a chromatic behavior, which requires that the X-ray emission is powered by a different source from the optical emission. One possibility is that the entire observed X-ray afterglow of these GRBs is powered by a long-lasting central engine model. It can be from a millisecond magnetar without collapsing into a black hole (e.g. [334]) or from a hyper-accreting black hole. Assuming a hyper-accreting black hole model for GRBs, [330,331] showed that the morphology of a canonical X-ray light curve – the steep decline of flux at the end of the prompt phase and a plateau following that – is similar to the time dependence of accretion rate onto the central object. The time dependence of the rate at which stellar material is added to the accretion disk, and the rate at which mass falls onto the central object, is a function of the density profile of the progenitor star [331]. The duration of the steeply declining early X-ray lightcurve – or the beginning of the plateau – is set by the dynamical timescale of the stellar core i.e.  $(R_c^3/GM_c)^{1/2}$ ; where  $R_c$  and  $M_c$  are the radius and mass of the progenitor star’s core. The X-ray flux & its rate of decline during the plateau is determined by the mass, radius, and the rotation rate of the stellar envelope, and therefore, the X-ray data can be *inverted* to obtain the GRB progenitor star structure as outlined in [330], and the result is shown in Fig. 37.

#### 8.4. Difference between the two types of engines

If we ever detect a milli-second pulsation in X-ray lightcurve of GRB prompt or afterglow radiation then that will clinch the case for the magnetar model. However, in the absence of this signature we have to look at other possible ways of determining whether the GRB central engine is an accreting black-hole or a milli-second magnetar. We describe a few of the main properties of the GRB prompt and afterglow lightcurves and how these could shed light on the nature of the central engine.

- (1) As already mentioned, a magnetar based model for GRBs cannot have total energy in the burst exceeding  $2 \times 10^{52}$  erg (Eq. (251)) which is the rotational energy of a neutron star that is spinning at close to the breakup speed; this total energy is the sum of the energy emitted during the prompt phase and the afterglow. On the other hand, a BH based central engine can in principle produce bursts with energy much larger than  $2 \times 10^{52}$  erg.

A major complication in determining the total energy output of a burst is the unknown collimation angle. Jet opening angle is measured for several long GRBs from the achromatic break in their multi-wavelength afterglow curves. Assuming that the opening angle for the jet during the prompt phase is same as the angle determined from afterglow data, the total collimation-corrected energy is found to be typically smaller than the upper limit of  $2 \times 10^{52}$  erg [26,37,200,28]. However, some bursts have energy close to or above this limit and that poses a challenge for the magnetar model [30,32,724].

Based on energy considerations alone, all that one can say is that magnetar model could produce less energetic bursts, and the BH model is needed for the most powerful explosions.

- (2) The specific angular momentum for a milli-second magnetar,  $j \sim R_{ns}^2 \Omega$ , is  $6 \times 10^{15} \text{ cm}^2 \text{ s}^{-1}$ , whereas for the innermost stable circular orbit of a maximally rotating Kerr black hole it is  $2GM/3^{1/2}c \sim 5 \times 10^{16} M_1 \text{ cm}^2 \text{ s}^{-1}$ ; where  $M_1$  is BH mass in units of  $10M_\odot$ . Thus, the requirement on the rotation rate of the GRB progenitor star is more severe for a BH model.
- (3) The steep decline of X-ray lightcurve at the end of the prompt GRB phase indicates that the central engine turns off very rapidly. A sharp decline of accretion rate onto the newly formed BH soon after the core collapse is found analytically and numerically for the collapsar model e.g. [331,333]. The steep decline occurs when the accretion flow makes a transition from a NDAF to an ADAF, and at roughly the same time an accretion shock forms and pushes back the in-falling gas that further reduces the accretion rate.

It is much more difficult for a magnetar to be turned off as rapidly as observations suggest. The luminosity of a magnetar wind, according to the dipole radiation model, fall off as  $t^{-2}$  which is far too slow. However, it is also the case that pulsar braking index  $n$  – defined as  $d\Omega/dt \propto \Omega^n$  – according to the dipole model is 3 whereas the index for 6 well studied pulsar is found to be between 1.4 and 2.9 [753]. If the braking index for a newly born magnetar were to be like these *much older* pulsars then that would suggest a faster fall off of the luminosity than  $t^{-2}$  and that might explain the observed steep decline of X-ray lightcurves.

Another possibility for the steep decline of lightcurve for the magnetar model is suggested by Metzger et al. [335]. According to these authors the steep decline is associated with a sharp increase of the magnetization parameter ( $\sigma_0$ ) from  $10^4$  to  $10^9$  as the neutron star becomes transparent to neutrinos, and the neutrino-driven mass-loss drops rapidly. They invoke inefficient acceleration, and radiation, for very high  $\sigma$  wind as the reason for the steeply declining X-ray lightcurve. It is not clear that a high  $\sigma$  wind is necessarily difficult to accelerate in a typical long-GRB setting. Adiabatic expansion of a wind of short spatial extent can lead to rapid acceleration e.g. [631]; see Section 7.10.1 for details. Moreover, for  $\sigma \gtrsim 10^6$  the jet becomes transparent to photons in the transverse direction while still inside the star and that causes a severe inverse-Compton drag on electrons bringing them quickly to almost standstill, and the resulting low current results in the dissipation of magnetic energy. If the Poynting jet with  $\sigma \gtrsim 10^6$  were to somehow escape this fate, it will become charge starved before reaching the deceleration radius, and consequently magnetic energy will be dissipated quickly. So it seems unlikely that a transition to high  $\sigma$  outflow necessarily leads to rapidly falling lightcurve, and hence a rapid turn-off of the central engine poses a challenge for the Magnetar model.

- (4) A plateau in jet luminosity can arise, according to the black-hole central engine, when the outer part of the star with  $\rho \propto R^{-2.5}$  is accreted onto the black hole [331,333].

According to the magnetar model the X-ray plateau is associated with its spindown time scale. Therefore, this model predicts that the average luminosity during the plateau should be inversely proportional to the duration of the plateau. This is something that observers should be able to verify and thus help determine the correct model for the GRB central engine; recent analysis of X-ray plateau data seems consistent with this expectation, e.g. [754–756,724].

Another point to note is that it is more natural for a magnetar model to produce a smooth lightcurve during the plateau, as is in fact observed, than for an accreting black hole model. The sharp decline of X-ray flux at the end of the plateau for a few GRBs (e.g. [294]) might seem inconsistent with the magnetar model. However, a sharp decline could perhaps arise when a supra-massive milli-second magnetar's rotation speed falls below a threshold value so that the centrifugal force is no longer able to prevent its collapse to a black hole. A black hole central engine may be also abruptly stopped if the accretion disk is suddenly blown away by a disk wind. However, the combination of a flat X-ray lightcurve (which would require a constant accretion rate) and a subsequent very rapid drop ( $\propto t^{-9}$ ) is difficult to arrange for the black hole central engine model.

- (5) It is much easier to understand X-ray flares when the central engine is a magnetar than when it is a black hole (e.g. [701,703]). X-ray flares, for a magnetar model, are analogous to Soft Gamma-ray Repeaters (SGRs). However, the energy of flares should not exceed  $\sim B^2 R_{\text{ns}}^3 / 5 \sim 10^{48} B_{15}^2$  erg if produced by dissipation of magnetic fields in a magnetar; bright X-ray flares in GRBs almost certainly violate this limit modulo the uncertainty regarding the beaming angle. Note that the magnetic field strength,  $B$ , cannot be much larger than  $\sim 10^{15}$  G, otherwise the duration of the plateau would be much smaller than the observed value of  $10^3$ – $10^4$  s.

According to [85] and [86] the average X-ray flare luminosity decreases with time (measured from  $\gamma$ -ray trigger) as  $\sim t^{-2.7}$ , and the energy in flares scales as  $\sim t^{-1.8}$ . Accretion onto a BH can give this steep decline in the CDAF regime. However, the sharp rise and fall off of X-ray flare lightcurve is puzzling to understand in this model. It is unclear why a magnetar model – where X-ray flare is produced by the dissipation of some fraction of the energy of the neutron star's magnetic field – should have flare luminosity falling off as  $\sim t^{-2.7}$ .

## 9. Progenitors of GRBs

### 9.1. Two physically distinct types of GRBs

Gamma-ray observations led to identification of two phenomenological classes of GRBs in the duration-hardness ( $T_{90}$  – HR) plane: long/soft vs. short/hard [3]. The boundary between the two classes is vague. The duration separation line is around 2 s in the BATSE band (30 keV – 2 MeV). Long and short GRBs roughly comprise 3/4 and 1/4 of the total population of the BATSE sample, but the short GRB fraction is smaller for other detectors [411–415]. This is because the duration  $T_{90}$  of a GRB is energy-dependent and detector-sensitivity-dependent [415]. It is possible that a short GRB detected by BATSE would appear as “long” by a detector with a softer bandpass (e.g. Swift). Indeed, in the Swift era, about 2% of GRBs have a short/hard spike typically shorter than or around 2 s, but with an extended emission (EE) lasting 10's to  $\sim 100$  seconds [430]. So the unfortunate consequence of the  $T_{90}$  classification is that the membership to a certain category of the same GRB could change when the detector is changed. Nonetheless, the confusion in  $T_{90}$  classification mostly arises in the “gray” area between the two classes.

Follow-up afterglow and host galaxy observations of GRBs led to the identification of at least two broad categories of progenitor. Observations led by BeppoSAX, HETE2, and Swift suggest that at least some long GRBs are associated with supernova Type Ic (e.g. [56–58,60,61]). Most long GRB host galaxies are found to be dwarf star-forming galaxies [51]. These facts establish the connection between long GRBs and deaths of massive stars [38]. The breakthrough led by Swift unveiled that some nearby short GRBs (or short GRBs with EE) have host galaxies that are elliptical or early-type, with little star formation [69,71,72]. Some others occur in star-forming galaxies, but the GRB location has a large offset from the host galaxy where the local star formation rate is low [70,757]. All these point toward another type of progenitor that does not involve massive stars, but is likely related to compact stars, such as NS–NS or NS–BH mergers (e.g. [77,758,78]).

The cozy picture that long GRBs are all physically related to massive star core collapses while short GRBs all physically related to compact star mergers was soon destroyed by several observations. GRB 060614 and GRB 060605 are both nearby long-duration GRBs, but deep searches show no association of a supernova accompanying the GRB [519,759–761], unlike other nearby long GRBs. Moreover, the gamma-ray properties of GRB 060614 share many properties with short GRBs [519], and it would resemble GRB 050724 (a smoking gun “short” GRB that has a definite non-massive star origin) if it were somewhat less luminous [762]. Although theoretically some massive star core collapses can have faint supernova signals (e.g. [763]), the available data for GRB 060614 do not demand such a scenario, since except the long duration all other properties are similar to those of other nearby short GRBs. Rather, it suggests that some GRBs that are not related to massive stars can have a long duration. Later, it was noticed that the three GRBs with the highest redshifts as of end of 2012, i.e. GRB 080913 at  $z = 6.7$  [764], GRB 090423 at  $z = 8.2$  [765,766], and GRB 090429B at  $z = 9.4$  [122] all have a “rest-frame duration”  $T_{90}/(1+z)$  shorter than 2 s.<sup>54</sup> Yet, various arguments suggest that they still originate from deaths of massive stars [512]. Later, an observer-frame short GRB 090426 at  $z = 2.609$  was discovered, which shared many properties of long GRBs with a massive star origin [769–772]. Independent arguments suggest that at least some short GRBs, especially those at high redshifts with high luminosities, are probably not related to compact star mergers [512,497,773,495].

Bromberg et al. [495] found that there exists a plateau in the  $dN/dT_{90}$  duration distribution of GRBs (for all samples with different detectors) and argued that this is an evidence for a massive star origin; the plateau, according to them, is due to the finite time it takes for GRB jets to clear a cavity and make their way out of the star. Bromberg et al. [410] suggest that 40% of the short-GRBs detected by the Swift satellite could arise from collapse of a massive star, and that the distinction between long and short bursts is detector dependent. This is consistent with previous works (e.g. [512,497,773]) that arrived at this conclusion using very different arguments. The host galaxy data, on the other hand, suggest that contamination of massive star GRBs in the short GRB sample may not be large [757,774]. Based on an analysis invoking an “amplitude” parameter  $f$

<sup>54</sup> Simulations suggest (e.g. [767,768]) that when a long GRB is progressively moved to high redshifts, the observer-frame duration may not increase noticeably due to the fact that some signals are buried below the background. As a result,  $T_{90}/(1+z) < 2$  s may not carry a direct clue about the progenitor, and rather could be due to a “tip-of-iceberg” selection effect.

(ratio between the peak flux and background flux) of short GRBs, [767] claimed that the massive star contamination becomes progressively important at low  $f$  values due to the “tip-of-iceberg” effect.

In view of the confusions in classification, suggestions have been made to distinguish the phenomenological classes (long vs. short) and the physically-motivated classes (massive star or Type II GRBs vs. compact star or Type I GRBs) [775,762,512]. The challenge is how to identify the physical class based on data. Zhang et al. [512] summarized a list of multi-wavelength observational criteria that could be connected to the physical nature of a GRB, and suggested to apply them to identify the physical class of a GRB. In particular, the observational criteria that are mostly related to the physical nature of GRBs include supernova association, host galaxy properties, as well as the location within the host galaxy. A flowchart to diagnose the physical category of a GRB based on multiple observational criteria was proposed [512], which was applied to study long and short GRBs observed in the Swift era [776,339].

The multi-wavelength data cannot be immediately obtained when a GRB is detected. So it is important to find a way of determining the physical class of a GRB from prompt  $\gamma$ -ray data alone. Several attempts have been made toward this goal. For example, [777] showed that for GRBs with known redshifts, the parameter  $\varepsilon \equiv E_{\gamma,\text{iso},52}/E_{p,z,2}^{5/3}$  has a more pronounced bimodal distribution; where  $E_{\gamma,\text{iso},52}$  is the GRB isotropic energy in units of  $10^{52}$  erg, and  $E_{p,z,2}$  is the peak of the  $\gamma$ -ray spectrum in units of 100 keV in GRB host galaxy rest frame at redshift  $z$ . The high- $\varepsilon$  vs. low- $\varepsilon$  categories are found to be more closely related to massive star GRBs vs. compact star GRBs, respectively. Lü et al. [767] suggested the “amplitude” of an observed lightcurve should be taken into account to classify GRBs based on duration. In particular, a low-amplitude short GRB can be the “tip-of-iceberg” of a long GRB, whose longer emission episode is buried beneath the background level. The rest-frame-short nature of high- $z$  GRBs can be naturally accounted for with this effect (see also [778]).

Sub-classes likely exist within these two broadly defined progenitor classes. For example, within the massive star GRBs, the low-luminosity bursts typically have smooth lightcurves and long durations, are more abundant, and probably form a distinct population in the luminosity function [54,492]. Physically, they may mark unsuccessful jets, and their emission is from a trans-relativistic shock breaking out from the star (e.g. [55,779]). Regular high-luminosity GRBs, in contrast, have successful jets, as manifested by the erratic variability in the lightcurves. The separation between the two populations is not so clear cut though, as several low luminosity GRBs with successful jets driven by a central engine have been observed (e.g. GRB 120422A, [310]).

Another potential sub-category of massive star GRBs was proposed to interpret several “ultra-long” GRBs (e.g. [780,781]). The ultra-long durations (of order  $10^3$ – $10^4$  s) of these events have led to the suggestion that they might be associated with a blue supergiant progenitor, in contrast to the standard Wolf-Rayet stars. The afterglow properties of these GRBs are not very different from the normal ones (e.g. [782]). Considering that long-lasting X-ray flares exist in a good fraction of GRBs, the possibility that these are the long-duration tail of the normal long GRBs is not ruled out [783].

## 9.2. Massive star GRBs

The progenitor of GRBs is hard to identify, since the progenitor is already destroyed when the GRB occurs. We do not know much regarding the GRB progenitors other than that there are two physically distinct types with one type related to deaths of massive stars and the other type not related to massive stars.

We know better the progenitor of GRBs that are associated with massive stars. This is because considerable amount of information is available about the properties of the supernovae that are associated with these GRBs and about their host galaxies.

### 9.2.1. Properties of supernovae associated with GRBs

A handful of long GRBs have ironclad associations with spectroscopically-identified SNe. The list includes GRB 980425/SN 1998bw at  $z = 0.0085$  [56], GRB 030329/SN 2003dh at  $z = 0.168$  [58,57], GRB 031203/SN 2003lw at  $z = 0.105$  [66], GRB 060218/SN 2006aj at  $z = 0.033$  [61,60], GRB 100316D/SN 2010bh at  $z = 0.059$  [63], GRB 101219B/SN 2010ma at  $z = 0.55$  [64], GRB 120422A/SN 2012bz at  $z = 0.283$  [65], and GRB 130427A/SN 2013cq at  $z = 0.34$  [67,68]. There are a lot more cases of association with various degrees of confidence level, some with a light curve bump as well as some spectroscopic evidence of the SN, some others with a clear light curve bump that is consistent with other GRB-SN associations (e.g. [784]). An optimistic statement that the data are consistent with the hypothesis that all long GRBs are associated with an underlying SN was made [785,10], until the null search results for GRB 060614 and 060505 were reported in 2006<sup>55</sup> [759–761].

The GRBs with firmly established associations with SNe are typically nearby events. As of July 2014, all bursts with SNe association, with the exception of GRBs 030329 and 130427A, are low luminosity GRBs or X-ray flashes. This is likely a selection effect, since the faint SN signal (especially the spectral features) can be only detected at low redshifts, and when the SNe flux is not too faint compared with the afterglow emission in the optical band. High luminosity GRBs have optical

<sup>55</sup> Observational properties (e.g. relatively short hard spike, short spectral lag, low specific star formation rate) of GRB 060614 make it more consistent with belonging to the compact star GRB category [519,759,762]. Indeed, [762] shows that it would look rather similar to the smoking-gun compact star GRB 050724 if it were somewhat less energetic. The case of GRB 060505 is more controversial, but it is by no means a typical long GRB.

afterglows that are brighter than SNe, and they are typically observed at  $z > 1$ . For these events, it is very difficult to detect their associated SNe. In any case, the identifications of SN 2003dh associated with a garden variety GRB 030329 at  $z = 0.168$ , and SN 2013cq associated with the nearby, high-luminosity GRB 130427A at  $z = 0.34$  suggest that high luminosity GRBs are also associated with SNe Ic, whose properties are similar to those associated with low luminosity GRBs.

The spectroscopically identified SNe associated with GRBs are of the Type Ic. These SNe are produced by core collapses of massive stars whose hydrogen and helium envelopes have been stripped before the explosions, so the progenitors were most likely Wolf–Rayet stars [10].

Not all Type Ic SNe have GRB associations. A systematic radio survey of Type Ibc SNe suggests that less than 3% are associated with GRBs [384]. The GRB-associated SNe are consistent with being broad-lined Type Ic, suggesting a large kinetic energy. They have diverse peak brightness, rise time, light curve width, and spectral broadness. Compared with regular Type Ic SNe, the few GRB-associated SNe appear to represent the brighter end of the Type Ic population. However, when non-detections and upper limits on SN light are taken into account, the GRB-associated Type Ic SNe may not be all that different compared with normal Type Ic SNe [10].

### 9.2.2. Host galaxy properties of long GRBs

The majority of long-GRB host galaxies are irregular, star-forming galaxies, and a few are spiral galaxies with active star formation [51]. Occasionally, one can have a GRB located in a galactic halo, (e.g. GRB 070125, [786]). A systematic study suggests that long-GRBs occur in the brightest region of the host galaxy, suggesting a very high specific star formation rate at the burst site [51]. All these properties are consistent with the massive star origin of long GRBs. Nonetheless, cases of long GRBs with relatively low local specific star formation rate have been also discovered (e.g. [787]).

One controversial aspect is whether long-GRBs prefer low metallicity environments. Claims that long GRB-hosts are relatively metal poor have been made (e.g. [788,789,51]). It was noted that GRB-SNe occur in environments that have a systematically lower metallicity than broad-lined Type Ic SNe [790]. Counter-arguments suggest that this apparent metal poor property of long GRB hosts is not intrinsic, but is rather a consequence of anti-correlation between star-formation and metallicity seen in general galaxy population [791]. Recently, [792] compared the metallicity of the hosts of long GRBs, broad-lined Type Ic SNe, and Type II SNe to each other, and to the metallicity distribution of local star-forming galaxies in the SDSS sample, and concluded that such an anti-correlation is not enough to explain the data, and that long GRBs indeed favor a low metallicity environment. This is consistent with the expectation of collapsar model of GRBs [40], as well as numerical simulations of GRB host galaxy luminosity function [793]. Nonetheless, some dark GRBs are found to be located in relatively metal-rich host galaxies (e.g. [794,795]), suggesting that low metallicity may not be the critical condition to produce a GRB.

### 9.2.3. Progenitor of long GRBs

With the above observational constraints, the progenitor of long GRBs can be narrowed down to massive stars with rapid spin (as required to launch a jet), relatively low metallicity, and stripped of their hydrogen and helium envelope. However, the explicit type of star is not identified. Theoretical arguments favor a Wolf–Rayet star with mass larger than  $10 M_{\odot}$  (but not too large, [796]). The leading candidate is a massive star directly collapsing to a black hole – the collapsar model [38,40]. But models invoking binary stars (e.g. [797]) or a magnetar central engine (e.g. [702,705]) are also viable candidates.

## 9.3. Compact star GRBs

A detailed review of observational evidences that many short GRBs are related to compact star mergers is presented in [774].

### 9.3.1. Non-detection of SN light

Deep searches of SNe associated with short-GRBs have been carried out for all nearby bursts. The upper limits on SNe luminosity vary from case to case (e.g. [339,774]), but so far no positive detection has been made. This is consistent with a compact star origin (rather than massive star origin) of these GRBs.

A weaker than supernova optical/IR signal, dubbed “macronova”, “kilonova”, “r-process nova”, or “mergernova” by various groups, has been predicted to be associated with NS–NS or NS–BH mergers [798–801]. Recently, a bright near-IR emission component was detected from the short-GRB 130603B with HST [802,803], which is consistent with the recent prediction of a “kilonova” – luminosity being  $\sim 10^3$  times the luminosity of a typical nova [801]. If a supra-massive magnetar is born during the merger, such a merger-nova could be brighter due to the additional energy injection into the ejecta from the magnetar [744,745]. It is speculated that most spin energy of the magnetar is carried away by gravitational waves, but extreme conditions are required to excite such a strong gravitational wave radiation in order to fit the data. More observations are needed to establish whether all short-GRBs are accompanied by a merger-nova, and to determine whether the central engine in these explosions is a black hole or a magnetar.

### 9.3.2. Host galaxy properties of short GRBs

Fong et al. [757] systematically analyzed the host galaxy properties of 10 nearby short GRBs and compared them with the hosts of long GRBs and Type II SNe. They found that short-GRB host galaxies have exponential disk profiles, but with a medium size twice as large as long-GRB hosts. More importantly, the GRB site has large offsets from the central star-forming regions. The accumulative fraction as a function of fractional flux is very different from long-GRBs, which show strong concentration to the brightest region in the host galaxy [51], and is also very different from that of the core-collapse supernovae. The short-GRBs appear to under-represent their host galaxy light in contrast to long-GRBs. This is consistent with the compact star merger scenarios, since compact stars born in asymmetric supernovae most likely received a “kick”, so that the binary system drifted away from the star forming regions when mergers occur [804].

There is a population of short GRBs that are “hostless”. They may be “kicked” away from their host, or reside in distant faint host galaxies [805].

### 9.3.3. Progenitor of short GRBs

Observations suggest that the progenitor of short GRBs is different from that of long GRBs. However, the explicit progenitor type is not identified. Leading candidates include mergers (or for a small fraction, collisions) of NS–NS and NS–BH systems [77,758,806]. An alternative candidate is accretion induced collapse of a NS to BH [807,808]. A small fraction of short GRBs can be the giant flares of soft gamma-ray repeaters in nearby galaxies [809].

One should be cautious and not jump to conclusion that all short/hard GRBs in the BATSE sample are due to the compact star merger origin. Even though the NS–NS merger model is claimed to be able to reproduce the Swift short GRB data [810] and the BATSE short GRB data [811], the model cannot simultaneously explain the z-known Swift sample, and the z-unknown BATSE sample [497]. In particular, the z-known sample demands a shallow luminosity function in order not to over-produce nearby low-luminosity short GRBs. For a reasonable redshift distribution of NS–NS mergers, such a shallow luminosity function is always translated to a shallow flux distribution, which is inconsistent with the BATSE data. A possible way out of this problem might be that some high-redshift, high-luminosity short-GRBs are related to massive stars [512,495].

Since giant flares of Galactic soft gamma-ray repeaters (SGRs) also generate a short, hard, emission episode, it has been speculated that some SGR giant flares in the nearby galaxies can give rise to apparent short hard GRBs [809]. Searches in nearby galaxies for well localized short GRBs suggest that such SGR contamination to the observed short-GRB population is low, below 15% [812,813].

## 9.4. Gravitational wave diagnosis of GRB progenitor

Probably the most definite diagnosis of GRB progenitor can be made when gravitational waves are jointly detected with GRBs. Different progenitors have distinct gravitational wave signatures (e.g. [814]). In particular, compact star mergers have a characteristic in-spiral chirp signal [815], detection of which would give definite identification of the short GRB progenitor (e.g. [816]). For NS–NS mergers, the post-merger product can be either a black hole or a supra-massive neutron star, which would give different gravitational wave signatures: a black hole engine would show a “ring-down” signal after the merger phase (e.g. [815,817,818,686]), while a supra-massive neutron star would give extended gravitational wave signals due to a secular bar-mode instability (e.g. [686,819]).

The gravitational wave signal due to a massive star core collapse is subject to large uncertainties. If collapse is asymmetric, bar-mode instability may develop in the accretion disk, so that strong gravitational waves can be released from the central engine of long GRBs [817,818,820].

Detecting gravitational waves from astrophysical objects is challenging. The upcoming advanced gravitational wave detectors such as Advanced LIGO [821] and Advanced VIRGO [822] are expected to expand the detection horizon to a few hundred Mpc as early as 2015. Detecting the electromagnetic counterparts of gravitational wave sources would increase the signal-to-noise ratio of the gravitational wave signal and confirm its astrophysical origin. If the final product of a compact star merger is a black hole, the electromagnetic signals associated with the gravitational wave burst include a short GRB, an optical “macronova” [798–800], and a long-lasting radio afterglow due to the interaction of the ejecta with the surrounding matter [823–829]. These signals are either beamed (short GRB) or very faint. On the other hand, if a NS–NS merger leaves behind a supra-massive millisecond magnetar which is possible based on uncertainties of our understanding of equation-of-state of nuclear matter [703,830], then very bright electromagnetic counterparts can be detected with gravitational wave bursts without a short GRB association. The signals include a bright early X-ray afterglow due to internal dissipation of a proto-magnetar wind [742], bright broad-band afterglow of a magnetar-powered ejecta [743], as well as a merger-nova brighter than the “kilo-nova” predicted for a black hole central engine [744,745]. The planned multi-messenger observations of GRBs would greatly enrich our understanding of GRB physics.

## 10. High energy neutrinos from GRBs

As energetic, non-thermal photon emitters, GRBs are believed to be efficient cosmic ray accelerators as well. The standard scenario invokes first order Fermi acceleration mechanism in relativistic shocks, both in internal shocks and the external (forward and reverse) shocks. Alternatively, magnetic reconnection can also accelerate cosmic rays to high energies.

The maximum proton energy can reach the ultra-high energy (UHE) range [831–833]. The maximum energy of the shock accelerated protons can be estimated by the condition  $t'_{\text{acc}} = \min(t'_{\text{dyn}}, t'_{\text{c}})$ , where  $t'_{\text{acc}} = \xi(\gamma_p m_p c/eB')$ ,  $t'_{\text{dyn}}$ , and  $t'_{\text{c}}$  are the acceleration, dynamical, and cooling time scales in the co-moving frame. For example, within the internal shock framework, when we ignore proton cooling via the photo-pion process (which can be important for UHE protons), the maximum proton energy is

$$E_{p,\text{max}} \simeq 4 \times 10^{20} \text{ eV} \xi^{-1} \left( \frac{\epsilon_{B,-1} L_{\gamma,52}}{\epsilon_{e,-1}} \right)^{1/2} \Gamma_{2.5}^{-1}, \quad (255)$$

which is in the UHE range. Protons with energies below this maximum value can produce neutrinos of different energies.

A GRB has multiple emission sites that can accelerate protons. These same sites usually are also permeated with photons. If protons in a GRB jet can be accelerated to an energy  $E_p$  so that the condition

$$E_p E_\gamma \gtrsim \frac{m_\Delta^2 - m_p^2}{4} \left( \frac{\Gamma}{1+z} \right)^2 = 0.16 \text{ GeV}^2 \left( \frac{\Gamma}{1+z} \right)^2 \quad (256)$$

is satisfied, significant neutrino emission is possible via the  $p\gamma$  mechanism at the  $\Delta$ -resonance

$$p\gamma \rightarrow (\Delta^+ \rightarrow) \begin{cases} n\pi^+ \rightarrow n\mu^+ \nu_\mu \rightarrow ne^+ \nu_e \bar{\nu}_\mu \nu_\mu, & \text{fraction 1/3} \\ p\pi^0 \rightarrow p\gamma\gamma, & \text{fraction 2/3.} \end{cases} \quad (257)$$

Here  $\Gamma$  is the bulk Lorentz factor,  $E_\gamma$  is photon energy in observer frame,  $m_\Delta = 1.232 \text{ GeV}$  and  $m_p = 0.938 \text{ GeV}$  are the rest masses of  $\Delta^+$  and proton, respectively. At  $\Delta$ -resonance, about 20% of the proton energy goes to  $\pi^+$  ( $\epsilon_{\pi^+} \sim 0.2\epsilon_p$ ), whose energy is evenly distributed to 4 leptons ( $\epsilon_\nu \sim 0.25\epsilon_{\pi^+}$ ). So overall

$$E_\nu \sim 0.05E_p. \quad (258)$$

Due to the high compactness of the ejecta, the  $p\gamma$  interaction can have high optical depth, so that  $\pi^+$  are copiously generated.  $\pi^+$  decay and subsequent  $\mu^+$  decay generate neutrinos ( $\nu_\mu$  and  $\nu_e$ ) and anti-neutrinos ( $\bar{\nu}_\mu$ ).

Another important neutrino production mechanism is hadronic collisions, including  $pp$  and  $pn$  processes, e.g.

$$\begin{aligned} pp &\rightarrow pn\pi^+/K^+ \rightarrow pn\mu^+ \nu_\mu \rightarrow pne^+ \nu_e \bar{\nu}_\mu \nu_\mu \\ pn &\rightarrow pp\pi^-/K^- \rightarrow pp\mu^- \bar{\nu}_\mu \rightarrow ppe^- \bar{\nu}_e \nu_\mu \bar{\nu}_\mu \\ pn &\rightarrow nn\pi^+/K^+ \rightarrow nn\mu^+ \nu_\mu \rightarrow nne^+ \nu_e \bar{\nu}_\mu \nu_\mu. \end{aligned} \quad (259)$$

Free neutrons will subsequently decay:  $n \rightarrow pe^- \bar{\nu}_e$ . These processes are important in a dense environment, such as inside the progenitor star.

### 10.1. PeV neutrinos

For GRBs, a guaranteed target photon source for  $p\gamma$  interaction is the burst itself. For the typical peak photon energy  $E_\gamma \sim$  several hundred keV, the corresponding neutrino energy is in the sub-PeV regime [834]. The standard model invokes internal shocks as the site of both gamma-ray photon emission and proton acceleration [98,834]. Alternatively, photons can be generated at the photosphere [590,112,835,113,836,118,117,837] or from magnetic field dissipation beyond the internal shock radii [107]. Protons can be accelerated in the same site or a different site from the gamma-ray emission region. Over the years, PeV neutrino flux from GRBs has been calculated both analytically and numerically [834,838–843,423]. We describe here a general formalism for calculating the strength of the neutrino signal that can be applied to any of the above mentioned models for GRB emission [844]:

For an observed “Band”-function photon flux spectrum

$$\begin{aligned} F_\gamma(E_\gamma) &= \frac{dN(E_\gamma)}{dE_\gamma} \\ &= f_\gamma \begin{cases} \left( \frac{\epsilon_\gamma}{\text{MeV}} \right)^{\alpha_\gamma} \left( \frac{E_\gamma}{\text{MeV}} \right)^{-\alpha_\gamma}, & E_\gamma < \epsilon_\gamma \\ \left( \frac{\epsilon_\gamma}{\text{MeV}} \right)^{\beta_\gamma} \left( \frac{E_\gamma}{\text{MeV}} \right)^{-\beta_\gamma}, & E_\gamma \geq \epsilon_\gamma \end{cases}, \end{aligned}$$

the observed neutrino number spectrum can be expressed as [834,845]

$$F_\nu(E_\nu) = \frac{dN(E_\nu)}{dE_\nu}$$

$$= f_\nu \begin{cases} \left(\frac{\epsilon_{\nu,1}}{\text{GeV}}\right)^{\alpha_\nu} \left(\frac{E_\nu}{\text{GeV}}\right)^{-\alpha_\nu}, & E_\nu < \epsilon_{\nu,1} \\ \left(\frac{\epsilon_{\nu,1}}{\text{GeV}}\right)^{\beta_\nu} \left(\frac{E_\nu}{\text{GeV}}\right)^{-\beta_\nu}, & \epsilon_{\nu,1} \leq E_\nu < \epsilon_{\nu,2}, \\ \left(\frac{\epsilon_{\nu,1}}{\text{GeV}}\right)^{\beta_\nu} \left(\frac{\epsilon_{\nu,2}}{\text{GeV}}\right)^{\gamma_\nu - \beta_\nu} \left(\frac{E_\nu}{\text{GeV}}\right)^{-\gamma_\nu}, & E_\nu \geq \epsilon_{\nu,2} \end{cases}$$

where

$$\alpha_\nu = p + 1 - \beta_\gamma, \quad \beta_\nu = p + 1 - \alpha_\gamma, \quad \gamma_\nu = \beta_\nu + 2, \quad (260)$$

and  $p$  is the proton spectral index defined by  $N(E_p)dE_p \propto E_p^{-p}dE_p$ . The indices  $\alpha_\nu$  and  $\beta_\nu$  are derived by assuming that the neutrino flux is proportional to the  $p\gamma$  optical depth  $\tau_{p\gamma}$ . This is valid when the fraction of proton energy that goes to pion production, i.e.  $f \equiv 1 - (1 - \langle \chi_{p \rightarrow \pi} \rangle)^{\tau_{p\gamma}}$ , is proportional to  $\tau_{p\gamma}$  ( $\langle \chi_{p \rightarrow \pi} \rangle \simeq 0.2$  is the average fraction of energy transferred from protons to pions), which is roughly valid when  $\tau_{p\gamma} < 3$ . In general, one can write [844]

$$\epsilon_{\nu,1} = \epsilon_{\nu,1}^0 \min(1, (\tau_{p\gamma}^p/3)^{1-\beta_\gamma}), \quad (261)$$

where

$$\epsilon_{\nu,1} = \epsilon_{\nu,1}^0 = 7.3 \times 10^5 \text{ GeV} (1+z)^{-2} \Gamma_{2.5}^2 \epsilon_{\gamma,\text{MeV}}^{-1}, \quad (262)$$

$$\epsilon_{\nu,2} = 3.4 \times 10^8 \text{ GeV} (1+z)^{-1} \epsilon_B^{-1/2} L_{w,52}^{-1/2} \Gamma_{2.5}^2 R_{14}, \quad (263)$$

and

$$\tau_{p\gamma}^p \equiv \tau_{p\gamma}(E_p^p) \simeq \frac{\Delta R'}{\lambda'_{p\gamma}(E_p^p)} = 0.8 L_{\gamma,52} \Gamma_{2.5}^{-2} R_{14}^{-1} \epsilon_{\gamma,\text{MeV}}^{-1}. \quad (264)$$

$\lambda'_{p\gamma}(E_p^p)$  is the comoving proton mean free path for  $p\gamma$  interaction at  $E_p^p$  ( $E_p^p$  is the energy of protons that interact with peak energy photons at  $\Delta$ -resonance),  $\Delta R'$  is the comoving width of the jet,  $R$  denotes the distance of proton acceleration site (rather than the photon emission site if the two sites are different) from the central engine,  $\epsilon_B$  is the fraction of dissipated jet energy in magnetic fields, and  $L_w$  is the luminosity of the dissipated wind. We further define

$$f_{\gamma/p} \equiv \frac{L_\gamma}{L_p}, \quad (265)$$

and

$$f_p \equiv \frac{\int_{E_{p,1}}^{E_{p,2}} dE_p E_p^2 dN(E_p)/dE_p}{\int_{E_{p,min}}^{E_{p,max}} dE_p E_p^2 dN(E_p)/dE_p} \simeq \frac{\ln(\epsilon_{\nu,2}/\epsilon_{\nu,1})}{\ln(E_{p,max}/E_{p,min})} \quad (\text{for } p = 2), \quad (266)$$

where  $E_{p,1}$  and  $E_{p,2}$  are proton energies corresponding to  $\epsilon_{\nu,1}$  and  $\epsilon_{\nu,2}$ , respectively (Eq. (258)), and  $E_{p,max}$  and  $E_{p,min}$  are the maximum and minimum proton energy. One can then normalize the neutrino spectrum with the total photon fluence [845]

$$\int_0^\infty dE_\nu E_\nu F_\nu(E_\nu) = \frac{1}{8} \frac{f_p}{f_{\gamma/p}} [1 - (1 - \langle \chi_{p \rightarrow \pi} \rangle)^{\tau_{p\gamma}^p}] \int_{1 \text{ keV}}^{10 \text{ MeV}} dE_\gamma E_\gamma F_\gamma(E_\gamma). \quad (267)$$

The coefficient  $1/8$  is the product of  $1/4$  (4 leptons share the energy of one  $\pi^+$ ) and  $1/2$  (on average roughly half of  $p\gamma$  interactions go to the  $\pi^+$  channel when all the  $\pi^+$  processes besides  $\Delta^+$  resonance, e.g. direct-pion production, and multiple pion production, are taken into account).

Over the years, the IceCube Collaboration have been searching for high energy neutrino signals coincident with GRBs in time and direction, and progressively deeper non-detection upper limits have been placed [845,846,606]. The current IceCube upper limit was claimed to be at least a factor of 3.7 smaller than the theoretical predictions for neutrino flux from GRBs according to the internal-shock model, which has raised further doubt regarding the viability of GRBs as sources of UHECRs [606]. More detailed, follow-up, calculations [847,848,366] suggest that the current limit is still not deep enough to provide significant constraints on the validity of the internal shock model. However, the model would be severely challenged if the upper limit continues to go down in the next few years.<sup>56</sup>

The internal shock model fails to explain prompt  $\gamma$ -ray spectra. Alternative prompt emission models (e.g. dissipative photosphere models and large-radius magnetic dissipation models) have been widely discussed in the literature. These

<sup>56</sup> As of July 2014, the IceCube upper limit on neutrino flux for GRBs has come down roughly by another factor of 3 since the upper limit reported in [606, 607], placing even tighter constraints on the internal shock and photosphere models.

different models have different predictions for the neutrino flux. Zhang and Kumar [844] compared the predictions of different models and concluded that the current upper limit already constrains the photosphere model unless  $f_{\gamma}/p > 0.1$  or protons are not accelerated to the desired energy to satisfy the  $\Delta$ -resonance condition. The internal shock model is barely constrained by the current data [366]. On the other hand, magnetic dissipation models that invoke a large emission radius (e.g. the ICMART model; [108]) predict a much lower neutrino flux, which is consistent with the current null result. If in the next few years the neutrino flux limit continues to go down, it would favor the magnetic dissipation models and further constrain the parameter space of the matter-dominated models.

The recent nearby, very bright GRB 130427A did not show a positive PeV neutrino signal. This non-detection makes even tighter constraints on the internal shock model and the photosphere model of GRBs [849].

Low-luminosity GRBs are more common and form a distinct population in the GRB luminosity function [494,54,492]. If these GRBs produce successful jets, since they are softer and have lower Lorentz factors, the characteristic neutrino energy in the traditional internal shocks is higher than that of the high-luminosity GRBs. These GRBs give a neutrino background in the sub EeV range with a flux level comparable to that by high luminosity GRBs [850,851].

## 10.2. Other neutrino emission components from GRBs

GRBs also have other sites that generate high energy neutrinos. Since the seed photon energies and Lorentz factor can be different at different sites, the characteristic energies of neutrinos are also different.

At the deceleration radius, the typical target photon energy may be  $\sim 1$  eV and  $\sim 1$  keV for the reverse and forward shock, respectively. Given  $\Gamma \sim 100$ , the  $\Delta$ -resonance condition gives the corresponding neutrino energy  $\epsilon_{\nu} \sim 5 \times 10^{19}$  eV and  $\sim 5 \times 10^{16}$  eV for the forward and reverse shock, respectively [852–854]. This is broadly in the EeV regime.

Due to a smaller Lorentz factor when the jet has not completed the acceleration phase while inside the star, internal shocks and proton acceleration can occur before the jet reaches the stellar surface. Neutrinos can be generated via both  $p\gamma$  and  $pp/pn$  collision mechanisms (if the envelope is large enough) [855,838,839,856]. Taking  $\Gamma \sim 10$ , and  $E_{\gamma} \sim 5$  keV (X-ray photons trapped in the jet), one can estimate  $E_p \sim 2 \times 10^{13}$  eV, and the typical neutrino energy  $\epsilon_{\nu} \sim 10^{12}$  eV (or TeV). Since this mechanism applies to both successful and failed GRBs, detecting this neutrino emission can probe failed jets in core-collapsing massive stars. Recent studies suggest that a relativistic photon-mediated shock is inefficient in accelerating protons (e.g. [857]). This would suppress high-energy neutrinos in successful GRBs, but low-luminosity GRBs remain good candidates to generate the high-energy neutrino background observed by IceCube [856].

For a neutron-rich ejecta, protons and neutrons can decouple and move with different Lorentz factors (see Section 7.7). If the relative speed between the two components is larger than about 0.5C, then pions, muons, and neutrinos are produced in inelastic collisions between protons and neutrons [258,259]; pion mass is about 140 MeV and proton mass 940 MeV. The neutrinos produced by this process have energies  $\sim 10$ – $10^2$  GeV. In this energy range, the atmospheric neutrino background is very strong, therefore, detecting these neutrinos from GRBs is very difficult with ground-based detectors. However, time- and space-coincidence with GRBs can help significantly reduce the background problem and improve the chances of detecting these quasi-thermal neutrinos with 10 year observations with IceCube (e.g. [858]).

Finally, the GRB central engine is expected to produce copious MeV neutrinos [570]. These MeV neutrinos are generic feature of all core collapse events. Positive detections have been made for SN 1987A. In order to detect MeV neutrinos from a GRB, the GRB has to be very close to earth. The event rate of such nearby GRBs whose MeV neutrinos are detectable is extremely low.

## 11. GRBs from the first stars (pop III stars) and their use for investigating the high redshift universe

The universe was essentially devoid of stars until the redshift of  $\sim 15$ – $20$ , when the first stars were born, and the strong UV radiation from them contributed to the reionization of the universe, and bringing to an end the cosmic dark age (e.g. [859–862]). A fraction of these stars likely ended their life as GRBs. In this section, we describe how GRBs can be used to study the end of the cosmic dark ages.

According to the cold dark matter (CDM) paradigm of hierarchical structure formation, the first generation of stars, or pop III stars, are expected to have formed in dark matter halos of mass  $\sim 10^6 M_{\odot}$  which decoupled from general expansion, and collapsed at about a redshift of 20 (e.g. [863,864]).

The first stars, free of metals, were born with mass larger than their metal rich descendants. Ten years ago it was thought that the typical mass of these stars might be more than  $10^2 M_{\odot}$  (e.g. [865–867]). The formation of metal free stars, in the absence of magnetic fields, is easier to understand than the much more complex physics behind the formation of later generation of stars where one needs to consider effects of magnetic fields and a complex network of radiative processes involving a rich variety of atoms. The characteristic mass scale of pop III stars is set by the Jeans mass for a primordial cloud that is cooled to a temperature of order 200 K by the rotational–vibrational transitions of molecular hydrogen; an upper limit to the density of the primordial clouds ( $n \sim 10^4$  cm $^{-3}$ ) from which stars are born is obtained by the requirement that the time scale for collisional de-excitation of H<sub>2</sub> should be longer than the time it takes for radiative transition to lower energy state (otherwise the cloud would be unable to cool and form stars). An additional complication one needs to deal

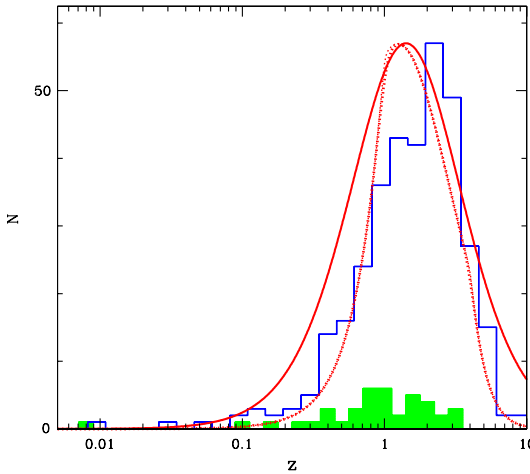


**Fig. 38.** This figure, showing redshift distribution of GRBs; the  $z$ -distributions of Swift GRBs and pre-Swift GRBs are in blue and green histograms, respectively (the higher redshift of Swift bursts,  $\langle z \rangle \sim 2.5$ , compared to  $\langle z \rangle \sim 1.2$  for pre-swift bursts is due to the higher sensitivity of Swift/BAT). The thick solid red curve is the evolution of a comoving volume element of the Universe for  $\Lambda$ -CDM model; the thin dotted red curve is a convolution of the comoving volume with a model for the star-formation rate as calculated by Yüksel et al. [880]. Credit: John Cannizzo. Source: Adapted from [13].

with is the fragmentation of clouds while it is undergoing collapse. Earlier simulations had underestimated this effect, and newer, higher resolution, simulations find that the typical mass of pop III stars is close to  $\sim 40 M_{\odot}$  (e.g. [868]).

Population III stars should have had a weak wind – massive stars have radiation driven winds which are launched by photons scattering off of metals, the most efficient of which for this purpose are the iron group of elements – and hence they retain their angular momentum and are rapidly spinning at the time of their death. These conditions – high mass and rapid rotation rate – are conducive to formation of an accretion disk when the star undergoes collapse at the end of its nuclear burning life cycle, and could produce a relativistic jet and a GRB. It is, therefore, speculated that a fraction of population III stars should produce GRBs when they die.

The recent discoveries of GRBs at redshifts of 8.26 [765,766] and 9.4 [122] have established that GRBs did indeed occur when the universe was young ( $z = 9.4$  corresponds to 525 million years after the big bang). These bursts were fairly typical of long-GRBs in terms of their luminosity and spectral properties, and bursts like these can be detected by the Swift satellite up to redshift of  $\sim 15$ . Thus, if the first stars to form in the universe, at the end of the cosmic dark age, were massive, and rapidly rotating, as suggested by theoretical calculations, then they should produce GRBs [796,869,870] and these can be detected by Swift and future GRB missions.

The observed redshift distribution of bursts is shown in Fig. 38, along with the star formation rate. It is clear that GRB rate is falling off less rapidly than the star formation rate at  $z > 2$ , which might be related to the claimed lower metallicity of GRB host galaxies. Correcting for the detector's sensitivity selection effect against detection of high- $z$  GRBs, this high- $z$  excess effect is even more significant. Detailed studies of this high- $z$  excess effect have been carried out in the last several years (e.g. [871–873,497,874,875]). The general conclusion from these studies is that the excess requires a low-metallicity preference for GRB progenitors, a possible evolution of GRB luminosity function, or even both [876,497]. Current observations of high- $z$  GRBs suggest that their rate per unit star formation is increasing with  $z$ , but the rate is not as large as previously estimated (e.g. [877–879]).

GRBs have some advantages over other astronomical objects for exploring the high redshift universe including the fact that the GRB afterglow is a factor  $\sim 10^4$  brighter than the brightest quasars and its spectrum is a featureless power law function. Due to their extreme luminosity [881], a favorable negative  $k$ -correction and time-dilation effect of optical/IR/radio afterglow [882,883], GRBs and their afterglows can be detected to a redshift  $z \sim 20$ . If a IR camera can observe the early afterglow phase and take a spectrum, one would be able to identify them as a high- $z$  GRB through the Gunn–Peterson “trough” [884]. Since the intrinsic GRB afterglow spectra are featureless, all the lines that are observed are due to atomic/molecular absorption in the burst-host-galaxy and by gas in the intergalactic medium. Thus, one can learn about gas density and composition at high redshifts from afterglow observations. By studying the damped Lyman  $\alpha$  systems of the high- $z$  GRB hosts [885,886], one can gain insights on structure formation in the early universe. High redshift GRBs could also serve as bright background sources for 21 cm absorption by neutral hydrogen (e.g. [887–889]) that would facilitate investigation of gas distribution at the dawn of galaxy formation, and for determining the reionization history of the universe [890,891]. Although we are far from there, properties of high- $z$  GRB progenitor stars can, in principle, be obtained from the prompt and early X-ray lightcurves.

Determining the atomic/molecular abundance of ISM at high redshifts would provide insight into the history of star formation and supernovae that enriched the ISM with metals cooked inside the first generation of stars. Infrared spectra of GRB afterglows would provide this information at distances of  $\gtrsim 10$  pc from the site of explosion. The medium within about

10 pc of the GRB is, however, completely ionized by the extreme luminosity of GRBs and their X-ray and UV afterglows. Thus, little information regarding the medium in the immediate vicinity of GRBs – which contains information about the GRB progenitor star and its mass loss history – can be obtained from afterglow spectra. We have to resort to other methods in order to obtain information regarding the ISM density within a few parsec of the GRB progenitor star.

## 12. Concluding thoughts and future prospects

It has been a long wild ride for people working on gamma-ray bursts to figure out the true nature and origin of these cosmic explosions. We provide a brief summary of things we have learned, and the questions still unanswered, regarding these powerful transient events.

### What are the things we know with confidence?

The distance to these events is well established from afterglow observations, and hence, we know the isotropic equivalent of energy release in  $\gamma$ -rays. The mean redshift for long duration bursts detected by the Swift satellite is  $z \sim 2.5$ , and for short bursts it is  $\sim 0.3$  [13]. The median isotropic energy in long (short) bursts is  $\sim 10^{52}$  erg ( $\sim 10^{50}$  erg).

These explosions have an outflow speed (whatever is its composition) that is close to that of light, with a Lorentz factor of a few hundred. There are numerous lines of evidence for the high outflow speed. The most direct ones are from radio observations that determine the angular size of the ejecta with time. The time dependence of ejecta size has been determined either directly using VLBI maps for a relatively nearby burst [49], or by using erratic variations of flux by a factor  $\sim 2$  (scintillation) for a period of a few weeks – which is produced when the source size is small – followed by a smooth decline when the source angular size becomes larger than the electron fluctuation scale in the inter-stellar medium [48,20]. These angular size measurements show that the LF of the outflow a few days after the explosion was  $\sim 10$  which when extrapolated back to about 1 min – when the GRB blast wave started decelerating due to interaction with the interstellar medium – yields a LF of  $\sim 10^2$ .

It is also certain that at least a part of the afterglow radiation in GeV, X-ray, optical, radio bands, is produced via the synchrotron process when the relativistic ejecta from the explosion drives a strong shock into the surrounding medium.

The relativistic outflow produced in GRBs are highly collimated. This is required by consideration of total energy – most energetic explosions release  $10^{55}$  ergs, if isotropic, and exceed the energy one can realistically expect from a stellar mass object – and also confirmed at least in a few cases where achromatic jet break is seen in X-ray and optical afterglow lightcurves.

There are at least two physically distinct types of GRBs. Most long duration bursts ( $t > 2$  s) occur in star forming galaxies, and several of these have spectroscopically identified supernova associated with them, giving a direct confirmation of their origin in the collapse of massive stars. On the other hand, several short duration GRBs have been found in low star forming galaxies, or low star forming regions in star forming galaxies, which implies that these were not produced in the collapse of massive, short lived, stars. A likely (but not proven) possibility is that they are produced from binary compact star mergers.

The black hole or neutron star produced in these explosions remains *active* and continues to produce relativistic jets for a long period of time, hours to days, as evidenced by flares seen in the X-ray band and occasionally in the optical.

### What we wish to know and how to get there?

Some of the foremost unanswered questions regarding GRBs are:

- what is the composition of jet/ejecta (baryonic,  $e^\pm$  or magnetic outflow)?
- how are  $\gamma$ -rays, particularly of energy less than  $\sim 10$  MeV, produced?
- is a black hole or a rapidly rotating, highly magnetized, neutron star (magnetar) produced in GRBs?
- what is the mechanism by which relativistic jets are launched? And how is their energy dissipated when they reach a large distance ( $\gtrsim 10^{12}$  cm) from their launching site?
- what are the properties of long and short duration GRB progenitor stars?

Since GRBs are short lived transient events, where the flux changes on time scale of seconds or less, it has been difficult to coordinate observing campaigns to cover the very broad segment of electromagnetic spectrum over which these bursts have significant radiation and capture their temporal behavior. An ideal observational campaign would be to obtain broad band data, from radio to GeV, for a period of several days starting from  $\gamma$ -ray trigger time. This demands wide-field, high-sensitivity detectors in a wide bandpass. Such detectors are not available, but the Swift observatory [274] and ground-based robotic optical telescopes with rapid slew capability have made possible monitoring of these events in optical and X-ray bands with excellent time coverage. Joint triggers by Swift and Fermi LAT [357], even though rare, can provide prompt data from  $\sim 10$  keV to  $10^2$  GeV. Future missions such as SVOM [892] and UFFO [893,894] would continue to allow rapid follow up observations of GRBs, and move the field forward.

Light on jet composition can be shed by measuring optical flux and spectrum during the prompt and the very early afterglow phase for a large sample of GRBs, e.g. with UFFO. Early observations in even longer wavelengths with telescopes such as The Expanded Very Large Array (EVLA, <http://www.aoc.nrao.edu/evla/>), Atacama Large Millimeter/submillimeter Array (ALMA, <http://www.almaobservatory.org>), and The LOw Frequency ARray (LOFAR, <http://www.lofar.org>) would also be very useful. These observations will help us determine whether the jet is heated by a reverse shock – which is strong for a baryonic jet and weak for jets of high magnetization ( $\sigma$ ) – and when the jet starts interacting with the external medium.

Firm determination of a thermal component to prompt  $\gamma$ -ray radiation is also an important, although not unique, signature of baryonic outflows. Detection or an order of magnitude improvement to the currently available upper limit for neutrino flux from GRBs would also be very important for answering the question of jet composition.

Measurement of polarization of  $\gamma$ -ray radiation will both help determine the jet composition and shed light on the radiation mechanism. Polarization measurement of early optical radiation is also very useful for this purpose.

Detection of gravitational waves from GRBs would rapidly advance our understanding of the GRB progenitor and the central engine.

We need a concerted theoretical effort to model multi-wavelength prompt and afterglow data to be able to extract information regarding the birth of a black hole/neutron star and the GRB progenitor star properties. Numerical simulations designed to study fundamental physical processes in extreme conditions, such as particle acceleration in relativistic shocks and in magnetic reconnection regions, and acceleration and dissipation of a Poynting jet, are also needed to attack this complex problem from “bottom-up”. Collecting more data, although very satisfying, is only truly rewarding when at least equal effort is invested to try to understand what the data is telling us about the underlying physics and astrophysics of the object. Otherwise we just keep collecting more data and do not advance any real understanding, which is like collecting fossil specimen, or cataloging plants/animals, without trying to figure out the underlying cause for the origin and diversity of life.

## Acknowledgments

PK thanks Rodolfo Barniol Duran, Jonathan Granot, Milos Milosavljević, Ramesh Narayan, Tsvi Piran, Craig Wheeler for numerous discussions. He is especially indebted to Alin Panaiteescu for nearly a decade long collaboration, and countless illuminating discussions.

We are grateful to Tsvi Piran and his group at the Hebrew university for carefully reading a draft of this review and discussing it over a period of about two months, and for providing extensive feedback that helped improve this work. We would like to thank a number of colleagues for providing comments, in particular Lorenzo Amati, Željka Bošnjak, Patrick Crumley, Rodolfo Barniol Duran, Zigao Dai, Yizhong Fan, Filippo Frontera, Jonathan Granot, Bruce Grossan, Kunihito Ioka, Peter Mészáros, Kohta Murase, Shigehiro Nagataki, Asaf Pe'er, Rodolfo Santana, Kenji Toma, Ryo Yamazaki, and Xiangyu Wang. We are indebted to the referee for taking the time to read this long review article and for providing extensive, constructive, comments and criticisms. Any remaining error or omission is obviously the responsibility of the authors. We also thank John Beacom, John Cannizzo, Patrick Crumley, Neil Gehrels, Savannah Kumar, Rodolfo Santana, and Bin-Bin Zhang for help with several figures.

PK is grateful to Dan Jaffe, Chairman of the Astronomy department at UT, for a semester off teaching and other administrative duties which were big help in completing this review, and he is indebted for the hospitality extended to him by KIAA, Beijing, and Jeremy Heyl at UBC where he worked uninterrupted for several weeks in very serene settings. BZ acknowledges UNLV faculty senate sabbatical committee for approving one-year on leave from UNLV, and the hospitality of KIAA and Department of Astronomy, Peking University. This work was funded in part by National Science Foundation grants AST-0909110 (PK), AST-0908362 (BZ), and NASA grants NNX10AP53G and NNX14AF85G (BZ).

## References

- [1] R.W. Klebesadel, I.B. Strong, R.A. Olson, Observations of Gamma-Ray Bursts of Cosmic Origin, *ApJ* 182 (1973) L85.
- [2] D. Band, J. Matteson, L. Ford, B. Schaefer, D. Palmer, B. Teegarden, T. Cline, M. Briggs, W. Paciesas, G. Pendleton, G. Fishman, C. Kouveliotou, C. Meegan, R. Wilson, P. Lestrade, BATSE observations of gamma-ray burst spectra. I - Spectral diversity, *ApJ* 413 (1993) 281–292.
- [3] C. Kouveliotou, C.A. Meegan, G.J. Fishman, N.P. Bhat, M.S. Briggs, T.M. Koshut, W.S. Paciesas, G.N. Pendleton, Identification of two classes of gamma-ray bursts, *ApJ* 413 (1993) L101–L104.
- [4] C.A. Meegan, G.J. Fishman, R.B. Wilson, J.M. Horack, M.N. Brock, W.S. Paciesas, G.N. Pendleton, C. Kouveliotou, Spatial distribution of gamma-ray bursts observed by BATSE, *Nature* 355 (1992) 143–145.
- [5] G.J. Fishman, C.A. Meegan, Gamma-ray bursts, *Ann. Rev. Astron. Astrophys.* 33 (1995) 415–458.
- [6] T. Piran, Gamma-ray bursts and the fireball model, *Physics Reports* 314 (1999) 575–667.
- [7] P. Mészáros, Theories of Gamma-Ray Bursts, *Ann. Rev. Astron. Astrophys.* 40 (2002) 137–169.
- [8] B. Zhang, P. Mészáros, Gamma-Ray Bursts: progress problems prospects, *Internat. J. Modern Phys. A* 19 (2004) 2385–2472.
- [9] T. Piran, The physics of gamma-ray bursts, *Rev. Modern Phys.* 76 (2004) 1143–1210.
- [10] S.E. Woosley, J.S. Bloom, The supernova gamma-ray burst connection, *Ann. Rev. Astron. Astrophys.* 44 (2006) 507–556.
- [11] D.B. Fox, P. Mészáros, GRB fireball physics: prompt and early emission, *New J. Phys.* 8 (2006) 199.
- [12] B. Zhang, Gamma-Ray Bursts in the swift era, *Chin. J. Astron. Astrophys.* 7 (2007) 1–50.
- [13] N. Gehrels, E. Ramirez-Ruiz, D.B. Fox, Gamma-Ray Bursts in the Swift Era, *Ann. Rev. Astron. Astrophys.* 47 (2009) 567–617.
- [14] S. Mao, B. Paczynski, On the cosmological origin of gamma-ray bursts, *ApJ* 388 (1992) L45–L48.
- [15] T. Piran, The implications of the Compton (GRO) observations for cosmological gamma-ray bursts, *ApJ* 389 (1992) L45–L48.
- [16] E.E. Fenimore, R.I. Epstein, C. Ho, R.W. Klebesadel, C. Lacey, J.G. Laros, M. Meier, T. Strohmayer, G. Pendleton, G. Fishman, C. Kouveliotou, C. Meegan, The intrinsic luminosity of  $\gamma$ -ray bursts and their host galaxies, *Nature* 366 (1993) 40–42.
- [17] E. Costa, F. Frontera, J. Heise, M. Feroci, J. in't Zand, F. Fiore, M.N. Cinti, D. Dal Fiume, L. Nicastro, M. Orlandini, E. Palazzi, M. Rapisarda#, G. Zavattini, R. Jager, A. Parmar, A. Owens, S. Molendi, G. Cusumano, M.C. Maccarone, S. Giarrusso, A. Coletta, L.A. Antonelli, P. Giommi, J.M. Muller, L. Piro, R.C. Butler, Discovery of an X-ray afterglow associated with the  $\gamma$ -ray burst of 28 February 1997, *Nature* 387 (1997) 783–785.
- [18] F. Frontera, E. Costa, L. Piro, J.M. Muller, L. Amati, M. Feroci, F. Fiore, G. Pizzichini, M. Tavani, A. Castro-Tirado, G. Cusumano, D. dal Fiume, J. Heise, K. Hurley, L. Nicastro, M. Orlandini, A. Owens, E. Palazzi, A.N. Parmar, J. in't Zand, G. Zavattini, Spectral properties of the prompt X-ray emission and afterglow from the gamma-ray burst of 1997 February 28, *ApJ* 493 (1998) L67.

- [19] J. van Paradijs, P.J. Groot, T. Galama, C. Kouveliotou, R.G. Strom, J. Telting, R.G.M. Rutten, G.J. Fishman, C.A. Meegan, M. Pettini, N. Tanvir, J. Bloom, H. Pedersen, H.U. Nørregaard-Nielsen, M. Linden-Vørnle, J. Melnick, G. van der Steene, M. Bremer, R. Naber, J. Heise, J. in'tZand, E. Costa, M. Feroci, L. Piro, F. Frontera, G. Zavattini, L. Nicastro, E. Palazzi, K. Bennet, L. Hanlon, A. Parmar, Transient optical emission from the error box of the  $\gamma$ -ray burst of 28 February 1997, *Nature* 386 (1997) 686–689.
- [20] D.A. Frail, S.R. Kulkarni, L. Nicastro, M. Feroci, G.B. Taylor, The radio afterglow from the  $\gamma$ -ray burst of 8 May 1997, *Nature* 389 (1997) 261–263.
- [21] S.R. Kulkarni, D.A. Frail, M.H. Wieringa, R.D. Ekers, E.M. Sadler, R.M. Wark, J.L. Higdon, E.S. Phinney, J.S. Bloom, Radio emission from the unusual supernova 1998bw and its association with the  $\gamma$ -ray burst of 25 April 1998, *Nature* 395 (1998) 663–669.
- [22] J.S. Bloom, S.R. Kulkarni, S.G. Djorgovski, A.C. Eichelberger, P. Côté, J.P. Blakeslee, S.C. Odewahn, F.A. Harrison, D.A. Frail, A.V. Filippenko, D.C. Leonard, A.G. Riess, H. Spinrad, D. Stern, A. Bunker, A. Dey, B. Grossan, S. Perlmutter, R.A. Knop, I.M. Hook, M. Feroci, The unusual afterglow of the  $\gamma$ -ray burst of 26 March 1998 as evidence for a supernova connection, *Nature* 401 (1999) 453–456.
- [23] S.R. Kulkarni, S.G. Djorgovski, S.C. Odewahn, J.S. Bloom, R.R. Gal, C.D. Koresko, F.A. Harrison, L.M. Lubin, L. Armus, R. Sari, G.D. Illingworth, D.D. Kelson, D.K. Magee, P.G.V. Dokkum, D.A. Frail, J.S. Mulchaey, M.A. Malkan, I.S. McClean, H.I. Teplitz, D. Koerner, D. Kirkpatrick, N. Kobayashi, I.-A. Yadigaroglu, J. Halpern, T. Piran, R.W. Goodrich, F.H. Chaffee, M. Feroci, E. Costa, The afterglow redshift and extreme energetics of the  $\gamma$ -ray burst of 23 January 1999, *Nature* 398 (1999) 389–394.
- [24] J.E. Rhoads, The Dynamics and Light Curves of Beamed Gamma-Ray Burst Afterglows, *ApJ* 525 (1999) 737–749.
- [25] R. Sari, T. Piran, J.P. Halpern, Jets in gamma-ray bursts, *ApJ* 519 (1999) L17–L20.
- [26] D.A. Frail, S.R. Kulkarni, R. Sari, S.G. Djorgovski, J.S. Bloom, T.J. Galama, D.E. Reichart, E. Berger, F.A. Harrison, P.A. Price, S.A. Yost, A. Diercks, R.W. Goodrich, F. Chaffee, Beaming in gamma-ray bursts: Evidence for a standard energy reservoir, *ApJ* 562 (2001) L55–L58.
- [27] A. Panaiteescu, P. Kumar, Fundamental physical parameters of collimated gamma-ray burst afterglows, *ApJ* 560 (2001) L49–L53.
- [28] E. Berger, S.R. Kulkarni, D.A. Frail, A standard kinetic energy reservoir in gamma-ray burst afterglows, *ApJ* 590 (2003) 379–385.
- [29] P.A. Curran, A.J. van der Horst, R.A.M.J. Wijers, Are the missing X-ray breaks in gamma-ray burst afterglow light curves merely hidden? *MNRAS* 386 (2008) 859–863.
- [30] E.-W. Liang, J.L. Racusin, B. Zhang, B.-B. Zhang, D.N. Burrows, A Comprehensive Analysis of Swift XRT Data. III. Jet Break Candidates in X-Ray and Optical Afterglow Light Curves, *ApJ* 675 (2008) 528–552.
- [31] J.L. Racusin, E.W. Liang, D.N. Burrows, A. Falcone, T. Sakamoto, B.B. Zhang, B. Zhang, P. Evans, J. Osborne, Jet Breaks and Energetics of Swift Gamma-Ray Burst X-Ray Afterglows, *ApJ* 698 (2009) 43–74.
- [32] S.B. Cenko, D.A. Frail, F.A. Harrison, S.R. Kulkarni, E. Nakar, P.C. Chandra, N.R. Butler, D.B. Fox, A. Gal-Yam, M.M. Kasliwal, J. Kelemen, D.-S. Moon, E.O. Ofek, P.A. Price, A. Rau, A.M. Soderberg, H.I. Teplitz, M.W. Werner, D.C.-J. Bock, J.S. Bloom, D.A. Starr, A.V. Filippenko, R.A. Chevalier, N. Gehrels, J.N. Nousek, T. Piran, The collimation and energetics of the brightest swift gamma-ray bursts, *ApJ* 711 (2010) 641–654.
- [33] M.J. Rees, P. Mészáros, Relativistic fireballs - Energy conversion and time-scales, *MNRAS* 258 (1992) 41P–43P.
- [34] B. Paczyński, J.E. Rhoads, Radio transients from gamma-ray bursters, *ApJ* 418 (1993) L5.
- [35] P. Mészáros, M.J. Rees, Relativistic fireballs and their impact on external matter — Models for cosmological gamma-ray bursts, *ApJ* 405 (1993) 278–284.
- [36] P. Mészáros, M.J. Rees, Optical and Long-Wavelength Afterglow from Gamma-Ray Bursts, *ApJ* 476 (1997) 232.
- [37] A. Panaiteescu, P. Kumar, Properties of relativistic jets in gamma-ray burst afterglows, *ApJ* 571 (2002) 779–789.
- [38] S.E. Woosley, Gamma-ray bursts from stellar mass accretion disks around black holes, *ApJ* 405 (1993) 273–277.
- [39] B. Paczyński, Are gamma-ray bursts in star-forming regions? *ApJ* 494 (1998) L45.
- [40] A.I. Macfadyen, S.E. Woosley, Collapsars: Gamma-Ray Bursts and Explosions in "Failed Supernovae", *ApJ* 524 (1999) 262–289.
- [41] Z.G. Dai, T. Lu, Gamma-ray burst afterglows: effects of radiative corrections and non-uniformity of the surrounding medium, *MNRAS* 298 (1998) 87–92.
- [42] R.A. Chevalier, Z.-Y. Li, Gamma-Ray Burst Environments and Progenitors, *ApJ* 520 (1999) L29–L32.
- [43] R.A. Chevalier, Z.-Y. Li, Wind interaction models for gamma-ray burst afterglows: The case for two types of progenitors, *ApJ* 536 (2000) 195–212.
- [44] E. Ramirez-Ruiz, L.M. Dray, P. Madau, C.A. Tout, Winds from massive stars: implications for the afterglows of  $\gamma$ -ray bursts, *MNRAS* 327 (2001) 829–840.
- [45] B. Paczyński, Gamma-ray bursters at cosmological distances, *ApJ* 308 (1986) L43–L46.
- [46] J. Goodman, Are gamma-ray bursts optically thick?, *ApJ* 308 (1986) L47–L50.
- [47] E.E. Fenimore, C.D. Madras, S. Nayakshin, Expanding relativistic shells and gamma-ray burst temporal structure, *ApJ* 473 (1996) 998.
- [48] J. Goodman, Radio scintillation of gamma-ray-burst afterglows, *New Astron.* 2 (1997) 449–460.
- [49] G.B. Taylor, D.A. Frail, E. Berger, S.R. Kulkarni, The angular size and proper motion of the afterglow of GRB 030329, *ApJ* 609 (2004) L1–L4.
- [50] J.S. Bloom, S.R. Kulkarni, P.A. Price, D. Reichart, T.J. Galama, B.P. Schmidt, D.A. Frail, E. Berger, P.J. McCarthy, R.A. Chevalier, J.C. Wheeler, J.P. Halpern, D.W. Fox, S.G. Djorgovski, F.A. Harrison, R. Sari, T.S. Axelrod, R.A. Kimble, J. Holtzman, K. Hurley, F. Frontera, L. Piro, E. Costa, Detection of a supernova signature associated with GRB 011121, *ApJ* 572 (2002) L45–L49.
- [51] A.S. Fruchter, A.J. Levan, L. Strolger, P.M. Vreeswijk, S.E. Thorsett, D. Bersier, I. Burud, J.M. Castro Cerón, A.J. Castro-Tirado, C. Conselice, T. Dahmen, H.C. Ferguson, J.P.U. Fynbo, P.M. Garnavich, R.A. Gibbons, J. Gorosabel, T.R. Gull, J. Hjorth, S.T. Holland, C. Kouveliotou, Z. Levay, M. Livio, M.R. Metzger, P.E. Nugent, L. Petro, E. Pian, J.E. Rhoads, A.G. Riess, K.C. Sahu, A. Smette, N.R. Tanvir, R.A.M.J. Wijers, S.E. Woosley, Long  $\gamma$ -ray bursts and core-collapse supernovae have different environments, *Nature* 441 (2006) 463–468.
- [52] L. Christensen, J. Hjorth, J. Gorosabel, UV star-formation rates of GRB host galaxies, *A&A* 425 (2004) 913–926.
- [53] J.M. Castro Cerón, M.J. Michałowski, J. Hjorth, D. Watson, J.P.U. Fynbo, J. Gorosabel, Star formation rates and Stellar masses in  $z \sim 1$  gamma-ray burst hosts, *ApJ* 653 (2006) L85–L88.
- [54] E. Liang, B. Zhang, F. Virgili, Z.G. Dai, Low-Luminosity Gamma-Ray Bursts as a Unique Population: Luminosity Function, Local Rate, and Beaming Factor, *ApJ* 662 (2007) 1111–1118.
- [55] O. Bromberg, E. Nakar, T. Piran, Are low-luminosity gamma-ray bursts generated by relativistic jets? *ApJ* 739 (2011) L55.
- [56] T.J. Galama, P.M. Vreeswijk, J. Vanparadijs, C. Kouveliotou, T. Augusteijn, H. Böhnhardt, J.P. Brewer, V. Doublier, J.-F. Gonzalez, B. Leibundgut, C. Lidman, O.R. Hainaut, F. Patat, J. Heise, J. In'tzand, K. Hurley, P.J. Groot, R.G. Strom, P.A. Mazzali, K. Iwamoto, K. Nomoto, H. Umeda, T. Nakamura, T.R. Young, T. Suzuki, T. Shigeyama, T. Koshut, M. Kipp, C. Robinson, P. de Wildt, R.A.M.J. Wijers, N. Tanvir, J. Greiner, E. Pian, E. Palazzi, F. Frontera, N. Masetti, L. Nicastro, M. Feroci, E. Costa, L. Piro, B.A. Peterson, C. Tinney, B. Boyle, R. Cannon, R. Stathakis, E. Sadler, M.C. Begam, P. Ianna, An unusual supernova in the error box of the  $\gamma$ -ray burst of 25 April 1998, *Nature* 395 (1998) 670–672.
- [57] J. Hjorth, J. Sollerman, P. Møller, J.P.U. Fynbo, S.E. Woosley, C. Kouveliotou, N.R. Tanvir, J. Greiner, M.I. Andersen, A.J. Castro-Tirado, J.M. Castro Cerón, A.S. Fruchter, J. Gorosabel, P. Jakobsson, L. Kaper, S. Klose, N. Masetti, H. Pedersen, K. Pedersen, E. Pian, E. Palazzi, J.E. Rhoads, E. Rol, E.P.J. van den Heuvel, P.M. Vreeswijk, D. Watson, R.A.M.J. Wijers, A very energetic supernova associated with the  $\gamma$ -ray burst of 29 March 2003, *Nature* 423 (2003) 847–850.
- [58] K.Z. Stanek, T. Matheson, P.M. Garnavich, P. Martini, P. Berlind, N. Caldwell, P. Challis, W.R. Brown, R. Schild, K. Krisciunas, M.L. Calkins, J.C. Lee, N. Hathi, R.A. Jansen, R. Windhorst, L. Echevarria, D.J. Eisenstein, B. Pindor, E.W. Olszewski, P. Harding, S.T. Holland, D. Bersier, Spectroscopic discovery of the supernova 2003dh associated with GRB 030329, *ApJ* 591 (2003) L17–L20.
- [59] M. Modjaz, K.Z. Stanek, P.M. Garnavich, P. Berlind, S. Blondin, W. Brown, M. Calkins, P. Challis, A.M. Diamond-Stanic, H. Hao, M. Hicken, R.P. Kirshner, J.L. Prieto, Early-Time Photometry and Spectroscopy of the Fast Evolving SN 2006aj Associated with GRB 060218, *ApJ* 645 (2006) L21–L24.
- [60] S. Campana, V. Manganò, A.J. Blustin, P. Brown, D.N. Burrows, G. Chincarini, J.R. Cummings, G. Cusumano, M. Della Valle, D. Malesani, P. Mészáros, J.A. Nousek, M. Page, T. Sakamoto, E. Waxman, B. Zhang, Z.G. Dai, N. Gehrels, S. Immler, F.E. Marshall, K.O. Mason, A. Moretti, P.T. O'Brien, J.P. Osborne, K.L. Page, P. Romano, P.W.A. Roming, G. Tagliaferri, L.R. Cominsky, P. Giommi, O. Godet, J.A. Kennea, H. Krimm, L. Angelini, S.D. Barthelmy, P.T. Boyd, D.M. Palmer, A.A. Wells, N.E. White, The association of GRB 060218 with a supernova and the evolution of the shock wave, *Nature* 442 (2006) 1008–1010.

- [61] E. Pian, P.A. Mazzali, N. Masetti, P. Ferrero, S. Klose, E. Palazzi, E. Ramirez-Ruiz, S.E. Woosley, C. Kouveliotou, J. Deng, A.V. Filippenko, R.J. Foley, J.P.U. Fynbo, D.A. Kann, W. Li, J. Hjorth, K. Nomoto, F. Patat, D.N. Sauer, J. Sollerman, P.M. Vreeswijk, E.W. Guenther, A. Levan, P. O'Brien, N.R. Tanvir, R.A.M.J. Wijers, C. Dumas, O. Hautain, D.S. Wong, D. Baade, L. Wang, L. Amati, E. Cappellaro, A.J. Castro-Tirado, S. Ellison, F. Frontera, A.S. Fruchter, J. Greiner, K. Kawabata, C. Ledoux, K. Maeda, P. Møller, L. Nicastro, E. Rol, R. Starling, An optical supernova associated with the X-ray flash XRF 060218, *Nature* 442 (2006) 1011–1013.
- [62] R. Chornock, E. Berger, E.M. Levesque, A.M. Soderberg, R.J. Foley, D.B. Fox, A. Frebel, J.D. Simon, J.J. Bochanski, P.J. Challis, R.P. Kirshner, P. Podsiadlowski, K. Roth, R.E. Rutledge, B.P. Schmidt, S.S. Sheppard, R.A. Simcoe, Spectroscopic Discovery of the Broad-Lined Type Ic Supernova 2010bh Associated with the Low-Redshift GRB 100316D, 2010. ArXiv e-prints.
- [63] R.L.C. Starling, K. Wiersema, A.J. Levan, T. Sakamoto, D. Bersier, P. Goldoni, S.R. Oates, A. Rowlinson, S. Campana, J. Sollerman, N.R. Tanvir, D. Malesani, J.P.U. Fynbo, S. Covino, P. D'Avanzo, P.T. O'Brien, K.L. Page, J.P. Osborne, S.D. Vergani, S. Barthelmy, D.N. Burrows, Z. Cano, P.A. Curran, M. Depasquale, V. D'Elia, P.A. Evans, H. Flores, A.S. Fruchter, P. Garnavich, N. Gehrels, J. Gorosabel, J. Hjorth, S.T. Holland, A.J. van der Horst, C.P. Hurkett, P. Jakobsson, A.P. Kamble, C. Kouveliotou, N.P.M. Kuin, L. Kaper, P.A. Mazzali, P.E. Nugent, E. Pian, M. Stamatikos, C.C. Thöne, S.E. Woosley, Discovery of the nearby long, soft GRB 100316D with an associated supernova, *MNRAS* 411 (2011) 2792–2803.
- [64] M. Sparre, J. Sollerman, J.P.U. Fynbo, D. Malesani, P. Goldoni, A. Deugartepesto, S. Covino, V. D'Elia, H. Flores, F. Hammer, J. Hjorth, P. Jakobsson, L. Kaper, G. Leloudas, A.J. Levan, B. Milvang-Jensen, S. Schulze, G. Tagliaferri, N.R. Tanvir, D.J. Watson, K. Wiersema, R.A.M.J. Wijers, Spectroscopic evidence for SN 2010ma associated with GRB 101219B, *ApJ* 735 (2011) L24.
- [65] A. Melandri, E. Pian, P. Ferrero, V. D'Elia, E.S. Walker, G. Ghirlanda, S. Covino, L. Amati, P. D'Avanzo, P.A. Mazzali, M. Della Valle, C. Guidorzi, L.A. Antonelli, M.G. Bernardini, D. Bersier, F. Bufano, S. Campana, A.J. Castro-Tirado, G. Chincarini, J. Deng, A.V. Filippenko, D. Fugazza, G. Ghisellini, C. Kouveliotou, K. Maeda, G. Marconi, N. Masetti, K. Nomoto, E. Palazzi, F. Patat, S. Piranomonte, R. Salvaterra, I. Saviane, R.L.C. Starling, G. Tagliaferri, M. Tanaka, S.D. Vergani, The optical SN 2012bz associated with the long GRB 120422A, *A&A* 547 (2012) A82.
- [66] D. Malesani, G. Tagliaferri, G. Chincarini, S. Covino, M. Della Valle, D. Fugazza, P. A. Mazzali, F. M. Zerbi, P. D'Avanzo, S. Kalogerakos, A. Simoncelli, L.A. Antonelli, L. Burderi, S. Campana, A. Cucchiara, F. Fiore, G. Ghirlanda, P. Goldoni, D. Götz, S. Mereghetti, I.F. Mirabel, P. Romano, L. Stella, T. Minezaki, Y. Yoshii, K. Nomoto, SN 2003lv and GRB 031203: a bright supernova for a faint gamma-ray burst, *ApJ* 609 (2004) L5–L8.
- [67] D. Xu, A. de Ugarte Postigo, G. Leloudas, T. Kruhler, Z. Cano, J. Hjorth, D. Malesani, J.P.U. Fynbo, C.C. Thoenen, R. Sanchez-Ramirez, S. Schulze, P. Jakobsson, L. Kaper, J. Sollerman, D.J. Watson, A. Cabrera-Lavers, C. Cao, S. Covino, H. Flores, S. Geier, J. Gorosabel, S.M. Hu, B. Milvang-Jensen, M. Sparre, L.P. Xin, T.M. Zhang, W.K. Zheng, Y.C. Zou, Discovery of the broad-lined Type Ic SN 2013cq associated with the very energetic GRB 130427A, May 2013, ArXiv e-prints.
- [68] A.J. Levan, N.R. Tanvir, A.S. Fruchter, J. Hjorth, E. Pian, P. Mazzali, D.A. Perley, Z. Cano, J. Graham, R.A. Hounsell, S.B. Cenko, J.P.U. Fynbo, C. Kouveliotou, A. Pe'er, K. Misra, K. Wiersema, Hubble Space Telescope observations of the afterglow, supernova and host galaxy associated with the extremely bright GRB 130427A, *ApJ* 792 (2014) 115–120.
- [69] N. Gehrels, C.L. Sarazin, P.T. O'Brien, B. Zhang, L. Barbier, S.D. Barthelmy, A. Blustin, D.N. Burrows, J. Cannizzo, J.R. Cummings, M. Goad, S.T. Holland, C.P. Hurkett, J.A. Kennea, A. Levan, C.B. Markwardt, K.O. Mason, P. Mészáros, M. Page, D.M. Palmer, E. Rol, T. Sakamoto, R. Willingale, L. Angelini, A. Beardmore, P.T. Boyd, A. Breeveld, S. Campana, M.M. Chester, G. Chincarini, L.R. Cominsky, G. Cusumano, M. Depasquale, E.E. Fenimore, P. Giommi, C. Gronwall, D. Grupe, J.E. Hill, D. Hinshaw, J. Hjorth, D. Hullinger, K.C. Hurley, S. Klose, S. Kobayashi, C. Kouveliotou, H.A. Krimm, V. Mangano, F.E. Marshall, K. McGowan, A. Moretti, R.F. Mushotzky, K. Nakazawa, J.P. Norris, J.A. Nousek, J.P. Osborne, K. Page, A.M. Parsons, S. Patel, M. Perri, T. Poole, P. Romano, P.W.A. Roming, S. Rosen, G. Sato, P. Schady, A.P. Smale, J. Sollerman, R. Starling, M. Still, M. Suzuki, G. Tagliaferri, T. Takahashi, M. Tashiro, J. Tueller, A.A. Wells, N.E. White, R.A.M.J. Wijers, A short  $\gamma$ -ray burst apparently associated with an elliptical galaxy at redshift  $z = 0.225$ , *Nature* 437 (2005) 851–854.
- [70] D.B. Fox, D.A. Frail, P.A. Price, S.R. Kulkarni, E. Berger, T. Piran, A.M. Soderberg, S.B. Cenko, P.B. Cameron, A. Gal-Yam, M.M. Kasliwal, D.-S. Moon, F.A. Harrison, E. Nakar, B.P. Schmidt, B. Penprase, R.A. Chevalier, P. Kumar, K. Roth, D. Watson, B.L. Lee, S. Shectman, M.M. Phillips, M. Roth, P.J. McCarthy, M. Rauch, L. Cowie, B.A. Peterson, J. Rich, N. Kawai, K. Aoki, G. Kosugi, T. Totani, H.-S. Park, A. Macfadyen, K.C. Hurley, The afterglow of GRB 050709 and the nature of the short-hard  $\gamma$ -ray bursts, *Nature* 437 (2005) 845–850.
- [71] S.D. Barthelmy, G. Chincarini, D.N. Burrows, N. Gehrels, S. Covino, A. Moretti, P. Romano, P.T. O'Brien, C.L. Sarazin, C. Kouveliotou, M. Goad, S. Vaughan, G. Tagliaferri, B. Zhang, L.A. Antonelli, S. Campana, J.R. Cummings, P. D'Avanzo, M.B. Davies, P. Giommi, D. Grupe, Y. Kaneko, J.A. Kennea, A. King, S. Kobayashi, A. Melandri, P. Mészáros, J.A. Nousek, S. Patel, T. Sakamoto, R.A.M.J. Wijers, An origin for short  $\gamma$ -ray bursts unassociated with current star formation, *Nature* 438 (2005) 994–996.
- [72] E. Berger, S.R. Kulkarni, D.B. Fox, A.M. Soderberg, F.A. Harrison, E. Nakar, D.D. Kelson, M.D. Gladders, J.S. Mulchaey, A. Oemler, A. Dressler, S.B. Cenko, P.A. Price, B.P. Schmidt, D.A. Frail, N. Morrell, S. Gonzalez, W. Krzeminski, R. Sari, A. Gal-Yam, D.-S. Moon, B.E. Penprase, R. Jayawardhana, A. Scholz, J. Rich, B.A. Peterson, G. Anderson, R. Mcnaught, T. Minezaki, Y. Yoshii, L.L. Cowie, K. Pimbblet, Afterglows, redshifts, and properties of swift gamma-ray bursts, *ApJ* 634 (2005) 501–508.
- [73] A. Panaitescu, The energetics and environment of the short-GRB afterglows 050709 and 050724, *MNRAS* 367 (2006) L42–L46.
- [74] J.S. Bloom, J.X. Prochaska, D. Pooley, C.H. Blake, R.J. Foley, S. Jha, E. Ramirez-Ruiz, J. Granot, A.V. Filippenko, S. Sigurdsson, A.J. Barth, H.-W. Chen, M.C. Cooper, E.E. Falco, R.R. Gal, B.F. Gerke, M.D. Gladders, J.E. Greene, J. Hennanwi, L.C. Ho, K. Hurley, B.P. Koester, W. Li, L. Lubin, J. Newman, D.A. Perley, G.K. Squires, W.M. Wood-Vasey, Closing in on a short-hard burst progenitor: Constraints from early-time optical imaging and spectroscopy of a possible host galaxy of GRB 050509b, *ApJ* 638 (2006) 354–368.
- [75] D. Guetta, T. Piran, The BATSE-Swift luminosity and redshift distributions of short-duration GRBs, *A&A* 453 (2006) 823–828.
- [76] E. Nakar, Short-hard gamma-ray bursts, *Physics Reports* 442 (2007) 166–236.
- [77] D. Eichler, M. Livio, T. Piran, D.N. Schramm, Nucleosynthesis, neutrino bursts and gamma-rays from coalescing neutron stars, *Nature* 340 (1989) 126–128.
- [78] R. Narayan, B. Paczynski, T. Piran, Gamma-ray bursts as the death throes of massive binary stars, *ApJ* 395 (1992) L83–L86.
- [79] G. Tagliaferri, M. Goad, G. Chincarini, A. Moretti, S. Campana, D.N. Burrows, M. Perri, S.D. Barthelmy, N. Gehrels, H. Krimm, T. Sakamoto, P. Kumar, P.J. Mészáros, S. Kobayashi, B. Zhang, L. Angelini, P. Banat, A.P. Beardmore, M. Capalbi, S. Covino, G. Cusumano, P. Giommi, O. Godet, J.E. Hill, J.A. Kennea, V. Mangano, D.C. Morris, J.A. Nousek, P.T. O'Brien, J.P. Osborne, C. Pagani, K.L. Page, P. Romano, L. Stella, A. Wells, An unexpectedly rapid decline in the X-ray afterglow emission of long  $\gamma$ -ray bursts, *Nature* 436 (2005) 985–988.
- [80] G. Chincarini, A. Moretti, P. Romano, S. Covino, G. Tagliaferri, S. Campana, M. Goad, S. Kobayashi, B. Zhang, L. Angelini, P. Banat, S. Barthelmy, A.P. Beardmore, P.T. Boyd, A. Breeveld, D.N. Burrows, M. Capalbi, M.M. Chester, G. Cusumano, E.E. Fenimore, N. Gehrels, P. Giommi, J.E. Hill, D. Hinshaw, S.T. Holland, J.A. Kennea, H.A. Krimm, V. La Parola, V. Mangano, F.E. Marshall, K.O. Mason, J.A. Nousek, P.T. O'Brien, J.P. Osborne, M. Perri, P. Mészáros, P.W.A. Roming, T. Sakamoto, P. Schady, M. Still, A.A. Wells, Prompt and afterglow early X-ray phases in the comoving frame. Evidence for Universal properties? 2005 ArXiv Astrophysics e-prints.
- [81] J.A. Nousek, C. Kouveliotou, D. Grupe, K.L. Page, J. Granot, E. Ramirez-Ruiz, S.K. Patel, D.N. Burrows, V. Mangano, S. Barthelmy, A.P. Beardmore, S. Campana, M. Capalbi, G. Chincarini, G. Cusumano, A.D. Falcone, N. Gehrels, P. Giommi, M.R. Goad, O. Godet, C.P. Hurkett, J.A. Kennea, A. Moretti, P.T. O'Brien, J.P. Osborne, P. Romano, G. Tagliaferri, A.A. Wells, Evidence for a Canonical Gamma-Ray Burst Afterglow Light Curve in the Swift XRT Data, *ApJ* 642 (2006) 389–400.
- [82] B. Zhang, Y.Z. Fan, J. Dyks, S. Kobayashi, P. Mészáros, D.N. Burrows, J.A. Nousek, N. Gehrels, Physical processes shaping gamma-ray burst X-Ray Afterglow Light Curves: Theoretical implications from the swift X-Ray telescope observations, *ApJ* 642 (2006) 354–370.
- [83] D.N. Burrows, P. Romano, A. Falcone, S. Kobayashi, B. Zhang, A. Moretti, P.T. O'Brien, M.R. Goad, S. Campana, K.L. Page, L. Angelini, S. Barthelmy, A.P. Beardmore, M. Capalbi, G. Chincarini, J. Cummings, G. Cusumano, D. Fox, P. Giommi, J.E. Hill, J.A. Kennea, H. Krimm, V. Mangano, F. Marshall, P. Mészáros, D.C. Morris, J.A. Nousek, J.P. Osborne, C. Pagani, M. Perri, G. Tagliaferri, A.A. Wells, Bright X-ray flares in gamma-ray burst afterglows, *Science* 309 (2005) 1833–1835.

- [84] G. Chincarini, A. Moretti, P. Romano, A.D. Falcone, D. Morris, J. Racusin, S. Campana, S. Covino, C. Guidorzi, G. Tagliaferri, D.N. Burrows, C. Pagani, M. Stroh, D. Grupe, M. Capalbi, G. Cusumano, N. Gehrels, P. Giommi, V. La Parola, V. Mangano, T. Mineo, J.A. Nousek, P.T. O'Brien, K.L. Page, M. Perri, E. Troja, R. Willingale, B. Zhang, The first survey of X-ray flares from gamma-ray bursts observed by swift: Temporal properties and morphology, *ApJ* 671 (2007) 1903–1920.
- [85] G. Chincarini, J. Mao, R. Margutti, M.G. Bernardini, C. Guidorzi, F. Pasotti, D. Giannios, M. Della Valle, A. Moretti, P. Romano, P. D'Avanzo, G. Cusumano, P. Giommi, Unveiling the origin of X-ray flares in gamma-ray bursts, *MNRAS* 406 (2010) 2113–2148.
- [86] R. Margutti, G. Bernardini, R. Barniol Duran, C. Guidorzi, R.F. Shen, G. Chincarini, On the average gamma-ray burst X-ray flaring activity, *MNRAS* 410 (2011) 1064–1075.
- [87] E. Nakar, T. Piran, Temporal properties of short gamma-ray bursts, *MNRAS* 330 (2002) 920–926.
- [88] K. Ioka, S. Kobayashi, B. Zhang, Variabilities of Gamma-Ray Burst Afterglows: Long-acting Engine, Anisotropic Jet, or Many Fluctuating Regions?, *ApJ* 631 (2005) 429–434.
- [89] E. Nakar, J. Granot, Smooth light curves from a bumpy ride: relativistic blast wave encounters a density jump, *MNRAS* 380 (2007) 1744–1760.
- [90] J.I. Katz, T. Piran, Persistent Counterparts to Gamma-Ray Bursts, *ApJ* 490 (1997) 772.
- [91] K. Hurley, B.L. Dingus, R. Mukherjee, P. Sreekumar, C. Kouveliotou, C. Meegan, G.J. Fishman, D. Band, L. Ford, D. Bertsch, T. Cline, C. Fichtel, R. Hartman, S. Hunter, D.J. Thompson, G. Kanbach, H. Mayer-Hasselwander, C. von Montigny, M. Sommer, Y. Lin, P. Nolan, P. Michelson, D. Kniffen, J. Mattox, E. Schneid, M. Boer, M. Niel, Detection of a gamma-ray burst of very long duration and very high energy, *Nature* 372 (1994) 652.
- [92] Y.Z. Fan, D.M. Wei, Late internal-shock model for bright X-ray flares in gamma-ray burst afterglows and GRB 011121, *MNRAS* 364 (2005) L42–L46.
- [93] D. Lazzati, R. Perna, X-ray flares and the duration of engine activity in gamma-ray bursts, *MNRAS* 375 (2007) L46–L50.
- [94] Y. Fan, T. Piran, Gamma-ray burst efficiency and possible physical processes shaping the early afterglow, *MNRAS* 369 (2006) 197–206.
- [95] A. Panaitescu, P. Mészáros, D. Burrows, J. Nousek, N. Gehrels, P. O'Brien, R. Willingale, Evidence for chromatic X-ray light-curve breaks in Swift gamma-ray burst afterglows and their theoretical implications, *MNRAS* 369 (2006) 2059–2064.
- [96] E.-W. Liang, B.-B. Zhang, B. Zhang, A Comprehensive Analysis of Swift XRT Data. II. Diverse Physical Origins of the Shallow Decay Segment, *ApJ* 670 (2007) 565–583.
- [97] G. Sato, R. Yamazaki, K. Ioka, T. Sakamoto, T. Takahashi, K. Nakazawa, T. Nakamura, K. Toma, D. Hullinger, M. Tashiro, A.M. Parsons, H.A. Krimm, S.D. Barthelmy, N. Gehrels, D.N. Burrows, P.T. O'Brien, J.P. Osborne, G. Chincarini, D.Q. Lamb, Swift discovery of gamma-ray bursts without a jet break feature in their X-Ray afterglows, *ApJ* 657 (2007) 359–366.
- [98] M.J. Rees, P. Mészáros, Unsteady outflow models for cosmological gamma-ray bursts, *ApJ* 430 (1994) L93–L96.
- [99] A.A. Abdo, M. Ackermann, M. Arimoto, K. Asano, W.B. Atwood, M. Axelsson, L. Baldini, J. Ballet, D.L. Band, G. Barbiellini, et al., Fermi observations of high-energy gamma-ray emission from GRB 080916C, *Science* 323 (2009) 1688.
- [100] A.A. Abdo, M. Ackermann, M. Ajello, M. Asano, W.B. Atwood, M. Axelsson, L. Baldini, J. Ballet, G. Barbiellini, M.G. Baring, et al., A limit on the variation of the speed of light arising from quantum gravity effects, *Nature* 462 (2009) 331–334.
- [101] M. Ackermann, K. Asano, W.B. Atwood, M. Axelsson, L. Baldini, J. Ballet, G. Barbiellini, M.G. Baring, D. Bastieri, K. Bechtol, et al., Fermi observations of GRB 090510: A short-hard gamma-ray burst with an additional, hard power-law component from 10 keV TO GeV energies, *ApJ* 716 (2010) 1178–1190.
- [102] M. Ackermann, M. Ajello, K. Asano, M. Axelsson, L. Baldini, J. Ballet, G. Barbiellini, M.G. Baring, D. Bastieri, K. Bechtol, et al., Detection of a spectral break in the extra hard component of GRB 090926A, *ApJ* 729 (2011) 114.
- [103] B.-B. Zhang, B. Zhang, E.-W. Liang, Y.-Z. Fan, X.-F. Wu, A. Pe'er, A. Maxham, H. Gao, Y.-M. Dong, A Comprehensive analysis of fermi gamma-ray burst data. I. Spectral components and the possible physical origins of LAT/GBM GRBs, *ApJ* 730 (2011) 141.
- [104] P. Kumar, R. Barniol Duran, On the generation of high-energy photons detected by the Fermi Satellite from gamma-ray bursts, *MNRAS* 400 (2009) L75–L79.
- [105] G. Ghisellini, G. Ghirlanda, L. Nava, A. Celotti, GeV emission from gamma-ray bursts: a radiative fireball? *MNRAS* 403 (2010) 926–937.
- [106] C.D. Dermer, K.E. Mitman, Short-timescale variability in the external shock model of gamma-ray bursts, *ApJ* 513 (1999) L5–L8.
- [107] M. Lyutikov, R. Blandford, Gamma ray bursts as electromagnetic outflows, Dec. 2003, ArXiv Astrophysics e-prints.
- [108] B. Zhang, H. Yan, The internal-collision-induced magnetic reconnection and turbulence (ICMART) model of gamma-ray bursts, *ApJ* 726 (2011) 90.
- [109] C. Thompson, A model of Gamma-Ray bursts, *MNRAS* 270 (1994) 480.
- [110] G. Ghisellini, A. Celotti, Quasi-thermal comptonization and Gamma-Ray bursts, *ApJ* 511 (1999) L93–L96.
- [111] P. Mészáros, M.J. Rees, Steep Slopes and Preferred Breaks in Gamma-Ray Burst Spectra: The Role of Photospheres and Comptonization, *ApJ* 530 (2000) 292–298.
- [112] A. Pe'er, P. Mészáros, M.J. Rees, The observable effects of a photospheric component on GRB and XRF prompt emission spectrum, *ApJ* 642 (2006) 995–1003.
- [113] A. Pe'er, Temporal evolution of thermal emission from relativistically expanding plasma, *ApJ* 682 (2008) 463–473.
- [114] D. Giannios, H.C. Spruit, Spectral and timing properties of a dissipative  $\gamma$ -ray burst photosphere, *A&A* 469 (2007) 1–9.
- [115] K. Ioka, K. Murase, K. Toma, S. Nagataki, T. Nakamura, Unstable GRB Photospheres and  $e^+e^-$  Annihilation Lines, *ApJ* 670 (2007) L77–L80.
- [116] K. Asano, T. Terasawa, Slow heating model of gamma-ray burst: photon spectrum and delayed emission, *ApJ* 705 (2009) 1714–1720.
- [117] D. Lazzati, M.C. Begelman, Non-thermal emission from the photospheres of gamma-ray burst outflows. I. high-frequency tails, *ApJ* 725 (2010) 1137–1145.
- [118] A.M. Beloborodov, Collisional mechanism for gamma-ray burst emission, *MNRAS* 407 (2010) 1033–1047.
- [119] K. Toma, X.-F. Wu, P. Mészáros, Photosphere-internal shock model of gamma-ray bursts: case studies of Fermi/LAT bursts, *MNRAS* 415 (2011) 1663–1680.
- [120] A. Mizuta, S. Nagataki, J. Aoi, Thermal radiation from gamma-ray burst jets, *ApJ* 732 (2011) 26.
- [121] H. Nagakura, H. Ito, K. Kiuchi, S. Yamada, Jet propagations breakouts and photospheric emissions in collapsing massive progenitors of long-duration gamma-ray bursts, *ApJ* 731 (2011) 80.
- [122] A. Cucchiara, A.J. Levan, D.B. Fox, N.R. Tanvir, T.N. Ukwatta, E. Berger, T. Krühler, A. Küpcü Yoldaş, X.F. Wu, K. Toma, J. Greiner, F.E. Olivares, A. Rowlinson, L. Amati, T. Sakamoto, K. Roth, A. Stephens, A. Fritz, J.P.U. Fynbo, J. Hjorth, D. Malesani, P. Jakobsson, K. Wiersema, P.T. O'Brien, A.M. Soderberg, R.J. Foley, A.S. Fruchter, J. Rhoads, R.E. Rutledge, B.P. Schmidt, M.A. Dopita, P. Podsiadlowski, R. Willingale, C. Wolf, S.R. Kulkarni, P. D'Avanzo, A Photometric Redshift of  $z \sim 9.4$  for GRB 090429B, *ApJ* 736 (2011) 7.
- [123] G.B. Rybicki, A.P. Lightman, Radiative Processes in Astrophysics, Wiley-Interscience, New York, 1979, p. 393.
- [124] M.S. Longair, High Energy Astrophysics, Cambridge University Press, 2010.
- [125] J.H. Krolik, Active galactic nuclei : from the central black hole to the galactic environment, Princeton University Press, 1999.
- [126] C.D. Dermer, G. Menon, High Energy Radiation from Black Holes: Gamma Rays, Cosmic Rays, and Neutrinos, Princeton University Press, 2009.
- [127] R.M. Kulsrud, Plasma physics for astrophysics, Princeton University Press, 2005.
- [128] E.E. Fenimore, J.J.M. in 't Zand, J.P. Norris, J.T. Bonnell, R.J. Nemiroff, Gamma-ray burst peak duration as a function of energy, *ApJ* 448 (1995) L101.
- [129] P. Kumar, A. Panaitescu, Afterglow emission from naked gamma-ray bursts, *ApJ* 541 (2000) L51–L54.
- [130] Z.L. Uhm, B. Zhang, Fast-cooling synchrotron radiation in a decaying magnetic field and  $\gamma$ -ray burst emission mechanism, *Nat. Phys.* 10 (2014) 351–356.
- [131] R. Sari, T. Piran, R. Narayan, Spectra and light curves of gamma-ray burst afterglows, *ApJ* 497 (1998) L17.
- [132] P. Kumar, R.A. Hernández, Ž Bošnjak, R.B. Duran, Maximum synchrotron frequency for shock-accelerated particles, *MNRAS* 427 (2012) L40–L44.
- [133] J.P. Rachen, P. Mészáros, Photohadronic neutrinos from transients in astrophysical sources, *Phys. Rev. D* 58 (12) (1998) 123005.
- [134] R.D. Blandford, C.F. McKee, Fluid dynamics of relativistic blast waves, *Phys. Fluids* 19 (1976) 1130–1138.
- [135] L. Rezzolla, O. Zanotti, Relativistic Hydrodynamics, Oxford University Press, ISBN-10:0198528906, 2013.

- [136] P. Mészáros, M.J. Rees, R.A.M.J. Wijers, Viewing Angle and Environment Effects in Gamma-Ray Bursts: Sources of Afterglow Diversity, *ApJ* 499 (1998) 301.
- [137] E. Cohen, T. Piran, Radiative efficiencies of continuously powered blast waves, *ApJ* 518 (1999) 346–355.
- [138] V.V. Usov, Millisecond pulsars with extremely strong magnetic fields as a cosmological source of gamma-ray bursts, *Nature* 357 (1992) 472–474.
- [139] Z.G. Dai, T. Lu, Gamma-ray burst afterglows and evolution of postburst fireballs with energy injection from strongly magnetic millisecond pulsars, *A&A* 333 (1998) L87–L90.
- [140] B. Zhang, P. Mészáros, Gamma-ray burst afterglow with continuous energy injection: Signature of a highly magnetized millisecond pulsar, *ApJ* 552 (2001) L35–L38.
- [141] M.J. Rees, P. Mészáros, Refreshed shocks and afterglow longevity in gamma-ray bursts, *ApJ* 496 (1998) L1.
- [142] J. Granot, R. Sari, The shape of spectral breaks in Gamma-Ray burst afterglows, *ApJ* 568 (2002) 820–829.
- [143] H. Gao, W.-H. Lei, Y.-C. Zou, X.-F. Wu, B. Zhang, A complete reference of the analytical synchrotron external shock models of gamma-ray bursts, *New Astron. Rev.* 57 (2013) 141–190.
- [144] S.A. Yost, F.A. Harrison, R. Sari, D.A. Frail, A study of the afterglows of four gamma-ray bursts: constraining the explosion and fireball model, *ApJ* 597 (2003) 459–473.
- [145] P. Kumar, The distribution of burst energy and shock parameters for GRBs, *ApJ* 538 (2000) L125–L128.
- [146] D.L. Freedman, E. Waxman, On the energy of gamma-ray bursts, *ApJ* 547 (2001) 922–928.
- [147] P. Meszaros, M.J. Rees, Gamma-Ray Bursts: Multiwaveband Spectral Predictions for Blast Wave Models, *ApJ* 418 (1993) L59.
- [148] R. Sari, T. Piran, Predictions for the very early afterglow and the optical flash, *ApJ* 520 (1999) 641–649.
- [149] C. Akerlof, R. Balsano, S. Barthelmy, J. Bloch, P. Butterworth, D. Caspersion, T. Cline, S. Fletcher, F. Frontera, G. Gisler, J. Heise, J. Hills, R. Kehoe, B. Lee, S. Marshall, T. McKay, R. Miller, L. Piro, W. Priedhorsky, J. Szymanski, J. Wren, Observation of contemporaneous optical radiation from a  $\gamma$ -ray burst, *Nature* 398 (1999) 400–402.
- [150] R. Sari, T. Piran, GRB 990123: The optical flash and the fireball model, *ApJ* 517 (1999) L109–L112.
- [151] P. Mészáros, M.J. Rees, GRB 990123: reverse and internal shock flashes and late afterglow behaviour, *MNRAS* 306 (1999) L39–L43.
- [152] R. Sari, T. Piran, Hydrodynamic timescales and temporal structure of gamma-ray bursts, *ApJ* 455 (1995) L143.
- [153] R. Sari, P. Mészáros, Impulsive and varying injection in gamma-ray burst afterglows, *ApJ* 535 (2000) L33–L37.
- [154] Z.L. Uhm, A.M. Beloborodov, On the mechanism of gamma-ray burst afterglows, *ApJ* 665 (2007) L93–L96.
- [155] F. Genet, F. Daigne, R. Mochkovitch, Can the early X-ray afterglow of gamma-ray bursts be explained by a contribution from the reverse shock?, *MNRAS* 381 (2007) 732–740.
- [156] Z.L. Uhm, B. Zhang, R. Hascoët, F. Daigne, R. Mochkovitch, I.H. Park, Dynamics and afterglow light curves of gamma-ray burst blast waves with a long-lived reverse shock, *ApJ* 761 (2012) 147.
- [157] Z.L. Uhm, B. Zhang, Dynamics and afterglow light curves of gamma-ray burst blast waves encountering a density bump or void, *ApJ* 789 (2014) 39.
- [158] S. Kobayashi, Light Curves of Gamma-Ray Burst Optical Flashes, *ApJ* 545 (2000) 807–812.
- [159] S. Kobayashi, B. Zhang, GRB 021004: Reverse Shock Emission, *ApJ* 582 (2003) L75–L78.
- [160] B. Zhang, S. Kobayashi, P. Mészáros, Gamma-ray burst early optical afterglows: Implications for the initial lorentz factor and the central engine, *ApJ* 595 (2003) 950–954.
- [161] P. Kumar, A. Panaitescu, A unified treatment of the gamma-ray burst 021211 and its afterglow, *MNRAS* 346 (2003) 905–914.
- [162] X.F. Wu, Z.G. Dai, Y.F. Huang, T. Lu, Optical flashes and very early afterglows in wind environments, *MNRAS* 342 (2003) 1131–1138.
- [163] S. Kobayashi, B. Zhang, Early Optical Afterglows from Wind-Type Gamma-Ray Bursts, *ApJ* 597 (2003) 455–458.
- [164] B. Zhang, S. Kobayashi, Gamma-Ray burst early afterglows: reverse shock emission from an arbitrarily magnetized ejecta, *ApJ* 628 (2005) 315–334.
- [165] P. Mimica, D. Giannios, M.A. Aloy, Deceleration of arbitrarily magnetized GRB ejecta: the complete evolution, *A&A* 494 (2009) 879–890.
- [166] R. Narayan, P. Kumar, A. Tchekhovskoy, Constraints on cold magnetized shocks in gamma-ray bursts, *MNRAS* 416 (2011) 2193–2201.
- [167] Y.Z. Fan, D.M. Wei, B. Zhang,  $\gamma$ -ray burst internal shocks with magnetization, *MNRAS* 354 (2004) 1031–1039.
- [168] C.F. Kennel, F.V. Coroniti, Confinement of the Crab pulsar's wind by its supernova remnant, *ApJ* 283 (1984) 694–709.
- [169] C.F. Kennel, F.V. Coroniti, Magnetohydrodynamic model of Crab nebula radiation, *ApJ* 283 (1984) 710–730.
- [170] E. Nakar, T. Piran, Early afterglow emission from a reverse shock as a diagnostic tool for gamma-ray burst outflows, *MNRAS* 353 (2004) 647–653.
- [171] E. McMahon, P. Kumar, T. Piran, Reverse shock emission as a probe of gamma-ray burst ejecta, *MNRAS* 366 (2006) 575–585.
- [172] Z.P. Jin, Y.Z. Fan, GRB 060418 and 060607A: the medium surrounding the progenitor and the weak reverse shock emission, *MNRAS* 378 (2007) 1043–1048.
- [173] L. Shao, Z.G. Dai, A reverse-shock model for the early afterglow of GRB 050525A, *ApJ* 633 (2005) 1027–1030.
- [174] D.W. Fox, P.A. Price, A.M. Soderberg, E. Berger, S.R. Kulkarni, R. Sari, D.A. Frail, F.A. Harrison, S.A. Yost, K. Matthews, B.A. Peterson, I. Tanaka, J. Christiansen, G.H. Moriarty-Schieven, Discovery of early optical emission from GRB 021211, *ApJ* 586 (2003) L5–L8.
- [175] W. Li, A.V. Filippenko, R. Chornock, S. Jha, The Early Light Curve of the Optical Afterglow of GRB 021211, *ApJ* 586 (2003) L9–L12.
- [176] A. Gomboc, S. Kobayashi, C. Guidorzi, M. Melandri, V. Mangano, B. Sbarufatti, C.G. Mundell, P. Schady, R.J. Smith, A.C. Updike, D.A. Kann, K. Misra, E. Rol, A. Pozanenko, A.J. Castro-Tirado, G.C. Anupama, D. Bersier, M.F. Bode, D. Carter, P. Curran, A. Fruchter, J. Graham, D.H. Hartmann, M. Ibrahimov, A. Levan, A. Monfardini, C.J. Mottram, P.T. O'Brien, P. Prema, D.K. Sahu, I.A. Steele, N.R. Tanvir, K. Wiersema, Multiwavelength analysis of the intriguing GRB 061126: The reverse shock scenario and magnetization, *ApJ* 687 (2008) 443–455.
- [177] E. Molinari, S.D. Vergani, D. Malesani, S. Covino, P. D'Avanzo, G. Chincarini, F.M. Zerbi, L.A. Antonelli, P. Conconi, V. Testa, G. Tosti, F. Vitali, F. D'Alessio, G. Malaspina, L. Nicastro, E. Palazzi, D. Guetta, S. Campana, P. Goldoni, N. Masetti, E.J.A. Meurs, A. Monfardini, L. Norci, E. Pian, S. Piranomonte, D. Rizzuto, M. Stefanon, L. Stella, G. Tagliaferri, P.A. Ward, G. Ihle, L. Gonzalez, A. Pizarro, P. Sinclair, J. Valenzuela, REM observations of GRB 060418 and GRB 060607A: the onset of the afterglow and the initial fireball Lorentz factor determination, *A&A* 469 (2007) L13–L16.
- [178] E.S. Rykoff, F. Aharonian, C.W. Akerlof, M.C.B. Ashley, S.D. Barthelmy, H.A. Flewelling, N. Gehrels, E. Göğüş, T. Güver, Ü. Kiziloğlu, H.A. Krimm, T.A. McKay, M. Öznel, A. Phillips, R.M. Quimby, G. Rowell, W. Rujopakarn, B.E. Schaefer, D.A. Smith, W.T. Vestrand, J.C. Wheeler, J. Wren, F. Yuan, S.A. Yost, Looking Into the Fireball: ROTSE-III and Swift Observations of Early Gamma-ray Burst Afterglows, *ApJ* 702 (2009) 489–505.
- [179] E.-W. Liang, S.-X. Yi, J. Zhang, H.-J. Lü, B.-B. Zhang, B. Zhang, Constraining Gamma-ray Burst Initial Lorentz Factor with the Afterglow Onset Feature and Discovery of a Tight  $\Gamma_0$ – $E_{\gamma, \text{iso}}$  Correlation, *ApJ* 725 (2010) 2209–2224.
- [180] J.E. Rhoads, How to Tell a Jet from a Balloon: A Proposed Test for Beaming in Gamma-Ray Bursts, *ApJ* 487 (1997) L1.
- [181] A. Panaitescu, P. Mészáros, Dynamical evolution, light curves, and spectra of spherical and collimated gamma-ray burst remnants, *ApJ* 526 (1999) 707–715.
- [182] P. Kumar, A. Panaitescu, Steepening of afterglow decay for jets interacting with stratified media, *ApJ* 541 (2000) L9–L12.
- [183] T. Piran, Gamma-ray bursts – a puzzle being resolved, *Physics Reports* 333 (2000) 529–553.
- [184] J. Granot, T. Piran, On the lateral expansion of gamma-ray burst jets, *MNRAS* 421 (2012) 570–587.
- [185] F. de Colle, E. Ramirez-Ruiz, J. Granot, D. Lopez-Camara, Simulations of gamma-ray burst jets in a stratified external medium: dynamics, afterglow light curves, jet breaks, and radio calorimetry, *ApJ* 751 (2012) 57.
- [186] P. Kumar, J. Granot, The Evolution of a Structured Relativistic Jet and Gamma-Ray Burst Afterglow Light Curves, *ApJ* 591 (2003) 1075–1085.
- [187] J. Granot, M. Miller, T. Piran, W.M. Stuen, P.A. Hughes, 2001, Light curves from an expanding relativistic jet. In: E. Costa, F. Frontera, J. Hjorth, (Eds.), *Gamma-ray Bursts in the Afterglow Era*, p. 312.
- [188] J.K. Cannizzo, N. Gehrels, E.T. Vishniac, A numerical gamma-ray burst simulation using three-dimensional relativistic hydrodynamics: the transition from spherical to jetlike expansion, *ApJ* 601 (2004) 380–390.
- [189] W. Zhang, A. MacFadyen, The dynamics and afterglow radiation of gamma-ray bursts. I. constant density medium, *ApJ* 698 (2009) 1261–1272.
- [190] H.J. van Eerten, A.I. MacFadyen, Gamma-ray burst afterglow scaling relations for the full blast wave evolution, *ApJ* 747 (2012) L30.

- [191] H. van Eerten, A. van der Horst, A. MacFadyen, Gamma-ray burst broadband fitting based directly on hydrodynamics simulations, *ApJ* 749 (2012) 44.
- [192] B.-B. Zhang, H. van Eerten, D.N. Burrows, et al. *ApJ* (2014), submitted for publication ([arXiv:1405.4867](#)).
- [193] G. Ryan, H. van Eerten, A. MacFadyen, B.-B. Zhang, *ApJ*, submitted for publication ([arXiv:1405.5516](#)).
- [194] E. Rossi, D. Lazzati, M.J. Rees, Afterglow light curves, viewing angle and the jet structure of  $\gamma$ -ray bursts, *MNRAS* 332 (2002) 945–950.
- [195] B. Zhang, P. Mészáros, Gamma-Ray burst beaming: a universal configuration with a standard energy reservoir? *ApJ* 571 (2002) 876–879.
- [196] B. Zhang, X. Dai, N.M. Lloyd-Ronning, P. Mészáros, Quasi-universal Gaussian Jets: A unified picture for gamma-ray bursts and x-ray flashes, *ApJ* 601 (2004) L119–L122.
- [197] Z.G. Dai, L.J. Gou, Gamma-ray burst afterglows from anisotropic jets, *ApJ* 552 (2001) 72–80.
- [198] A. Panaiteescu, Jets, structured outflows and energy injection in gamma-ray burst afterglows: numerical modelling, *MNRAS* 363 (2005) 1409–1423.
- [199] J. Granot, P. Kumar, Constraining the structure of gamma-ray burst jets through the afterglow light curves, *ApJ* 591 (2003) 1086–1096.
- [200] J.S. Bloom, D.A. Frail, S.R. Kulkarni, Gamma-ray burst energetics and the gamma-ray burst hubble diagram: promises and limitations, *ApJ* 594 (2003) 674–683.
- [201] R. Perna, R. Sari, D. Frail, Jets in Gamma-Ray Bursts: Tests and Predictions for the Structured Jet Model, *ApJ* 594 (2003) 379–384.
- [202] E. Nakar, J. Granot, D. Guetta, Testing the predictions of the universal structured Gamma-Ray burst jet model, *ApJ* 606 (2004) L37–L40.
- [203] N.M. Lloyd-Ronning, X. Dai, B. Zhang, On the Structure of Quasi-universal Jets for Gamma-Ray Bursts, *ApJ* 601 (2004) 371–379.
- [204] X. Dai, B. Zhang, A global test of a quasi-universal gamma-ray burst jet model through monte carlo simulations, *ApJ* 621 (2005) 875–883.
- [205] Y.F. Huang, X.F. Wu, Z.G. Dai, H.T. Ma, T. Lu, Rebrightening of XRF 030723: Further Evidence for a Two-Component Jet in a Gamma-Ray Burst, *ApJ* 605 (2004) 300–306.
- [206] F. Peng, A. Königl, J. Granot, Two-component jet models of gamma-ray burst sources, *ApJ* 626 (2005) 966–977.
- [207] X.F. Wu, Z.G. Dai, Y.F. Huang, T. Lu, Gamma-ray bursts: polarization of afterglows from two-component jets, *MNRAS* 357 (2005) 1197–1204.
- [208] E. Berger, S.R. Kulkarni, G. Pooley, D.A. Frail, V. McIntyre, R.M. Wark, R. Sari, A.M. Soderberg, D.W. Fox, S. Yost, P.A. Price, A common origin for cosmic explosions inferred from calorimetry of GRB030329, *Nature* 426 (2003) 154–157.
- [209] J.L. Racusin, S.V. Karpov, M. Sokolowski, J. Granot, X.F. Wu, V. Pal'Shin, S. Covino, A.J. van der Horst, S.R. Oates, P. Schady, R.J. Smith, J. Cummings, R.L.C. Starling, L.W. Piotrowski, B. Zhang, P.A. Evans, S.T. Holland, K. Malek, M.T. Page, L. Vetere, R. Margutti, C. Guidorzi, A.P. Kamble, P.A. Curran, A. Beardmore, C. Kouveliotou, L. Mankiewicz, A. Melandri, P.T. O'Brien, K.L. Page, T. Piran, N.R. Tanvir, G. Wrochna, R.L. Aptekar, S. Barthelmy, C. Bartolini, G.M. Beskin, S. Bondar, M. Bremer, S. Campana, A. Castro-Tirado, A. Cucchiara, M. Ciwoł, P. D'Avanzo, V. D'Elia, M.D. Valle, A. Deugarpestigo, W. Dominik, A. Falcone, F. Fiore, D.B. Fox, D.D. Frederiks, A.S. Fruchter, D. Fugazza, M.A. Garrett, N. Gehrels, S. Golenetskii, A. Gomboc, J. Gorosabel, G. Greco, A. Guarneri, S. Immler, M. Jelinek, G. Kasprzowicz, V. Laparola, A.J. Levan, V. Manganò, E.P. Mazets, E. Molinari, A. Moretti, K. Nawrocki, P.P. Oleynik, J.P. Osborne, C. Pagani, S.B. Pandey, Z. Paragi, M. Perri, A. Piccioni, E. Ramirez-Ruiz, P.W.A. Roming, I.A. Steele, R.G. Strom, V. Testa, G. Tosti, M.V. Ulánov, K. Wiersma, R.A.M.J. Wijers, J.M. Winters, A.F. Zarnecki, F. Zerbini, P. Mészáros, G. Chincarini, D.N. Burrows, Broadband observations of the naked-eye  $\gamma$ -ray burst GRB080319B, *Nature* 455 (2008) 183–188.
- [210] E. Ramirez-Ruiz, A. Celotti, M.J. Rees, Events in the life of a cocoon surrounding a light, collapsar jet, *MNRAS* 337 (2002) 1349–1356.
- [211] W. Zhang, S.E. Woosley, A. Heger, The propagation and eruption of relativistic jets from the stellar progenitors of gamma-ray bursts, *ApJ* 608 (2004) 365–377.
- [212] P. Kumar, T. Piran, Energetics and luminosity function of gamma-ray bursts, *ApJ* 535 (2000) 152–157.
- [213] R. Yamazaki, K. Ioka, T. Nakamura, Peak energy-isotropic energy relation in the off-axis gamma-ray burst model, *ApJ* 606 (2004) L33–L36.
- [214] R. Narayan, P. Kumar, A turbulent model of gamma-ray burst variability, *MNRAS* 394 (2009) L117–L120.
- [215] P. Kumar, R. Narayan, GRB 080319B: evidence for relativistic turbulence, not internal shocks, *MNRAS* 395 (2009) 472–489.
- [216] A. Lazar, E. Nakar, T. Piran, Gamma-Ray Burst light curves in the relativistic turbulence and relativistic subjet models, *ApJ* 695 (2009) L10–L14.
- [217] B. Zhang, B. Zhang, Gamma-Ray burst prompt emission light curves and power density spectra in the IC-MART model, *ApJ* 782 (2014) 92.
- [218] J. Granot, A. Panaiteescu, P. Kumar, S.E. Woosley, Off-Axis afterglow emission from jetted gamma-ray bursts, *ApJ* 570 (2002) L61–L64.
- [219] Y.F. Huang, Z.G. Dai, T. Lu, Failed gamma-ray bursts and orphan afterglows, *MNRAS* 332 (2002) 735–740.
- [220] T. Totani, A. Panaiteescu, Orphan afterglows of collimated gamma-ray bursts: Rate predictions and prospects for detection, *ApJ* 576 (2002) 120–134.
- [221] A. Levinson, E.O. Ofek, E. Waxman, A. Gal-Yam, Orphan gamma-ray burst radio afterglows: Candidates and constraints on beaming, *ApJ* 576 (2002) 923–931.
- [222] E. Nakar, T. Piran, J. Granot, The detectability of orphan afterglows, *ApJ* 579 (2002) 699–705.
- [223] Y.C. Zou, X.F. Wu, Z.G. Dai, Estimation of the detectability of optical orphan afterglows, *A&A* 461 (2007) 115–119.
- [224] S.B. Cenko, S.R. Kulkarni, A. Horesh, A. Corsi, D.B. Fox, J. Carpenter, D.A. Frail, P.E. Nugent, D.A. Perley, D. Gruber, A. Gal-Yam, P.J. Groot, G. Hallinan, E.O. Ofek, A. Rau, C.L. Macleod, A.A. Miller, J.S. Bloom, A.V. Filippenko, M.M. Kasliwal, N.M. Law, A.N. Morgan, D. Polishook, D. Poznanski, R.M. Quimby, B. Sesar, K.J. Shen, J.M. Silverman, A. Sternberg, Discovery of a cosmological, relativistic outburst via its rapidly fading optical emission, *ApJ* 769 (2013) 130.
- [225] C.D. Dermer, J. Chiang, M. Böttcher, Fireball loading and the blast-wave model of gamma-ray bursts, *ApJ* 513 (1999) 656–668.
- [226] Y.F. Huang, Z.G. Dai, T. Lu, A generic dynamical model of gamma-ray burst remnants, *MNRAS* 309 (1999) 513–516.
- [227] M. Böttcher, C.D. Dermer, Early gamma-ray burst afterglows from relativistic blast waves in general radiative regimes, *ApJ* 532 (2000) 281–285.
- [228] L. Nava, L. Sironi, G. Ghisellini, A. Celotti, G. Ghirlanda, Afterglow emission in gamma-ray bursts - I. Pair-enriched ambient medium and radiative blast waves, *MNRAS* 433 (2013) 2107–2121.
- [229] C.D. Dermer, Curvature effects in gamma-ray burst colliding shells, *ApJ* 614 (2004) 284–292.
- [230] E.W. Liang, B. Zhang, P.T. O'Brien, R. Willingale, L. Angelini, D.N. Burrows, S. Campana, G. Chincarini, A. Falcone, N. Gehrels, M.R. Goad, D. Grupe, S. Kobayashi, P. Mészáros, J.A. Nousek, J.P. Osborne, K.L. Page, G. Tagliaferri, Testing the Curvature Effect and Internal Origin of Gamma-Ray Burst Prompt Emissions and X-Ray Flares with Swift Data, *ApJ* 646 (2006) 351–357.
- [231] P. Kumar, T. Piran, Some observational consequences of gamma-ray burst shock models, *ApJ* 532 (2000) 286–293.
- [232] B. Zhang, P. Mészáros, Gamma-Ray bursts with continuous energy injection and their afterglow signature, *ApJ* 566 (2002) 712–722.
- [233] M. Nardini, J. Greiner, T. Krühler, R. Filgas, S. Klose, P. Afonso, C. Clemens, A.N.E. Guelbenzu, F. Olivares, A. Rau, A. Rossi, A. Updike, A. Küpcü Yoldaş, A. Yoldaş, D. Burlon, J. Elliott, D.A. Kann, On the nature of the extremely fast optical rebrightening of the afterglow of GRB 081029, *A&A* 531 (2011) A39.
- [234] Z.G. Dai, T. Lu, Spectrum and duration of delayed MeV–GeV emission of gamma-ray bursts in cosmic background radiation fields, *ApJ* 580 (2002) 1013–1016.
- [235] D. Lazzati, E. Rossi, S. Covino, G. Ghisellini, D. Malesani, The afterglow of GRB 021004: Surfing on density waves, *A&A* 396 (2002) L5–L9.
- [236] Z.G. Dai, X.F. Wu, GRB 030226 in a density-jump medium, *ApJ* 591 (2003) L21–L24.
- [237] A. Pe'er, R.A.M.J. Wijers, The signature of a wind reverse shock in gamma-ray burst afterglows, *ApJ* 643 (2006) 1036–1046.
- [238] E. Nakar, T. Piran, J. Granot, Variability in GRB afterglows and GRB 021004, *New Astronomy* 8 (2003) 495–505.
- [239] J.J. Geng, X.F. Wu, L. Li, Y.F. Huang, Z.G. Dai, Revisiting the emission from relativistic blast waves in a density-jump medium, *ApJ* 792 (2014) 31.
- [240] D.M. Wei, T. Lu, Diverse temporal properties of gamma-ray burst afterglows, *ApJ* 505 (1998) 252–254.
- [241] A. Panaiteescu, P. Kumar, Analytic light curves of gamma-ray burst afterglows: Homogeneous versus wind external media, *ApJ* 543 (2000) 66–76.
- [242] R. Sari, A.A. Esin, On the synchrotron self-compton emission from relativistic shocks and its implications for gamma-ray burst afterglows, *ApJ* 548 (2001) 787–799.
- [243] P. Mészáros, M.J. Rees, H. Papathanassiou, Spectral properties of blast-wave models of gamma-ray burst sources, *ApJ* 432 (1994) 181–193.
- [244] B. Zhang, P. Mészáros, High-energy spectral components in gamma-ray burst afterglows, *ApJ* 559 (2001) 110–122.
- [245] E.V. Derishev, V.V. Kocharyan, V.V. Kocharyan, Physical parameters and emission mechanism in gamma-ray bursts, *A&A* 372 (2001) 1071–1077.
- [246] E. Nakar, S. Ando, R. Sari, Klein–Nishina effects on optically thin synchrotron and synchrotron self-compton spectrum, *ApJ* 703 (2009) 675–691.

- [247] F. Daigne, Ž Bošnjak, G. Dubus, Reconciling observed gamma-ray burst prompt spectra with synchrotron radiation? *A&A* 526 (2011) A110.
- [248] R. Barniol Duran, Ž Bošnjak, P. Kumar, Inverse-Compton cooling in Klein–Nishina regime and gamma-ray burst prompt spectrum, *MNRAS* 424 (2012) 3192–3200.
- [249] X.-Y. Wang, H.-N. He, Z. Li, X.-F. Wu, Z.-G. Dai, Klein–Nishina effects on the high-energy afterglow emission of Gamma-ray bursts, *ApJ* 712 (2010) 1232–1240.
- [250] P. Kumar, R. Barniol Duran, External forward shock origin of high-energy emission for three gamma-ray bursts detected by Fermi, *MNRAS* 409 (2010) 226–236.
- [251] M. Ackermann, M. Ajello, K. Asano, W.B. Atwood, M. Axelsson, L. Baldini, J. Ballet, G. Barbiellini, M.G. Baring, D.e.a. Bastieri, Fermi-LAT observations of the gamma-ray burst GRB 130427A, *Science* 343 (2014) 42–47.
- [252] Y.-Z. Fan, P.H.T. Tam, F.-W. Zhang, Y.-F. Liang, H.-N. He, B. Zhou, R.-Z. Yang, Z.-P. Jin, D.-M. Wei, High-energy emission of GRB 130427A: Evidence for inverse compton radiation, *ApJ* 776 (2013) 95.
- [253] R.-Y. Liu, X.-Y. Wang, X.-F. Wu, Interpretation of the Unprecedentedly Long-lived High-energy Emission of GRB 130427A, *ApJ* 773 (2013) L20.
- [254] Z.G. Dai, K.S. Cheng, Afterglow emission from highly collimated jets with flat electron spectra: application to the GRB 010222 case?, *ApJ* 558 (2001) L109–L112.
- [255] D. Bhattacharya, Flat spectrum gamma ray burst afterglows, *Bulletin of the Astronomical Society of India* 29 (2001) 107–114.
- [256] L. Resmi, D. Bhattacharya, Hard electron energy distribution in the relativistic shocks of gamma-ray burst afterglows, *MNRAS* 388 (2008) 144–158.
- [257] E.V. Derishev, V.V. Kocharyan, V.V. Kocharyan, The neutron component in fireballs of gamma-ray bursts: dynamics and observable imprints, *ApJ* 521 (1999) 640–649.
- [258] J.N. Bahcall, P. Mészáros, 5–10 GeV neutrinos from gamma-ray burst fireballs, *Phys. Rev. Lett.* 85 (2000) 1362–1365.
- [259] P. Mészáros, M.J. Rees, Multi-GeV Neutrinos from Internal Dissipation in Gamma-Ray Burst Fireballs, *ApJ* 541 (2000) L5–L8.
- [260] A.M. Beloborodov, Nuclear composition of gamma-ray burst fireballs, *ApJ* 588 (2003) 931–944.
- [261] A.M. Beloborodov, Neutron-fed afterglows of gamma-ray bursts, *ApJ* 585 (2003) L19–L22.
- [262] Y.Z. Fan, B. Zhang, D.M. Wei, Early optical afterglow light curves of neutron-fed gamma-ray bursts, *ApJ* 628 (2005) 298–314.
- [263] P. Madau, C. Thompson, Relativistic Winds from Compact Gamma-Ray Sources. I. Radiative Acceleration in the Klein–Nishina Regime, *ApJ* 534 (2000) 239–247.
- [264] C. Thompson, P. Madau, Relativistic winds from compact Gamma-Ray sources. II. pair loading and radiative acceleration in gamma-ray bursts, *ApJ* 538 (2000) 105–114.
- [265] P. Mészáros, E. Ramirez-Ruiz, M.J. Rees,  $e^{+/-}$  Pair Cascades and Precursors in Gamma-Ray Bursts, *ApJ* 554 (2001) 660–666.
- [266] A.M. Beloborodov, Radiation front sweeping the ambient medium of gamma-ray bursts, *ApJ* 565 (2002) 808–828.
- [267] P. Kumar, A. Panaitescu, Creation of electron-positron wind in gamma-ray bursts and its effect on the early afterglow emission, *MNRAS* 354 (2004) 252–258.
- [268] Z.G. Dai, T. Lu, The afterglow of GRB 990123 and a dense medium, *ApJ* 519 (1999) L155–L158.
- [269] M. Livio, E. Waxman, Toward a Model for the Progenitors of Gamma-Ray Bursts, *ApJ* 538 (2000) 187–191.
- [270] A. Pe'er, Dynamical model of an expanding shell, *ApJ* 752 (2012) L8.
- [271] Y.F. Huang, K.S. Cheng, Gamma-ray bursts: optical afterglows in the deep Newtonian phase, *MNRAS* 341 (2003) 263–269.
- [272] A.J. van der Horst, A. Kamble, L. Resmi, R.A.M.J. Wijers, D. Bhattacharya, B. Scheers, E. Rol, R. Strom, C. Kouveliotou, T. Oosterloo, C.H. Ishwara-Chandra, Detailed study of the GRB 030329 radio afterglow deep into the non-relativistic phase, *A&A* 480 (2008) 35–43.
- [273] J.I. Katz, Two populations and models of gamma-ray bursts, *ApJ* 422 (1994) 248–259.
- [274] N. Gehrels, G. Chincarini, P. Giommi, K.O. Mason, J.A. Nousek, A.A. Wells, N.E. White, S.D. Barthelmy, D.N. Burrows, L.R. Cominsky, K.C. Hurley, F.E. Marshall, P. Mészáros, P.W.A. Roming, L. Angelini, L.M. Barbier, T. Belloni, S. Campana, P.A. Caraveo, M.M. Chester, O. Citterio, T.L. Cline, M.S. Cropper, J.R. Cummings, A.J. Dean, E.D. Feigelson, E.E. Fenimore, D.A. Frail, A.S. Fruchter, G.P. Garnire, K. Gendreau, G. Ghisellini, J. Greiner, J.E. Hill, S.D. Hunsberger, H.A. Krimm, S.R. Kulkarni, P. Kumar, F. Lebrun, N.M. Lloyd-Ronning, C.B. Markwardt, B.J. Mattson, R.F. Mushotzky, J.P. Norris, J. Osborne, B. Paczynski, D.M. Palmer, H.-S. Park, A.M. Parsons, J. Paul, M.J. Rees, C.S. Reynolds, J.E. Rhoads, T.P. Sasseen, B.E. Schaefer, A.T. Short, A.P. Smale, I.A. Smith, L. Stella, G. Tagliaferri, T. Takahashi, M. Tashiro, L.K. Townsley, J. Tueller, M. Vietri, W. Voges, M.J. Ward, R. Willingale, F.M. Zerbi, W.W. Zhang, The swift gamma-ray burst mission, *ApJ* 611 (2004) 1005–1020.
- [275] R.A.M.J. Wijers, M.J. Rees, P. Mészáros, Shocked by GRB 970228: the afterglow of a cosmological fireball, *MNRAS* 288 (1997) L51–L56.
- [276] F.A. Harrison, J.S. Bloom, D.A. Frail, R. Sari, S.R. Kulkarni, S.G. Djorgovski, T. Axelrod, J. Mould, B.P. Schmidt, M.H. Wieringa, R.M. Wark, R. Subrahmanyam, D. McConnell, P.J. McCarthy, B.E. Schaefer, R.G. McMahon, R.O. Markze, E. Firth, P. Soffitta, L. Amati, Optical and radio observations of the Afterglow from GRB 990510: Evidence for a jet, *ApJ* 523 (1999) L121–L124.
- [277] D.A. Frail, E. Waxman, S.R. Kulkarni, A 450 day light curve of the radio afterglow of GRB 970508: Fireball calorimetry, *ApJ* 537 (2000) 191–204.
- [278] R.A.M.J. Wijers, T.J. Galama, Physical parameters of GRB 970508 and GRB 971214 from their afterglow synchrotron emission, *ApJ* 523 (1999) 177–186.
- [279] S.T. Holland, M. Weidinger, J.P.U. Fynbo, J. Gorosabel, J. Hjorth, K. Pedersen, J. Méndez Alvarez, T. Augusteijn, J.M. Castro Cerón, A. Castro-Tirado, H. Dahle, M.P. Egholm, P. Jakobsson, B.L. Jensen, A. Levan, P. Møller, H. Pedersen, T. Pursimo, P. Ruiz-Lapuente, B. Thomsen, Optical photometry of GRB 021004: The first month, *AJ* 125 (2003) 2291–2298.
- [280] Y.M. Lipkin, E.O. Ofek, A. Gal-Yam, E.M. Leibowitz, D. Poznanski, S. Kaspi, D. Polishook, S.R. Kulkarni, D.W. Fox, E. Berger, N. Mirabal, J. Halpern, M. Bureau, K. Fathi, P.A. Price, B.A. Peterson, A. Frebel, B. Schmidt, J.A. Orosz, J.B. Fitzgerald, J.S. Bloom, P.G. van Dokkum, C.D. Bailyn, M.M. Buxton, M. Barsony, The Detailed Optical Light Curve of GRB 030329, *ApJ* 606 (2004) 381–394.
- [281] J.I. Katz, T. Piran, R. Sari, Implications of the Visible and X-Ray Counterparts to GRB 970228, *Phys. Rev. Lett.* 80 (1998) 1580–1581.
- [282] J. Granot, E. Nakar, T. Piran, Astrophysics: refreshed shocks from a  $\gamma$ -ray burst, *Nature* 426 (2003) 138–139.
- [283] R. Yamazaki, K. Ioka, T. Nakamura, A unified model of short and long gamma-ray bursts, X-Ray-rich gamma-ray bursts, and X-ray flashes, *ApJ* 607 (2004) L103–L106.
- [284] D.N. Burrows, J.E. Hill, J.A. Nousek, J.A. Kennea, A. Wells, J.P. Osborne, A.F. Abbey, A. Beardmore, K. Mukerjee, A.D.T. Short, G. Chincarini, S. Campana, O. Citterio, A. Moretti, C. Pagani, G. Tagliaferri, P. Giommi, M. Capalbi, F. Tamburelli, L. Angelini, G. Cusumano, H.W. Bräuning, W. Burkert, G.D. Hartner, The swift x-ray telescope, *Space Science Reviews* 120 (2005) 165–195.
- [285] P.W.A. Roming, T.E. Kennedy, K.O. Mason, J.A. Nousek, L. Ahr, R.E. Bingham, P.S. Broos, M.J. Carter, B.K. Hancock, H.E. Huckle, S.D. Hunsberger, H. Kawakami, R. Killough, T.S. Koch, M.K. Mclelland, K. Smith, P.J. Smith, J.C. Soto, P.T. Boyd, A.A. Breeveld, S.T. Holland, M. Ivanushkina, M.S. Pryzby, M.D. Still, J. Stock, The swift ultra-violet/optical telescope, *Space Sci. Rev.* 120 (2005) 95–142.
- [286] S.D. Barthelmy, L.M. Barbier, J.R. Cummings, E.E. Fenimore, N. Gehrels, D. Hullinger, H.A. Krimm, C.B. Markwardt, D.M. Palmer, A. Parsons, G. Sato, M. Suzuki, T. Takahashi, M. Tashiro, J. Tueller, The burst alert telescope (BAT) on the SWIFT midex mission, *Space Sci. Rev.* 120 (2005) 143–164.
- [287] Y.-Z. Fan, Z.-G. Dai, Y.-F. Huang, T. Lu, Optical flash of GRB 990123: Constraints on the physical parameters of the reverse shock, *Chin. J. Astron. Astrophys.* 2 (2002) 449–453.
- [288] S.R. Kulkarni, D.A. Frail, R. Sari, G.H. Moriarty-Schieven, D.S. Shepherd, P. Udomprasert, A.C.S. Readhead, J.S. Bloom, M. Feroci, E. Costa, Discovery of a Radio Flare from GRB 990123, *ApJ* 522 (1999) L97–L100.
- [289] P.A. Evans, A.P. Beardmore, K.L. Page, L.G. Tyler, J.P. Osborne, M.R. Goad, P.T. O'Brien, L. Vetere, J. Racusin, D. Morris, D.N. Burrows, M. Capalbi, M. Perri, N. Gehrels, P. Romano, An online repository of Swift/XRT light curves of  $\gamma$ -ray bursts, *A&A* 469 (2007) 379–385.
- [290] P.A. Evans, A.P. Beardmore, K.L. Page, J.P. Osborne, P.T. O'Brien, R. Willingale, R.L.C. Starling, D.N. Burrows, O. Godet, L. Vetere, J. Racusin, M.R. Goad, K. Wiersema, L. Angelini, M. Capalbi, G. Chincarini, N. Gehrels, J.A. Kennea, R. Margutti, D.C. Morris, C.J. Mountford, C. Pagani, M. Perri, P. Romano, N. Tanvir, Methods and results of an automatic analysis of a complete sample of Swift-XRT observations of GRBs, *MNRAS* 397 (2009) 1177–1201.
- [291] S.D. Barthelmy, J.K. Cannizzo, N. Gehrels, G. Cusumano, V. Mangano, P.T. O'Brien, S. Vaughan, B. Zhang, D.N. Burrows, S. Campana, G. Chincarini, M.R. Goad, C. Kouveliotou, P. Kumar, P. Mészáros, J.A. Nousek, J.P. Osborne, A. Panaitescu, J.N. Reeves, T. Sakamoto, G. Tagliaferri, R.A.M.J. Wijers, Discovery of an afterglow extension of the prompt phase of two gamma-ray bursts observed by swift, *ApJ* 635 (2005) L133–L136.

- [292] R. Barniol Duran, P. Kumar, Adiabatic expansion, early X-ray data and the central engine in GRBs, MNRAS 395 (2009) 955–961.
- [293] A. Panaiteescu, P. Mészáros, N. Gehrels, D. Burrows, J. Nousek, Analysis of the X-ray emission of nine Swift afterglows, MNRAS 366 (2006) 1357–1366.
- [294] E. Troja, G. Cusumano, P.T. O'Brien, B. Zhang, B. Sbarufatti, V. Mangano, R. Willingale, G. Chincarini, J.P. Osborne, F.E. Marshall, D.N. Burrows, S. Campana, N. Gehrels, C. Guidorzi, H.A. Krimm, V. Laparola, E.W. Liang, T. Mineo, A. Moretti, K.L. Page, P. Romano, G. Tagliaferri, B.B. Zhang, M.J. Page, P. Schady, Swift observations of GRB 070110: An extraordinary X-Ray afterglow powered by the central engine, ApJ 665 (2007) 599–607.
- [295] L. Piro, M. Depasquale, P. Soffitta, D. Lazzati, L. Amati, E. Costa, M. Feroci, F. Frontera, C. Guidorzi, J.M.J. In'tZand, E. Montanari, L. Nicastro, Probing the environment in gamma-ray bursts: The case of an X-Ray precursor, afterglow late onset, and wind versus constant density profile in GRB 011121 and GRB 011211, ApJ 623 (2005) 314–324.
- [296] A. Maxham, B. Zhang, Modeling gamma-ray burst x-ray flares within the internal shock model, ApJ 707 (2009) 1623–1633.
- [297] R. Margutti, C. Guidorzi, G. Chincarini, M.G. Bernardini, F. Genet, J. Mao, F. Pasotti, Lag-luminosity relation in  $\gamma$ -ray burst X-ray flares: a direct link to the prompt emission, MNRAS 406 (2010) 2149–2167.
- [298] P.T. O'Brien, R. Willingale, J. Osborne, M.R. Goad, K.L. Page, S. Vaughan, E. Rol, A. Beardmore, O. Godet, C.P. Hurkett, A. Wells, B. Zhang, S. Kobayashi, D.N. Burrows, J.A. Nousek, J.A. Kennea, A. Falcone, D. Grupe, N. Gehrels, S. Barthelmy, J. Cannizzo, J.E. Hill, H. Krimm, G. Chincarini, G. Tagliaferri, S. Campana, A. Moretti, P. Giommi, M. Perri, V. Mangano, V. Laparola, The Early X-Ray Emission from GRBs, ApJ 647 (2006) 1213–1237.
- [299] R. Willingale, P.T. O'Brien, J.P. Osborne, O. Godet, K.L. Page, M.R. Goad, D.N. Burrows, B. Zhang, E. Rol, N. Gehrels, G. Chincarini, Testing the standard fireball model of gamma-ray bursts using late X-Ray afterglows measured by swift, ApJ 662 (2007) 1093–1110.
- [300] G. Ghisellini, M. Nardini, G. Ghirlanda, A. Celotti, A unifying view of gamma-ray burst afterglows, MNRAS 393 (2009) 253–271.
- [301] N. Lyons, P.T. O'Brien, B. Zhang, R. Willingale, E. Troja, R.L.C. Starling, Can X-ray emission powered by a spinning-down magnetar explain some gamma-ray burst light-curve features?, MNRAS 402 (2010) 705–712.
- [302] Y.-Z. Fan, T. Piran, D. Xu, The interpretation and implication of the afterglow of GRB 060218, J. Cosmol. Astropart. Phys. 9 (2006) 13.
- [303] K.Y. Huang, Y. Urata, P.H. Kuo, W.H. Ip, K. Ioka, T. Aoki, C.W. Chen, W.P. Chen, M. Isogai, H.C. Lin, K. Makishima, H. Mito, T. Miyata, Y. Nakada, S. Nishiura, K. Onda, Y. Qiu, T. Soyano, T. Tamagawa, K. Tarusawa, M. Tashiro, T. Yoshioka, Multicolor Shallow Decay and Chromatic Breaks in the GRB 050319 Optical Afterglow, ApJ 654 (2007) L25–L28.
- [304] X.G. Wang, et al. ApJ (2015), to be submitted.
- [305] R. Sari, T. Piran, Variability in Gamma-Ray Bursts: A Clue, ApJ 485 (1997) 270.
- [306] B.-B. Zhang, E.-W. Liang, B. Zhang, A comprehensive analysis of swift XRT Data. I. apparent spectral evolution of gamma-ray burst X-ray tails, ApJ 666 (2007) 1002–1011.
- [307] B.-B. Zhang, B. Zhang, E.-W. Liang, X.-Y. Wang, Curvature effect of a non-power spectrum and spectral evolution of GRB X-Ray Tails, ApJ 690 (2009) L10–L13.
- [308] F. Genet, J. Granot, Realistic analytic model for the prompt and high-latitude emission in GRBs, MNRAS 399 (2009) 1328–1346.
- [309] V. Mangano, B. Sbarufatti, Modeling the spectral evolution in the decaying tail of gamma-ray bursts observed by Swift, Adv. Space Res. 47 (2011) 1367–1373.
- [310] B.-B. Zhang, Y.-Z. Fan, R.-F. Shen, D. Xu, F.-W. Zhang, D.-M. Wei, D.N. Burrows, B. Zhang, N. Gehrels, GRB 120422A: A low-luminosity gamma-ray burst driven by a central engine, ApJ 756 (2012) 190.
- [311] A. Pe'er, P. Mészáros, M.J. Rees, Radiation from an expanding cocoon as an explanation of the steep decay observed in GRB early afterglow light curves, ApJ 652 (2006) 482–489.
- [312] C.D. Dermer, Rapid X-ray declines and plateaus in swift GRB light curves explained by a highly radiative blast wave, ApJ 664 (2007) 384–396.
- [313] M. Petropoulou, A. Mastichiadis, T. Piran, Effects of a low electron distribution cutoff on multiwavelength spectra and light curves of GRB afterglows, A&A 531 (2011) A76.
- [314] X.F. Wu, Z.G. Dai, X.Y. Wang, Y.F. Huang, L.L. Feng, T. Lu, X-ray flares from late internal and late external shocks, in: 36th COSPAR Scientific Assembly, in: COSPAR, Plenary Meeting, vol. 36, 2006, pp. 731–+.
- [315] D. Giannios, Flares in GRB afterglows from delayed magnetic dissipation, A&A 455 (2006) L5–L8.
- [316] A.M. Beloborodov, F. Daigne, R. Mochkovitch, Z.L. Uhm, Is gamma-ray burst afterglow emission intrinsically anisotropic? MNRAS 410 (2011) 2422–2427.
- [317] J. Granot, A. Königl, T. Piran, Implications of the early X-ray afterglow light curves of Swift gamma-ray bursts, MNRAS 370 (2006) 1946–1960.
- [318] Y. Fan, T. Piran, Gamma-ray burst efficiency and possible physical processes shaping the early afterglow, MNRAS 369 (2006) 197–206.
- [319] V. Mangano, V. Laparola, G. Cusumano, T. Mineo, D. Malesani, J. Dyks, S. Campana, M. Capalbi, G. Chincarini, P. Giommi, A. Moretti, M. Perri, P. Romano, G. Tagliaferri, D.N. Burrows, N. Gehrels, O. Godet, S.T. Holland, J.A. Kennea, K.L. Page, J.L. Racusin, P.W.A. Roming, B. Zhang, Swift XRT observations of the Afterglow of XRF 050416A, ApJ 654 (2007) 403–412.
- [320] D. Grupe, C. Gronwall, X.-Y. Wang, P.W.A. Roming, J. Cummings, B. Zhang, P. Mészáros, M.D. Trigo, P.T. O'Brien, K.L. Page, A. Beardmore, O. Godet, D.E. Vandenberg, P.J. Brown, S. Koch, D. Morris, M. Stroh, D.N. Burrows, J.A. Nousek, M. Mcmathchester, S. Immler, V. Mangano, P. Romano, G. Chincarini, J. Osborne, T. Sakamoto, N. Gehrels, Swift and XMM-Newton observations of the extraordinary Gamma-Ray Burst 060729: More than 125 Days of X-Ray Afterglow, ApJ 662 (2007) 443–458.
- [321] M. de Pasquale, P. Evans, S. Oates, M. Page, S. Zane, P. Schady, A. Breeveld, S. Holland, P. Kuin, M. Still, P. Roming, P. Ward, Jet breaks at the end of the slow decline phase of Swift GRB light curves, MNRAS 392 (2009) 153–169.
- [322] K. Ioka, K. Toma, R. Yamazaki, T. Nakamura, Efficiency crisis of swift gamma-ray bursts with shallow X-ray afterglows: prior activity or time-dependent microphysics?, A&A 458 (2006) 7–12.
- [323] R. Shen, C.D. Matzner, Coasting external shock in wind medium: An origin for the X-ray plateau decay component in swift gamma-ray burst afterglows, ApJ 744 (2012) 36.
- [324] L. Shao, Z.G. Dai, Behavior of X-Ray dust scattering and implications for X-Ray afterglows of gamma-ray bursts, ApJ 660 (2007) 1319–1325.
- [325] R. Shen, R. Willingale, P. Kumar, P.T. O'Brien, P.A. Evans, The dust scattering model cannot explain the shallow X-ray decay in GRB afterglows, MNRAS 393 (2009) 598–606.
- [326] R. Yamazaki, Prior emission model for X-ray plateau phase of gamma-ray burst afterglows, ApJ 690 (2009) L118–L121.
- [327] T. Birnbaum, B. Zhang, B.-B. Zhang, E.-W. Liang, Observational constraints on the external shock prior emission hypothesis of gamma-ray bursts, MNRAS 422 (2012) 393–400.
- [328] A.D. Falcone, D. Morris, J. Racusin, G. Chincarini, A. Moretti, P. Romano, D.N. Burrows, C. Pagani, M. Stroh, D. Grupe, S. Campana, S. Covino, G. Tagliaferri, R. Willingale, N. Gehrels, The first survey of x-ray flares from gamma-ray bursts observed by swift: spectral properties and energetics, ApJ 671 (2007) 1921–1938.
- [329] G. Ghisellini, G. Ghirlanda, L. Nava, C. Firmani, “Late Prompt” emission in gamma-ray bursts? ApJ 658 (2007) L75–L78.
- [330] P. Kumar, R. Narayan, J.L. Johnson, Mass fall-back and accretion in the central engine of gamma-ray bursts, MNRAS (2008) 750.
- [331] P. Kumar, R. Narayan, J.L. Johnson, Properties of gamma-ray burst progenitor stars, Science 321 (2008) 376.
- [332] J.K. Cannizzo, N. Gehrels, A new paradigm for gamma-ray bursts: Long-term accretion rate modulation by an external accretion disk, ApJ 700 (2009) 1047–1058.
- [333] C.C. Lindner, M. Milosavljević, S.M. Couch, P. Kumar, Collapsar Accretion and the Gamma-Ray Burst X-Ray Light Curve, ApJ 713 (2010) 800–815.
- [334] Y.-W. Yu, K.S. Cheng, X.-F. Cao, The role of newly born magnetars in gamma-ray burst X-ray afterglow emission: Energy injection and internal emission, ApJ 715 (2010) 477–484.
- [335] B.D. Metzger, D. Giannios, T.A. Thompson, N. Bucciantini, E. Quataert, The protomagnetar model for gamma-ray bursts, MNRAS 413 (2011) 2031–2056.
- [336] A. Panaiteescu, P. Kumar, R. Narayan, Observational prospects for afterglows of short-duration gamma-ray bursts, ApJ 561 (2001) L171–L174.

- [337] N. Gehrels, S.D. Barthelmy, D.N. Burrows, J.K. Cannizzo, G. Chincarini, E. Fenimore, C. Kouveliotou, P. O'Brien, D.M. Palmer, J. Racusin, P.W.A. Roming, T. Sakamoto, J. Tueller, R.A.M.J. Wijers, B. Zhang, Correlations of prompt and afterglow emission in swift long and short gamma-ray bursts, *ApJ* 689 (2008) 1161–1172.
- [338] M. Nysewander, A.S. Fruchter, A. Pe'er, A Comparison of the Afterglows of Short- and Long-duration Gamma-ray Bursts, *ApJ* 701 (2009) 824–836.
- [339] D.A. Kann, S. Klose, B. Zhang, S. Covino, N.R. Butler, D. Malesani, E. Nakar, A.C. Wilson, L.A. Antonelli, G. Chincarini, B.E. Cobb, P. D'Avanzo, V. D'Elia, M. Della Valle, P. Ferrero, D. Fugazza, J. Gorosabel, G.L. Israel, F. Mannucci, S. Piranomonte, S. Schulze, L. Stella, G. Tagliaferri, K. Wiersema, The Afterglows of Swift-era Gamma-Ray Bursts. II. Type I GRB versus Type II GRB Optical Afterglows, *ApJ* 734 (2011) 96.
- [340] B. Zhang, E. Liang, K.L. Page, D. Grupe, B.-B. Zhang, S.D. Barthelmy, D.N. Burrows, S. Campana, G. Chincarini, N. Gehrels, S. Kobayashi, P. Mészáros, A. Moretti, J.A. Nousek, P.T. O'Brien, J.P. Osborne, P.W.A. Roming, T. Sakamoto, P. Schady, R. Willingale, GRB radiative efficiencies derived from the swift data: GRBs versus XRFs, Long versus Sh ort, *ApJ* 655 (2007) 989–1001.
- [341] Ž Bošnjak, F. Daigne, G. Dubus, Prompt high-energy emission from gamma-ray bursts in the internal shock model, *A&A* 498 (2009) 677–703.
- [342] C.D. Dermer, J. Chiang, K.E. Mitman, Beaming, baryon loading, and the synchrotron self-compton component in gamma-ray bursts, *ApJ* 537 (2000) 785–795.
- [343] X.Y. Wang, Z.G. Dai, T. Lu, Prompt high-energy gamma-ray emission from the synchrotron self-compton process in the reverse shocks of gamma-ray bursts, *ApJ* 546 (2001) L33–L37.
- [344] X.Y. Wang, Z.G. Dai, T. Lu, The inverse compton emission spectra in the very early afterglows of gamma-ray bursts, *ApJ* 556 (2001) 1010–1016.
- [345] J. Granot, D. Guetta, Explaining the high-energy spectral component in GRB 941017, *ApJ* 598 (2003) L11–L14.
- [346] A. Pe'er, E. Waxman, The High-Energy Tail of GRB 941017: Comptonization of synchrotron self-absorbed photons, *ApJ* 603 (2004) L1–L4.
- [347] N. Gupta, B. Zhang, Prompt emission of high-energy photons from gamma ray bursts, *MNRAS* 380 (2007) 78–92.
- [348] Y.-Z. Fan, T. Piran, High-energy  $\gamma$ -ray emission from gamma-ray bursts before GLAST, *Front. Phys. China* 3 (2008) 306–330.
- [349] Y.-C. Zou, Y.-Z. Fan, T. Piran, The possible high-energy emission from GRB 080319B and origins of the GeV emission of GRBs 080514B, 080916C and 081024B, *MNRAS* 396 (2009) 1163–1170.
- [350] P. Mészáros, M.J. Rees, Delayed GEV Emission from Cosmological Gamma-Ray Bursts – Impact of a Relativistic Wind on External Matter, *MNRAS* 269 (1994) L41.
- [351] A.M. Beloborodov, Optical and GeV–TeV flashes from gamma-ray bursts, *ApJ* 618 (2005) L13–L16.
- [352] Y.Z. Fan, B. Zhang, D.M. Wei, Early photon-shock interaction in a stellar wind: a sub-gev photon flash and high-energy neutrino emission from long gamma-ray bursts, *ApJ* 629 (2005) 334–340.
- [353] R. Plaga, Detecting intergalactic magnetic fields using time delays in pulses of gamma-rays, *Nature* 374 (1995) 430.
- [354] Z.G. Dai, B. Zhang, L.J. Gou, P. Mészáros, E. Waxman, GeV emission from tev blazars and intergalactic magnetic fields, *ApJ* 580 (2002) L7–L10.
- [355] X.Y. Wang, K.S. Cheng, Z.G. Dai, T. Lu, Constraining the origin of TeV photons from Gamma-Ray Bursts with Delayed MeV–GeV Emission Formed by interaction with cosmic infrared/microwave background photons, *ApJ* 604 (2004) 306–311.
- [356] K. Murase, B. Zhang, K. Takahashi, S. Nagataki, Possible effects of pair echoes on gamma-ray burst afterglow emission, *MNRAS* 396 (2009) 1825–1832.
- [357] W.B. Atwood, A.A. Abdo, M. Ackermann, W. Althouse, B. Anderson, M. Axelsson, L. Baldini, J. Ballet, D.L. Band, G. Barbiellini, et al., The large area telescope on the Fermi gamma-ray space telescope mission, *ApJ* 697 (2009) 1071–1102.
- [358] C. Meegan, G. Lichti, P.N. Bhat, E. Bissaldi, M.S. Briggs, V. Connaughton, R. Diehl, G. Fishman, J. Greiner, A.S. Hoover, A.J. van der Horst, A. Vonkienlin, R.M. Kippen, C. Kouveliotou, S. McBreer, W.S. Paciesas, R. Preece, H. Steinle, M.S. Wallace, R.B. Wilson, C. Wilson-Hodge, The Fermi Gamma-ray burst monitor, *ApJ* 702 (2009) 791–804.
- [359] A.A. Abdo, M. Ackermann, M. Ajello, K. Asano, W.B. Atwood, M. Axelsson, L. Baldini, J. Ballet, G. Barbiellini, M.G. Baring, et al., Fermi observations of GRB 090902B: A distinct spectral component in the prompt and delayed emission, *ApJ* 706 (2009) L138–L144.
- [360] A.M. Beloborodov, R. Hascoet, I. Vurm, On the origin of GeV emission in gamma-ray bursts, *ApJ* 788 (2014) 36–54.
- [361] R. Barniol Duran, P. Kumar, Implications of electron acceleration for high-energy radiation from gamma-ray bursts, *MNRAS* 412 (2011) 522–528.
- [362] T. Piran, E. Nakar, On the external shock synchrotron model for gamma-ray Bursts' GeV emission, *ApJ* 718 (2010) L63–L67.
- [363] E.-W. Liang, H.-J. Lü, S.-J. Hou, B.-B. Zhang, B. Zhang, A Comprehensive Analysis of Swift/X-Ray Telescope Data. IV. Single Power-Law Decaying Light Curves Versus Canonical Light Curves and Implications for a Unified Origin of X-Rays, *ApJ* 707 (2009) 328–342.
- [364] A.A. Abdo, M. Ackermann, M. Ajello, L. Baldini, J. Ballet, G. Barbiellini, M.G. Baring, D. Bastieri, K. Bechtol, R.e.a. Bellazzini, Detection of high-energy gamma-ray emission during the X-ray flaring activity in GRB 100728A, *ApJ* 734 (2011) L27.
- [365] X.-Y. Wang, Z. Li, P. Mészáros, GeV–TeV and X-Ray flares from gamma-ray bursts, *ApJ* 641 (2006) L89–L92.
- [366] H.-N. He, R.-Y. Liu, X.-Y. Wang, S. Nagataki, K. Murase, Z.-G. Dai, Icecube nondetection of gamma-ray bursts: Constraints on the fireball properties, *ApJ* 752 (2012) 29.
- [367] M. de Pasquale, P. Schady, N.P.M. Kuin, M.J. Page, P.A. Curran, S. Zane, S.R. Oates, S.T. Holland, A.A. Breeveld, E.A.e.a. Hoversten, Swift and fermi observations of the early afterglow of the short gamma-ray burst 090510, *ApJ* 709 (2010) L146–L151.
- [368] M. Ackermann, M. Ajello, K. Asano, L. Baldini, G. Barbiellini, M.G. Baring, D. Bastieri, R. Bellazzini, R.D. Blandford, E. Bonamente, et al., Multiwavelength observations of GRB 110731A: GeV emission from onset to afterglow, *ApJ* 763 (2013) 71.
- [369] W. Gao, J. Mao, D. Xu, Y. Fan, GRB 080916C and GRB 090510: The high-energy emission and the afterglow, *ApJ* 706 (2009) L33–L36.
- [370] A. Maxham, B.-B. Zhang, B. Zhang, Is GeV emission from Gamma-Ray Bursts of external shock origin? *MNRAS* 415 (2011) 77–82.
- [371] H.-N. He, X.-F. Wu, K. Toma, X.-Y. Wang, P. Mészáros, On the high-energy emission of the short GRB 090510, *ApJ* 733 (2011) 22.
- [372] R.-Y. Liu, X.-Y. Wang, Modeling the Broadband Emission of GRB 090902B, *ApJ* 730 (2011) 1.
- [373] M. Ackermann, M. Ajello, K. Asano, M. Axelsson, L. Baldini, J. Ballet, G. Barbiellini, D. Bastieri, K. Bechtol, Bellazzini, et al., The first Fermi-LAT gamma-ray burst catalog, *ApJ* 209 (2013) 11.
- [374] E.S. Weibel, Spontaneously growing transverse waves in a plasma due to an anisotropic velocity distribution, *Phys. Rev. Lett.* 2 (1959) 83–84.
- [375] M.V. Medvedev, A. Loeb, Generation of magnetic fields in the relativistic shock of gamma-ray burst sources, *ApJ* 526 (1999) 697–706.
- [376] E. Berger, A.M. Soderberg, D.A. Frail, S.R. Kulkarni, A Radio Flare from GRB 020405: Evidence for a Uniform Medium around a Massive Stellar Progenitor, *ApJ* 587 (2003) L5–L8.
- [377] G. Björnsson, E.H. Gudmundsson, G. Jóhannesson, Energy injection episodes in gamma-ray bursts: The light curves and polarization properties of GRB 021004, *ApJ* 615 (2004) L77–L80.
- [378] P. Chandra, D.A. Frail, D. Fox, S. Kulkarni, E. Berger, S.B. Cenko, D.C.-J. Bock, F. Harrison, M. Kasliwal, Discovery of radio afterglow from the most distant cosmic explosion, *ApJ* 712 (2010) L31–L35.
- [379] A. Corsi, D. Guetta, L. Piro, GeV emission from short gamma-ray bursts: the case of GRB 081024B, *A&A* 524 (2010) A92.
- [380] P.A. Curran, A.J. van der Horst, R.A.M.J. Wijers, R.L.C. Starling, A.J. Castro-Tirado, J.P.U. Fynbo, J. Gorosabel, A.S. Järvinen, D. Malesani, E. Rol, N.R. Tanvir, K. Wiersema, M.R. Burleigh, S.L. Casewell, P.D. Dobbie, S. Guziy, P. Jakobsson, M. Jelinek, P. Laursen, A.J. Levan, C.G. Mundell, J. Näränen, S. Piranomonte, GRB060206 and the quandary of achromatic breaks in afterglow light curves, *MNRAS* 381 (2007) L65–L69.
- [381] W.-H. Gao, Optical/Infrared Flares of GRB 080129 from late internal shocks, *ApJ* 697 (2009) 1044–1047.
- [382] A. Rossi, S. Schulze, S. Klose, D.A. Kann, A. Rau, H.A. Krimm, G. Jóhannesson, A. Panaiteescu, F. Yuan, P. Ferrero, T. Krühler, J. Greiner, P. Schady, S.B. Pandey, L. Amati, P.M.J. Afonso, C.W. Akerlof, L.A. Arnold, C. Clemens, R. Filgas, D.H. Hartmann, A. Küpcü Yoldaş, S. McBreen, T.A McKay, A. Nicuesa Guelbenzu, F.E. Olivares, B. Paciesas, E.S. Rykoff, G. Szokoly, A.C. Updike, A. Yoldaş, The Swift/Fermi GRB 080928 from 1 eV to 150 keV, *A&A* 529 (2011) A142.
- [383] A.M. Soderberg, E. Berger, M. Kasliwal, D.A. Frail, P.A. Price, B.P. Schmidt, S.R. Kulkarni, D.B. Fox, S.B. Cenko, A. Gal-Yam, E. Nakar, K.C. Roth, The afterglow, energetics, and host galaxy of the short-hard gamma-ray burst 051221a, *ApJ* 650 (2006) 261–271.
- [384] A.M. Soderberg, The radio properties of type Ibc supernovae, in: S. Immler, K. Weiler, R. McCray (Eds.), *Supernova 1987A: 20 Years After: Supernovae and Gamma-Ray Bursters*, in: American Institute of Physics Conference Series, vol. 937, 2007, pp. 492–499.

- [385] D. Xu, R.L.C. Starling, J.P.U. Fynbo, J. Sollerman, S. Yost, D. Watson, S. Foley, P.T. O'Brien, J. Hjorth, In search of progenitors for supernovaless gamma-ray bursts 060505 and 060614: Re-examination of their afterglows, *ApJ* 696 (2009) 971–979.
- [386] R. Santana, R. Barniol Duran, P. Kumar, Magnetic fields in relativistic collisionless shocks, *ApJ* 785 (2014) 29.
- [387] L. Sironi, A. Spitkovsky, Particle acceleration in relativistic magnetized collisionless electron-ion shocks, *ApJ* 726 (2011) 75.
- [388] L.O. Silva, R.A. Fonseca, J.W. Tonge, J.M. Dawson, W.B. Mori, M.V. Medvedev, Interpenetrating plasma shells: near-equipartition magnetic field generation and nonthermal particle acceleration, *ApJ* 596 (2003) L121–L124.
- [389] P. Chang, A. Spitkovsky, J. Arons, Long-term evolution of magnetic turbulence in relativistic collisionless shocks: electron-positron plasmas, *ApJ* 674 (2008) 378–387.
- [390] M. Lemoine, Z. Li, X.-Y. Wang, On the magnetisation of gamma-ray burst blast waves, *MNRAS* 435 (2014) 3009–3016.
- [391] E. Rossi, M.J. Rees, Gamma-ray burst afterglow emission with a decaying magnetic field, *MNRAS* 339 (2003) 881–886.
- [392] A. Pe'er, B. Zhang, Synchrotron emission in small-scale magnetic fields as a possible explanation for prompt emission spectra of gamma-ray bursts, *ApJ* 653 (2006) 454–461.
- [393] M. Milosavljević, E. Nakar, The Cosmic-Ray Precursor of Relativistic Collisionless Shocks: A Missing Link in Gamma-Ray Burst Afterglows, *ApJ* 651 (2006) 979–984.
- [394] L. Sironi, J. Goodman, Production of magnetic energy by macroscopic turbulence in GRB afterglows, *ApJ* 671 (2007) 1858–1867.
- [395] J. Goodman, A. Macfadyen, Ultra-relativistic geometrical shock dynamics and vorticity, *J. Fluid Mech.* 604 (2008) 325–338.
- [396] S.M. Couch, M. Milosavljević, E. Nakar, Shock vorticity generation from accelerated ion streaming in the precursor of ultrarelativistic gamma-ray burst external shocks, *ApJ* 688 (2008) 462–469.
- [397] T. Inoue, K. Asano, K. Ioka, Three-dimensional Simulations of Magnetohydrodynamic Turbulence Behind Relativistic Shock Waves and Their Implications for Gamma-Ray Bursts, *ApJ* 734 (2011) 77.
- [398] J. Bednarz, M. Ostrowski, Energy spectra of cosmic rays accelerated at ultrarelativistic shock waves, *Phys. Rev. Lett.* 80 (1998) 3911–3914.
- [399] J.G. Kirk, A.W. Guthmann, Y.A. Gallant, A. Achterberg, Particle Acceleration at Ultrarelativistic Shocks: An Eigenfunction Method, *ApJ* 542 (2000) 235–242.
- [400] A. Achterberg, Y.A. Gallant, J.G. Kirk, A.W. Guthmann, Particle acceleration by ultrarelativistic shocks: theory and simulations, *MNRAS* 328 (2001) 393–408.
- [401] M. Lemoine, G. Pelletier, Particle transport in tangled magnetic fields and Fermi acceleration at relativistic shocks, *ApJ* 589 (2003) L73–L76.
- [402] R. Shen, P. Kumar, E.L. Robinson, No universality for the electron power-law index ( $p$ ) in gamma-ray bursts and other relativistic sources, *MNRAS* 371 (2006) 1441–1447.
- [403] P.A. Curran, R.L.C. Starling, A.J. van der Horst, R.A.M.J. Wijers, Testing the blast wave model with Swift GRBs, *MNRAS* 395 (2009) 580–592.
- [404] P.A. Curran, P.A. Evans, M. de Pasquale, M.J. Page, A.J. van der Horst, On the electron energy distribution index of swift gamma-ray burst afterglows, *ApJ* 716 (2010) L135–L139.
- [405] S. Mukherjee, E.D. Feigelson, G. Jogesh Babu, F. Murtagh, C. Fraley, A. Raftery, Three types of gamma-ray bursts, *ApJ* 508 (1998) 314–327.
- [406] I. Horváth, A third class of gamma-ray bursts? *ApJ* 508 (1998) 757–759.
- [407] J. Hakkila, T.W. Giblin, R.J. Roiger, D.J. Haglin, W.S. Paciesas, C.A. Meegan, How sample completeness affects gamma-ray burst classification, *ApJ* 582 (2003) 320–329.
- [408] I. Horváth, Z. Bagoly, L.G. Baláz, A. de Ugarte Postigo, P. Veres, A. Mészáros, Detailed classification of swift's gamma-ray bursts, *ApJ* 713 (2010) 552–557.
- [409] P. Veres, Z. Bagoly, I. Horváth, A. Mészáros, L.G. Baláz, A distinct peak-flux distribution of the third class of gamma-ray bursts: a possible signature of X-ray flashes? *ApJ* 725 (2010) 1955–1964.
- [410] O. Bromberg, E. Nakar, T. Piran, R. Sari, Short versus Long and Collapsars versus non-collapsars: A quantitative classification of gamma-ray bursts, *ApJ* 764 (2013) 179.
- [411] T. Sakamoto, S.D. Barthelmy, L. Barbier, J.R. Cummings, E.E. Fenimore, N. Gehrels, D. Hullinger, H.A. Krimm, C.B. Markwardt, D.M. Palmer, A.M. Parsons, G. Sato, M. Stamatikos, J. Tueller, T.N. Ukwatta, B. Zhang, The first swift BAT gamma-ray burst catalog, *ApJ* 175 (2008) 179–190.
- [412] T. Sakamoto, S.D. Barthelmy, W.H. Baumgartner, J.R. Cummings, E.E. Fenimore, N. Gehrels, H.A. Krimm, C.B. Markwardt, D.M. Palmer, A.M. Parsons, G. Sato, M. Stamatikos, J. Tueller, T.N. Ukwatta, B. Zhang, The second swift burst alert telescope gamma-ray burst catalog, *ApJ* 195 (2011) 2.
- [413] W.S. Paciesas, C.A. Meegan, A. Vonkienlin, P.N. Bhat, E. Bissaldi, M.S. Briggs, J.M. Burgess, V. Chaplin, V. Connaughton, R. Diehl, G.J. Fishman, G. Fitzpatrick, S. Foley, M. Gibby, M. Giles, A. Goldstein, J. Greiner, D. Gruber, S. Guiriec, A.J. van der Horst, R.M. Kippen, C. Kouveliotou, G. Lichti, L. Lin, S. Mcbrean, R.D. Preece, A. Rau, D. Tierney, C. Wilson-Hodge, The Fermi GBM gamma-ray burst catalog: The first two years, *ApJ* 199 (2012) 18.
- [414] F.-W. Zhang, L. Shao, J.-Z. Yan, D.-M. Wei, Revisiting the long/soft-short/hard classification of gamma-ray bursts in the fermi era, *ApJ* 750 (2012) 88.
- [415] Y. Qin, E.-W. Liang, Y.-F. Liang, S.-X. Yi, L. Lin, B.-B. Zhang, J. Zhang, H.-J. Lü, R.-J. Lu, L.-Z. Lü, B. Zhang, A comprehensive analysis of fermi gamma-ray burst data. iii. energy-dependent  $t_{90}$  distributions of gbm grbs and instrumental selection effect on duration classification, *ApJ* 763 (2013) 15.
- [416] T.M. Koshut, C. Kouveliotou, W.S. Paciesas, J. van Paradijs, G.N. Pendleton, M.S. Briggs, G.J. Fishman, C.A. Meegan, Gamma-Ray Burst Precursor Activity as Observed with BATSE, *ApJ* 452 (1995) 145.
- [417] D. Burlon, G. Ghirlanda, G. Ghisellini, J. Greiner, A. Celotti, Time resolved spectral behavior of bright BATSE precursors, *A&A* 505 (2009) 569–575.
- [418] D. Lazzati, Precursor activity in bright, long BATSE gamma-ray bursts, *MNRAS* 357 (2005) 722–731.
- [419] D. Burlon, G. Ghirlanda, G. Ghisellini, D. Lazzati, L. Nava, M. Nardini, A. Celotti, Precursors in swift gamma ray bursts with redshift, *ApJ* 685 (2008) L19–L22.
- [420] Y.-D. Hu, E.-W. Liang, S.-Q. Xi, F.-K. Peng, R.-J. Lu, L.-Z. Lü, B. Zhang, Internal energy dissipation of gamma-ray bursts observed with swift: Precursors, Prompt Gamma-Rays, Extended Emission, and Late X-Ray Flares, *ApJ* 789 (2014) 145.
- [421] A.M. Beloborodov, On the efficiency of internal shocks in gamma-ray bursts, *ApJ* 539 (2000) L25–L28.
- [422] L. Vetere, E. Massaro, E. Costa, P. Softitta, G. Ventura, Slow and fast components in the X-ray light curves of gamma-ray bursts, *A&A* 447 (2006) 499–513.
- [423] H. Gao, B.-B. Zhang, B. Zhang, Stepwise filter correlation method and evidence of superposed variability components in gamma-ray burst prompt emission light curves, *ApJ* 748 (2012) 134.
- [424] B. Mcbrean, K.J. Hurley, R. Long, L. Metcalfe, Lognormal distributions in gamma-ray bursts and cosmic lightning, *MNRAS* 271 (1994) 662.
- [425] H. Li, E.E. Fenimore, Log-normal distributions in gamma-ray burst time histories, *ApJ* 469 (1996) L115.
- [426] E. Nakar, T. Piran, Time-scales in long gamma-ray bursts, *MNRAS* 331 (2002) 40–44.
- [427] J.P. Norris, J.T. Bonnell, D. Kazanas, J.D. Scargle, J. Hakkila, T.W. Giblin, Long-Lag, Wide-Pulse Gamma-Ray Bursts, *ApJ* 627 (2005) 324–345.
- [428] J.P. Norris, G.F. Marani, J.T. Bonnell, Connection between Energy-dependent Lags and Peak Luminosity in Gamma-Ray Bursts, *ApJ* 534 (2000) 248–257.
- [429] J.P. Norris, Implications of the lag-luminosity relationship for unified gamma-ray burst paradigms, *ApJ* 579 (2002) 386–403.
- [430] J.P. Norris, J.T. Bonnell, Short gamma-ray bursts with extended emission, *ApJ* 643 (2006) 266–275.
- [431] T. Yi, E. Liang, Y. Qin, R. Lu, On the spectral lags of the short gamma-ray bursts, *MNRAS* 367 (2006) 1751–1756.
- [432] M.S. Briggs, D.L. Band, R.M. Kippen, R.D. Preece, C. Kouveliotou, J. van Paradijs, G.H. Share, R.J. Murphy, S.M. Matz, A. Connors, C. Winkler, M.L. McConnell, J.M. Ryan, O.R. Williams, C.A. Young, B. Dingus, J.R. Catelli, R.A.M.J. Wijers, Observations of GRB 990123 by the compton gamma ray observatory, *ApJ* 524 (1999) 82–91.
- [433] R.D. Preece, M.S. Briggs, R.S. Mallozzi, G.N. Pendleton, W.S. Paciesas, D.L. Band, The BATSE gamma-ray burst spectral catalog. I. high time resolution spectroscopy of bright bursts using high energy resolution data, *ApJ* 126 (2000) 19–36.
- [434] Z. Bosnjak, D. Gotz, L. Bouchet, S. Schanne, B. Cordier, The spectral catalogue of INTEGRAL gamma-ray bursts: results of the joint IBIS/SPI spectral analysis, *AA* 561 (2014) 25–39.

- [435] T. Sakamoto, D. Hullinger, G. Sato, R. Yamazaki, L. Barbier, S.D. Barthelmy, J.R. Cummings, E.E. Fenimore, N. Gehrels, H.A. Krimm, D.Q. Lamb, C.B. Markwardt, J.P. Osborne, D.M. Palmer, A.M. Parsons, M. Stamatikos, J. Tueller, Global properties of X-Ray flashes and X-Ray-Rich gamma-ray bursts observed by swift, *ApJ* 679 (2008) 570–586.
- [436] L. Nava, G. Ghirlanda, G. Ghisellini, A. Celotti, Spectral properties of 438 GRBs detected by Fermi/GBM, *A&A* 530 (2011) A21.
- [437] T. Sakamoto, D.Q. Lamb, N. Kawai, A. Yoshida, C. Graziani, E.E. Fenimore, T.Q. Donaghy, M. Matsuoka, M. Suzuki, G. Ricker, J.-L. Atteia, Y. Shirasaki, T. Tamagawa, K. Torii, M. Galassi, J. Doty, R. Vanderspek, G.B. Crew, J. Villasenor, N. Butler, G. Prigozhin, J.G. Jernigan, C. Barraud, M. Boer, J.-P. Dezalay, J.-F. Olive, K. Hurley, A. Levine, G. Monnelly, F. Martel, E. Morgan, S.E. Woosley, T. Cline, J. Braga, R. Manchanda, G. Pizzichini, K. Takagishi, M. Yamauchi, Global characteristics of X-Ray flashes and X-Ray-Rich gamma-ray bursts observed by HETE-2, *ApJ* 629 (2005) 311–327.
- [438] F. Ryde, The cooling behavior of thermal pulses in gamma-ray bursts, *ApJ* 614 (2004) 827–846.
- [439] F. Ryde, A. Pe'er, Quasi-blackbody component and radiative efficiency of the prompt emission of gamma-ray bursts, *ApJ* 702 (2009) 1211–1229.
- [440] G. Ghirlanda, Z. Bošnjak, G. Ghisellini, F. Tavecchio, C. Firmani, Blackbody components in gamma-ray bursts spectra? *MNRAS* 379 (2007) 73–85.
- [441] F. Frontera, L. Amati, R. Farinelli, S. Dichiara, C. Guidorzi, R. Landi, L. Titarchuk, Comptonization signatures in the prompt emission of Gamma Ray Bursts, *ApJ* 779 (2013) 175–193.
- [442] B. Zhang, A. Pe'er, Evidence of an Initially Magnetically Dominated Outflow in GRB 080916C, *ApJ* 700 (2009) L65–L68.
- [443] F. Ryde, M. Axelsson, B.B. Zhang, S. McGlynn, A. Pe'er, C. Lundman, S. Larsson, M. Battelino, B. Zhang, E. Bissaldi, J. Bregeon, M.S. Briggs, J. Chiang, F. de Palma, S. Guiriec, J. Larsson, F. Longo, S. McBreen, N. Omodei, V. Petrosian, R. Preece, A.J. vanderHorst, Identification and properties of the photospheric emission in GRB090902B, *ApJ* 709 (2010) L172–L177.
- [444] M.M. González, B.L. Dingus, Y. Kaneko, R.D. Preece, C.D. Dermer, M.S. Briggs, A  $\gamma$ -ray burst with a high-energy spectral component inconsistent with the synchrotron shock model, *Nature* 424 (2003) 749–751.
- [445] S. Guiriec, V. Connaughton, M.S. Briggs, M. Burgess, F. Ryde, F. Daigne, P. Mészáros, A. Goldstein, J. McEnery, N. Omodei, P.N. Bhat, E. Bissaldi, A. Camero-Arranz, V. Chaplin, R. Diehl, R. Diehl, G. Fishman, S. Foley, M. Gibby, M.M. Giles, J. Greiner, D. Gruber, A. Vonkienlin, M. Kippen, C. Kouveliotou, S. McBreen, C.A. Meegan, W. Paciesas, R. Preece, A. Rau, D. Tierney, A.J. van der Horst, C. Wilson-Hodge, Detection of a thermal spectral component in the prompt emission of GRB 100724B, *ApJ* 727 (2011) L33.
- [446] M. Axelsson, L. Baldini, G. Barbiellini, M.G. Baring, R. Bellazzini, J. Bregeon, M. Brigida, P. Bruel, R. Buehler, G.A. Caliandro, et al., GRB110721A: An extreme peak energy and signatures of the photosphere, *ApJ* 757 (2012) L31.
- [447] S. Guiriec, F. Daigne, R. Hascoët, G. Vianello, F. Ryde, R. Mochkovitch, C. Kouveliotou, S. Xiong, P.N. Bhat, S. Foley, D. Gruber, J.M. Burgess, S. McGlynn, J. McEnery, N. Gehrels, Evidence for a photospheric component in the prompt emission of the short GRB 120323A and its effects on the GRB hardness-luminosity relation, *ApJ* 770 (2013) 32.
- [448] J.M. Burgess, R.D. Preece, F. Ryde, P. Veres, P. Mészáros, V. Connaughton, M. Briggs, A. Pe'er, S. Iyyani, A. Goldstein, M. Axelsson, M.G. Baring, P.N. Bhat, D. Byrne, G. Fitzpatrick, S. Foley, D. Kocevski, N. Omodei, W.S. Paciesas, V. Pelassa, C. Kouveliotou, S. Xiong, H.-F. Yu, B. Zhang, S. Zhu, An observed correlation between thermal and non-thermal emission in gamma-ray bursts, *ApJ* 784 (2014) L43.
- [449] X.-Y. Wang, Z. Li, E. Waxman, P. Mészáros, Nonthermal gamma-Ray/X-Ray flashes from shock breakout in gamma-ray burst-associated supernovae, *ApJ* 664 (2007) 1026–1032.
- [450] J.P. Norris, G.H. Share, D.C. Messina, B.R. Dennis, U.D. Desai, T.L. Cline, S.M. Matz, E.L. Chupp, Spectral evolution of pulse structures in gamma-ray bursts, *ApJ* 301 (1986) 213–219.
- [451] S.V. Golenetskii, E.P. Mazets, R.L. Aptekar, V.N. Ilinskii, Correlation between luminosity and temperature in gamma-ray burst sources, *Nature* 306 (1983) 451–453.
- [452] R.-J. Lu, S.-J. Hou, E.-W. Liang, The  $E_p$ -flux correlation in the rising and decaying phases of gamma-ray burst pulses: evidence for viewing angle effect? *ApJ* 720 (2010) 1146–1154.
- [453] R.-J. Lu, J.-J. Wei, E.-W. Liang, B.-B. Zhang, H.-J. Lü, L.-Z. Lü, W.-H. Lei, B. Zhang, A comprehensive analysis of Fermi Gamma-Ray Burst Data. II.  $E_p$  evolution patterns and implications for the observed spectrum-luminosity relations, *ApJ* 756 (2012) 112.
- [454] G. Ghirlanda, G. Ghisellini, L. Nava, D. Burlon, Spectral evolution of Fermi/GBM short gamma-ray bursts, *MNRAS* 410 (2011) L47–L51.
- [455] J. Hakkila, R.D. Preece, Unification of pulses in long and short gamma-ray bursts: Evidence from pulse properties and their correlations, *ApJ* 740 (2011) 104.
- [456] K. Toma, X. Wu, P. Mészáros, An Up-Scattered cocoon emission model of gamma-ray burst high-energy lags, *ApJ* 707 (2009) 1404–1416.
- [457] S. Razzaque, C.D. Dermer, J.D. Finke, Synchrotron radiation from ultra-high energy protons and the Fermi observations of GRB 080916C, *Open Astron. J.* 3 (2010) 150–155.
- [458] Z. Li, Prompt GeV Emission from Residual Collisions in Gamma-Ray Burst Outflows: Evidence from Fermi Observations of Grb 080916c, *ApJ* 709 (2010) 525–534.
- [459] P. Mészáros, M.J. Rees, GeV emission from collisional magnetized gamma-ray bursts, *ApJ* 733 (2011) L40.
- [460] K. Asano, P. Mészáros, Delayed onset of high-energy emissions in leptonic and hadronic models of gamma-ray bursts, *ApJ* 757 (2012) 115.
- [461] Ž. Bošnjak, P. Kumar, Magnetic jet model for GRBs and the delayed arrival of > 100 MeV photons, *MNRAS* 421 (2012) L39–L43.
- [462] P. Beniamini, D. Guetta, E. Nakar, T. Piran, Limits on the GeV emission from gamma-ray bursts, *MNRAS* 416 (2011) 3089–3097.
- [463] M. Ackermann, M. Ajello, L. Baldini, G. Barbiellini, M.G. Baring, K. Bechtol, R. Bellazzini, R.D. Blandford, E.D. Bloom, E.e.a. Bonamente, Constraining the high-energy emission from gamma-ray bursts with fermi, *ApJ* 754 (2012) 121.
- [464] J. Kakutawa, K. Murase, K. Toma, S. Inoue, R. Yamazaki, K. Ioka, Prospects for detecting gamma-ray bursts at very high energies with the Cherenkov Telescope Array, *MNRAS* 425 (2012) 514–526.
- [465] S. Inoue, J. Granot, P.T. O'Brien, K. Asano, A. Bouvier, A. Carosi, V. Connaughton, M. Garczarczyk, R. Gilmore, J. Hinton, Y. Inoue, K. Ioka, J. Kakutawa, S. Markoff, K. Murase, J.P. Osborne, A.N. Otte, R. Starling, H. Tajima, M. Teshima, K. Toma, S. Wagner, R.A.M.J. Wijers, D.A. Williams, T. Yamamoto, R. Yamazaki, CTA Consortium, Gamma-ray burst science in the era of the cherenkov telescope array, *Astropart. Phys.* 43 (2013) 252–275.
- [466] P. Romano, A. Moretti, P.L. Banat, D.N. Burrows, S. Campana, G. Chincarini, S. Covino, D. Malesani, G. Tagliaferri, S. Kobayashi, B. Zhang, A.D. Falcone, L. Angelini, S. Barthelmy, A.P. Beardmore, M. Capalbi, G. Cusumano, P. Giommi, M.R. Goad, O. Godet, D. Grupe, J.E. Hill, J.A. Kennea, V. Laparola, V. Mangano, P. Mészáros, D.C. Morris, J.A. Nousek, P.T. O'Brien, J.P. Osborne, A. Parsons, M. Perri, C. Pagani, K.L. Page, A.A. Wells, N. Gehrels, X-ray flare in XRF 050406: evidence for prolonged engine activity, *A&A* 450 (2006) 59–68.
- [467] K.L. Page, R. Willingale, J.P. Osborne, B. Zhang, O. Godet, F.E. Marshall, A. Melandri, J.P. Norris, P.T. O'Brien, V. Pal'Shin, E. Rol, P. Romano, R.L.C. Starling, P. Schady, S.A. Yost, S.D. Barthelmy, A.P. Beardmore, G. Cusumano, D.N. Burrows, M. Depasquale, M. Ehle, P.A. Evans, N. Gehrels, M.R. Goad, S. Golenetskii, C. Guidorzi, C. Mundell, M.J. Page, G. Ricker, T. Sakamoto, B.E. Schaefer, M. Stamatikos, E. Troja, M. Ulanov, F. Yuan, H. Ziaeepour, GRB 061121: Broadband spectral evolution through the prompt and afterglow phases of a bright burst, *ApJ* 663 (2007) 1125–1138.
- [468] C.H. Blake, J.S. Bloom, D.L. Starr, E.E. Falco, M. Skrutskie, E.E. Fenimore, G. Duchêne, A. Szentgyorgyi, S. Hornstein, J.X. Prochaska, C. McCabe, A. Ghez, Q. Konopacky, K. Stapelfeldt, K. Hurley, R. Campbell, M. Kassis, F. Chaffee, N. Gehrels, S. Barthelmy, J.R. Cummings, D. Hullinger, H.A. Krimm, C.B. Markwardt, D. Palmer, A. Parsons, K. McLean, J. Tueller, An infrared flash contemporaneous with the  $\gamma$ -rays of GRB 041219a, *Nature* 435 (2005) 181–184.
- [469] W.T. Vestrand, P.R. Wozniak, J.A. Wren, E.E. Fenimore, T. Sakamoto, R.R. White, D. Caspersion, H. Davis, S. Evans, M. Galassi, K.E. McGowan, J.A. Schier, J.W. Asa, S.D. Barthelmy, J.R. Cummings, N. Gehrels, D. Hullinger, H.A. Krimm, C.B. Markwardt, K. McLean, D. Palmer, A. Parsons, J. Tueller, A link between prompt optical and prompt  $\gamma$ -ray emission in  $\gamma$ -ray bursts, *Nature* 435 (2005) 178–180.
- [470] W.T. Vestrand, J.A. Wren, P.R. Wozniak, R. Aptekar, S. Golentsev, V. Pal'Shin, T. Sakamoto, R.R. White, S. Evans, D. Caspersion, E. Fenimore, Energy input and response from prompt and early optical afterglow emission in  $\gamma$ -ray bursts, *Nature* 442 (2006) 172–175.
- [471] G. Beskin, S. Karpov, S. Bondar, G. Greco, A. Guarneri, C. Bartolini, A. Piccioni, Fast optical variability of a naked-eye burst manifestation of the periodic activity of an internal engine, *ApJ* 719 (2010) L10–L14.

- [472] W. Zheng, R.F. Shen, T. Sakamoto, A.P. Beardmore, M. Depasquale, X.F. Wu, J. Gorosabel, Y. Urata, S. Sugita, B.E.A. Zhang, Panchromatic observations of the textbook GRB 110205A: Constraining physical mechanisms of prompt emission and afterglow, *ApJ* 751 (2012) 90.
- [473] A. Cucchiara, S.B. Cenko, J.S. Bloom, A. Melandri, A. Morgan, S. Kobayashi, R.J. Smith, D.A. Perley, W. Li, J.L. Hora, R.L. da Silva, J.X. Prochaska, P.A. Milne, N.R. Butler, B. Cobb, G. Worseck, C.G. Mundell, I.A. Steele, A.V. Filippenko, M. Fumagalli, C.R. Klein, A. Stephens, A. Bluck, R. Mason, Constraining gamma-ray burst emission physics with extensive early-time, multiband follow-up, *ApJ* 743 (2011) 154.
- [474] B. Gendre, J.L. Atteia, M. Boér, F. Colas, A. Klotz, F. Kugel, M. Laas-Bourez, C. Rinner, J. Strajnic, G. Stratta, F. Vachier, GRB 110205A: Anatomy of a long gamma-ray burst, *ApJ* 748 (2012) 59.
- [475] D.A. Perley, S.B. Cenko, A. Corsi, N.R. Tanvir, A.J. Levan, D.A. Kann, E. Sonbas, K. Wiersema, W. Zheng, X.-H. Zhao, J.-M. Bai, L. Chang, K. Clubb, D. Frail, A. Fruchter, E. Göğüş, J. Greiner, T. Güver, A. Horesh, A.V. Filippenko, S. Klose, J. Mao, A.N. Morgan, S. Schmidl, B. Stecklum, M. Tanga, J.-G. Wang, Y.-X. Xin, The Afterglow of GRB 130427A from 1 to  $10^{16}$  GHz, *ApJ* 781 (2014) 37–57.
- [476] R. Shen, B. Zhang, Prompt optical emission and synchrotron self-absorption constraints on emission site of GRBs, *MNRAS* 398 (2009) 1936–1950.
- [477] P. Kumar, A. Panaiteescu, What did we learn from gamma-ray burst 080319B?, *MNRAS* 391 (2008) L19–L23.
- [478] Y. Fan, B. Zhang, D. Wei, Naked-eye optical flash from gamma-ray burst 080319B: Tracing the decaying neutrons in the outflow, *Phys. Rev. D* 79 (2) (2009) 021301.
- [479] Y.W. Yu, X.Y. Wang, Z.G. Dai, Optical and  $\gamma$ -ray Emissions from Internal Forward-Reverse Shocks: Application to GRB 080319B?, *ApJ* 692 (2009) 1662–1668.
- [480] W. Coburn, S.E. Boggs, Polarization of the prompt  $\gamma$ -ray emission from the  $\gamma$ -ray burst of 6 December 2002, *Nature* 423 (2003) 415–417.
- [481] R.E. Rutledge, D.B. Fox, Re-analysis of polarization in the  $\gamma$ -ray flux of GRB 021206, *MNRAS* 350 (2004) 1288–1300.
- [482] D.R. Willis, E.J. Barlow, A.J. Bird, D.J. Clark, A.J. Dean, M.L. McConnell, L. Moran, S.E. Shaw, V. Sguera, Evidence of polarisation in the prompt gamma-ray emission from GRB 930131 and GRB 960924, *A&A* 439 (2005) 245–253.
- [483] E. Kalemci, S.E. Boggs, C. Kouveliotou, M. Finger, M.G. Baring, Search for Polarization from the Prompt Gamma-Ray Emission of GRB 041219a with SPI on INTEGRAL, *ApJ* 169 (2007) 75–82.
- [484] S. McGlynn, D.J. Clark, A.J. Dean, L. Hanlon, S. McBrean, D.R. Willis, B. McBrean, A.J. Bird, S. Foley, Polarisation studies of the prompt gamma-ray emission from GRB 041219a using the spectrometer aboard INTEGRAL, *A&A* 466 (2007) 895–904.
- [485] D. Yonetoku, T. Murakami, S. Gunji, T. Mihara, K. Toma, T. Sakashita, Y. Morihara, T. Takahashi, N. Toukairin, H. Fujimoto, Y. Kodama, S. Kubo, IKAROS Demonstration Team, Detection of gamma-ray polarization in prompt emission of GRB 100826A, *ApJ* 743 (2011) L30.
- [486] D. Yonetoku, T. Murakami, S. Gunji, T. Mihara, K. Toma, Y. Morihara, T. Takahashi, Y. Wakashima, H. Yonemochi, T. Sakashita, N. Toukairin, H. Fujimoto, Y. Kodama, Magnetic structures in gamma-ray burst jets probed by gamma-ray polarization, *ApJ* 758 (2012) L1.
- [487] C.G. Mundell, I.A. Steele, S. Kobayashi, A. Melandri, C. Guidorzi, A. Gomboc, C.J. Mottram, D. Clarke, A. Monfardini, D. Carter, D. Bersier, Early optical polarization of a gamma-ray burst afterglow, *Science* 315 (2007) 1822.
- [488] I.A. Steele, C.G. Mundell, R.J. Smith, S. Kobayashi, C. Guidorzi, Ten per cent polarized optical emission from GRB?090102, *Nature* 462 (2009) 767–769.
- [489] T. Uehara, K. Toma, K.S. Kawabata, S. Chiyonobu, Y. Fukazawa, Y. Ikejiri, T. Inoue, R. Itoh, T. Komatsu, H. Miyamoto, T. Mizuno, O. Nagae, H. Nakaya, T. Ohsugi, K. Sakimoto, M. Sasada, H. Tanaka, M. Uemura, M. Yamashita, T. Yamashita, R. Yamazaki, M. Yoshida, GRB 091208B: First detection of the optical polarization in early forward shock emission of a gamma-ray burst afterglow, *ApJ* 752 (2012) L6.
- [490] C.G. Mundell, D. Kopač, D.M. Arnold, I.A. Steele, A. Gomboc, S. Kobayashi, R.M. Harrison, R.J. Smith, C. Guidorzi, F.J. Virgili, A. Melandri, J. Japelj, Highly polarized light from stable ordered magnetic fields in GRB120308A, *Nature* 504 (2013) 119–121.
- [491] K. Wiersema, S. Covino, K. Toma, A.J. van der Horst, K. Varela, M. Min, J. Greiner, R.L.C. Starling, N.R. Tanvir, R.A.M.J. Wijers, S. Campana, P.A. Curran, Y. Fan, J.P.U. Fynbo, J. Gorosabel, A. Gomboc, D. Gotz, J. Hjorth, Z.P. Jin, S. Kobayashi, C. Kouveliotou, C. Mundell, P.T. O'Brien, E. Pian, A. Rowlinson, D.M. Russell, R. Salvaterra, S. di Serego Alighieri, G. Tagliaferri, S.D. Vergani, J. Elliott, C. Farina, O.E. Hartoog, R. Karjalainen, S. Klose, F. Knust, A.J. Levan, P. Schady, V. Sudilovsky, R. Willingale, Circular polarization in the optical afterglow of GRB 121024A, *Nature* 509 (2014) 201–204.
- [492] F.J. Virgili, E.-W. Liang, B. Zhang, Low-luminosity gamma-ray bursts as a distinct GRB population: a firmer case from multiple criteria constraints, *MNRAS* 392 (2009) 91–103.
- [493] D. Wanderman, T. Piran, The luminosity function and the rate of Swift's gamma-ray bursts, *MNRAS* 406 (2010) 1944–1958.
- [494] A.M. Soderberg, S.R. Kulkarni, E. Nakar, E. Berger, P.B. Cameron, D.B. Fox, D. Frail, A. Gal-Yam, R. Sari, S.B. Cenko, M. Kasliwal, R.A. Chevalier, T. Piran, P.A. Price, B.P. Schmidt, G. Pooley, D.-S. Moon, B.E. Penprase, E. Ofek, A. Rau, N. Gehrels, J.A. Nousek, D.N. Burrows, S.E. Persson, P.J. McCarthy, Relativistic ejecta from X-ray flash XRF 060218 and the rate of cosmic explosions, *Nature* 442 (2006) 1014–1017.
- [495] O. Bromberg, E. Nakar, T. Piran, R. Sari, An observational imprint of the collapsar model of long gamma-ray bursts, *ApJ* 749 (2012) 110.
- [496] D. Guetta, L. Stella, Short  $\gamma$ -ray bursts and gravitational waves from dynamically formed merging binaries, *A&A* 498 (2009) 329–333.
- [497] F.J. Virgili, B. Zhang, P. O'Brien, E. Troja, Are all short-hard gamma-ray bursts produced from mergers of compact stellar objects? *ApJ* 727 (2011) 109.
- [498] D. Wanderman, T. Piran, The rate, luminosity function and time delay of non-Collapsar short GRBs, May 2014, ArXiv e-prints.
- [499] L. Amati, F. Frontera, M. Tavani, J.J.M. in't Zand, A. Antonelli, E. Costa, M. Feroci, C. Guidorzi, J. Heise, N. Masetti, E. Montanari, L. Nicastro, E. Palazzi, E. Pian, L. Piro, P. Soffitta, Intrinsic spectra and energetics of BeppoSAX Gamma-Ray Bursts with known redshifts, *A&A* 390 (2002) 81–89.
- [500] L. Amati, The  $E_{p,i}$ – $E_{iso}$  correlation in gamma-ray bursts: updated observational status, re-analysis and main implications, *MNRAS* 372 (2006) 233–245.
- [501] F. Frontera, L. Amati, C. Guidorzi, R. Landi, J. in't Zand, Broadband time-resolved  $E_{p,i}$  –  $E_{iso}$  correlation in gamma-ray bursts, *ApJ* 754 (2012) 138.
- [502] T. Sakamoto, L. Barbier, S.D. Barthelmy, J.R. Cummings, E.E. Fenimore, N. Gehrels, D. Hullinger, H.A. Krimm, C.B. Markwardt, D.M. Palmer, A.M. Parsons, G. Sato, J. Tueller, Confirmation of the  $E_{peak}^{src}$  –  $E_{iso}$  (Amati) Relation from the X-Ray Flash XRF 050416A Observed by the Swift Burst Alert Telescope, *ApJ* 636 (2006) L73–L76.
- [503] E. Nakar, T. Piran, Outliers to the peak energy-isotropic energy relation in gamma-ray bursts, *MNRAS* 360 (2005) L73–L76.
- [504] D.L. Band, R.D. Preece, Testing the gamma-ray burst energy relationships, *ApJ* 627 (2005) 319–323.
- [505] N.R. Butler, D. Kocevski, J.S. Bloom, J.L. Curtis, A complete catalog of swift gamma-ray burst spectra and durations: Demise of a physical origin for pre-swift high-energy correlations, *ApJ* 671 (2007) 656–677.
- [506] D. Kocevski, On the Origin of High-energy Correlations in Gamma-Ray Bursts, *ApJ* 747 (2012) 146.
- [507] G. Ghirlanda, L. Nava, G. Ghisellini, C. Firmani, J.I. Cabrera, The  $E_{peak}$ – $E_{iso}$  plane of long gamma-ray bursts and selection effects, *MNRAS* 387 (2008) 319–330.
- [508] D.M. Wei, W.H. Gao, Are there cosmological evolution trends on gamma-ray burst features? *MNRAS* 345 (2003) 743–746.
- [509] D. Yonetoku, T. Murakami, T. Nakamura, R. Yamazaki, A.K. Inoue, K. Ioka, Gamma-ray burst formation rate inferred from the spectral peak energy-peak luminosity relation, *ApJ* 609 (2004) 935–951.
- [510] E.W. Liang, Z.G. Dai, X.F. Wu, The Luminosity- $E_p$  Relation within Gamma-Ray Bursts and the Implications for Fireball Models, *ApJ* 606 (2004) L29–L32.
- [511] R. Preece, J.M. Burgess, A. Vonkienlin, P.N. Bhat, M.S. Briggs, D. Byrne, V. Chaplin, W. Cleveland, A.C. Collazzi, V.e.a. Connaughton, The first pulse of the extremely bright GRB 130427A: A test lab for synchrotron shocks, *Science* 343 (2014) 51–54.
- [512] B. Zhang, B. Zhang, F.J. Virgili, E. Liang, D.A. Kann, X. Wu, D. Proga, H. Lv, K. Toma, P. Mészáros, D.N. Burrows, P.W.A. Roming, N. Gehrels, Discerning the Physical Origins of Cosmological Gamma-ray Bursts Based on Multiple Observational Criteria: The Cases of  $z = 6.7$  GRB 080913,  $z = 8.2$  GRB 090423, and Some Short/Hard GRBs, *ApJ* 703 (2009) 1696–1724.
- [513] G. Ghirlanda, L. Nava, G. Ghisellini, A. Celotti, C. Firmani, Short versus long gamma-ray bursts: spectra, energetics, and luminosities, *A&A* 496 (2009) 585–595.
- [514] R. Tsutsui, D. Yonetoku, T. Nakamura, K. Takahashi, Y. Morihara, Possible existence of the  $E_p$ – $L_p$  and  $E_p$ – $E_{iso}$  correlations for short gamma-ray bursts with a factor 5–100 dimmer than those for long gamma-ray bursts, *MNRAS* 431 (2013) 1398–1404.
- [515] G. Ghirlanda, G. Ghisellini, D. Lazzati, The collimation-corrected gamma-ray burst energies correlate with the peak energy of their  $\nu F_\nu$  spectrum, *ApJ* 616 (2004) 331–338.
- [516] D. Kocevski, N. Butler, Gamma-Ray Burst Energetics in the Swift Era, *ApJ* 680 (2008) 531–538.

- [517] E. Liang, B. Zhang, Model-independent Multivariable Gamma-Ray Burst Luminosity Indicator and Its Possible Cosmological Implications, *ApJ* 633 (2005) 611–623.
- [518] C. Firmani, G. Ghisellini, V. Avila-Reese, G. Ghirlanda, Discovery of a tight correlation among the prompt emission properties of long gamma-ray bursts, *MNRAS* 370 (2006) 185–197.
- [519] N. Gehrels, J.P. Norris, S.D. Barthelmy, J. Granot, Y. Kaneko, C. Kouveliotou, C.B. Markwardt, P. Mészáros, E. Nakar, J.A. Nousek, P.T. O'Brien, M. Page, D.M. Palmer, A.M. Parsons, P.W.A. Roming, T. Sakamoto, C.L. Sarazin, P. Schady, M. Stamatikos, S.E. Woosley, A new  $\gamma$ -ray burst classification scheme from GRB060614, *Nature* 444 (2006) 1044–1046.
- [520] T.N. Ukwatta, K.S. Dhuga, M. Stamatikos, C.D. Dermer, T. Sakamoto, E. Sonbas, W.C. Parke, L.C. Maximon, J.T. Linnemann, P.N. Bhat, A. Eskandarian, N. Gehrels, A.U. Abeysekara, K. Tolleson, J.P. Norris, The lag-luminosity relation in the GRB source frame: an investigation with Swift BAT bursts, *MNRAS* 419 (2012) 614–623.
- [521] E.-W. Liang, B.-B. Zhang, M. Stamatikos, B. Zhang, J. Norris, N. Gehrels, J. Zhang, Z.G. Dai, Temporal Profiles and Spectral Lags of XRF 060218, *ApJ* 653 (2006) L81–L84.
- [522] S. McBreen, S. Foley, D. Watson, L. Hanlon, D. Malesani, J.P.U. Fynbo, D.A. Kann, N. Gehrels, S. McGlynn, D. Palmer, The spectral lag of GRB 060505: A likely member of the long-duration class, *ApJ* 677 (2008) L85–L88.
- [523] E.E. Fenimore, E. Ramirez-Ruiz, Redshifts For 220 BATSE gamma-ray bursts determined by variability and the cosmological consequences, 2000, ArXiv Astrophysics e-prints.
- [524] D.E. Reichart, D.Q. Lamb, E.E. Fenimore, E. Ramirez-Ruiz, T.L. Cline, K. Hurley, A possible cepheid-like luminosity estimator for the long gamma-ray bursts, *ApJ* 552 (2001) 57–71.
- [525] C. Guidorzi, F. Frontera, E. Montanari, F. Rossi, L. Amati, A. Gomboc, K. Hurley, C.G. Mundell, The gamma-ray burst variability-peak luminosity correlation: new results, *MNRAS* 363 (2005) 315–325.
- [526] J. Lü, Y.-C. Zou, W.-H. Lei, B. Zhang, Q. Wu, D.-X. Wang, E.-W. Liang, H.-J. Lü, Lorentz-factor-Isotropic-luminosity/Energy Correlations of Gamma-Ray Bursts and Their Interpretation, *ApJ* 751 (2012) 49.
- [527] W.-H. Lei, B. Zhang, E.-W. Liang, Hyperaccreting Black Hole as Gamma-Ray Burst Central Engine. I. Baryon Loading in Gamma-Ray Burst Jets, *ApJ* 765 (2013) 125.
- [528] Y.-Z. Fan, D.-M. Wei, F.-W. Zhang, B.-B. Zhang, The photospheric radiation model for the prompt emission of gamma-ray bursts: interpreting four observed correlations, *ApJ* 755 (2012) L6.
- [529] D. Lazzati, B.J. Morsanyi, R. Margutti, M.C. Begelman, Photospheric emission as the dominant radiation mechanism in long-duration gamma-ray bursts, *ApJ* 765 (2013) 103.
- [530] B.E. Schaefer, Gamma-ray burst hubble diagram to  $z = 4.5$ , *ApJ* 583 (2003) L67–L70.
- [531] Z.G. Dai, E.W. Liang, D. Xu, Constraining  $\Omega_M$  and dark energy with gamma-ray bursts, *ApJ* 612 (2004) L101–L104.
- [532] G. Ghirlanda, G. Ghisellini, D. Lazzati, C. Firmani, Gamma-Ray Bursts: New rulers to measure the universe, *ApJ* 613 (2004) L13–L16.
- [533] D. Xu, Z.G. Dai, E.W. Liang, Can gamma-ray bursts be used to measure cosmology? A further analysis, *ApJ* 633 (2005) 603–610.
- [534] L. Amati, C. Guidorzi, F. Frontera, M. Della Valle, F. Finelli, R. Landi, E. Montanari, Measuring the cosmological parameters with the  $E_{p,i} - E_{iso}$  correlation of gamma-ray bursts, *MNRAS* 391 (2008) 577–584.
- [535] L. Amati, M.D. Valle, Measuring cosmological parameters with gamma ray bursts, *Internat. J. Modern Phys. D* 22 (2013) 30028.
- [536] B.E. Schaefer, The hubble diagram to redshift  $>6$  from 69 gamma-ray bursts, *ApJ* 660 (2007) 16–46.
- [537] E. Liang, B. Zhang, Calibration of gamma-ray burst luminosity indicators, *MNRAS* 369 (2006) L37–L41.
- [538] G. Ghirlanda, G. Ghisellini, C. Firmani, L. Nava, F. Tavecchio, D. Lazzati, Cosmological constraints with GRBs: homogeneous medium vs. wind density profile, *A&A* 452 (2006) 839–844.
- [539] N. Liang, W.K. Xiao, Y. Liu, S.N. Zhang, A Cosmology-Independent Calibration of Gamma-Ray Burst Luminosity Relations and the Hubble Diagram, *ApJ* 685 (2008) 354–360.
- [540] Y. Kodama, D. Yonetoku, T. Murakami, S. Tanabe, R. Tsutsui, T. Nakamura, Gamma-ray bursts between  $z$  of 1.8 and 5.6 suggest that the time variation of the dark energy is small, *MNRAS* 391 (2008) L1–L4.
- [541] V.V. Usov, On the nature of nonthermal radiation from cosmological Gamma-Ray bursters, *MNRAS* 267 (1994) 1035–1038.
- [542] J.I. Katz, Yet Another Model of Gamma-Ray Bursts, *ApJ* 490 (1997) 633–641.
- [543] P. Mészáros, M.J. Rees, Poynting Jets from Black Holes and Cosmological Gamma-Ray Bursts, *ApJ* 482 (1997) L29.
- [544] G. Cavallo, M.J. Rees, A qualitative study of cosmic fireballs and gamma-ray bursts, *MNRAS* 183 (1978) 359–365.
- [545] A. Shemi, T. Piran, The appearance of cosmic fireballs, *ApJ* 365 (1990) L55–L58.
- [546] P. Mészáros, P. Laguna, M.J. Rees, Gasdynamics of relativistically expanding gamma-ray burst sources – Kinematics, energetics, magnetic fields, and efficiency, *ApJ* 415 (1993) 181–190.
- [547] T. Piran, A. Shemi, R. Narayan, Hydrodynamics of relativistic fireballs, *MNRAS* 263 (1993) 861.
- [548] P. Mészáros, E. Ramirez-Ruiz, M.J. Rees, B. Zhang, X-Ray-rich Gamma-Ray Bursts, Photospheres, and Variability, *ApJ* 578 (2002) 812–817.
- [549] S. Kobayashi, T. Piran, R. Sari, Hydrodynamics of a Relativistic Fireball: The Complete Evolution, *ApJ* 513 (1999) 669–678.
- [550] J.L. Racusin, S.R. Oates, P. Schady, D.N. Burrows, M. de Pasquale, D. Donato, N. Gehrels, S. Koch, J. McEney, T. Piran, P. Roming, T. Sakamoto, C. Swenson, E. Troja, V. Vasileiou, F. Virgili, D. Wanderman, B. Zhang, Fermi and swift gamma-ray burst afterglow population studies, *ApJ* 738 (2011) 138.
- [551] N. Gupta, B. Zhang, Diagnosing the site of gamma-ray burst prompt emission with spectral cut-off energy, *MNRAS* 384 (2008) L11–L15.
- [552] J. Granot, J. Cohen-Tanugi, E. do Couto e Silva, Opacity buildup in impulsive relativistic sources, *ApJ* 677 (2008) 92–126.
- [553] Y.-Z. Zou, Y.-Z. Fan, T. Piran, A revised limit of the lorentz factors of gamma-ray bursts with two emitting regions, *ApJ* 726 (2011) L2.
- [554] X.-H. Zhao, Z. Li, J.-M. Bai, The bulk lorentz factors of fermi-lat gamma ray bursts, *ApJ* 726 (2011) 89.
- [555] R. Hascoët, F. Daigne, R. Mochkovitch, V. Vennin, Do Fermi Large Area Telescope observations imply very large Lorentz factors in gamma-ray burst outflows?, *MNRAS* 421 (2012) 525–545.
- [556] E. Nakar, T. Piran, R. Sari, Pure and loaded fireballs in soft gamma-ray repeater giant flares, *ApJ* 635 (2005) 516–521.
- [557] W. Deng, B. Zhang, Low energy spectral index and  $E_p$  evolution of quasi-thermal photosphere emission of gamma-ray bursts, *ApJ* 785 (2014) 112.
- [558] C. Lundman, A. Pe'er, F. Ryde, A theory of photospheric emission from relativistic, collimated outflows, *MNRAS* 428 (2013) 2430–2442.
- [559] Y. Lithwick, R. Sari, Lower Limits on Lorentz Factors in Gamma-Ray Bursts, *ApJ* 555 (2001) 540–545.
- [560] F. Daigne, R. Mochkovitch, The expected thermal precursors of gamma-ray bursts in the internal shock model, *MNRAS* 336 (2002) 1271–1280.
- [561] K. Murase, K. Ioka, Closure relations for  $e^{+/-}$  pair signatures in gamma-ray bursts, *ApJ* 676 (2008) 1123–1129.
- [562] S.A. Yost, H.F. Swan, E.S. Rykoff, F. Aharonian, C.W. Akerlof, A. Alday, M.C.B. Ashley, S. Barthelmy, D. Burrows, E.A. Depoy, Exploring broadband GRB behavior during  $\gamma$ -ray emission, *ApJ* 657 (2007) 925–941.
- [563] D. Kopač, S. Kobayashi, A. Gomboc, J. Japelj, C.G. Mundell, C. Guidorzi, A. Melandri, D. Bersier, Z. Cano, R.J. Smith, I.A. Steele, F.J. Virgili, GRB 090727 and Gamma-Ray Bursts with Early-time Optical Emission, *ApJ* 772 (2013) 73.
- [564] M. Lyutikov, Did Swift measure gamma-ray burst prompt emission radii?, *MNRAS* 369 (2006) L5–L8.
- [565] D. Lazzati, M.C. Begelman, Thick Fireballs and the Steep Decay in the Early X-Ray Afterglow of Gamma-Ray Bursts, *ApJ* 641 (2006) 972–977.
- [566] R. Hascoët, F. Daigne, R. Mochkovitch, Accounting for the XRT early steep decay in models of the prompt gamma-ray burst emission, *A&A* 542 (2012) L29.
- [567] R. Willingale, F. Genet, J. Granot, P.T. O'Brien, The spectral-temporal properties of the prompt pulses and rapid decay phase of gamma-ray bursts, *MNRAS* 403 (2010) 1296–1316.
- [568] P. Kumar, E. McMahon, A. Panaiteescu, R. Willingale, P. O'Brien, D. Burrows, J. Cummings, N. Gehrels, S. Holland, S.B. Pandey, D. van den Berk, S. Zane, The nature of the outflow in gamma-ray bursts, *MNRAS* 376 (2007) L57–L61.
- [569] S. Kobayashi, T. Piran, R. Sari, Can Internal Shocks Produce the Variability in Gamma-Ray Bursts?, *ApJ* 490 (1997) 92.

- [570] P. Kumar, Gamma-Ray Burst Energetics, *ApJ* 523 (1999) L113–L116.
- [571] A. Panaiteescu, M. Spada, P. Mészáros, Power density spectra of gamma-ray bursts in the internal shock model, *ApJ* 522 (1999) L105–L108.
- [572] S. Kobayashi, R. Sari, Ultraefficient Internal Shocks, *ApJ* 551 (2001) 934–939.
- [573] R. Sari, R. Narayan, T. Piran, Cooling timescales and temporal structure of gamma-ray bursts, *ApJ* 473 (1996) 204.
- [574] G. Ghisellini, A. Celotti, D. Lazzati, Constraints on the emission mechanisms of gamma-ray bursts, *MNRAS* 313 (2000) L1–L5.
- [575] P. Kumar, E. McMahon, A general scheme for modelling  $\gamma$ -ray burst prompt emission, *MNRAS* 384 (2008) 33–63.
- [576] P. Beniamini, T. Piran, Constraints on the synchrotron emission mechanism in gamma-ray bursts, *ApJ* 769 (2013) 69.
- [577] K. Murase, K. Asano, T. Terasawa, P. Mészáros, The role of stochastic acceleration in the prompt emission of gamma-ray bursts: Application to hadronic injection, *ApJ* 746 (2012) 164.
- [578] T. Piran, R. Sari, Y.-C. Zou, Observational limits on inverse Compton processes in gamma-ray bursts, *MNRAS* 393 (2009) 1107–1113.
- [579] B. Zhang, P. Mészáros, An analysis of gamma-ray burst spectral break models, *ApJ* 581 (2002) 1236–1247.
- [580] L. Resmi, B. Zhang, Gamma-ray burst prompt emission variability in synchrotron and synchrotron self-Compton light curves, *MNRAS* 426 (2012) 1385–1395.
- [581] Z. Li, E. Waxman, Prompt Optical Emission from Residual Collisions in Gamma-Ray Burst Outflows, *ApJ* 674 (2008) L65–L68.
- [582] Y. Zou, T. Piran, R. Sari, Clues from the prompt emission of GRB 080319B, *ApJ* 692 (2009) L92–L95.
- [583] E.M. Rossi, A.M. Beloborodov, M.J. Rees, Neutron-loaded outflows in gamma-ray bursts, *MNRAS* 369 (2006) 1797–1807.
- [584] I. Vurm, A.M. Beloborodov, J. Poutanen, Gamma-ray bursts from magnetized collisionally heated jets, *ApJ* 738 (2011) 77.
- [585] J.I. Katz, Nonrelativistic Compton scattering and models of quasars, *ApJ* 206 (1976) 910–916.
- [586] S.L. Shapiro, A.P. Lightman, D.M. Eardley, A two-temperature accretion disk model for Cygnus X-1 – Structure and spectrum, *ApJ* 204 (1976) 187–199.
- [587] R.A. Sunyaev, L.G. Titarchuk, Comptonization of X-rays in plasma clouds – Typical radiation spectra, *A&A* 86 (1980) 121–138.
- [588] G. Ghisellini, Radiative Processes in High Energy Astrophysics, Feb. 2012, ArXiv e-prints.
- [589] D. Eichler, A. Levinson, A compact fireball model of gamma-ray bursts, *ApJ* 529 (2000) 146–150.
- [590] M.J. Rees, P. Mészáros, Dissipative photosphere models of gamma-ray bursts and X-Ray flashes, *ApJ* 628 (2005) 847–852.
- [591] D. Lazzati, B.J. Morsony, M.C. Begelman, Very high efficiency photospheric emission in long-duration  $\gamma$ -ray bursts, *ApJ* 700 (2009) L47–L50.
- [592] H. Ito, S. Nagataki, M. Ono, S.-H. Lee, J. Mao, S. Yamada, A. Pe'er, A. Mizuta, S. Harikae, Photospheric emission from stratified jets, *ApJ* 777 (2013) 62–78.
- [593] A.M. Beloborodov, Regulation of the spectral peak in gamma-ray bursts, *ApJ* 764 (2013) 157.
- [594] B. Zhang, R.-J. Lu, E.-W. Liang, X.-F. Wu, GRB 110721A: Photosphere "Death Line" and the physical origin of the GRB band function, *ApJ* 758 (2012) L34.
- [595] P. Veres, B.-B. Zhang, P. Mészáros, The extremely high peak energy of GRB 110721A in the context of a dissipative photosphere synchrotron emission model, *ApJ* 761 (2012) L18.
- [596] I. Vurm, Y. Lyubarsky, T. Piran, On thermalization in gamma-ray burst jets and the peak energies of photospheric spectra, *ApJ* 764 (2013) 143.
- [597] K. Asano, P. Mészáros, Photon and neutrino spectra of time-dependent photospheric models of gamma-ray bursts, *JCAP* 9 (2013) 8.
- [598] M. Böttcher, C.D. Dermer, High-energy gamma rays from ultra-high-energy cosmic-ray protons in gamma-ray bursts, *ApJ* 499 (1998) L131.
- [599] T. Totani, TEV Burst of gamma-ray bursts and ultra-high-energy cosmic rays, *ApJ* 509 (1998) L81–L84.
- [600] F.A. Aharonian, TeV gamma rays from BL Lac objects due to synchrotron radiation of extremely high energy protons, *New Astron.* 5 (2000) 377–395.
- [601] A. Mücke, R.J. Protheroe, R. Engel, J.P. Rachen, T. Stanev, BL Lac objects in the synchrotron proton blazar model, *Astropart. Phys.* 18 (2003) 593–613.
- [602] A. Reimer, R.J. Protheroe, A.-C. Donea, M87 – a misaligned synchrotron-proton blazar?, *New Astron. Rev.* 48 (2004) 411–413.
- [603] K. Asano, S. Inoue, P. Mészáros, Prompt high-energy emission from proton-dominated gamma-ray bursts, *ApJ* 699 (2009) 953–957.
- [604] P. Crumley, P. Kumar, Hadronic models for Large Area Telescope prompt emission observed in Fermi gamma-ray bursts, *MNRAS* 429 (2013) 3238–3251.
- [605] J. Greiner, C. Clemens, T. Kröhler, A. Vonkienlin, A. Rau, R. Sari, D.B. Fox, N. Kawai, P. Afonso, M. Ajello, E. Berger, S.B. Cenko, A. Cucchiara, R. Filgas, S. Klose, A. Küpcü Yıldız, G.G. Lichti, S. Löw, S. McBreen, T. Nagayama, A. Rossi, S. Sato, G. Szokoly, A. Yıldız, X.-L. Zhang, The redshift and afterglow of the extremely energetic gamma-ray burst GRB 080916C, *A&A* 498 (2009) 89–94.
- [606] R. Abbasi, Y. Abdou, T. Abu-Zayyad, M. Ackermann, J. Adams, J.A. Aguilar, M. Ahlers, D. Altmann, K. Andeen, J. Auffenberg, et al., An absence of neutrinos associated with cosmic-ray acceleration in  $\gamma$ -ray bursts, *Nature* 484 (2012) 351–354.
- [607] IceCube Collaboration: M.G. Aartsen, et al., 2014, ArXiv:1412.6510.
- [608] H.A. Bethe, L.C. Maximon, *Phys. Rev.* 93 (1954) 768.
- [609] J.P. Rachen, Interaction Processes and Statistical Properties of the Propagation of Cosmic Rays in Photon Backgrounds (Ph.D. thesis), University of Bonn, 1996, p. 159.
- [610] S.S. Komissarov, Time-dependent, force-free, degenerate electrodynamics, *MNRAS* 336 (2002) 759–766.
- [611] Z.-Y. Li, T. Chiueh, M.C. Begelman, Electromagnetically driven relativistic jets – A class of self-similar solutions, *ApJ* 394 (1992) 459–471.
- [612] N. Vlahakis, A. Königl, Relativistic magnetohydrodynamics with application to gamma-ray burst outflows. i. theory and semianalytic Trans-Alfvénic solutions, *ApJ* 596 (2003) 1080–1103.
- [613] N. Vlahakis, F. Peng, A. Königl, Neutron-rich hydromagnetic outflows in gamma-ray burst sources, *ApJ* 594 (2003) L23–L26.
- [614] V.S. Beskin, E.E. Nokhrina, The effective acceleration of plasma outflow in the paraboloidal magnetic field, *MNRAS* 367 (2006) 375–386.
- [615] Y.E. Lyubarsky, Transformation of the Poynting flux into kinetic energy in relativistic jets, *MNRAS* 402 (2010) 353–361.
- [616] S. Heinz, M.C. Begelman, Jet acceleration by tangled magnetic fields, *ApJ* 535 (2000) 104–117.
- [617] S.S. Komissarov, Direct numerical simulations of the Blandford–Znajek effect, *MNRAS* 326 (2001) L41–L44.
- [618] S.S. Komissarov, Electrodynamics of black hole magnetospheres, *MNRAS* 350 (2004) 427–448.
- [619] J.C. McKinney, General relativistic force-free electrodynamics: a new code and applications to black hole magnetospheres, *MNRAS* 367 (2006) 1797–1807.
- [620] S.S. Komissarov, Multidimensional numerical scheme for resistive relativistic magnetohydrodynamics, *MNRAS* 382 (2007) 995–1004.
- [621] S.S. Komissarov, M.V. Barkov, N. Vlahakis, A. Königl, Magnetic acceleration of relativistic active galactic nucleus jets, *MNRAS* 380 (2007) 51–70.
- [622] J.C. McKinney, R. Narayan, Disc-jet coupling in black hole accretion systems – I. General relativistic magnetohydrodynamical models, *MNRAS* 375 (2007) 513–530.
- [623] A. Tchekhovskoy, J.C. McKinney, R. Narayan, Simulations of ultrarelativistic magnetodynamic jets from gamma-ray burst engines, *MNRAS* 388 (2008) 551–572.
- [624] S.S. Komissarov, N. Vlahakis, A. Königl, M.V. Barkov, Magnetic acceleration of ultrarelativistic jets in gamma-ray burst sources, *MNRAS* 394 (2009) 1182–1212.
- [625] J.C. McKinney, R.D. Blandford, Stability of relativistic jets from rotating, accreting black holes via fully three-dimensional magnetohydrodynamic simulations, *MNRAS* 394 (2009) L126–L130.
- [626] A. Tchekhovskoy, J.C. McKinney, R. Narayan, Efficiency of magnetic to kinetic energy conversion in a monopole magnetosphere, *ApJ* 699 (2009) 1789–1808.
- [627] A. Tchekhovskoy, R. Narayan, J.C. McKinney, Magnetohydrodynamic simulations of gamma-ray burst jets: Beyond the progenitor star, *New Astron.* 15 (2010) 749–754.
- [628] P. Goldreich, W.H. Julian, Stellar winds, *ApJ* 160 (1970) 971.
- [629] S.S. Komissarov, N. Vlahakis, A. Königl, Rarefaction acceleration of ultrarelativistic magnetized jets in gamma-ray burst sources, *MNRAS* 407 (2010) 17–28.
- [630] J. Contopoulos, A simple type of magnetically driven jets: an astrophysical plasma gun, *ApJ* 450 (1995) 616.
- [631] J. Granot, S.S. Komissarov, A. Spitkovsky, Impulsive acceleration of strongly magnetized relativistic flows, *MNRAS* 411 (2011) 1323–1353.
- [632] G. Drenkhahn, H.C. Spruit, Efficient acceleration and radiation in Poynting flux powered GRB outflows, *A&A* 391 (2002) 1141–1153.

- [633] G. Drenkhahn, Acceleration of GRB outflows by Poynting flux dissipation, *A&A* 387 (2002) 714–724.
- [634] H.R. Takahashi, T. Kudoh, Y. Masada, J. Matsumoto, Scaling law of relativistic Sweet–Parker-type magnetic reconnection, *ApJ* 739 (2011) L53.
- [635] J.C. McKinney, D.A. Uzdensky, A reconnection switch to trigger gamma-ray burst jet dissipation, *MNRAS* 419 (2012) 573–607.
- [636] P.A. Sweet, The neutral point theory of solar flares, in: B. Lehnert (Ed.), Electromagnetic Phenomena in Cosmical Physics, in: IAU Symposium, vol. 6, 1958, pp. 123–+.
- [637] E.N. Parker, Sweet's mechanism for merging magnetic fields in conducting fluids, *JGR* 62 (1957) 509–520.
- [638] M. Lyutikov, D. Uzdensky, Dynamics of relativistic reconnection, *ApJ* 589 (2003) 893–901.
- [639] Y.E. Lyubarsky, On the relativistic magnetic reconnection, *MNRAS* 358 (2005) 113–119.
- [640] H.E. Petschek, Magnetic Field Annihilation, vol. 50, NASA Special Publication, 1964, p. 425.
- [641] D.A. Uzdensky, R.M. Kulsrud, Two-dimensional numerical simulation of the resistive reconnection layer, *Phys. Plasmas* 7 (2000) 4018–4030.
- [642] N.F. Loureiro, A.A. Schekochihin, S.C. Cowley, Instability of current sheets and formation of plasmoid chains, *Phys. Plasmas* 14 (10) (2007) 100703.
- [643] R. Samtaney, N.F. Loureiro, D.A. Uzdensky, A.A. Schekochihin, S.C. Cowley, Formation of plasmoid chains in magnetic reconnection, *Phys. Rev. Lett.* 103 (10) (2009) 105004.
- [644] A. Lazarian, E.T. Vishniac, Reconnection in a weakly Stochastic field, *ApJ* 517 (1999) 700–718.
- [645] G. Kowal, A. Lazarian, E.T. Vishniac, K. Otmianowska-Mazur, Numerical Tests of Fast Reconnection in Weakly Stochastic Magnetic Fields, *ApJ* 700 (2009) 63–85.
- [646] J. Zrake, A.I. MacFadyen, Numerical simulations of driven relativistic magnetohydrodynamic turbulence, *ApJ* 744 (2012) 32.
- [647] D. Giannios, UHECRs from magnetic reconnection in relativistic jets, *MNRAS* 408 (2010) L46–L50.
- [648] M. Hesse, S. Zenitani, Dissipation in relativistic pair-plasma reconnection, *Phys. Plasmas* 14 (11) (2007) 112102.
- [649] D.A. Uzdensky, B. Cerutti, M.C. Begelman, Reconnection-powered Linear Accelerator and Gamma-Ray Flares in the Crab Nebula, *ApJ* 737 (2011) L40.
- [650] N. Bessho, A. Bhattacharjee, Fast magnetic reconnection and particle acceleration in relativistic low-density electron-positron plasmas without guide field, *ApJ* 750 (2012) 129.
- [651] S. Zenitani, M. Hoshino, The generation of nonthermal particles in the relativistic magnetic reconnection of pair plasmas, *ApJ* 562 (2001) L63–L66.
- [652] S. Zenitani, M. Hoshino, Particle acceleration and magnetic dissipation in relativistic current sheet of pair plasmas, *ApJ* 670 (2007) 702–726.
- [653] S. Zenitani, M. Hoshino, The role of the guide field in relativistic pair plasma reconnection, *ApJ* 677 (2008) 530–544.
- [654] C.H. Jaroschek, R.A. Treumann, H. Lesch, M. Scholer, Fast reconnection in relativistic pair plasmas: Analysis of particle acceleration in self-consistent full particle simulations, *Phys. Plasmas* 11 (2004) 1151–1163.
- [655] N. Bessho, A. Bhattacharjee, Fast collisionless reconnection in electron-positron plasmas, *Phys. Plasmas* 14 (5) (2007) 056503.
- [656] J. Pétri, Y. Lyubarsky, Magnetic reconnection at the termination shock in a striped pulsar wind, *A&A* 473 (2007) 683–700.
- [657] W. Liu, H. Li, L. Yin, B.J. Albright, K.J. Bowers, E.P. Liang, Particle energization in 3D magnetic reconnection of relativistic pair plasmas, *Phys. Plasmas* 18 (5) (2011) 052105.
- [658] L. Sironi, A. Spitkovsky, Particle acceleration at the termination shock of striped pulsar winds, *Internat. J. Modern Phys. Conf. Ser.* 8 (2012) 144.
- [659] D. Kagan, M. Milosavljević, A. Spitkovsky, A Flux rope network and particle acceleration in Three-dimensional relativistic magnetic reconnection, *ApJ* 774 (2013) 41.
- [660] E.G. Zweibel, M. Yamada, Magnetic reconnection in astrophysical and laboratory plasmas, *Ann. Rev. Astron. Astrophys.* 47 (2009) 291–332.
- [661] J.F. Drake, M. Swisdak, H. Che, M.A. Shay, Electron acceleration from contracting magnetic islands during reconnection, *Nature* 443 (2006) 553–556.
- [662] M.M. Romanova, R.V.E. Lovelace, Magnetic field, reconnection, and particle acceleration in extragalactic jets, *A&A* 262 (1992) 26–36.
- [663] D.A. Larabee, R.V.E. Lovelace, M.M. Romanova, Lepton acceleration by relativistic collisionless magnetic reconnection, *ApJ* 586 (2003) 72–78.
- [664] B. Cerutti, G.R. Werner, D.A. Uzdensky, M.C. Begelman, Beaming and rapid variability of high-energy radiation from relativistic pair plasma reconnection, *ApJ* 754 (2012) L33.
- [665] B. Cerutti, G.R. Werner, D.A. Uzdensky, M.C. Begelman, Three-dimensional relativistic pair plasma reconnection with radiative feedback in the crab nebula, *ApJ* 782 (2014) 104.
- [666] D. Lazzati, G. Ghisellini, A. Celotti, M.J. Rees, Compton-dragged gamma-ray bursts associated with supernovae, *ApJ* 529 (2000) L17–L20.
- [667] A.E. Broderick, Supernovae in helium star–compact object binaries: a possible  $\gamma$ -ray burst mechanism, *MNRAS* 361 (2005) 955–964.
- [668] A. Dar, A. de Rújula, Towards a complete theory of gamma-ray bursts, *Physics Reports* 405 (2004) 203–278.
- [669] S. Dado, A. Dar, A. Deružula, The Discovery of a Hyperluminous Source in the Radio Afterglow of GRB 030329, 2004. ArXiv Astrophysics e-prints.
- [670] R. Ruffini, C.L. Bianco, F. Fraschetti, S.-S. Xue, P. Chardonnet, Relative spacetime transformations in gamma-ray bursts, *ApJ* 555 (2001) L107–L111.
- [671] M.G. Bernardini, C.L. Bianco, L. Caito, M.G. Dainotti, R. Guida, R. Ruffini, GRB 970228 and a class of GRBs with an initial spikelike emission, *A&A* 474 (2007) L13–L16.
- [672] R. Ruffini, C.L. Bianco, F. Fraschetti, S.-S. Xue, P. Chardonnet, On the interpretation of the burst structure of gamma-ray bursts, *ApJ* 555 (2001) L113–L116.
- [673] C.L. Bianco, R. Ruffini, Exact versus Approximate Solutions in Gamma-Ray Burst Afterglows, *ApJ* 633 (2005) L13–L16.
- [674] R. Ruffini, G. Vereshchagin, S.-S. Xue, Electron–positron pairs in physics and astrophysics: From heavy nuclei to black holes, *Physics Reports* 487 (2010) 1–140.
- [675] W.H. Lei, D.X. Wang, B.P. Gong, C.Y. Huang, A model of the light curves of gamma-ray bursts, *A&A* 468 (2007) 563–569.
- [676] G.E. Romero, M.M. Reynoso, H.R. Christiansen, Gravitational radiation from precessing accretion disks in gamma-ray bursts, *A&A* 524 (2010) A4.
- [677] T. Liu, E.-W. Liang, W.-M. Gu, X.-H. Zhao, Z.-G. Dai, J.-F. Lu, Jet precession driven by neutrino-cooled disk for gamma-ray bursts, *A&A* 516 (2010) A16.
- [678] D. Fargion, GRBs by thin persistent precessing lepton jets: the long life GRB110328 and the Neutrino signal, *Mem. Soc. Astron. It.* 83 (2012) 312.
- [679] K. Ioka, Y. Ohira, N. Kawanaka, A. Mizuta, Gamma-Ray Burst without Baryonic and Magnetic Load?, *Progr. Theoret. Phys.* 126 (2011) 555–564.
- [680] L. Titarchuk, R. Farinelli, F. Frontera, L. Amati, An upscattering spectral formation model for the prompt emission of gamma-ray bursts, *ApJ* 752 (2012) 116.
- [681] D. Kazanas, M. Georganopoulos, A. Mastichiadis, The “Supercritical Pile” Model for Gamma-Ray Bursts: Getting the  $\nu F$  Peak at 1 MeV, *ApJ* 578 (2002) L15–L18.
- [682] M. Ruffert, H.-T. Janka, Gamma-ray bursts from accreting black holes in neutron star mergers, *A&A* 344 (1999) 573–606.
- [683] S. Rosswog, E. Ramirez-Ruiz, M.B. Davies, High-resolution calculations of merging neutron stars – III. Gamma-ray bursts, *MNRAS* 345 (2003) 1077–1090.
- [684] M.A. Aloy, H.-T. Janka, E. Müller, Relativistic outflows from remnants of compact object mergers and their viability for short gamma-ray bursts, *A&A* 436 (2005) 273–311.
- [685] W.H. Lee, E. Ramirez-Ruiz, The progenitors of short gamma-ray bursts, *New J. Phys.* 9 (2007) 17.
- [686] L. Baiotti, B. Giacomazzo, L. Rezzolla, Accurate evolutions of inspiralling neutron-star binaries: Prompt and delayed collapse to a black hole, *Phys. Rev. D* 78 (8) (2008) 084033.
- [687] L. Dessart, C. Ott, A. Burrows, S. Rosswog, E. Livne, Neutrino signatures and the neutrino-driven wind in Binary Neutron Star Mergers, *ApJ* 690 (2009) 1681–1705.
- [688] L. Rezzolla, B. Giacomazzo, L. Baiotti, J. Granot, C. Kouveliotou, M.A. Aloy, The missing link: Merging neutron stars naturally produce jet-like structures and can power short gamma-ray bursts, *ApJ* 732 (2011) L6.
- [689] R. Popham, S.E. Woosley, C. Fryer, Hyperaccreting black holes and gamma-ray bursts, *ApJ* 518 (1999) 356–374.
- [690] H.K. Lee, R.A.M.J. Wijers, G.E. Brown, The Blandford–Znajek process as a central engine for a gamma-ray burst, *Physics Reports* 325 (2000) 83–114.
- [691] R. Narayan, T. Piran, P. Kumar, Accretion models of gamma-ray bursts, *ApJ* 557 (2001) 949–957.
- [692] T. Di Matteo, R. Perna, R. Narayan, Neutrino Trapping and Accretion Models for Gamma-Ray Bursts, *ApJ* 579 (2002) 706–715.
- [693] D.X. Wang, K. Xiao, W.H. Lei, Evolution characteristics of the central black hole of a magnetized accretion disc, *MNRAS* 335 (2002) 655–664.
- [694] J.C. McKinney, Total and Jet Blandford–Znajek Power in the Presence of an Accretion Disk, *ApJ* 630 (2005) L5–L8.

- [695] D.A. Uzdensky, A.I. Macfadyen, Stellar explosions by magnetic towers, *ApJ* 647 (2006) 1192–1212.
- [696] W.-X. Chen, A.M. Beloborodov, Neutrino-cooled accretion disks around spinning black holes, *ApJ* 657 (2007) 383–399.
- [697] W.H. Lei, D.X. Wang, L. Zhang, Z.M. Gan, Y.C. Zou, Y. Xie, Magnetically torqued neutrino-dominated accretion flows for gamma-ray bursts, *ApJ* 700 (2009) 1970–1976.
- [698] F. Yuan, B. Zhang, Episodic jets as the central engine of gamma-ray bursts, *ApJ* 757 (2012) 56.
- [699] S. Nagataki, Development of a general relativistic magnetohydrodynamic code and its application to the central engine of long gamma-ray bursts, *ApJ* 704 (2009) 937–950.
- [700] S. Nagataki, Rotating black holes as central engines of long gamma-ray bursts: faster is better, *Pub. Astro. Soc. of Japan* 63 (2011) 1243–1249.
- [701] W. Klužniak, M. Ruderman, The central engine of Gamma-Ray bursters, *ApJ* 505 (1998) L113–L117.
- [702] J.C. Wheeler, I. Yi, P. Höflich, L. Wang, Asymmetric supernovae, pulsars, magnetars, and gamma-ray bursts, *ApJ* 537 (2000) 810–823.
- [703] Z.G. Dai, X.Y. Wang, X.F. Wu, B. Zhang, X-ray flares from postmerger millisecond pulsars, *Science* 311 (2006) 1127–1129.
- [704] N. Bucciantini, E. Quataert, J. Arons, B.D. Metzger, T.A. Thompson, Relativistic jets and long-duration gamma-ray bursts from the birth of magnetars, *MNRAS* 383 (2008) L25–L29.
- [705] N. Bucciantini, E. Quataert, B.D. Metzger, T.A. Thompson, J. Arons, L. Del Zanna, Magnetized relativistic jets and long-duration GRBs from magnetar spin-down during core-collapse supernovae, *MNRAS* 396 (2009) 2038–2050.
- [706] R.D. Blandford, R.L. Znajek, Electromagnetic extraction of energy from Kerr black holes, *MNRAS* 179 (1977) 433–456.
- [707] K. Kohri, S. Mineshige, Can Neutrino-cooled Accretion Disks Be an Origin of Gamma-Ray Bursts?, *ApJ* 577 (2002) 311–321.
- [708] K. Kohri, R. Narayan, T. Piran, Neutrino-dominated Accretion and Supernovae, *ApJ* 629 (2005) 341–361.
- [709] I. Zalamea, A.M. Beloborodov, Neutrino heating near hyper-accreting black holes, *MNRAS* 410 (2011) 2302–2308.
- [710] Y.-Z. Qian, S.E. Woosley, Nucleosynthesis in neutrino-driven winds. I. the physical conditions, *ApJ* 471 (1996) 331.
- [711] L.-X. Li, Toy model for the Blandford–Znajek mechanism, *Phys. Rev. D* 61 (8) (2000) 084016.
- [712] A. Tchekhovskoy, J.C. McKinney, Prograde and retrograde black holes: whose jet is more powerful? *MNRAS* 423 (2012) L55–L59.
- [713] A. Levinson, D. Eichler, Baryon loading of gamma-ray burst by neutron pickup, *ApJ* 594 (2003) L19–L22.
- [714] D. Lynden-Bell, Magnetic collimation by accretion discs of quasars and stars, *MNRAS* 279 (1996) 389–401.
- [715] B.J. Morsany, D. Lazzati, M.C. Begelman, Temporal and angular properties of gamma-ray burst jets emerging from massive stars, *ApJ* 665 (2007) 569–598.
- [716] M.A. Aloy, E. Müller, J.M. Ibáñez, J.M. Martí, A. Macfadyen, Relativistic jets from collapsars, *ApJ* 531 (2000) L119–L122.
- [717] P. Mészáros, M.J. Rees, Collapsar Jets, Bubbles, and Fe Lines, *ApJ* 556 (2001) L37–L40.
- [718] C.D. Matzner, Supernova hosts for gamma-ray burst jets: dynamical constraints, *MNRAS* 345 (2003) 575–589.
- [719] O. Bromberg, E. Nakar, T. Piran, R. Sari, The propagation of relativistic jets in external media, *ApJ* 740 (2011) 100.
- [720] W. Zhang, S.E. Woosley, A.I. Macfadyen, Relativistic jets in collapsars, *ApJ* 586 (2003) 356–371.
- [721] A. Levinson, M.C. Begelman, Collimation and confinement of magnetic jets by external media, *ApJ* 764 (2013) 148.
- [722] O. Bromberg, J. Granot, Y. Lyubarsky, T. Piran, The dynamics of a highly magnetized jet propagating inside a star, *MNRAS* 443 (2014) 1532–1548.
- [723] H. Nagakura, K. Hotokezaka, Y. Sekiguchi, M. Shibata, K. Ioka, Jet collimation in the ejecta of double neutron star mergers: A new canonical picture of short gamma-ray bursts, *ApJ* 784 (2014) L28.
- [724] H.-J. Lü, B. Zhang, A Test of the Millisecond Magnetar Central Engine Model of Gamma-Ray Bursts with Swift Data, *ApJ* 785 (2014) 74.
- [725] K. Kiuchi, K. Kyutoku, M. Shibata, Three-dimensional evolution of differentially rotating magnetized neutron stars, *Phys. Rev. D* 86 (6) (2012) 064008.
- [726] D.M. Siegel, R. Ciolfi, L. Rezzolla, Magnetically driven winds from differentially rotating neutron stars and X-Ray afterglows of short gamma-ray bursts, *ApJ* 785 (2014) L6.
- [727] M.A. Ruderman, L. Tao, W. Klužniak, A central engine for cosmic gamma-ray burst sources, *ApJ* 542 (2000) 243–250.
- [728] Z.G. Dai, Relativistic wind bubbles and afterglow signatures, *ApJ* 606 (2004) 1000–1005.
- [729] S. Dall’osso, G. Stratta, D. Guetta, S. Covino, G. De Cesare, L. Stella, Gamma-ray bursts afterglows with energy injection from a spinning down neutron star, *A&A* 526 (2011) A121.
- [730] J. Granot, P. Kumar, Distribution of gamma-ray burst ejecta energy with Lorentz factor, *MNRAS* 366 (2006) L13–L16.
- [731] A. Rowlinson, P.T. O’Brien, N.R. Tanvir, B. Zhang, P.A. Evans, N. Lyons, A.J. Levan, R. Willingale, K.L. Page, O. Onal, D.N. Burrows, A.P. Beardmore, T.N. Ukwatta, E. Berger, J. Hjorth, A.S. Fruchter, R.L. Tunnicliffe, D.B. Fox, A. Cucchiara, The unusual X-ray emission of the short Swift GRB 090515: evidence for the formation of a magnetar?, *MNRAS* 409 (2010) 531–540.
- [732] A. Rowlinson, P.T. O’Brien, B.D. Metzger, N.R. Tanvir, A.J. Levan, Signatures of magnetar central engines in short GRB light curves, *MNRAS* 430 (2013) 1061–1087.
- [733] W.-H. Gao, Y.-Z. Fan, Short-living supermassive magnetar model for the early X-ray Flares following short GRBs, *Chin. J. Astron. Astrophys.* 6 (2006) 513–516.
- [734] Y.-Z. Fan, D. Xu, The X-ray afterglow flat segment in short GRB 051221A: Energy injection from a millisecond magnetar? *MNRAS* 372 (2006) L19–L22.
- [735] B.D. Metzger, E. Quataert, T.A. Thompson, Short-duration gamma-ray bursts with extended emission from protomagnetar spin-down, *MNRAS* 385 (2008) 1455–1460.
- [736] Y.T. Liu, S.L. Shapiro, Z.B. Etienne, K. Taniguchi, General relativistic simulations of magnetized binary neutron star mergers, *Phys. Rev. D* 78 (2) (2008) 024012.
- [737] M. Anderson, E.W. Hirschmann, L. Lehner, S.L. Liebling, P.M. Motl, D. Nielsen, C. Palenzuela, J.E. Tohline, Magnetized neutron-star mergers and gravitational-wave signals, *Phys. Rev. Lett.* 100 (19) (2008) 191101.
- [738] B. Giacomazzo, L. Rezzolla, L. Baiotti, Accurate evolutions of inspiralling and magnetized neutron stars: Equal-mass binaries, *Phys. Rev. D* 83 (4) (2011) 044014.
- [739] Y.-Z. Fan, X.-F. Wu, D.-M. Wei, Signature of gravitational wave radiation in afterglows of short gamma-ray bursts? *Phys. Rev. D* 88 (6) (2013) 067304.
- [740] K.S. Cheng, Z.G. Dai, Conversion of neutron stars to strange stars as a possible origin of  $\gamma$ -ray bursts, *Phys. Rev. Lett.* 77 (1996) 1210–1213.
- [741] P. Chen, L. Labun, Electromagnetic signal of the QCD phase transition in neutron star mergers, *Phys. Rev. D* 88 (8) (2013) 083006.
- [742] B. Zhang, Early X-Ray and optical afterglow of gravitational wave bursts from mergers of binary neutron stars, *ApJ* 763 (2013) L22.
- [743] H. Gao, X. Ding, X.-F. Wu, B. Zhang, Z.-G. Dai, Bright broadband afterglows of gravitational wave bursts from mergers of binary neutron stars, *ApJ* 771 (2013) 86.
- [744] Y.-W. Yu, B. Zhang, H. Gao, Bright "merger-nova" from the remnant of a neutron star binary merger: A signature of a newly born, massive, millisecond magnetar, *ApJ* 776 (2013) L40–44.
- [745] B.D. Metzger, A.L. Piro, Optical and X-ray emission from stable millisecond magnetars formed from the merger of binary neutron stars, *MNRAS* 439 (2014) 3916–3930.
- [746] J.I. Katz, T. Piran, What have we learned from GRB afterglows? in: C. Meegan, R. Preece, T. M. Koshut, (Eds.), Gamma-Ray Bursts, 4th Huntsville Symposium in: American Institute of Physics Conference Series, vol. 428, 1998 pp. 689–699.
- [747] A. King, P.T. O’Brien, M.R. Goad, J. Osborne, E. Olsson, K. Page, Gamma-Ray Bursts: Restarting the Engine, *ApJ* 630 (2005) L113–L115.
- [748] R. Perna, P.J. Armitage, B. Zhang, Flares in long and short gamma-ray bursts: A common origin in a hyperaccreting accretion disk, *ApJ* 636 (2006) L29–L32.
- [749] D. Proga, B. Zhang, The late time evolution of gamma-ray bursts: ending hyperaccretion and producing flares, *MNRAS* 370 (2006) L61–L65.
- [750] X. Cao, E.-W. Liang, Y.-F. Yuan, Episodic jet power extracted from a spinning black hole surrounded by a neutrino-dominated accretion flow in gamma-ray bursts, *ApJ* 789 (2014) 129.
- [751] W.H. Lee, E. Ramirez-Ruiz, D. López-Cámará, Phase Transitions and He-Synthesis-Driven Winds in Neutrino Cooled Accretion Disks: Prospects for Late Flares in Short Gamma-Ray Bursts, *ApJ* 699 (2009) L93–L96.
- [752] B. Zhang, A possible connection between fast radio bursts and gamma-ray bursts, *ApJ* 780 (2014) L21.

- [753] D.R. Lorimer, Binary and Millisecond Pulsars, *Living Rev. Rel.* 8 (2005) 7.
- [754] M.G. Bernardini, R. Margutti, J. Mao, E. Zaninoni, G. Chincarini, The X-ray light curve of gamma-ray bursts: clues to the central engine, *A&A* 539 (2012) A3.
- [755] M. Xu, Y.F. Huang, New three-parameter correlation for gamma-ray bursts with a plateau phase in the afterglow, *A&A* 538 (2012) A134.
- [756] M.G. Dainotti, V. Petrosian, J. Singal, M. Ostrowski, Determination of the intrinsic Luminosity Time Correlation in the X-ray Afterglows of GRBs, *ApJ* 774 (2013) 157–165.
- [757] W. Feng, E. Berger, D.B. Fox, Hubble space telescope observations of short gamma-ray burst host galaxies: Morphologies, offsets, and local environments, *ApJ* 708 (2010) 9–25.
- [758] B. Paczynski, Cosmological gamma-ray bursts, *Acta Astronom.* 41 (1991) 257–267.
- [759] A. Gal-Yam, D.B. Fox, P.A. Price, E.O. Ofek, M.R. Davis, D.C. Leonard, A.M. Soderberg, B.P. Schmidt, K.M. Lewis, B.A. Peterson, S.R. Kulkarni, E. Berger, S.B. Cenko, R. Sari, K. Sharon, D. Frail, D.-S. Moon, P.J. Brown, A. Cucchiara, F. Harrison, T. Piran, S.E. Persson, P.J. McCarthy, B.E. Penprase, R.A. Chevalier, A.I. Macfadyen, A novel explosive process is required for the  $\gamma$ -ray burst GRB 060614, *Nature* 444 (2006) 1053–1055.
- [760] J.P.U. Fynbo, D. Watson, C.C. Thöne, J. Sollerman, J.S. Bloom, T.M. Davis, J. Hjorth, P. Jakobsson, U.G. Jørgensen, J.F. Graham, A.S. Fruchter, D. Bersier, L. Kewley, A. Cassan, J.M. Castro Cerón, S. Foley, J. Gorosabel, T.C. Hinse, K.D. Horne, B.L. Jensen, S. Klose, D. Kocevski, J.-B. Marquette, D. Perley, E. Ramirez-Ruiz, M.D. Stritzinger, P.M. Vreeswijk, R.A.M. Wijers, K.G. Woller, D. Xu, M. Zub, No supernovae associated with two long-duration  $\gamma$ -ray bursts, *Nature* 444 (2006) 1047–1049.
- [761] M. Della Valle, G. Chincarini, N. Panagia, G. Tagliaferri, D. Malesani, V. Testa, D. Fugazza, S. Campana, S. Covino, V. Mangano, L.A. Antonelli, P. D'Avanzo, K. Hurley, I.F. Mirabel, L.J. Pellizza, S. Piranomonte, L. Stella, An enigmatic long-lasting  $\gamma$ -ray burst not accompanied by a bright supernova, *Nature* 444 (2006) 1050–1052.
- [762] B. Zhang, B.-B. Zhang, E.-W. Liang, N. Gehrels, D.N. Burrows, P. Mészáros, Making a short gamma-ray burst from a long one: implications for the nature of GRB 060614, *ApJ* 655 (2007) L25–L28.
- [763] K. Nomoto, N. Tominaga, M. Tanaka, K. Maeda, T. Suzuki, J.S. Deng, P.A. Mazzali, Diversity of the supernova–gamma-ray burst connection, *Nuovo Cimento B Serie 121* (2006) 1207–1222.
- [764] J. Greiner, T. Krühler, J.P.U. Fynbo, A. Rossi, R. Schwarz, S. Klose, S. Savaglio, N.R. Tanvir, S. Mcbreen, T. Totani, B.B. Zhang, X.F. Wu, D. Watson, S.D. Barthelmy, A.P. Beardmore, P. Ferrero, N. Gehrels, D.A. Kann, N. Kawai, A.K. Yoldaş, P. Mészáros, B. Milvang-Jensen, S.R. Oates, D. Pierini, P. Schady, K. Toma, P.M. Vreeswijk, A. Yoldaş, B. Zhang, P. Afonso, K. Aoki, D.N. Burrows, C. Clemens, R. Filgas, Z. Haiman, D.H. Hartmann, G. Hasinger, J. Hjorth, E. Jehin, A.J. Levan, E.W. Liang, D. Malesani, T. Pyo, S. Schulze, G. Szokoly, K. Terada, K. Wiersema, GRB 080913 at Redshift 6.7, *ApJ* 693 (2009) 1610–1620.
- [765] N.R. Tanvir, D.B. Fox, A.J. Levan, E. Berger, K. Wiersema, J.P.U. Fynbo, A. Cucchiara, T. Krühler, N. Gehrels, J.S. Bloom, J. Greiner, P.A. Evans, E. Rol, F. Olivares, J. Hjorth, P. Jakobsson, J. Farhi, R. Willingale, R.L.C. Starling, S.B. Cenko, D. Perley, J.R. Maund, J. Duke, R.A.M.J. Wijers, A.J. Adamson, A. Allan, M.N. Bremer, D.N. Burrows, A.J. Castro-Tirado, B. Cavanagh, A. Deugartepesto, M.A. Dopita, T.A. Fatkhullin, A.S. Fruchter, R.J. Foley, J. Gorosabel, J. Kennea, T. Kerr, S. Klose, H.A. Krimm, V.N. Komarova, S.R. Kulkarni, A.S. Moskvitin, C.G. Mundell, T. Naylor, K. Page, B.E. Penprase, M. Perri, P. Podsiadlowski, K. Roth, R.E. Rutledge, T. Sakamoto, P. Schady, B.P. Schmidt, A.M. Soderberg, J. Sollerman, A.W. Stephens, G. Stratta, T.N. Ukwatta, D. Watson, E. Westra, T. Wold, C. Wolf, A  $\gamma$ -ray burst at a redshift of  $z \sim 8.2$ , *Nature* 461 (2009) 1254–1257.
- [766] R. Salvaterra, M. Della Valle, S. Campana, G. Chincarini, S. Covino, P. D'Avanzo, A. Fernández-Soto, C. Guidorzi, F. Mannucci, R. Margutti, C.C. Thöne, L.A. Antonelli, S.D. Barthelmy, M. Depasquale, V. D'Elia, F. Fiore, D. Fugazza, L.K. Hunt, E. Maiorano, S. Marinoni, F.E. Marshall, E. Molinari, J. Nosek, E. Pian, J.L. Racusin, L. Stella, L. Amati, G. Andreuzzi, G. Cusumano, E.E. Fenimore, P. Ferrero, P. Giommi, D. Guetta, S.T. Holland, K. Hurley, G.L. Israel, J. Mao, C.B. Markwardt, N. Masetti, C. Pagani, E. Palazzi, D.M. Palmer, S. Piranomonte, G. Tagliaferri, V. Testa, GRB090423 at a redshift of  $z \sim 8.1$ , *Nature* 461 (2009) 1258–1260.
- [767] H.-J. Lü, B. Zhang, E.-W. Liang, B.-B. Zhang, T. Sakamoto, The ‘amplitude’ parameter of gamma-ray bursts and its implications for GRB classification, *MNRAS* 442 (2014) 1922–1929.
- [768] O.M. Littlejohns, N.R. Tanvir, R. Willingale, P.A. Evans, P.T. O'Brien, A.J. Levan, Are gamma-ray bursts the same at high redshift and low redshift?, *MNRAS* 436 (2013) 3640–3655.
- [769] E.M. Levesque, J.S. Bloom, N.R. Butler, D.A. Perley, S.B. Cenko, J.X. Prochaska, L.J. Kewley, A. Bunker, H. Chen, R. Chornock, A.V. Filippenko, K. Glazebrook, S. Lopez, J. Masiero, M. Modjaz, A. Morgan, D. Poznanski, GRB090426: the environment of a rest-frame 0.35-s gamma-ray burst at a redshift of 2.609, *MNRAS* 401 (2010) 963–972.
- [770] L.A. Antonelli, P. D'Avanzo, R. Perna, L. Amati, S. Covino, S. Cutini, V. D'Elia, S. Gallozzo, A. Grazian, E. Palazzi, S. Piranomonte, A. Rossi, S. Spiro, L. Stella, V. Testa, G. Chincarini, A. di Paola, F. Fiore, D. Fugazza, E. Giallongo, E. Maiorano, N. Masetti, F. Pedichini, R. Salvaterra, G. Tagliaferri, S. Vergani, GRB 090426: the farthest short gamma-ray burst? *A&A* 507 (2009) L45–L48.
- [771] L.-P. Xin, E.-W. Liang, J.-Y. Wei, B. Zhang, H.-J. Lv, W.-K. Zheng, Y. Urata, M. Im, J. Wang, Y.-L. Qiu, J.-S. Deng, K.-Y. Huang, J.-Y. Hu, Y. Jeon, H.-L. Li, X.-H. Han, Probing the nature of high-z short GRB 090426 with its early optical and X-ray afterglows, *MNRAS* 410 (2011) 27–32.
- [772] C.C. Thöne, S. Campana, D. Lazzati, A. Deugartepesto, J.P.U. Fynbo, L. Christensen, A.J. Levan, M.A. Aloy, J. Hjorth, P. Jakobsson, E.M. Levesque, D. Malesani, B. Milvang-Jensen, P.W.A. Roming, N.R. Tanvir, K. Wiersema, M. Gladders, E. Wuyts, H. Dahle, Variable Ly $\alpha$  sheds light on the environment surrounding GRB 090426, *MNRAS* 414 (2011) 479–488.
- [773] X.-H. Cui, S. Nagataki, J. Aoi, R.-X. Xu, Origins of short gamma-ray bursts deduced from offsets in their host galaxies revisited, *Research in Astronomy and Astrophysics* 12 (2012) 1255–1268.
- [774] E. Berger, Short-duration gamma-ray bursts, *Ann. Rev. Astron. Astrophys.* 52 (2014) 43–105.
- [775] B. Zhang, Astrophysics: A burst of new ideas, *Nature* 444 (2006) 1010–1011.
- [776] D.A. Kann, S. Klose, B. Zhang, D. Malesani, E. Nakar, A. Pozanenko, A.C. Wilson, N.R. Butler, P. Jakobsson, S. Schulze, M. Andreev, L.A. Antonelli, I.F. Bikmaev, V. Biryukov, M. Böttcher, R.A. Burenin, J.M. Castro Cerón, A.J. Castro-Tirado, G. Chincarini, B.E. Cobb, S. Covino, P. D'Avanzo, V. D'Elia, M. Della Valle, A. de Ugarte Postigo, Y. Efimov, P. Ferrero, D. Fugazza, J.P.U. Fynbo, M. Gál Falk, F. Grundahl, J. Gorosabel, S. Gupta, S. Guziy, B. Hafizov, J. Hjorth, K. Holjhjem, M. Ibrahimov, M. Im, G.L. Israel, M. Jelínek, B.L. Jensen, R. Karimov, I.M. Khamitov, Ü. Kiziloglu, E. Klunko, P. Kubánek, A.S. Kutyrav, P. Laursen, A.J. Levan, F. Mannucci, C.M. Martin, A. Mescheryakov, N. Mirabal, J.P. Norris, J.-E. Ovaldsen, D. Paraficz, E. Pavlenko, S. Piranomonte, A. Rossi, V. Rumyantsev, R. Salinas, A. Sergeev, D. Sharapov, J. Sollerman, B. Stecklum, L. Stella, G. Tagliaferri, N.R. Tanvir, J. Telting, V. Testa, A.C. Updike, A. Volnova, D. Watson, K. Wiersema, D. Xu, The Afterglows of Swift-era Gamma-ray Bursts. I. Comparing pre-Swift and Swift-era Long/Soft (Type II) GRB Optical Afterglows, *ApJ* 720 (2010) 1513–1558.
- [777] H.-J. Lü, E.-W. Liang, B.-B. Zhang, B. Zhang, A New Classification Method for Gamma-ray Bursts, *ApJ* 725 (2010) 1965–1970.
- [778] D. Kocevski, V. Petrosian, On the Lack of Time Dilation Signatures in Gamma-Ray Burst Light Curves, *ApJ* 765 (2013) 116.
- [779] E. Nakar, R. Sari, Relativistic Shock Breakouts — A Variety of Gamma-Ray Flares: From Low-luminosity Gamma-Ray Bursts to Type Ia Supernovae, *ApJ* 747 (2012) 88.
- [780] B. Gendre, G. Stratta, J.L. Atteia, S. Basa, M. Boér, D.M. Coward, S. Cutini, V. D'Elia, E.J. Howell, A. Klotz, L. Piro, The ultra-long gamma-ray burst 111209A: The collapse of a blue supergiant?, *ApJ* 766 (2013) 30.
- [781] A.J. Levan, N.R. Tanvir, R.L.C. Starling, K. Wiersema, K.L. Page, D.A. Perley, S. Schulze, G.A. Wynn, R. Chornock, J. Hjorth, S.B. Cenko, A.S. Fruchter, P.T. O'Brien, G.C. Brown, R.L. Tunnicliffe, D. Malesani, P. Jakobsson, D. Watson, E. Berger, D. Bersier, B.E. Cobb, S. Covino, A. Cucchiara, A. de Ugarte Postigo, D.B. Fox, A. Gal-Yam, P. Goldoni, J. Gorosabel, L. Kaper, T. Krühler, R. Karjalainen, J.P. Osborne, E. Pian, R. Sánchez-Ramírez, B. Schmidt, I. Skillen, G. Tagliaferri, C. Thöne, O. Vaduvescu, R.A.M.J. Wijers, B.A. Zauderer, A new population of ultra-long duration gamma-ray bursts, *ApJ* 781 (2014) 13.
- [782] F.J. Virgili, C.G. Mundell, V. Pal'Shin, C. Guidorzi, R. Margutti, A. Melandri, R. Harrison, S. Kobayashi, R. Chornock, A. Henden, A.C. Updike, S.B. Cenko, N.R. Tanvir, I.A. Steele, A. Cucchiara, A. Gomboc, A. Levan, Z. Cano, C.J. Mottram, N.R. Clay, D. Bersier, D. Kopac, J. Japelj, A.V. Filippenko, W. Li, D. Svinkin, S. Golenetskii, D.H. Hartmann, P.A. Milne, G. Williams, P.T. O'Brien, D.B. Fox, E. Berger, GRB 091024A and the nature of ultra-long gamma-ray bursts, *ApJ* 778 (2013) 54.
- [783] B.-B. Zhang, B. Zhang, K. Murase, V. Connaughton, M.S. Briggs, How long does a burst burst? *ApJ* 787 (2014) 66.

- [784] J. Hjorth, J.S. Bloom, The Gamma-Ray Burst – Supernova Connection, ArXiv e-prints, Apr 2011.
- [785] A. Zeh, S. Klose, D.H. Hartmann, A systematic analysis of supernova light in gamma-ray burst afterglows, *ApJ* 609 (2004) 952–961.
- [786] S.B. Cenko, D.B. Fox, B.E. Penprase, A. Cucchiara, P.A. Price, E. Berger, S.R. Kulkarni, F.A. Harrison, A. Gal-Yam, E.O. Ofek, A. Rau, P. Chandra, D.A. Frail, M.M. Kasliwal, B.P. Schmidt, A.M. Soderberg, P.B. Cameron, K.C. Roth, GRB 070125: The first long-duration gamma-ray burst in a halo environment, *ApJ* 677 (2008) 441–447.
- [787] E.M. Levesque, R. Chornock, A.M. Soderberg, E. Berger, R. Lunnan, Host galaxy properties of the subluminous GRB 120422A/SN 2012bz, *ApJ* 758 (2012) 92.
- [788] J.P.U. Fynbo, P. Jakobsson, P. Möller, J. Hjorth, B. Thomsen, M.I. Andersen, A.S. Fruchter, J. Gorosabel, S.T. Holland, C. Ledoux, H. Pedersen, J. Rhoads, M. Weidinger, R.A.M.J. Wijers, On the Lyalpha emission from gamma-ray burst host galaxies: Evidence for low metallicities, *A&A* 406 (2003) L63–L66.
- [789] J.X. Prochaska, J.S. Bloom, H.-W. Chen, K.C. Hurley, J. Melbourne, A. Dressler, J.R. Graham, D.J. Osip, W.D. Vacca, The host galaxy of GRB 031203: Implications of its low metallicity, low redshift, and starburst nature, *ApJ* 611 (2004) 200–207.
- [790] M. Modjaz, L. Kewley, R.P. Kirshner, K.Z. Stanek, P. Challis, P.M. Garnavich, J.E. Greene, P.L. Kelly, J.L. Prieto, Measured Metallicities at the Sites of Nearby Broad-Lined Type Ic Supernovae and Implications for the Supernovae Gamma-Ray Burst Connection, *AJ* 135 (2008) 1136–1150.
- [791] S. Savaglio, K. Glazebrook, D. Le Borgne, The galaxy population hosting gamma-ray bursts, *ApJ* 691 (2009) 182–211.
- [792] J.F. Graham, A.S. Fruchter, The metal aversion of long-duration gamma-ray bursts, *ApJ* 774 (2013) 119.
- [793] Y. Niino, J.-H. Choi, M.A.R. Kobayashi, K. Nagamine, T. Totani, B. Zhang, Luminosity Distribution of Gamma-ray Burst Host Galaxies at Redshift  $z = 1$  in Cosmological Smoothed Particle Hydrodynamic Simulations: Implications for the Metallicity Dependence of GRBs, *ApJ* 726 (2011) 88.
- [794] S.T. Holland, B. Sbarufatti, R. Shen, P. Schady, J.R. Cummings, E. Fonseca, J.P.U. Fynbo, P. Jakobsson, E. Leitet, S. Linné, P.W.A. Roming, M. Still, B. Zhang, GRB 090417B and its host galaxy: A step toward an understanding of optically dark gamma-ray bursts, *ApJ* 717 (2010) 223–234.
- [795] D.A. Perley, A.J. Levan, N.R. Tanvir, S.B. Cenko, J.S. Bloom, J. Hjorth, T. Kruehler, A.V. Filippenko, A. Fruchter, J.P.U. Fynbo, P. Jakobsson, J. Kalirai, B. Milvang-Jensen, A.N. Morgan, J.X. Prochaska, J.M. Silverman, A population of massive, luminous galaxies hosting heavily dust-obscured gamma-ray bursts: Implications for the use of GRBs as tracers of cosmic star formation, *ApJ* 778 (2013) 128–162.
- [796] S.E. Woosley, Models for Gamma-Ray Burst Progenitors and Central Engines, May 2011, ArXiv e-prints.
- [797] C.L. Fryer, S.E. Woosley, D.H. Hartmann, Formation rates of black hole accretion disk gamma-ray bursts, *ApJ* 526 (1999) 152–177.
- [798] L.-X. Li, B. Paczyński, Transient Events from Neutron Star Mergers, *ApJ* 507 (1998) L59–L62.
- [799] S.R. Kulkarni, Modeling Supernova-like Explosions Associated with Gamma-ray Bursts with Short Durations, ArXiv Astrophysics e-prints, 2005.
- [800] B.D. Metzger, G. Martínez-Pinedo, S. Darbha, E. Quataert, A. Arcones, D. Kasen, R. Thomas, P. Nugent, I.V. Panov, N.T. Zinner, Electromagnetic counterparts of compact object mergers by the radioactive decay of r-process nuclei, *MNRAS* 406 (2010) 2650–2662.
- [801] J. Barnes, D. Kasen, Effect of a high opacity on the light curves of radioactively powered transients from compact object mergers, *ApJ* 775 (2013) 18.
- [802] N.R. Tanvir, A.J. Levan, A.S. Fruchter, J. Hjorth, R.A. Hounsell, K. Wiersema, R.L. Tunnicliffe, A ‘kilonova’ associated with the short-duration  $\gamma$ -ray burst GRB130603B, *Nature* 500 (2013) 547–549.
- [803] E. Berger, W. Fong, R. Chornock, An r-process Kilonova associated with the short-hard GRB 130603B, *ApJ* 774 (2013) L23.
- [804] J.S. Bloom, S.R. Kulkarni, S.G. Djorgovski, The observed offset distribution of gamma-ray bursts from their host galaxies: a robust clue to the nature of the progenitors, *AJ* 123 (2002) 1111–1148.
- [805] E. Berger, The environments of short-duration gamma-ray bursts and implications for their progenitors, *New Astron. Rev.* 55 (2011) 1–22.
- [806] S. Rosswog, T. Piran, E. Nakar, The multimessenger picture of compact object encounters: binary mergers versus dynamical collisions, *MNRAS* 430 (2013) 2585–2604.
- [807] B. Qin, X.-P. Wu, M.-C. Chu, L.-Z. Fang, J.-Y. Hu, The Collapse of Neutron Stars in High-Mass Binaries as the Energy Source for the Gamma-Ray Bursts, *ApJ* 494 (1998) L57.
- [808] A.I. Macfadyen, E. Ramirez-Ruiz, W. Zhang, X-ray flares following short gamma-ray bursts from shock heating of binary stellar companions, Oct. 2005, ArXiv Astrophysics e-prints.
- [809] D.M. Palmer, S. Barthelmy, N. Gehrels, R.M. Kippen, T. Cayton, C. Kouveliotou, D. Eichler, R.A.M.J. Wijers, P.M. Woods, J. Granot, Y.E. Lyubarsky, E. Ramirez-Ruiz, L. Barbier, M. Chester, J. Cummings, E.E. Fenimore, M.H. Finger, B.M. Gaensler, D. Hullinger, H. Krimm, C.B. Markwardt, J.A. Nosek, A. Parsons, S. Patel, T. Sakamoto, G. Sato, M. Suzuki, J. Tueller, A giant  $\gamma$ -ray flare from the magnetar SGR 1806 – 20, *Nature* 434 (2005) 1107–1109.
- [810] E. Nakar, A. Gal-Yam, D.B. Fox, The local rate and the progenitor lifetimes of short-hard gamma-ray bursts: synthesis and predictions for the laser interferometer gravitational-wave observatory, *ApJ* 650 (2006) 281–290.
- [811] D. Guetta, T. Piran, The luminosity and redshift distributions of short-duration GRBs, *A&A* 435 (2005) 421–426.
- [812] N.R. Tanvir, R. Chapman, A.J. Levan, R.S. Priddey, An origin in the local Universe for some short  $\gamma$ -ray bursts, *Nature* 438 (2005) 991–993.
- [813] E. Nakar, A. Gal-Yam, T. Piran, D.B. Fox, The distances of short-hard gamma-ray bursts and the soft gamma-ray repeater connection, *ApJ* 640 (2006) 849–853.
- [814] I. Bartos, P. Brady, S. Márka, How gravitational-wave observations can shape the gamma-ray burst paradigm, *Classical Quantum Gravity* 30 (12) (2013) 123001.
- [815] É É Flanagan, S.A. Hughes, Measuring gravitational waves from binary black hole coalescences. I. Signal to noise for inspiral, merger, and ringdown, *Phys. Rev. D* 57 (1998) 4535–4565.
- [816] C.S. Kochanek, T. Piran, Gravitational Waves and gamma -Ray Bursts, *ApJ* 417 (1993) L17.
- [817] T. Piran, Gamma-Ray bursts – a primer for relativists, in: N.T. Bishop, S.D. Maharaj (Eds.), *General Relativity and Gravitation*, 2002, pp. 259–275.
- [818] S. Kobayashi, P. Mészáros, Gravitational Radiation from Gamma-Ray Burst Progenitors, *ApJ* 589 (2003) 861–870.
- [819] A. Corsi, P. Mészáros, Gamma-ray burst afterglow plateaus and gravitational waves: multi-messenger signature of a millisecond magnetar? *ApJ* 702 (2009) 1171–1178.
- [820] C.D. Ott, E. Abdikamalov, E. O'Connor, C. Reisswig, R. Haas, P. Kalmus, S. Drasco, A. Burrows, E. Schnetter, Correlated gravitational wave and neutrino signals from general-relativistic rapidly rotating iron core collapse, *Phys. Rev. D* 86 (2) (2012) 024026.
- [821] B.P. Abbott, R. Abbott, R. Adhikari, P. Ajith, B. Allen, G. Allen, R.S. Amin, S.B. Anderson, W.G. Anderson, M.A. Arain, et al., LIGO: the laser interferometer gravitational-wave observatory, *Rep. Prog. Phys.* 72 (7) (2009) 076901.
- [822] F. Acernese, M. Alshourbagy, P. Amico, F. Antonucci, S. Aoudia, P. Astone, S. Avino, L. Baggio, G. Ballardin, F.e.a. Barone, Status of Virgo, *Classical Quantum Gravity* 25 (11) (2008) 114045.
- [823] L. Rezzolla, L. Baiotti, B. Giacomazzo, D. Link, J.A. Font, Accurate evolutions of unequal-mass neutron-star binaries: properties of the torus and short GRB engines, *Classical Quantum Gravity* 27 (11) (2010) 114105.
- [824] E. Nakar, T. Piran, Detectable radio flares following gravitational waves from mergers of binary neutron stars, *Nature* 478 (2011) 82–84.
- [825] M. Shibata, Y. Suwa, K. Kiuchi, K. Ioka, Afterglow of a binary neutron star merger, *ApJ* 734 (2011) L36.
- [826] B.D. Metzger, E. Berger, What is the Most Promising Electromagnetic Counterpart of a Neutron Star Binary Merger?, *ApJ* 746 (2012) 48.
- [827] T. Piran, E. Nakar, S. Rosswog, The electromagnetic signals of compact binary mergers, *MNRAS* 430 (2013) 2121–2136.
- [828] K. Kyutoku, K. Ioka, M. Shibata, Ultra-relativistic counterparts to binary neutron star mergers in every direction, X-ray-to-radio bands and second-to-day timescales, *MNRAS* 437 (2014) L6–L10.
- [829] K. Kyutoku, K. Ioka, M. Shibata, Anisotropic mass ejection from black hole–neutron star binaries: diversity of electromagnetic counterparts, *PhRvD* 88 (2014) 1503.
- [830] B. Giacomazzo, R. Perna, Formation of stable magnetars from binary neutron star mergers, *ApJ* 771 (2013) L26.
- [831] E. Waxman, Cosmological gamma-ray bursts and the highest energy cosmic rays, *Phys. Rev. Lett.* 75 (1995) 386–389.
- [832] M. Vietri, The acceleration of ultra-high-energy cosmic rays in gamma-ray bursts, *ApJ* 453 (1995) 883.
- [833] M. Milgrom, V. Usov, Possible Association of Ultra-High-Energy Cosmic-Ray Events with Strong Gamma-Ray Bursts, *ApJ* 449 (1995) L37.
- [834] E. Waxman, J. Bahcall, High energy neutrinos from cosmological gamma-ray burst fireballs, *Phys. Rev. Lett.* 78 (1997) 2292–2295.

- [835] C. Thompson, P. Mészáros, M.J. Rees, Thermalization in relativistic outflows and the correlation between spectral hardness and apparent luminosity in gamma-ray bursts, *ApJ* 666 (2007) 1012–1023.
- [836] D. Giannios, Prompt GRB emission from gradual energy dissipation, *A&A* 480 (2008) 305–312.
- [837] K. Ioka, Very High Lorentz Factor Fireballs and Gamma-Ray Burst Spectra, *Progr. Theoret. Phys.* 124 (2010) 667–710.
- [838] S. Razzaque, P. Mészáros, E. Waxman, High energy neutrinos from gamma-ray bursts with precursor supernovae, *Phys. Rev. Lett.* 90 (24) (2003) 241103.
- [839] S. Razzaque, P. Mészáros, E. Waxman, Neutrino tomography of gamma ray bursts and massive stellar collapses, *Phys. Rev. D* 68 (8) (2003) 083001.
- [840] D. Guetta, R. Perna, L. Stella, M. Vietri, Are All Gamma-Ray Bursts Like GRB 980425, GRB 030329, and GRB 031203?, *ApJ* 615 (2004) L73–L76.
- [841] K. Murase, S. Nagataki, High energy neutrino emission and neutrino background from gamma-ray bursts in the internal shock model, *Phys. Rev. D* 73 (6) (2006) 063002.
- [842] K. Murase, Prompt high-energy neutrinos from gamma-ray bursts in photospheric and synchrotron self-Compton scenarios, *Phys. Rev. D* 78 (10) (2008) 101302.
- [843] X.-Y. Wang, Z.-G. Dai, Prompt TeV neutrinos from the dissipative photospheres of gamma-ray bursts, *ApJ* 691 (2009) L67–L71.
- [844] B. Zhang, P. Kumar, Model-dependent high-energy neutrino flux from gamma-ray bursts, *Phys. Rev. Lett.* 110 (12) (2013) 121101.
- [845] R. Abbasi, Y. Abdou, T. Abu-Zayyad, J. Adams, J.A. Aguilar, M. Ahlers, K. Andeen, J. Auffenberg, X. Bai, M. Baker, et al., Search for muon neutrinos from gamma-ray bursts with the icecube neutrino telescope, *ApJ* 710 (2010) 346–359.
- [846] R. Abbasi, Y. Abdou, T. Abu-Zayyad, J. Adams, J.A. Aguilar, M. Ahlers, K. Andeen, J. Auffenberg, X. Bai, M. Baker, et al., Limits on neutrino emission from gamma-ray bursts with the 40 string icecube detector, *Phys. Rev. Lett.* 106 (14) (2011) 141101.
- [847] Z. Li, Note on the normalization of predicted gamma-ray burst neutrino flux, *Phys. Rev. D* 85 (2) (2012) 027301.
- [848] S. Hümmer, P. Baerwald, W. Winter, Neutrino emission from gamma-ray burst fireballs, revised, *Phys. Rev. Lett.* 108 (23) (2012) 231101.
- [849] S. Gao, K. Kashiyama, P. Mészáros, On the neutrino non-detection of GRB 130427A, *ApJ* 772 (2013) L4.
- [850] K. Murase, K. Ioka, S. Nagataki, T. Nakamura, High-Energy Neutrinos and Cosmic Rays from Low-Luminosity Gamma-Ray Bursts?, *ApJ* 651 (2006) L5–L8.
- [851] N. Gupta, B. Zhang, Neutrino spectra from low and high luminosity populations of gamma ray bursts, *Astropart. Phys.* 27 (2007) 386–391.
- [852] E. Waxman, J.N. Bahcall, Neutrino afterglow from gamma-ray bursts:  $10^{18}$  EV, *ApJ* 541 (2000) 707–711.
- [853] Z.G. Dai, T. Lu, Neutrino afterglows and progenitors of gamma-ray bursts, *ApJ* 551 (2001) 249–253.
- [854] C.D. Dermer, Neutrino, neutron, and cosmic-ray production in the external shock model of gamma-ray bursts, *ApJ* 574 (2002) 65–87.
- [855] P. Mészáros, E. Waxman, TeV Neutrinos from Successful and Choked Gamma-Ray Bursts, *Phys. Rev. Lett.* 87 (17) (2001) 171102.
- [856] K. Murase, K. Ioka, TeV-PeV Neutrinos from Low-Power Gamma-Ray Burst Jets inside Stars, *Phys. Rev. Lett.* 111 (12) (2013) 121102.
- [857] A. Levinson, O. Bromberg, Relativistic photon mediated shocks, *Phys. Rev. Lett.* 100 (13) (2008) 131101.
- [858] K. Murase, K. Kashiyama, P. Meszaros, Subphotospheric neutrinos from gamma-ray bursts: the role of neutrons, *PhRvL* 111 (2013) 1102–1105.
- [859] J. Tumlinson, J.M. Shull, Zero-Metallicity stars and the effects of the first stars on reionization, *ApJ* 528 (2000) L65–L68.
- [860] D. Schaerer, On the properties of massive Population III stars and metal-free stellar populations, *A&A* 382 (2002) 28–42.
- [861] A. Venkatesan, J.W. Truran, The ionizing efficiency of the first stars, *ApJ* 594 (2003) L1–L4.
- [862] V. Bromm, R.B. Larson, The first stars, *Ann. Rev. Astron. Astrophys.* 42 (2004) 79–118.
- [863] M. Tegmark, J. Silk, M.J. Rees, A. Blanchard, T. Abel, F. Palla, How small were the first cosmological objects? *ApJ* 474 (1997) 1.
- [864] N. Yoshida, T. Abel, L. Hernquist, N. Sugiyama, Simulations of early structure formation: primordial gas clouds, *ApJ* 592 (2003) 645–663.
- [865] V. Bromm, P.S. Coppi, R.B. Larson, Forming the first stars in the universe: The fragmentation of primordial gas, *ApJ* 527 (1999) L5–L8.
- [866] T. Abel, G.L. Bryan, M.L. Norman, The formation and fragmentation of primordial molecular clouds, *ApJ* 540 (2000) 39–44.
- [867] F. Nakamura, M. Umemura, On the initial mass function of population III stars, *ApJ* 548 (2001) 19–32.
- [868] A. Stacy, T.H. Greif, V. Bromm, The first stars: formation of binaries and small multiple systems, *MNRAS* 403 (2010) 45–60.
- [869] Y. Suwa, K. Ioka, Can Gamma-ray burst jets break out the first stars? *ApJ* 726 (2011) 107.
- [870] H. Nagakura, Y. Suwa, K. Ioka, Population III gamma-ray bursts and breakout criteria for accretion-powered jets, *ApJ* 754 (2012) 85.
- [871] M.D. Kistler, H. Yüksel, J.F. Beacom, K.Z. Stanek, An Unexpectedly Swift Rise in the Gamma-Ray Burst Rate, *ApJ* 673 (2008) L119–L122.
- [872] M.A. Campisi, L.-X. Li, P. Jakobsson, Redshift distribution and luminosity function of long gamma-ray bursts from cosmological simulations, *MNRAS* 407 (2010) 1972–1980.
- [873] S. Qin, E. Liang, R. Lu, J. Wei, S. Zhang, Simulations on high-z long gamma-ray burst rate, *MNRAS* 406 (2010) 558–565.
- [874] B.E. Robertson, R.S. Ellis, Connecting the Gamma Ray Burst Rate and the Cosmic Star Formation History: Implications for Reionization and Galaxy Evolution, *ApJ* 744 (2012) 95.
- [875] M. Trenti, R. Perna, S. Tacchella, Gamma-Ray burst and star formation rates: The physical origin for the redshift evolution of their ratio, *ApJ* 773 (2013) L22.
- [876] F. Daigne, E.M. Rossi, R. Mochkovitch, The redshift distribution of Swift gamma-ray bursts: evidence for evolution, *MNRAS* 372 (2006) 1034–1042.
- [877] V. Bromm, A. Loeb, The expected redshift distribution of gamma-ray bursts, *ApJ* 575 (2002) 111–116.
- [878] V. Bromm, A. Loeb, High-redshift gamma-ray bursts from population III progenitors, *ApJ* 642 (2006) 382–388.
- [879] R.S de Souza, N. Yoshida, K. Ioka, Populations III.1 and III.2 gamma-ray bursts: constraints on the event rate for future radio and X-ray surveys, *A&A* 533 (2011) A32.
- [880] H. Yüksel, M.D. Kistler, J.F. Beacom, A.M. Hopkins, Revealing the high-redshift star formation rate with gamma-ray bursts, *ApJ* 683 (2008) L5–L8.
- [881] D.Q. Lamb, D.E. Reichart, Gamma-ray bursts as a probe of the very high redshift universe, *ApJ* 536 (2000) 1–18.
- [882] B. Ciardi, A. Loeb, Expected number and flux distribution of gamma-ray burst afterglows with high redshifts, *ApJ* 540 (2000) 687–696.
- [883] L.J. Gou, P. Mészáros, T. Abel, B. Zhang, Detectability of Long Gamma-Ray Burst Afterglows from Very High Redshifts, *ApJ* 604 (2004) 508–520.
- [884] R. Barkana, A. Loeb, The physics and early history of the intergalactic medium, *Reports on Progress in Physics* 70 (2007) 627–657.
- [885] K. Nagamine, B. Zhang, L. Hernquist, Incidence rate of GRB-host DLAs at high redshift, *ApJ* 686 (2008) L57–L60.
- [886] A. Pontzen, A. Deason, F. Governato, M. Pettini, J. Wadsley, T. Quinn, A. Brooks, J. Bellovary, J.P.U. Fynbo, The nature of HIabsorbers in gamma-ray burst afterglows: clues from hydrodynamic simulations, *MNRAS* 402 (2010) 1523–1535.
- [887] K. Ioka, P. Mészáros, Radio Afterglows of Gamma-Ray Bursts and Hypernovae at High Redshift and Their Potential for 21 Centimeter Absorption Studies, *ApJ* 619 (2005) 684–696.
- [888] K. Toma, T. Sakamoto, P. Mészáros, Population III gamma-ray burst afterglows: constraints on stellar masses and external medium densities, *ApJ* 731 (2011) 127.
- [889] B. Ciardi, P. Labropoulos, A. Maselli, R. Thomas, S. Zaroubi, L. Graziani, J.S. Bolton, G. Bernardi, M. Brentjens, A.G. de Bruyn, S. Daiboo, G.J.A Harker, V. Jelic, S. Kazemi, L.V.E. Koopmans, O. Martinez, G. Mellema, A.R. Offringa, V.N. Pandey, J. Schaye, V. Veligatla, H. Vedantham, S. Yatawatta, Prospects for detecting the 21 cm forest from the diffuse intergalactic medium with LOFAR, *MNRAS* 428 (2013) 1755–1765.
- [890] N. Kawai, G. Kosugi, K. Aoki, T. Yamada, T. Totani, K. Ohta, M. Iye, T. Hattori, W. Aoki, H. Furusawa, K. Hurley, K.S. Kawabata, N. Kobayashi, Y. Komiyama, Y. Mizumoto, K. Nomoto, J. Noumaru, R. Ogasawara, R. Sato, K. Sekiguchi, Y. Shirasaki, M. Suzuki, T. Takata, T. Tamagawa, H. Terada, J. Watanabe, Y. Yatsu, A. Yoshida, An optical spectrum of the afterglow of a  $\gamma$ -ray burst at a redshift of  $z = 6.295$ , *Nature* 440 (2006) 184–186.
- [891] T. Totani, N. Kawai, G. Kosugi, K. Aoki, T. Yamada, M. Iye, K. Ohta, T. Hattori, Implications for cosmic reionization from the optical afterglow spectrum of the gamma-ray burst 050904 at  $z = 6.3$ , *Pub. Astro. Soc. of Japan* 58 (2006) 485–498.
- [892] J. Paul, J. Wei, S. Basa, S.-N. Zhang, The Chinese-French SVOM mission for gamma-ray burst studies, *Comptes Rendus Physique* 12 (2011) 298–308.
- [893] B. Grossan, I.H. Park, S. Ahmad, K.B. Ahn, P. Barrillon, S. Brandt, C. Budtz-Jørgensen, A.J. Castro-Tirado, P. Chen, H.S. Choi, Y.J. Choi, P. Connell, S. Dagoret-Campagne, C. Delataille, C. Eyles, I. Hermann, M.-H.A. Huang, A. Jung, S. Jeong, J.E. Kim, M. Kim, S.-W. Kim, Y.W. Kim, J. Lee, H. Lim, E.V. Linder, T.-C. Liu, N. Lund, K.W. Min, G.W. Na, J.W. Nam, M.I. Panasyuk, J. Ripa, V. Reglero, J.M. Rodrigo, G.F. Smoot, J.E. Suh, S. Svertilov, N. Vedenkin, M.-Z. Wang, I. Yashin, M.H. Zhao, 2012. A next generation Ultra-Fast Flash Observatory (UFFO-100) for IR/optical observations of the rise phase of gamma-ray bursts, in: Society of Photo-Optical Instrumentation Engineers (SPIE) Conference Series, vol. 8443.
- [894] I.H. Park, S. Brandt, C. Budtz-Jørgensen, A.J. Castro-Tirado, P. Chen, P. Connell, C. Eyles, B. Grossan, M.-H.A. Huang, S. Jeong, A. Jung, J.E. Kim, S.-W. Kim, J. Lee, H. Lim, E.V. Linder, T.-C. Liu, K.W. Min, G.W. Na, J.W. Nam, M.I. Panasyuk, V. Reglero, J. Ripa, J.M. Rodrigo, G.F. Smoot, S. Svertilov, N. Vedenkin, I. Yashin, Ultra-Fast Flash Observatory for the observation of early photons from gamma-ray bursts, *New J. Phys.* 15 (2) (2013) 023031.